Bacteria-targeted infection imaging

Heuker, Marjolein

DOI:
10.33612/diss.177500497

Bacteria-targeted infection imaging

Towards a faster diagnosis of bacterial infection

Marjolein Heuker

Cover design:
Gonny Huijink

Lay-out:
Lisanne Braams and Marjolein Heuker

Print:
Ipskamp Printing, Enschede, The Netherlands

rijksuniversiteit
groningen

Bacteria-targeted infection imaging

Towards a faster diagnosis of bacterial infection

Proefschrift

ter verkrijging van de graad van doctor aan de
Rijksuniversiteit Groningen
op gezag van de
rector magnificus prof. dr. C. Wijmenga
en volgens besluit van het College voor Promoties

De openbare verdediging zal plaatsvinden op

woensdag 8 september 2021 om 11.00 uur

door

Mattje Heuker

geboren op 8 december 1992
te Groningen

Promotores
Prof. dr. J.M. van Dijl
Prof. dr. G.M. van Dam

Copromotor
Dr. M. van Oosten

Beoordelingscommissie
Prof. dr. H.J. Busscher
Prof. dr. R.A.J.O. Dierckx
Prof. dr. J.A.G. van Strijp

Paranimfen
Jorrit W. A. Schoenmakers
Lisanne M. Braams
Mafalda Bispo

The work described in this thesis was mainly performed in the Laboratory of Molecular Bacteriology, Department of Medical Microbiology of the University of Groningen and the University Medical Center Groningen (The Netherlands). The research described in this thesis was financially supported by the University Medical Center Groningen and the University of Groningen.

Printing of this thesis was financially supported by the Graduate School of Medical Sciences of the University of Groningen, the Groningen University Library, Mauna Kea Technologies, Gino software, and Studio Apenzaken.

Table of contents

Chapter 1

General introduction

History of infectious diseases

Infectious diseases have been a serious concern for many years.[1] In 1683, bacteria were first observed under the microscope by the Dutch biologist Antoni van Leeuwenhoek. More than 150 years later, Friedrich Henle proposed the 'germ theory' of disease, in which micro-organisms are responsible for causing human disease. In the 1870s and 1880s this theory was confirmed by proving that micro-organisms were responsible for causing infectious diseases like anthrax, rabies, cholera and tuberculosis.[2]

For centuries, large epidemics like small pox, leprosy, cholera, poliomyelitis and tuberculosis have caused severe patient morbidity and mortality all over the world. Nowadays, these infectious diseases are not common anymore due to improved hygiene, increased knowledge of disease transmission and the introduction of vaccines and antibiotics. Confidence that infectious diseases can be successfully prevented and fought has risen, and the research community turned its attention more prominently to other major diseases, such as cancer.[1] However, in 1981 the world got a wake-up call from the acquired immune deficiency syndrome (AIDS) pandemic, which has spread across the planet and caused many deaths.[1] Since then, we have witnessed the emergence of various other dangerous micro-organisms causing severe morbidity and mortality, as exemplified by outbreaks of the Ebola virus in several African countries and the current SARS-CoV-2 pandemic.[3,4]

Bacterial infections

Bacterial infections are a frequently occurring problem in hospital settings worldwide, and they are responsible for major patient morbidity and mortality.[5] Moreover, their incidence is rising due to an increasing elderly population and advanced healthcare support, which includes the use of implanted biomaterials and organ transplantations. In addition, a second wake-up call that infectious diseases are still a serious threat to human health and wellbeing came from the emergence and spread of multiple drug-resistant microbes.[1] The rapid increase of bacteria that are insensitive to different classes of antibiotics has made bacterial infections increasingly difficult to treat.[6,7] In principle, micro-organisms can infect and disrupt all parts and functions of the human body and, consequently, there are numerous different infectious diseases. Three particular diseases that are in the focus of the research presented in this PhD thesis are bloodstream infections, biomaterial-associated infections and pneumonia.

Bloodstream infections

Bloodstream infections (BSIs) are amongst the most severe infectious diseases that lead to high morbidity and mortality. These infections, where viable micro-organisms enter the bloodstream and regularly cause sepsis (i.e. an extreme immune response to these micro-organisms), are leading

causes of death, especially in critically ill patients.[8,9] The high mortality rates observed for patients with BSIs are mainly related to delayed and ineffective antimicrobial treatment.[8] Treatment delays are often due to difficulties in early-stage diagnosis of BSI, and therapeutic interventions may be challenged by drug-resistant micro-organisms.[10]

Biomaterial-associated infections

Fracture-related infections (FRIs) and prosthetic joint infections (PJIs) are devastating post-operative complications after, respectively, bone fracture treatment or joint replacement. These dreaded complications and the following device failure are responsible for serious patient morbidity and decrease of quality of life.[11,12] Both biomaterial-associated infections often result in prolonged hospital-stay and a high disability.[13] Non-living surfaces, such as implanted biomaterials and dead bone fragments, are susceptible to the formation of bacterial biofilms in which bacteria are able to hide from the host's immune system. In addition, the biofilm functions as an impermeable barrier for antibiotics, which makes FRIs and PJIs extremely difficult to treat.[14]

Pneumonia

Another frequently occurring infection that often requires intensive therapy, is pneumonia. This infectious disease affects the lower respiratory tract and is still one of the leading causes of death.[15] Besides the increased mortality, pneumonia often leads to hospitalisation and prolonged treatment, which significantly increase healthcare costs. The mortality rate can even rise till more than 70% in mechanically ventilated patients, who may develop ventilator-associated pneumonia frequently caused by a high-risk pathogen with increased antibiotic resistance.[16]

Clinical challenges in diagnosing infections

The diagnosis of different bacterial infections faces several challenges. Clinical diagnosis of infection is mainly based on patients' signs and symptoms, general inflammation markers and the visualisation with non-specific imaging techniques, such as computed tomography (CT), magnetic resonance imaging (MRI), ultrasound (US), positron emission tomography (PET), single-photon emission computed tomography (SPECT) and scintigraphy. Unfortunately, these imaging techniques are unable to distinguish bacterial infection from sterile inflammation or other pathologies (i.e. viral or fungal infections).[5,17–19] Culture and/or molecular detection techniques are therefore needed to identify the causative micro-organisms, which can take many hours to usually several days. Meanwhile, empirical management of infection needs to be started with broad-spectrum antibiotics.

As an example, blood culture is considered to be the gold standard to diagnose BSIs. However, this method to detect infections is time consuming and it may take many days before a causative agent is identified.[8] To achieve a sensitivity of >95%, the results of at least two sets of blood cultures have to be obtained, ideally prior to the administration of antibiotics, which is unfortunately not always possible.[20] Moreover, identifying slow-growing fastidious micro-organisms can be problematic. Of importance, it is crucial to start with appropriate antimicrobial therapy within the first hour after a clinical suspicion of sepsis, to reduce the morbidity and mortality of the respective patients.[21]

Diagnosing biomaterial-associated infections, especially to distinguish bacterial infection from sterile inflammation, also represents a difficult technical challenge.[22] Specifically, in case of low-grade infections it is extremely difficult to achieve a diagnosis due to the absence of clinical signs and symptoms. Unfortunately, there is no single detection method to accurately detect FRIs or PJIs, and pre-operative imaging techniques are often inconclusive.[23] Accordingly, the diagnosis is usually based on a combination of clinical, laboratory, histopathological, microbiological and non-specific imaging results.[23] Pre-operative synovial fluid aspiration or intra-operative tissue sampling for culture form the cornerstones in the identification of the causative micro-organisms for specific antimicrobial treatment. Besides the fact that these procedures are invasive and time-consuming, it is not always possible to obtain appropriate material for culturing, which further complicates the diagnostic process.

Also the diagnosis of pneumonia faces several challenges, being based on clinical signs and symptoms, radiography and the results of sputum culture. Although radiography often reveals pulmonary infiltration, a reliable distinction of pneumonia from other causes of pulmonary infiltration is not possible.[16,24] In addition, the identification of pathogens in sputum cultures, or ideally in cultures of broncho-alveolar samples, is needed to provide accurate information on the causative bacterial species and its antibiotic resistance profile. However, it may be challenging to obtain sufficient and representative material for sputum culture and, often, it cannot be obtained due to the clinical condition of the patient. Moreover, due to the time-consuming nature of culturing, broad-spectrum antibiotic therapy is usually started before a definitive diagnosis can be made.

These three examples of frequently encountered infectious diseases highlight the urgent need for rapid and accurate detection and identification of micro-organisms. A fast detection of bacteria is particularly needed to optimise antibiotic therapy, limit therapeutic side effects, and decrease medical costs. In addition, specific treatment with the right antibiotics will help to prevent the selection and spread of antimicrobial resistant micro-organisms.

New diagnostic imaging modalities

A sensitive and specific imaging modality that allows for a quick and reliable detection of infecting bacteria in real-time is highly desirable. The above-mentioned current imaging modalities (i.e. anatomical imaging techniques, such as CT, MRI and US, and functional imaging modalities, such as PET, SPECT and scintigraphy) do unfortunately not meet this requirement. A major drawback of these imaging modalities nowadays is the inability to reliably distinguish infection from sterile inflammation or other pathologies at a cellular level. Hence, new imaging modalities that allow for fast and accurate direct detection of the infecting micro-organisms, and that ideally even provide specific information on the causative agent and its antibiotic resistances, would be of high value in clinical practice.

Fluorescence imaging

Fluorescence imaging or optical imaging is an upcoming and elegant imaging modality. The principle of fluorescence imaging is based on the excitation of a fluorophore, where its electrons become excited. When these electrons return to their ground state, light of a longer wavelength is emitted, which can be detected using a fluorescence camera. Human tissue exerts some (low) degree of auto-fluorescence, which is mainly detectable in the visible light range (400-600 nm). Of importance, fluorophores emit stronger signals than observed upon auto-fluorescence of human tissue. Fluorophores that emit signals in the near-infrared range (NIR; 700-1000 nm) are best detectable, with maximum tissue penetration, whereas the auto-fluorescence in the NIR range of the spectrum is minimal.[25] Fluorescence imaging offers various advantages, such as a high resolution, minimal invasive imaging, no evolvement of radiation and real-time visualisation.[25] The limited penetration depth of ~1 cm using NIR fluorophores and even less for fluorophores with shorter wavelengths, makes this imaging modality mainly suitable for surface and endoscopic imaging.[26]

Bacteria-targeted imaging

Bacteria-targeted imaging is based on a targeting agent (e.g. an antibody, antibiotic or antimicrobial peptide) that specifically targets bacteria or other micro-organisms, coupled to an imaging agent such as a radionuclide or fluorophore. Bacteria-targeted imaging not only allows for the localisation of infection, but it can also identify a specific micro-organism.[19,27] Fluorescence-targeted imaging of bacterial infections has multiple promising applications. These include the possibility of intra-operative real-time infection imaging, imaging of infections by arthroscopy or bronchoscopy, or *ex vivo* diagnostic infection imaging. Consequently, targeted fluorescence imaging has the potential to serve as a 'red-flag' in identifying infecting micro-organisms.

Scope and outline of this thesis

As described in the above paragraphs, fluorescence-targeted imaging of infecting bacteria shows great promise for diagnosing infectious diseases. Therefore, the aim of this PhD research was to develop and test new bacteria-specific imaging tools to improve the diagnosis of bacterial infections. An extensive overview of the different approaches that have been explored and described in the literature is presented in **Chapter 2** of this thesis. In addition, this chapter presents future opportunities for bacteria-targeted imaging in the detection of diverse infectious diseases.

Chapter 3 of this thesis is dedicated to the currently used and clinically well-known functional imaging modality PET with fluorine-18-fluorodeoxyglucose (^{18}F-FDG), which is frequently used to track sites of infection and inflammation. Diagnosing infections with ^{18}F-FDG-PET remains challenging, due to the fact that, for instance, malignancies, sterile inflammation and physiological wound healing can result in similarly high signals.[28] In particular, this chapter describes the accumulation of ^{18}F-FDG in diverse bacterial pathogens and the bacterial contribution to the signals observed in the currently applied FDG-PET infection imaging.

The following sections of this thesis, **Chapters 4** to **6**, focus on preclinical staphylococcal-targeted imaging approaches. **Chapter 4** presents a novel human monoclonal antibody-based tracer for bacteria-targeted imaging. The respective antibody binds specifically to the immunodominant staphylococcal antigen A (Isa A) which is exposed on the bacterial cell surface. Pre-clinical feasibility for *Staphylococcus*-specific imaging is demonstrated in a human *post-mortem* infection model and an *in vivo* murine skin infection model. Another promising *Staphylococcus*-specific tracer detects enzymatic activity of the micrococcal nuclease, which is specifically secreted by *S. aureus*. The results described in **Chapter 5** highlight the sensitivity and specificity of this nuclease activity-based tracer and demonstrate its stability in human blood and plasma. Importantly, the investigated nuclease-specific tracer is 'smart-activatable', because it only emits a fluorescence signal when it is cleaved by the target enzyme. Subsequently, evidence for future clinical implementation of the nuclease-activatable tracer for early diagnosis of *S. aureus* bacteraemia is presented in **Chapter 6**.

In the last sections of this thesis, **Chapters 7** to **9**, different clinical applications of bacteria-targeted fluorescence imaging are presented. **Chapter 7** describes the possible application of a recently developed fluorescent tracer based on the antibiotic vancomycin and the NIR fluorophore IRDye800CW. This tracer, denoted as vanco-800CW, is capable of detecting most Gram-positive bacteria, thereby targeting the vast majority of biomaterial-associated infections.[29] This chapter reports on the first *ex vivo* fluorescence imaging of clinical bacterial biofilms on osteosynthesis devices with vanco-800CW. Importantly, the results show that bacteria-targeted fluorescence imaging reduces the time to diagnosis from days to less than 30 min. In addition, surgeons could benefit from real-time visual information on the presence and extent of FRIs. To develop this fluorescence imaging technique further for the detection of PJIs, arthroscopic imaging with vanco-800CW was performed. This proof-of-principle study is described in **Chapter 8**. The last clinical

application presented in this thesis addresses the fluorescence-targeted imaging of bacterial colonisation and infection in the human lung. Accordingly, **Chapter 9** describes probe-based confocal laser endomicroscopy combined with fluorescence-targeted imaging of micro-organisms in the alveolar space of human resected lungs. Using two previously described tracers, respectively based on ubiquicidin and colistin (polymyxin E),[30–32] the presence of bacteria and yeast could be visualised even when the gold standard of microbiological culturing failed.

Lastly, **Chapter 10** presents a summary of the overall conclusions and a general discussion to place the present results in a more general perspective for the area for microbial infection imaging. Possible implications for future research and clinical implementation are highlighted.

References

1. Lederberg, J. Infectious history. *Science.* **14**, 287–293 (2000).
2. Murray, P. R., Rosenthal, K. S. & Pfaller, M. A. *Medical Microbiology.* 6th ed. p.3. Elsevier (2009).
3. World Health Organization. Ebola virus disease. Available from: https://www.who.int/health-topics/ebola/#tab=tab_1. [Accessed 15th December 2020].
4. World Health Organization. Coronavirus disease (COVID-19) pandemic. Available from: https://www.who.int/emergencies/diseases/novel-coronavirus-2019. [Accessed 15th December 2020].
5. Love, C. & Palestro, C. J. Radionuclide imaging of infection. *J. Nucl. Med. Technol.* **32**, 47–57 (2004).
6. Laxminarayan, R. *et al.* Antibiotic resistance-the need for global solutions. *Lancet Infect. Dis.* **13**, 1057–1098 (2013).
7. World Health Organization. The evolving threat of antimicrobial resistance – options for action. Available from: https://apps.who.int/iris/bitstream/handle/10665/44812/9789241503181_eng.pdf?sequence=1&isAllowed=y (2016). [Accessed 11th February 2021].
8. Peker, N., Couto, N., Sinha, B. & Rossen, J. W. Diagnosis of bloodstream infections from positive blood cultures and directly from blood samples: recent developments in molecular approaches. *Clin. Microbiol. Infect.* **24**, 944–955 (2018).
9. Bearman, G. M. L. & Wenzel, R. P. Bacteremias: a leading cause of death. *Arch. Med. Res.* **36**, 646–659 (2005).
10. Inagaki, K., Lucar, J., Blackshear, C. & Hobbs, C. V. Methicillin-susceptible and Methicillin-resistant *Staphylococcus aureus* Bacteremia: Nationwide Estimates of 30-Day Readmission, In-hospital Mortality, Length of Stay, and Cost in the United States. *Clin. Infect. Dis.* **69**, 2112–2118 (2019).
11. Kurtz, S., Ong, K., Lau, E., Mowat, F. & Halpern, M. Projections of primary and revision hip and knee arthroplasty in the United States from 2005 to 2030. *J. Bone Joint Surg.* **89**, 780–785 (2007).
12. Kurtz, S. M., Lau, E., Watson, H., Schmier, J. K. & Parvizi, J. Economic burden of periprosthetic joint infection in the united states. *J. Arthroplasty.* **27**, 61-65 (2012).
13. Maleb, A. *et al.* Bacteriological aspects of chronic osteoarticular infections in adults: The influence of the osteosynthesis material. *BMC Res. Notes.* **10**, 1–5 (2017).
14. Morgenstern, M. *et al.* Diagnostic challenges and future perspectives in fracture-related infection. *Injury.* **49**, S83–S90 (2018).
15. Mizgerd, J. Acute lower respiratory tract infection. *N. Engl. J. Med.* **358**, 716–727 (2008).
16. Chastre, J. & Fagon, J. State of the Art Ventilator-associated Pneumonia. *Am. J. Respir. Crit. Care Med.* **165**, 867–903 (2002).
17. Love, C., Tomas, M. B., Tronco, G. G. & Palestro, C. J. FDG PET of infection and inflammation. *Radiographics.* **25**, 1357–1368 (2005).
18. Strobel, K. & Stumpe, K. D. M. PET/CT in musculoskeletal infection. *Semin. Musculoskelet. Radiol.* **11**, 353–364 (2007).
19. van Oosten, M. *et al.* Targeted imaging of bacterial infections: advances, hurdles and hopes. *FEMS Microbiol. Rev.* **39**, 892–916

(2015).

20. Dubourg, G. & Raoult, D. Emerging methodologies for pathogen identification in positive blood culture testing. *Expert Rev. Mol. Diagn.* **16**, 97–111 (2016).
21. Rhodes, A. *et al.* Surviving Sepsis Campaign: International Guidelines for Management of Sepsis and Septic Shock: 2016. *Intensive Care Medicine.* **3**, 304-377 (2017).
22. Govaert, G. A. M. *et al.* Diagnosing Fracture-Related Infection: Current Concepts and Recommendations. *J. Orthop. Trauma.* **34**, 8–17 (2020).
23. Trampuz, A. & Zimmerli, W. Diagnosis and treatment of infections associated with fracture-fixation devices. *Injury.* **37**, 59–66 (2006).
24. Fàbregas, N. *et al.* Clinical diagnosis of ventilator associated pneumonia revisited: Comparative validation using immediate *post-mortem* lung biopsies. *Thorax.* **54**, 867–873 (1999).
25. Luo, S., Zhang, E., Su, Y., Cheng, T. & Shi, C. A review of NIR dyes in cancer targeting and imaging. *Biomaterials.* **32**, 7127–7138 (2011).
26. Pleijhuis, R. G. *et al.* Near-infrared fluorescence (NIRF) imaging in breast-conserving surgery: Assessing intraoperative techniques in tissue-simulating breast phantoms. *Eur. J. Surg. Oncol.* **37**, 32–39 (2011).
27. Mills, B., Bradley, M. & Dhaliwal, K. Optical imaging of bacterial infections. *Clin. Transl. Imaging.* **4**, 163–174 (2016).
28. Glaudemans, A. W. J. M., Israel, O. & Slart, R. H. J. A. Pitfalls and Limitations of Radionuclide and Hybrid Imaging in Infection and Inflammation. *Semin. Nucl. Med.* **45**, 500–512 (2015).
29. van Oosten, M. *et al.* Real-time *in vivo* imaging of invasive- and biomaterial-associated bacterial infections using fluorescently labelled vancomycin. *Nat. Commun.* **4**, 2548 (2013).
30. Akram, A. R. *et al.* A labelled-ubiquicidin antimicrobial peptide for immediate *in situ* optical detection of live bacteria in human alveolar lung tissue. *Chem. Sci.* **6**, 6971–6979 (2015).
31. Akram, A. R. *et al. In situ* identification of Gram-negative bacteria in human lungs using a topical fluorescent peptide targeting lipid A. *Sci. Transl. Med.* **10**, eaal0033 (2018).
32. Akram, A. R. *et al.* Enhanced avidity from a multivalent fluorescent antimicrobial peptide enables pathogen detection in a human lung model. *Sci. Rep.* **9**, 8422 (2019).

Chapter 2

Preclinical studies and prospective clinical applications for bacteria targeted imaging: *the future is bright*

Marjolein Heuker, Anna Gomes, Jan Maarten van Dijl, Gooitzen M. van Dam, Alexander W. Friedrich, Bhanu N.M. Sinha and Marleen van Oosten

Clinical and Translational Imaging (2016) 4:253-264

Abstract

Bacterial infections are a frequently occurring and major complication in human healthcare, in particular due to the rapid increase of antimicrobial resistance and the emergence of pan-drug resistant microbes. Current anatomical and functional imaging modalities are insufficiently capable of distinguishing sites of bacterial infection from sterile inflammation. Therefore, definitive diagnosis of an infection can often only be obtained by tissue biopsy and subsequent culture, and occasionally, a definite diagnosis even appears to be impossible. To accurately diagnose bacterial infections early, novel imaging modalities are urgently needed. In this regard, bacteria-targeted imaging is an attractive option due to its specificity. Here, different bacteria-targeted imaging approaches are reviewed, and their promising future perspectives are discussed.

Keywords: *imaging; infection; bacteria; tracer; fluorescence, radioisotope*

Introduction

Bacterial infections are of major concern both in hospital and community settings worldwide. Although much fundamental knowledge has been gained about micro-organisms and antimicrobial therapy, infections remain responsible for substantial patient morbidity and mortality these days.[1] In addition, infections become increasingly difficult to treat due to the rapid increase of antimicrobial resistance and the spread of pan-drug-resistant microbes.[2,3] Besides the fact that drug-resistant infections are difficult to treat, their associated healthcare costs are substantially higher. For example, 1-2% of the total joint arthroplasties will become infected, and the costs of treating such infections can amount up to $107.000 per case if caused by a resistant micro-organism. By comparison, the costs of treating infections with antibiotic-sensitive bacteria are substantially lower, revolving around $68.000.[4]

Despite a vast array of new technologies for the detection and typing of pathogens,[5] diagnosing infections is often complex or even problematic. This results in a relatively, or even completely, blind management of infections. This complexity is a consequence of the fact that diagnosis is based on the combination of several non-specific signs and symptoms, systemic inflammation markers, and visualisation with fairly unspecific imaging techniques.[6–8] A definite diagnosis of infectious disease, with evidence of infection and identification of the causative microbial species, can only be obtained by culture and/or molecular detection. Ideally, this involves obtaining material directly from the infective focus, which often requires tissue biopsy for deep-seated infections. This invasive diagnostic procedure takes many hours or even several days to yield an answer, and occasionally it is not even possible to obtain a representative biopsy. However, infections can be treated better when diagnosed accurately and early. Therefore reliable and fast diagnostic processes are desirable.[9]

Current imaging modalities to diagnose infectious disease comprise anatomical imaging modalities, such as computed tomography (CT), magnetic resonance imaging (MRI), and ultrasound (US), as well as functional imaging modalities, such as positron emission tomography (PET), single-photon emission computed tomography (SPECT), and scintigraphy. Unfortunately, these clinical imaging modalities by themselves are unable to differentiate bacterial infection from other infections (i.e. viral, fungal or parasitic), or from sterile inflammation.[1,10] Ideally, an imaging modality would allow for a reliable detection of infection, differentiate infection from other causes of inflammation, and thereby circumvent the need of more invasive methods. Hence, a new imaging modality that allows for sensitive and specific imaging of bacterial infection, ideally even providing species and resistance information to guide optimal therapy, would be of high value in clinical practice. Such an imaging modality is most likely to be found in bacteria-targeted imaging approaches.

In this review we present several bacteria-targeted imaging approaches and promising future perspectives of targeted imaging to diagnose infections.

Methods

A literature search was performed in PubMed, searching for publications in English, in the period between January 1980 and February 2016. The following search terms and variations thereof were used: imaging, detection, specific, targeted, bacterial, radionuclide, optical and/or fluorescence. Of the publications thus retrieved, only those that were aimed at bacteria-specific *in vivo* imaging, in animals or humans, were selected. CT, MRI, and US were not included, because in a separate search using the terms computed tomography, magnetic resonance imaging, and ultrasound, targeted, specific, bacterial, detection, articles describing *in vivo* bacteria-specific imaging with CT, MRI or US were identified. Only those tracers closest to clinical introduction are reported.

Targeted imaging

In recent years, an increasing interest in targeted imaging has been raised. Targeted imaging is based on an imaging agent, such as a radionuclide or fluorophore, coupled to a molecule (e.g. an antibody, an antibiotic, an antimicrobial peptide, a metabolizable compound, a bacteriophage, or a DNA/RNA-binding compound) that targets specific bacteria or other pathogens.[9,11] Besides visualisation of the site of infection, targeted imaging might also allow for the identification of the causative micro-organism. For additional information on the matter, we refer to the article of Mills *et al.* in this edition.[11] A more extensive review on targeted imaging was recently published by van Oosten *et al.*[9]

Radionuclide imaging

The functional non-targeted imaging modalities PET with fluorine-18-fluorodeoxyglucose (^{18}F-FDG) and leukocyte scintigraphy are nowadays frequently used to track down sites of both infection and inflammation.[12] Imaging of infections with ^{18}F-FDG-PET remains challenging due to the fact that all tissues with a high glucose uptake, such as brain, heart, malignancies, sterile inflammation and physiological wound healing, show increased FDG-uptake.[10] Leukocyte scintigraphy partly overcomes this drawback as it allows to some extent the distinction between inflammation and infection by comparing images at different acquisition times.[13] However, a major drawback of leukocyte scintigraphy is that it is very laborious, since it involves the drawing of blood from the patient, harvesting and radiolabelling of leukocytes, and re-administering of the labelled leukocytes to the patient. Altogether, this procedure takes several hours. Other non-targeted radionuclide imaging techniques used to detect infections are ^{67}Gallium-citrate imaging and bone scintigraphy.[10] In addition, two-step scintigraphy with streptavidin and ^{111}Indium-biotin (^{111}In-biotin) has been described by several research groups.[14,15] The latter approach is based on the fact that streptavidin binds ^{111}In-biotin with high affinity. However, this approach is unlikely to be bacteria-targeted as

streptavidin accumulates at sites of infection as well as sites of inflammation.[15]

The importance of non-invasive, specific, bacterial imaging in real-time has become widely recognised. Most current knowledge on radionuclide-targeted imaging concerns ^{99m}Technetium-ciprofloxacin (^{99m}Tc-ciprofloxacin; Infecton®). In this regard, a large multi-centre clinical trial showed a sensitivity of 85.4% and specificity of 81.7% for detecting bacterial infections with ^{99m}Tc-ciprofloxacin.[16] Although the sensitivity seems promising, its specificity is relatively low. Several other studies showed similar concern about the specificity of this imaging agent.[17–19] Indeed, ^{18}F-labelled ciprofloxacin did not allow for bacteria-specific imaging in humans.[20] PET-scans in four patients with bacterial soft tissue infections showed increased uptake of the tracer in infected areas. However, the signal was not retained in infected tissue and vanished at similar elimination half-life as in healthy tissue. It was, therefore, suggested that the radioactive signal was related to increased blood flow and vascular permeability in local infection.[20] Furthermore, there is a disadvantage of using ciprofloxacin due to the widespread resistance against this antibiotic.[21,22] Besides ^{99m}Tc-ciprofloxacin, other antibiotic-based tracers used in patients are radiolabelled ceftriaxone or fleroxacin.[23,24] ^{99m}Techneticum-labelled ceftriaxone allowed for successful visualisation of infections in patients, but studies were too small to draw a final conclusion about the sensitivity and specificity of this tracer.[23] Also, many other antibiotics have been radiolabelled and tested, mainly in animal models.[9]

As an alternative for labelled antibiotics, radiolabelled synthetic fragments of the antimicrobial peptide ubiquicidin can be used for detection of bacterial or fungal infections in patients. Ubiquicidin is a peptide originally isolated from mouse macrophages, and synthetic fragments of ubiquicidin were shown to bind to both Gram-positive and Gram-negative bacteria as well as to fungi. Small clinical trials investigating radiolabelled ubiquicidin, showed a sensitivity of 100% and a specificity from 80 to 100% for detection of bacterial and fungal infections.[25–28] Altogether, ten successful clinical studies have been reported on specific imaging of infections with radiolabelled ubiquicidin.[29] Importantly, ^{99m}Tc-ubiquicidin allowed the detection of infections with 93.7% accuracy and with a pooled data sensitivity and specificity of 97.5% and 89%, respectively. No immunological side effects were observed. Furthermore, a radionuclide-mediated tracer based on the nucleoside analogue fialuridine (1-(2-deoxy-2-fluoro-β-D-arabino-furanosyl)-5-iodouracil; FIAU), has been evaluated in patients. It was shown that FIAU is taken-up by bacteria and incorporated into their DNA, while this was not the case in human cells. Successful visualisation of bacterial infections using ^{124}Iodine-labelled FIAU has been reported, with apparently no false-positive or false-negative results in seven patients.[30] In contrast, a recent study investigating the use of ^{124}Iodine-FIAU to image prosthetic joint infections in patients did not establish a clear correlation between the infection status and imaging results.[31] Moreover, two clinical studies addressing the use of ^{124}Iodine-FIAU were terminated because of poor image quality, and a lack of correlation between FIAU uptake and bone biopsy results (clinicaltrials.gov: NCT01705496 and NCT01764919). Therefore, the future role of radiolabelled FIAU in infection imaging is currently unclear.

Another extensively described approach, which is hardly used anymore, is the imaging of infections with radiolabelled human polyclonal immunoglobulin (HIG).[32–34] HIG was supposed to accumulate at sites of infection, but it is apparently not bacteria-specific since the reported specificity ranges from 50 to 90%. This compromised specificity is mainly due to the fact that inflammation often results in a false-positive signal.

Not explored in humans so far, but promising as bacteria-specific imaging agents, are compounds that are exclusively metabolized by bacteria. Recently, detection of bacteria with the sugar 6-[^{18}F]-fluoromaltose (^{18}F-FM) has been reported.[35] Maltose and maltodextrins appear to be used as energy sources by the vast majority, if not all bacteria, since they express the maltodextrin transport complex in contrast to mammalian cells. ^{18}F-FM therefore allows specific detection of all classes of bacteria and distinction of bacterial infection from other causes of inflammation. Another promising sugar for imaging purposes is sorbitol, which is a sugar alcohol mainly metabolized by Gram-negative bacteria, especially *Enterobacteriaceae.* 2-[^{18}F]-fluoro-deoxy-sorbitol (^{18}F-FDS) was shown to allow for the specific detection of infections with *Escherichia coli* or *Klebsiella pneumoniae* in mice.[36] Importantly, ^{18}F-FDS neither accumulated in healthy nor malignant mammalian cells *in vitro*. Thus, ^{18}F-FM, ^{18}F-FDS and other labelled compounds that can only be metabolized by bacteria have a high potential for bacteria-targeted imaging and clinical translation.

Optical imaging

Use of optical (i.e. fluorescent) tracers for bacteria-targeted imaging is an upcoming and interesting topic nowadays. Optical imaging of infections seems highly feasible and has some important advantages over radionuclide imaging, such as (I) a high resolution, (II) the absence of ionizing radiation and its associated risks, (III) the possibility of real-time visualisation, and (IV) lower costs.[37–39] An important drawback of optical imaging is its limited penetration depth of maximally 1-2 cm using near-infrared tracers, and even less for tracers with shorter wavelengths. This limited penetration depth makes fluorescence imaging suitable mainly for imaging of surfaces and superficially located structures, and thus solely applicable in superficially located infections, such as soft tissue or superficial implant infections, or in intra-operative applications.[40]

Over the past decades much experience has been gained in optical imaging, for example in the visualisation of tumours in image-guided surgery.[41–43] Indeed, tumour-specific intra-operative fluorescence imaging of ovarian cancer was shown feasible in 2011 by targeting the overexpressed folate receptor-α in patients.[44] Especially intra- and peri-operative fluorescence imaging is likely to be of great value and major improvements, such as enhanced visual information during surgery and as a consequence improved sensitivity and specificity and more optimal resection margins, can be expected. In addition, deeper signal penetration might be feasible with improvements in fluorescent dyes and charge-coupled device (CCD) cameras.

Despite the fact that many different fluorophores are available, only a few fluorophores are approved and tested for clinical use today, including fluorescein isothiocyanate (FITC; emission

maximum: 518 nm), indocyanine green (ICG; emission maximum: 790 nm) and IRDye-800CW (emission maximum: 800 nm). To date, bacteria-targeted fluorescence imaging is only described in a few *in vivo* studies, but with very promising results. First, Ning *et al.* showed specific uptake of fluorescently labelled maltodextrin by different bacterial strains and it was feasible to distinguish bacterial infections from sterile inflammation with high target-to-normal tissue (T/N) ratios in rats.[45] Second, Panizzi *et al.* used fluorescently and radiolabelled inactivated prothrombin, which binds to the staphylococcal coagulase produced by *Staphylococcus aureus*. These authors were able to make a distinction between *S. aureus*-induced versus *Staphylococcus epidermidis*-induced endocarditis, or sterile vegetations in mice.[46] Third, several research groups described the use of a fluorescent bis zinc (II)-dipicolylamine complex for infection imaging.[47,48] This tracer attaches to the negatively charged membranes of bacteria. Unfortunately, the specificity of the fluorescent bis zinc (II)-dipicolylamine complex seems to be relatively low since this tracer also binds to negatively charged apoptotic cells.[48] Moreover, apoptotic cells are usually phagocytosed by macrophages which may further reduce the specificity. Lastly, non-invasive *in vivo* detection of infection caused by the Gram-positive bacterium *S. aureus* was shown using fluorescently labelled vancomycin.[37] Vancomycin-IRDye800CW (in short vanco-800CW) allowed the detection of *S. aureus* infection *in vivo* through several millimetres of tissue using a specialised CCD camera (**Figure 1**). This was not only shown in a mouse model, but also in a human *post-mortem* model for a biomaterial-associated infection. Vancomycin and IRDye-800CW are both approved substances for use in clinical practice, and it is therefore anticipated that vanco-800CW may be introduced safely for clinical use in the near future allowing for exploration of clinical applications. Whether the actual clinical application of vanco-800CW could be limited by increased vancomycin resistance in Gram-positive bacteria is currently unknown, but this is clearly a potential drawback of all antibiotic-based tracers.[9]

Optoacoustic imaging

The relatively new detection technology of optoacoustic imaging has been recently suggested for use in clinical imaging. Like optical imaging, this technique is based on absorption of light of a certain wavelength by an appropriate fluorophore coupled to a specific targeting molecule. After absorption of light, the fluorophore molecules will undergo thermo-elastic expansion, which leads to the emission of ultrasonic pressure waves. In optoacoustic imaging, these ultrasonic waves are detected by specialised sensors.[49] Optoacoustic imaging allows for deeper visualisation in tissue (around 11 cm in muscle tissue), since ultrasonic waves have longer wavelengths and deeper penetration than light.[50] This deeper penetration can particularly be valuable in the visualisation of e.g. bacterial infections of biomaterials or endocarditis. Next to these advantages, optoacoustic imaging offers a high resolution and high contrast comparable to that of MRI.[49]

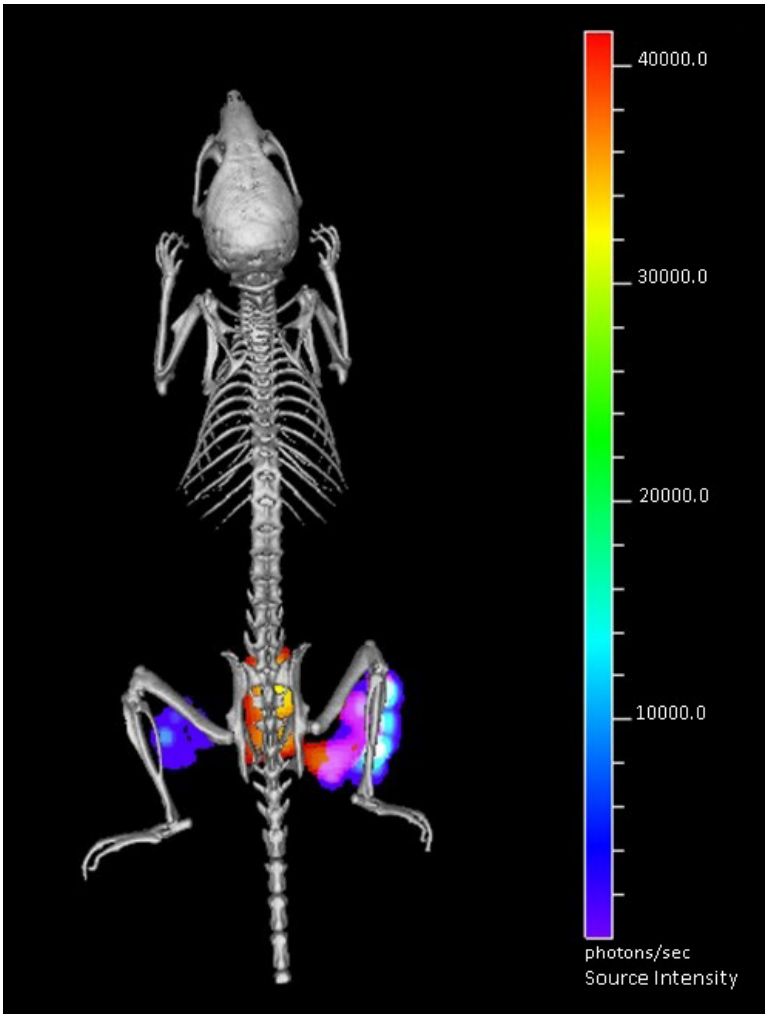

Figure 1. *In vivo* optical imaging of *Staphylococcus aureus* infection. Micro-computed tomography image of a mouse that was infected with a bioluminescent *S. aureus* strain in the right hind limb, and with a bioluminescent *Escherichia coli* strain in the left hind limb. The near-infrared (NIR) tracer vanco-800CW was administered intravenously.[37] The bioluminescence signal emitted by the infecting *S. aureus* and *E. coli* cells is depicted in rainbow scale, and the fluorescence signal due to vanco-800CW-binding in red-yellow scale. A clear co-registration of bioluminescence and NIR fluorescence was detected at the site of *S. aureus* infection. Moreover, a NIR fluorescence signal was detected in the bladder (in this image visible behind the spine). This bladder signal reflects the renal excretion of the tracer. (Reprinted with permission).[37]

Other imaging modalities

Specific imaging with CT and MRI scanning has been reported for imaging of malignancies, using targeted modality-specific contrast agents.[51,52] To the best of our knowledge, examples of bacteria-targeted imaging with CT or MRI *in vivo* have not yet been documented.[9] Neither were reports found addressing bacteria-specific targeting *in vivo* with the gas-filled microbubbles that are used as contrast agents in US.[9] Nevertheless, Anastasiadis *et al.* showed feasibility of a combined optical and acoustic evaluation *in vitro*, using targeted encapsulated gas bubbles for detection of early- and late-stage biofilm formation, potentially allowing for biofilm-specific imaging with US *in vivo*.[53]

Smart-activatable tracers

An exciting approach in the field of infection-targeted imaging is the detection of bacteria with so called 'smart-activatable tracers' (**Figure 2**). Smart-activatable tracers are optical tracers that are quenched in their normal state, and thus do not emit any signal. When the tracer encounters its target, the tracer is cleaved by bacterial enzymes, resulting in removal of the quencher. Subsequently, a fluorescence signal is emitted that can be detected. Imaging with smart-activatable tracers usually results in a higher T/N ratio as compared to conventional tracers, and consequently in more efficient imaging. Successful use of smart-activatable tracers has been reported for imaging tumours, as well as bacteria.[54–56] However, for infection imaging, results have so far only been obtained in animal studies. Kong *et al.* designed a smart-activatable tracer based on a β-lactam ring, which is hydrolysed by bacterial β-lactamases, leading to activation of the fluorophore.[55] Successful imaging with this tracer has been shown for *Mycobacterium tuberculosis* infection in mice. Although only *M. tuberculosis* infection imaging has been described, this tracer might be applicable for all β-lactamase-producing bacteria. No T/N ratios have been reported yet for this β-lactam smart-activatable tracer and, thus it is not clear whether the smart-activatable tracer in this case indeed offers the increased T/N ratios required.

Furthermore, Hernandez *et al.* reported the non-invasive detection of *S. aureus* infection in mice, with an intravenously administered nuclease-activated tracer.[56] The quenched fluorescent oligonucleotide tracer is specifically activated by micrococcal nuclease (MN), a nuclease secreted by *S. aureus*. This tracer is proven to be MN- and thus *S. aureus*-specific, since the mutated nuclease-deficient *S. aureus* showed a significantly lower signal. For this tracer good T/N ratios have been reported.

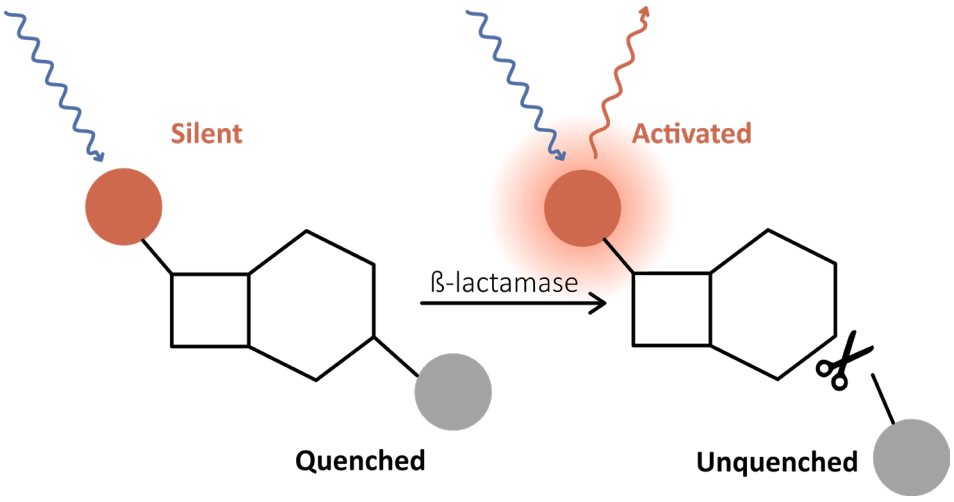

Figure 2. Mechanistic principle of β-lactam-based smart-activatable tracers. The intact tracer does not emit light due to the presence of a quencher (grey sphere). After hydrolysis of the β-lactam ring by a β-lactamase, the quencher is detached from the fluorophore (red sphere) and the tracer emits light.

Multi-modality tracers

A combination of imaging modalities allows for the concurrent application of the advantageous properties of each single modality, and thereby optimisation of diagnosis. Multi-modality tracers are based on a targeting molecule, coupled to two or more imaging modality agents, such as radionuclides, fluorophores, CT contrast agents, MRI contrast agents, or microbubbles.[57] Such a multi-modality tracer allows for imaging of a target with one single tracer by two or more different imaging modalities simultaneously. For example, this potentially offers an opportunity for pre-operative detection of infection and tracking down its localisation, and subsequently it offers a possibility for optical visualisation during invasive procedures. Such multi-modality tracers have been described for targeting inflammation (e.g. CD20 on B-cells, integrins and matrix metalloproteinases).[58] Notably, a bacteria-targeted multi-modality tracer based on the antimicrobial peptide ubiquicidin has recently been described.[59] Ubiquicidin was conjugated to a radioisotope and fluorophore and this dual-modality tracer was able to detect *S. aureus* and *K. pneumoniae* infections *in vivo* using a combined imaging system. In our opinion, these multi-modality tracers are potentially of great value in bacterial infection imaging.

Photodynamic therapy

Besides using targeted modalities to optimise diagnosis of infection, targeted therapy could be used to improve infection treatment. In particular, targeted photodynamic therapy (PDT) could play an important role in the treatment of infections. PDT is based on excitation of photosensitive molecules with light of a certain wavelength, resulting in an optical signal as well as cytotoxic molecules that are capable of destructing the targeted cells.[60,61] Treatment characteristics of this approach are promising, but untargeted PDT leads to damage of healthy tissue due to the non-specific uptake of photodynamic molecules, currently limiting this form of PDT to skin and dental infections.[60,62] Targeted PDT might solve this drawback and was already shown to be successful in cancer treatment.[61,63] It seems conceivable that targeted PDT could play an important role in the treatment of bacterial infections as well. Unfortunately, PDT would be limited to localised, easily accessible or superficial infections due to a limited penetration depth of available lasers. To date, there is little experience with targeted PDT in infections *in vivo*. Ragàs *et al.* showed eradication of methicillin-resistant *S. aureus* (MRSA) infection in a murine burn wound model.[64] A cationic photosensitizer, which was topically administered, was used to target the bacteria. Although, this technique eradicated MRSA, it is questionable whether this tracer is really 'targeted', since the photosensitizer binds to the negatively charged bacterial cell walls based on the cationic molecules, which probably would also have affinity for other negatively charged structures, such as apoptotic tissue. There is some more experience with targeted PDT in *in vitro* infection models. In this regard, feasibility has been shown for antibody-directed and antimicrobial peptides-directed PDT.[65–67] Suci *et al.* described successful targeted PDT based on a biotinylated photosensitizer and a biotinylated antibody specific for *Aggregatibacter actinomycetemcomitans*, coupled by streptavidin.[68] These results seem promising for the treatment of periodontal biofilms. Overall, PDT seems to be an interesting diagnostic and therapeutic application for locoregional infections.

Potential clinical applications of targeted imaging

Targeted imaging could enable earlier detection of infections, resulting in earlier institution of an accurate treatment. The more accurate treatment will subsequently represent a crucial element in the fight against bacterial resistance. Besides the application of targeted imaging in pre-operative diagnostics and post-operative follow-up of infections, it could also be used for intra-operative surgical guidance, theoretically leading to a more optimal resection of infected tissue and minimised damage in healthy tissue. Potential use of tracers for different infections is outlined in **Table 1**.

Table 1. Overview of infections, with most common causative micro-organisms, and potentially suitable tracers for detection

Infection	Common causative microorganisms (>10%)	Potential tracers for detection	Remarks
Bacteraemia	Miscellaneous	BLA, CEF, CIP, FIAU, MALT, NUC, PRO, SOR, UBI, VAN	
Infective endocarditis	Coagulase negative staphylococci, enterococci, HACEK organisms*, *Staphylococcus aureus,* viridans streptococci	CEF, CIP, FIAU, MALT, NUC, PRO, UBI, VAN	
Infected surgical grafts and meshes	Coagulase negative staphylococci, enterococci, *Staphylococcus aureus,* streptococci	CEF, CIP, FIAU, MALT, NUC, PRO, UBI, VAN	
Meningitis	*Haemophilus influenzae, Listeria monocytogenes*, Neisseria meningitides, Streptococcus pneumoniae*	CEF, FIAU, MALT, UBI	The tracer has to cross the blood-brain barrier
Necrotizing fasciitis	(An)aerobic mixed flora, *Clostridium perfringens*,* other clostridia*, *Staphylococcus aureus*, *Streptococcus pyogenes*, other β-hemolytic streptococci	CEF, CIP, FIAU, MALT, UBI, VAN	
Pneumonia	*Haemophilus influenzae,* Hospital-acquired pneumonia: miscellaneous, *Staphylococcus aureus, Streptococcus pneumoniae*	BLA, CEF, CIP, FIAU, MALT, NUC, PRO, SOR, UBI	
Septic arthritis	*Neisseria gonorrhoeae, Staphylococcus aureus,* streptococci	CEF, CIP, FIAU, FLER, MALT, NUC, PRO, UBI, VAN	

Tracers can be suitable in two possible ways, namely I) detection of infection by targeting the vast majority of causative pathogens, or II) by detection of particular species, which would have direct implications for the choice of therapy. Ideally, future approaches would offer both possibilities. Potentially usable tracers not only include the tracers in their current published structures but also future variants (e.g. modification from radiolabelled to optically labelled, or *vice versa*). Micro-organisms and tracers are mentioned in alphabetical order. The specific tracers listed are: ^{99m}Tc-ceftriaxone (CEF), ^{99m}Tc-ciprofloxacin/^{18}F-ciprofloxacin (CIP), ^{124}Iodine-FIAU (FIAU), ^{18}F-fleroxacin (FLER), 6-[^{18}F]-fluoromaltose/maltodextrin-based optical tracer (MALT), activatable nuclease-targeted optical tracer (*S. aureus*-directed; NUC), prothrombin-based optical/radiolabelled tracer (PRO), 2-[^{18}F]-fluoro-deoxy-sorbitol (SOR), ^{99m}Tc-ubiquicidin (UBI), vanco-800CW (VAN), activatable β-lactamase-targeted optical tracer (BLA).

* Marks micro-organisms that occur in less than 10% of the cases, but are classically associated with the respective infection. HACEK organisms (fastidious Gram-negative bacilli): *Haemophilus spp.*, *Aggregatibacter actinomycetemcomitans*, *Cardiobacterium hominis*, *Eikenella corrodens*, *Kingella kingae/Kingella denitrificans.*

Bacteraemia

The gold standard for diagnosis of bacteraemia (in case of sepsis or endocarditis) is the isolation of micro-organisms from a blood culture. Ideally, blood cultures are obtained prior to antimicrobial therapy. Unfortunately, it takes several days of culture until the causative micro-organism with its matching resistance pattern is identified. In case of infection with a fastidious micro-organism or antibiotic usage prior to the blood culture collection, identification of the bacterial species can be problematic. Real-time detection of bacteria in the blood stream of a patient would therefore be of great value. In particular optical targeted imaging might be ideal for this application, since this makes real-time bedside measurements feasible. For instance, the diagnosis of infection could potentially be made much faster by implementing continuous measurement systems. This could involve optical smart-activatable tracers and dedicated sensors. Subsequently, this would also allow for treatment follow-up, to detect whether the bacterial load in the blood stream is decreasing.

Infective endocarditis

Infective endocarditis (IE) causes serious morbidity and mortality (40% of all patients die in 1 year).[69] Therefore, early and accurate diagnosis is crucial. Unfortunately, diagnosing IE remains a challenge in current clinical practice, due to its variable clinical presentation of both cardiac and extra-cardiac manifestations. Diagnosis of IE is largely based on the modified Duke criteria, of which blood cultures and echocardiography are cornerstones.[70] These criteria have only a sensitivity and specificity of around 80% when no artificial material is involved,[70] and the ultimate diagnosis has still to be made by expert clinical judgement. Echocardiography has been shown to miss life-threatening complications in 30% of patients.[71] In addition, blood cultures show no causative micro-organism in up to 31% of all cases of IE,[72] partly due to prior antimicrobial therapy. This poses considerable diagnostic and therapeutic dilemmas in clinical practice, as anatomic information guides indication and timing of surgical treatment. Furthermore, it is essential to determine the causative micro-organism and its resistance pattern to implement appropriate antimicrobial therapy. Here, opportunities for improved imaging are, obviously, highly desirable. Promising results in this direction have been published using conventional ^{18}F-FDG-PET/CT and leukocyte scintigraphy.[73] These functional techniques use, respectively, ^{18}F-FDG as tracer and PET/CT for detection, or radiolabelled white blood cells (e.g. with ^{99m}Tc-HMPAO) as tracers and SPECT/CT for detection. Pizzi *et al.* have reported the largest study to date evaluating ^{18}F-FDG-PET/CT in endocarditis. Their results show that the largest group of 50 patients with possible endocarditis (54%) could

be reduced to 5 (5%).[74] Furthermore, Rouzet *et al.* compared both imaging techniques in IE, and their results mainly indicate that ^{18}F-FDG-PET/CT is more sensitive, whereas leukocyte scintigraphy is more specific.[75] However, even when taking most recent (non-specific) imaging developments into account,[73] more specific diagnosis of IE could prove critical in a vast amount of remaining cases with diagnostic uncertainty. In addition, opportunities to accelerate accurate diagnosis and treatment could prove lifesaving. Therefore, targeted imaging represents an appealing option for IE diagnosis. For example, targeted imaging could disclose the pathogenic bacterium in cases of negative blood cultures, so that adequate antibiotic therapy can be given. Besides, targeted imaging could point towards additional and distant sites of cardiac infection, which should be taken into account in the individualised therapy plan. On top of this, intra-operative targeted imaging could visualise the exact borders of infected tissue of which radical resection could potentially improve patient outcome. This is likely to be highly important in this condition since it is mandatory to immediately implant prosthetic material in the area of infected tissue.

Infected surgical meshes

Surgical meshes are commonly used to support tissue. In particular, these meshes are useful for permanent support in the repair of abdominal and inguinal hernias. Occasionally, a wound infection will occur after surgical intervention, and on longer term, intestinal-cutaneous fistulas can occur after abdominal surgery. Often it is difficult to determine whether and to what extent implanted meshes are involved in these infectious processes. This is highly relevant to predict prognosis and determine most optimal therapy. Targeted imaging could provide information on (I) whether the mesh is involved in the infectious process, and (II) what is the causing bacterial species. Due to the minimal-invasive targeted imaging technique, a more invasive technique, with ultimately preventive removal of the mesh, may be avoided.

Infected vascular grafts

Superficial (i.e. dialysis shunts) and deeper seated (e.g. aortic aneurysm repair) vascular graft infections are responsible for high patient morbidity and mortality, if not treated immediately.[76] Frequently, only the outside of the graft is infected resulting in negative blood cultures. Nowadays, ^{18}F-FDG-PET and/or leukocyte scintigraphy are used for the diagnosis of vascular graft infections in addition to the CT-scan. Both give information about inflammatory activity, in addition to the anatomic information derived from a simultaneous and/or separate CT-scan. However, infection cannot be reliably distinguished from sterile inflammation or physiological wound healing using ^{18}F-FDG-PET nor CT. Therefore, early infected vascular grafts cannot always be readily detected.[77] Also, notwithstanding its high sensitivity (91%), ^{18}F-FDG-PET is not an ideal imaging approach for detection of infected vascular grafts since its specificity is rather low (64%).[76] Leukocyte scintigraphy seems to allow for a higher specificity, especially early post-operatively, and is recommended if the CT-scan is inconclusive.[78,79] Nevertheless, a non-invasive specific targeted imaging technique

is highly desirable for detection of infected vascular grafts. The most important advantage of such a targeted approach is that an invasive surgical procedure is not needed to diagnose bacterial infection, to determine which vascular grafts are involved in infection, and to what extent these grafts are affected. Targeted imaging that allows for determination of the causative bacterial pathogen would highly aid in directing optimal therapy. This would be especially helpful in detecting fastidious micro-organisms that cannot be routinely cultured, such as *Coxiella burnetii*. Besides, intra-operative targeted imaging could aid for determining the extent of infected tissue and grafts, and for determining most optimal resection borders.

Meningitis

The diagnosis of meningitis is currently based on blood tests (i.e. C-reactive protein and complete blood count), blood cultures, and most importantly examination of the cerebrospinal fluid (CSF). CSF should be obtained of every patient with a suspicion of meningitis to identify the causative micro-organism unless a lumbar puncture is contraindicated (e.g. brain tumour, abscess, or a high intracranial pressure). In selected patients a CT-scan or MRI-scan is recommended prior to lumbar puncture to check for the existence of contraindications, which delays the actual puncture. As it is of great importance to treat meningitis quickly with antibiotics, in these cases broad-spectrum antimicrobial treatment is commonly initiated before lumbar puncture to prevent treatment delay. Unfortunately, this early start of antibiotic treatment often interferes with finding the causative agent, whereas culture of CSF that is obtained after start of antibiotic treatment has a substantially lower sensitivity. A sensitive imaging modality to detect meningitis at an early stage and to discriminate between different causative pathogens would be highly desirable.[80] Especially the new hybrid PET/MRI approach seems very promising for distinguishing meningitis from other pathologies such as abscesses and encephalitis.[81–83] This might even allow a distinction of meningitis caused by viruses from bacterial meningitis by pattern recognition. Bacteria-targeted PET-tracers, such as ^{18}F-FDS or ^{18}F-FM, which detect a subset or all bacterial species, could more clearly distinguish bacterial infections from other pathologies, and especially tracers that identify particular bacterial groups or even species could enable quick and more accurate treatment. An extra challenge might be found in designing tracers that reliably pass the blood-brain barrier upon intravenous administration. Also, it remains to be seen whether the bacterial load in meningitis is high enough for detection with the current PET cameras, which have a relative low resolution (3-4 mm). Clearly, a rapid and highly sensitive test for the presence of bacteria using fluorescent tracers could improve diagnostic accuracy and accelerate diagnosis in patients where CSF has been obtained. This option could make use of optical smart-activatable tracers and dedicated sensors which might be even used as bedside tests.

Necrotizing fasciitis

Necrotizing fasciitis is a rapidly progressive infection of the deeper layers of skin and subcutaneous tissues, which requires immediate aggressive surgery and antibiotic therapy. To date, surgeons mainly rely on visual and tactile information during surgery. Infection borders of necrotizing fasciitis are difficult to recognise and can only be analysed during surgery using frozen sections. Unfortunately, this is an indirect method giving information only about the small site of tissue where a biopsy was taken. Clearly, it is desirable to develop new methods that provide the needed information in real-time and intra-operatively. Using targeted imaging, surgeons can be provided with extra visual information. In targeted imaging of ovarian cancer in patients, surgeons were able to detect small tumour spots of <1 mm.[84] Hypothetically, intra-operative targeted imaging can also result in better detection of infection, and more precise and radical resection, while sparing as much as possible healthy tissue. This may eventually lead to a better prognosis for patients with less mutilating outcomes. Presumably, targeted imaging would be of great value for necrotizing fasciitis-related surgery in the future.

Pneumonia

Currently, diagnosis of pneumonia comprises clinical symptoms and signs, radiography and sputum culture. Radiography reveals in most cases pulmonary infiltrates, but differentiation between infection and other causes of pulmonary infiltration (e.g. atelectasis, infarction, haemorrhage, acute respiratory distress syndrome and malignancy) remains difficult with a specificity of only 33-70%.[85,86] Sputum culture, or even more optimal broncho-alveolar sample culture, can provide relevant information, but it takes several days before a reliable identification of the causative agent and its drug-resistance profile is available, if at all. Besides, representative respiratory material is often not obtainable due to the clinical situation of the patient. As a consequence, physicians substantially overtreat patients by early empirical initiation of broad-spectrum antibiotic therapy. Thus, there is currently an unmet need for fast and accurate diagnosis of pneumonia and identification of its causative agent to allow narrow-spectrum treatment and avoid unnecessary antibiotic usage. Development of a set of infection-targeted optical tracers for direct detection of pneumonia is a highly promising approach. First clinical trials on bacteria-targeted imaging are currently initiated at the Royal Infirmary in Edinburgh in order to detect bacterial pneumonia using a bronchoscope combined with confocal laser endomicroscopy (clinicaltrials.gov: NCT02558062 and NCT02491164). Potentially, this approach can visualise pneumonia *in situ*, not only providing direct cues about the presence and localisation of pneumonia, but also offering the possibility of focused sample collection for subsequent microbiological analysis (i.e. microscopy, culture or molecular analysis).

Septic arthritis

Septic arthritis is most commonly caused by bacteria, but fungi or viruses can be the causative agents as well. Notably, also sterile inflammatory diseases, such as rheumatoid arthritis or gout, are very

common causes of arthritis. Arthritis caused by bacterial pathogens is often rapidly destructive, and thereby of the most fulminant subtype. In daily practice, the causative agent of arthritis is difficult to establish from the outside, and arthrocentesis is used to collect synovial fluid. Subsequent microbiological culturing is needed to find evidence of infection and to identify the responsible bacteria. Minimal-invasive targeted imaging techniques would be of great importance in this clinical situation, to: (I) quickly and adequately distinguish bacterial arthritis from other pathologies, and (II) start early with appropriate antibiotic therapy. This may lead to a better prognosis for patients and a lowered chance of eliciting bacterial resistance.

Conclusion

Bacteria-targeted imaging is of significant upcoming interest. Progress has been made in the development of specific tracers, as well as in the development of imaging modalities to visualise infection. It remains difficult to predict which tracers or modalities will prove most appropriate for clinical use, but it is to be expected that some of the approaches described in this review will eventually find their place in routine clinical diagnostic settings. The further implementation of new imaging techniques, such as multi-modality imaging or optoacoustic imaging, and smart-activatable tracers, holds even greater promise for quick and accurate detection of infections. This may ultimately be extended to antibacterial therapy in case of targeted PDT. We thus conclude that bacteria-targeted imaging has a bright future.

Author contributions

MH, AG and MvO: Literature search and review, content planning and manuscript writing. JMvD, GMvD, AWF and BNMS: Content planning, manuscript writing and editing.

Compliance with ethics guidelines

Conflict of interest

MH, AG, JMvD, GMvD, AWF, BNMS and MvO have no conflict of interest to disclose.

Human and animal studies

This article does not contain any unpublished studies with human or animal subjects performed by any of the authors.

References

1. Love, C. & Palestro, C. J. Radionuclide imaging of infection. *J. Nucl. Med. Technol.* **32**, 47–57 (2004).
2. Laxminarayan, R. *et al.* Antibiotic resistance- the need for global solutions. *Lancet Infect. Dis.* **13**, 1057–1098 (2013).
3. World Health Organization. The evolving threat of antimicrobial resistance – options for action. Available from: https://apps.who.int/iris/bitstream/handle/10665/44812/9789241503181_eng.pdf?sequence=1&isAllowed=y (2016). [Accessed 25th February 2016].
4. Parvizi, J. *et al.* Periprosthetic Joint Infection - The Economic Impact of Methicillin-Resistant Infections. J. *Arthroplasty.* **25**, 103–107 (2010).
5. Sabat, A. J. *et al.* Overview of molecular typing methods for outbreak detection and epidemiological surveillance. *Eurosurveillance.* **18**, 1–15 (2013).
6. Carek, P. J., Dickerson, L. M. & Sack, J. L. Diagnosis and Management of Osteomyelitis. *Am. Fam. Physician.* **63**, 2413–2420 (2001).
7. Hatzenbuehler, J. & Pulling, T. J. Diagnosis and Management of Osteomyelitis. *Am. Fam. Physician.* **84**, 1027–1033 (2011).
8. Trampuz, A. & Zimmerli, W. Diagnosis and treatment of infections associated with fracture-fixation devices. *Injury.* **37**, 59–66 (2006).
9. van Oosten, M. *et al.* Targeted imaging of bacterial infections: advances, hurdles and hopes. *FEMS Microbiol. Rev.* **39**, 892–916 (2015).
10. Love, C., Tomas, M. B., Tronco, G. G. & Palestro, C. J. FDG PET of infection and inflammation. *Radiographics.* **25**, 1357–1368 (2005).
11. Mills, B., Bradley, M. & Dhaliwal, K. Optical imaging of bacterial infections. *Clin. Transl. Imaging.* **4**, 163–174 (2016).
12. El-Haddad, G., Zhuang, H., Gupta, N. & Alavi, A. Evolving role of positron emission tomography in the management of patients with inflammatory and other benign disorders. *Semin. Nucl. Med.* **34**, 313–329 (2004).
13. Glaudemans, A. W. J. M., Galli, F., Pacilio, M. & Signore, A. Leukocyte and bacteria imaging in prosthetic joint infection. *Eur. Cells Mater.* **25**, 61–77 (2013).
14. Fogarasi, M., Pullman, J., Winnard, P., Hnatowich, D. J. & Rusckowski, M. Pretargeting of bacterial endocarditis in rats with streptavidin and ^{111}In-labeled biotin. *J. Nucl. Med.* **40**, 484–490 (1999).
15. Lazzeri, E. *et al.* Clinical feasibility of two-step streptavidin / ^{111}In-biotin scintigraphy in patients with suspected vertebral osteomyelitis. *Eur. J. Nucl. Med. Mol. Imaging.* **31**, 1505–1511 (2004).
16. Britton, K. E. *et al.* Imaging bacterial infection with ^{99m}Tc-ciprofloxacin (Infecton). *J. Clin. Pathol.* **55**, 817–823 (2002).
17. Sarda, L. *et al.* Inability of ^{99m}Tc-Ciprofloxacin Scintigraphy to Discriminate Between Septic and Sterile Osteoarticular Diseases. *J. Nucl. Med.* **44**, 920–926 (2003).
18. Siaens, R. H., Rennen, H. J., Boerman, O. C., Dierckx, R. & Slegers, G. Synthesis and Comparison of ^{99m}Tc-Enrofloxacin and ^{99m}Tc-Ciprofloxacin. *J. Nucl. Med.* **45**, 2088–2094 (2004).
19. Dumarey, N., Blocklet, D., Appelboom, T., Tant, L. & Schoutens, A. Infecton is not specific for

bacterial osteo-articular infective pathology. *Eur. J. Nucl. Med.* **29**, 530–535 (2002).

20. Langer, O. *et al. In vitro* and *in vivo* evaluation of [^{18}F] ciprofloxacin for the imaging of bacterial infections with PET. *Eur. J. Nucl. Med. Mol. Imaging.* **32**, 143–150 (2005).
21. Hall, A. V., Solanki, K. K., Vinjamuri, S., Britton, K. E. & Das, S. S. Evaluation of the efficacy of ^{99m}Tc-infecton, a novel agent for detecting sites of infection. *J. Clin. Pathol*. **51**, 215–219 (1998).
22. Malamitsi, J. *et al.* Infecton: a ^{99m}Tc-ciprofloxacin radiopharmaceutical for the detection of bone infection. *Clin. Microbiol. Infect.* **9**, 101–109 (2003).
23. Kaul, A. *et al.* Preliminary evaluation of technetium-99m-labeled ceftriaxone: Infection imaging agent for the clinical diagnosis of orthopedic infection. *Int. J. Infect. Dis.* **17**, 263–270 (2013).
24. Fischman, A. J. *et al.* Pharmacokinetics of [^{18}F] fleroxacin in patients with acute exacerbations of chronic bronchitis and complicated urinary tract infection studied by positron emission tomography. *Antimicrob. Agents Chemother.* **40**, 659–664 (1996).
25. Assadi, M. *et al.* Diagnostic value of ^{99m}Tc-ubiquicidin scintigraphy for osteomyelitis and comparisons with ^{99m}Tc-methylene diphosphonate scintigraphy and magnetic resonance imaging. *Nucl. Med. Commun.* **32**, 716–723 (2011).
26. Akhtar, M. S. *et al.* Antimicronial Peptide ^{99m}Tc-Ubiquicidin 29-41 as Human Infection-Imaging Agent: Clinical Trial. *J. Nucl. Med.* **46**, 567–573 (2005).
27. Meléndez-Alafort, L. *et al.* Biokinetics of ^{99m}Tc-UBI 29-41 in humans. *Nucl. Med. Biol.* **31**, 373–379 (2004).
28. Gandomkar, M. *et al.* Clinical evaluation of antimicrobial peptide [^{99m}Tc/Tricine/HYNIC0] ubiquicidin 29-41 as a human-specific infection imaging agent. *Nucl. Med. Biol.* **36**, 199–205 (2009).
29. Ostovar, A. *et al.* A Pooled Analysis of Diagnostic Value of ^{99m}Tc-Ubiquicidin (UBI) Scintigraphy in Detection of an Infectious Process. *Clin. Nucl. Med.* **38**, 808–9 (2013).
30. Diaz, L. A. *et al.* Imaging of musculoskeletal bacterial infections by [^{124}I]FIAU-PET/CT. *PLoS One.* **2**, 1007 (2007).
31. Zhang, X. M. *et al.* [^{124}I] FIAU: Human dosimetry and infection imaging in patients with suspected prosthetic joint infection. *Nucl. Med. Biol.* **43**, 273–279 (2016).
32. Nijhof, M. W. *et al.* Evaluation of Infections of the Locomotor System with Indium-111-Labeled Human IgG Scintigraphy. *J. Nucl. Med.* **38**, 1300–1305 (1997).
33. Buscombe, J. R. *et al*. Indium-111-Labeled Polyclonal Human Immunoglobulin: Identifying Focal Infection in Patients Positive for Human Immunodeficiency Virus. *J. Nucl. Med.* **34**, 1621–1625 (1993).
34. Buscombe, J. R., Oyen, W. J. G., Corstens, F. H. M., Ell, P. J. & Miller, R. F. A comparison of ^{111}In-HIG scintigraphy and chest radiology in the identification of pulmonary infection in patients with HIV infection. *Nucl. Med. Commun.* **16**, 327–335 (1995).
35. Gowrishankar, G. *et al.* Investigation of 6-[^{18}F]-fluoromaltose as a novel PET tracer for imaging bacterial infection. *PLoS One.* ***9***, 6–11 (2014).
36. Weinstein, E. A. *et al.* Imaging *Enterobacteriaceae* infection *in vivo* with ^{18}F-fluorodeoxysorbitol positron emission tomography. *Sci. Transl. Med.* **6**, 1–20 (2014).

37. van Oosten, M. *et al.* Real-time *in vivo* imaging of invasive- and biomaterial-associated bacterial infections using fluorescently labelled vancomycin. *Nat. Commun.* **4**, 2584 (2013).
38. Luo, S., Zhang, E., Su, Y., Cheng, T. & Shi, C. A review of NIR dyes in cancer targeting and imaging. *Biomaterials.* **32**, 7127–7138 (2011).
39. Hellebust, A. & Richards-Kortum, R. Advances in molecular imaging: Targeted optical contrast agents for cancer diagnostics. *Nanomedicine.* **7**, 429–445 (2012).
40. Pleijhuis, R. G. *et al.* Near-infrared fluorescence (NIRF) imaging in breast-conserving surgery: Assessing intraoperative techniques in tissue-simulating breast phantoms. *Eur. J. Surg. Oncol.* **37**, 32–39 (2011).
41. Witjes, J. A. *et al.* Hexaminolevulinate-Guided Fluorescence Cystoscopy in the Diagnosis and Follow-Up of Patients with Non-Muscle-Invasive Bladder Cancer: Review of the Evidence and Recommendations. *Eur. Urol.* **57**, 607–614 (2010).
42. Colditz, M. J. & Jeffree, R. L. Aminolevulinic acid (ALA)-protoporphyrin IX fluorescence guided tumour resection. Part 1: Clinical, radiological and pathological studies. *J. Clin. Neurosci.* **19**, 1471–1474 (2012).
43. Vahrmeijer, A. L., Hutteman, M., van der Vorst, J. R., van de Velde, C. J. H. & Frangioni, J. V. Image-guided cancer surgery using near-infrared fluorescence. *Nat. Rev. Clin. Oncol.* **10**, 507–518 (2013).
44. van Dam, G. M. *et al.* Intraoperative tumor-specific fluorescence imaging in ovarian cancer by folate receptor-α targeting: first in-human results. *Nat. Med.* **17**, 1315–1319 (2011).
45. Ning, X. *et al.* Maltodextrin-based imaging probes detect bacteria *in vivo* with high sensitivity and specificity. *Nat. Mater.* **10**, 602–607 (2011).
46. Panizzi, P. *et al. In vivo* detection of *Staphylococcus aureus* endocarditis by targeting pathogen-specific prothrombin activation. *Nat. Med.* **17**, 1142–1146 (2011).
47. Leevy, W. M. *et al.* Noninvasive Optical Imaging of *Staphylococcus aureus* Bacterial Infection in Living Mice Using a Bis-Dipicolylamine-Zinc(II) Affinity Group Conjugated to a Near-Infrared Fluorophore. *Bioconjug. Chem.* **19**, 686–692 (2008).
48. Thakur, M. L. *et al.* Targeting Apoptosis for Optical Imaging of Infection. *Mol. Imaging Biol.* **14**, 163–171 (2012).
49. Ntziachristos, V. & Razansky, D. Molecular imaging by means of multispectral optoacoustic tomography (MSOT). *Chem. Rev.* **110**, 2783–2794 (2010).
50. Ntziachristos, V. Going deeper than microscopy: the optical imaging frontier in biology. *Nat. Methods.* **7**, 603–614 (2010).
51. Tan, M. *et al.* An Effective Targeted Nanoglobular Manganese(II) Chelate Conjugate for Magnetic Resonance Molecular Imaging of Tumor Extracellular Matrix. *Mol. Pharm.* **7**, 936–943 (2010).
52. Reuveni, T., Motiei, M., Popovtzer, A. & Popovtzer, R. Targeted gold nanoparticles enable molecular CT imaging of cancer: an *in vivo* study. *Int. J. Nanomedicine.* **6**, 2859–2864 (2011).
53. Anastasiadis, P., Mojica, K. D. A., Allen, J. S. & Matter, M. L. Detection and quantification of bacterial biofilms combining high-frequency acoustic microscopy and targeted lipid microparticles. *J. Nanobiotechnology.* **12**, 1–11 (2014).

54. Elias, D. R., Thorek, D. L. J., Chen, A. K., Czupryna, J. & Tsourkas, A. *In vivo* imaging of cancer biomarkers using activatable molecular probes. *Cancer Biomarkers.* **4**, 287–305 (2008).
55. Kong, Y. *et al.* Imaging tuberculosis with endogenous β -lactamase reporter enzyme fluorescence in live mice. *PNAS.* **107**, 12239-12244 (2010).
56. Hernandez, F. J. *et al.* Noninvasive imaging of *Staphylococcus aureus* infections with a nuclease-activated probe. *Nat. Med.* **20**, 301–306 (2014).
57. Lee, S. & Chen, X. Dual-modality probes for *in vivo* molecular imaging. *Mol. Imaging.* **8**, 87–100 (2009).
58. Azhdarinia, A., Ghosh, P., Ghosh, S., Wilganowski, N. & Sevick-Muraca, E. M. Dual-labeling strategies for nuclear and fluorescence molecular imaging: A review and analysis. *Mol. Imaging Biol.* **14**, 261–276 (2012).
59. Welling, M. M. *et al.* Development of a Hybrid Tracer for SPECT and Optical Imaging of Bacterial Infections. *Bioconjug. Chem.* **26**, 839–849 (2015).
60. Rajesh, S., Koshi, E., Philip, K. & Mohan, A. Antimicrobial photodynamic therapy: An overview. *J Indian Soc Periodontol.* **15**, 323–327 (2011).
61. Mitsunaga, M. *et al.* Cancer Cell-Selective *In Vivo* Near Infrared Photoimmunotherapy Targeting Specific Membrane Molecules. *Nat. Med.* **17**, 1685–1691 (2011).
62. Kharkwal, G. B., Sharma, S. K., Huang, Y., Dai, T. & Hamblin, M. R. Photodynamic Therapy for Infections: Clinical Applications. *Lasers Surg. Med.* **43**, 755–767 (2011).
63. Mitsunaga, M. *et al.* Immediate *in vivo* target-specific cancer cell death after near infrared photoimmunotherapy. *BMC Cancer.* **12**, 345 (2012).
64. Ragàs, X. *et al.* Cationic porphycenes as potential photosensitizers for antimicrobial photodynamic therapy. *J Med Chem.* **53**, 7796–7803 (2010).
65. Bhatti, M. *et al.* Antibody-targeted lethal photosensitization of *Porphyromonas gingivalis*. *Antimicrob. Agents Chemother.* **44**, 2615–2618 (2000).
66. Demidova, T. N. & Hamblin, M. R. Photodynamic therapy targeted to pathogens. *Int. J. Immunopathol. Pharmacol.* **17**, 245–254 (2004).
67. Dosselli, R. *et al.* Synthesis, characterization, and photoinduced antibacterial activity of porphyrin-type photosensitizers conjugated to the antimicrobial peptide apidaecin 1b. *J. Med. Chem.* **56**, 1052–1063 (2013).
68. Suci, P., Kang, S., Gmür, R., Douglas, T. & Young, M. Targeted delivery of a photosensitizer to *Aggregatibacter actinomycetemcomitans* biofilm. *Antimicrob. Agents Chemother.* **54**, 2489–2496 (2010).
69. Murdoch, D. R. *et al.* Clinical Presentation, Etiology and Outcome of Infective Endocarditis in the 21st Century: The International Collaboration on Endocarditis-Prospective Cohort Study. *Arch. Intern. Med.* **169**, 463–473 (2013).
70. Li, J. S. *et al.* Proposed Modifications to the Duke Criteria for the Diagnosis of Infective Endocarditis. *Clin. Infect. Dis.* **30**, 633–638 (2000).
71. Habets, J. *et al.* Cardiac computed tomography angiography results in diagnostic and therapeutic change in prosthetic heart valve endocarditis. *Int. J. Cardiovasc. Imaging.* **30**,

377–387 (2014).

72. Habib, G. *et al.* 2015 ESC Guidelines for the management of infective endocarditis. *European Heart Journal.* **36**, 3075-3123 (2015).
73. Gomes, A. *et al.* Diagnostic value of imaging in infective endocarditis: a systematic review. *Lancet Infect. Dis.* **17**, 1–14 (2017).
74. Pizzi, M. N. *et al*. Improving the Diagnosis of Infective Endocarditis in Prosthetic Valves and Intracardiac Devices With ^{18}F-Fluordeoxyglucose Positron Emission Tomography / Computed Tomography Angiography. *Circulation.* **132**, 1113–1126 (2015).
75. Rouzet, F. *et al.* Respective Performance of ^{18}F-FDG PET and Radiolabeled Leukocyte Scintigraphy for the Diagnosis of Prosthetic Valve Endocarditis. *J. Nucl. Med.* **55**, 1980–1985 (2014).
76. Fukuchi, K. *et al.* Detection of aortic graft infection by fluorodeoxyglucose positron emission tomography: Comparison with computed tomographic findings. *J. Vasc. Surg.* **42**, 919–925 (2005).
77. Keidar, Z., Pirmisashvili, N., Leiderman, M., Nitecki, S. & Israel, O. ^{18}F-FDG uptake in noninfected prosthetic vascular grafts: Incidence, patterns, and changes over time. *J. Nucl. Med.* **55**, 392–395 (2014).
78. Bruggink, J. L. M., Slart, R. H. J. A., Pol, J. A., Reijnen, M. M. P. J. & Zeebregts, C. J. Current role of imaging in diagnosing aortic graft infections. *Semin. Vasc. Surg.* **24**, 182–190 (2011).
79. Erba, P. A. *et al.* Radiolabelled leucocyte scintigraphy versus conventional radiological imaging for the management of late, low-grade vascular prosthesis infections. *Eur. J. Nucl. Med. Mol. Imaging.* **41**, 357–368 (2014).
80. Iovino, F., Seinen, J., Henriques-Normark, B. & van Dijl, J. M. How Does *Streptococcus pneumoniae* Invade the Brain? *Trends Microbiol.* **24**, 307–315 (2016).
81. Nensa, F., Beiderwellen, K., Heusch, P. & Wetter, A. Clinical applications of PET/MRI: current status and future perspectives. *Diagnostic Interv. Radiol.* **20**, 438–447 (2014).
82. Yang, Z. L. & Zhang, L. J. PET/MRI of central nervous system: current status and future perspective. *Eur. Radiol.* **26**, 3534–3541 (2016).
83. Beyer, T., Freudenberg, L. S., Czernin, J. & Townsend, D. W. The future of hybrid imaging - part 3: PET/MR, small-animal imaging and beyond. *Insights Imaging.* **2**, 235–246 (2011).
84. Terwisscha van Scheltinga, A. G. T. *et al.* Intraoperative near-infrared fluorescence tumor imaging with vascular endothelial growth factor and human epidermal growth factor receptor 2 targeting antibodies. *J. Nucl. Med.* **52**, 1778–1785 (2011).
85. Fàbregas, N. *et al.* Clinical diagnosis of ventilator associated pneumonia revisited: Comparative validation using immediate *post-mortem* lung biopsies. *Thorax.* **54**, 867–873 (1999).
86. Chastre, J. & Fagon, J.Y. State of the Art Ventilator-associated Pneumonia. *Am J Respir Crit Care Med.* **165**, 867–903 (2002).

Chapter 3

In vitro imaging of bacteria using ^{18}F-fluorodeoxyglucose micro positron emission tomography

Marjolein Heuker, Jürgen W.A. Sijbesma, Rocío Aguilar Suárez, Johan R. de Jong, Hendrikus H. Boersma, Gert Luurtsema, Philip H. Elsinga, Andor W.J.M. Glaudemans, Gooitzen M. van Dam, Jan Maarten van Dijl, Riemer H.J.A. Slart and Marleen van Oosten

Scientific Reports (2017) 4:253-264

Abstract

Positron emission tomography (PET) with fluorine-18-fluorodeoxyglucose (^{18}F-FDG) can be applied to detect infection and inflammation. However, it was so far not known to what extent bacterial pathogens may contribute to the PET signal. Therefore, we investigated whether clinical isolates of frequently encountered bacterial pathogens take up ^{18}F-FDG *in vitro*, and whether FDG inhibits bacterial growth as previously shown for 2-deoxy-glucose. 22 isolates of Gram-positive and Gram-negative bacterial pathogens implicated in fever and inflammation were incubated with ^{18}F-FDG and uptake of ^{18}F-FDG was assessed by gamma-counting and µPET imaging. Possible growth inhibition by FDG was assayed with *Staphylococcus aureus* and the Gram-positive model bacterium *Bacillus subtilis*. The results show that all tested isolates accumulated ^{18}F-FDG actively. Further, ^{18}F-FDG uptake was hampered in *B. subtilis pts* mutants impaired in glucose uptake. FDG inhibited growth of *S. aureus* and *B. subtilis* only to minor extents, and this effect was abrogated by *pts* mutations in *B. subtilis*. These observations imply that bacteria may contribute to the signals observed in FDG-PET infection imaging *in vivo*. Active bacterial FDG uptake is corroborated by the fact that the *B. subtilis* phosphotransferase system is needed for ^{18}F-FDG uptake, while *pts* mutations protect against growth inhibition by FDG.

Keywords: *^{18}F-FDG; PET; imaging; infection; bacteria*

Introduction

Bacterial infections represent a major problem in hospital and community settings worldwide. In particular, due to increasingly ageing populations, higher rates of organ transplantations and expanding possibilities for chemotherapy, the numbers of immune-compromised patients who are at risk of bacterial infections are steadily increasing. Moreover, this problem is exacerbated by increased use of implanted biomaterials and medical devices, which are particularly susceptible to bacterial contaminations and infection.[1] Another major contributor to the problem of bacterial infections is the rapid increase of resistance to multiple antibiotics.[2] Infections caused by such multidrug-resistant microbes are difficult to treat and responsible for substantial patient morbidity and mortality.[2,3]

The diagnosis of bacterial infections is nowadays mainly based on a combination of several specific and/or non-specific symptoms, systemic inflammation markers and the detection of pathogens by culturing, mass spectrometry, polymerase chain reaction (PCR) or serology. In the ideal situation, the causative agent is identified by culturing, but this takes time and is often challenging since sites of infection may be poorly accessible. Also, there is always a risk of contaminations by other bacteria not related to the actual infection resulting in false-positive culture outcomes. Since these challenges often lead to blind management of bacterial infections, there is an urgent need for diagnostic tools that allow real-time detection of infecting bacteria in the patient, for example by infection imaging.[1,4,5]

Although several promising approaches for the direct imaging of infecting bacteria have been proposed and explored, with the exception of ^{99m}Technetium-ciprofloxacin (^{99m}Tc-ciprofloxacin Infecton®),[6] there are currently no bacteria-specific imaging approaches in clinical use.[1,4] A clinically applied alternative is positron emission tomography (PET) with fluorine-18-fluorodeoxyglucose (^{18}F-FDG), which can serve as a diagnostic tool for localising infections, inflammatory conditions and unknown origins of fever.[7,8] In this case, it is generally believed that the infection-specific signal originates from increased glucose uptake by cells involved in the inflammatory process, such as leukocytes, monocytes, lymphocytes, giant cells and macrophages.[9] Importantly, ^{18}F-FDG-PET is safe, sensitive, easy and rapid to use,[3,10–12] and it is potentially applicable in the monitoring of treatment.[13] Furthermore, the view that ^{18}F-FDG-PET imaging enables the visualisation of bacterial infections and evaluation of antimicrobial therapy has been confirmed in animal experiments and clinical studies.[14–18] On the other hand, diagnosing infections with ^{18}F-FDG-PET still remains challenging due to the fact that, for instance, malignancies, sterile inflammation and physiological wound healing, may result in similarly high levels of ^{18}F-FDG uptake as infections.[9,15–17]

An intriguing question that has, so far, received little attention is whether infecting bacteria could potentially contribute to the signal derived in ^{18}F-FDG-PET imaging. Specifically, it was not known whether different bacteria can accumulate ^{18}F-FDG, and whether the uptake of FDG is potentially toxic for bacteria as is known to be the case for the structurally related glucose analogue 2-deoxy-

glucose (2-DG).[19] The aims of this study were, therefore, to determine whether clinical isolates of different bacterial pathogens actively take up ^{18}F-FDG *in vitro*, and whether this may lead to impaired bacterial growth.

Material and methods

Bacteria

Clinical isolates of different bacterial pathogens were collected from the diagnostic laboratory of the Department of Medical Microbiology at the University Medical Center Groningen (UMCG; July-November 2015, 15 isolates derived from 15 different patients, **Table 1**). Identification of these bacterial isolates was performed using matrix-assisted laser desorption/ionization time-of-flight (MALDI-TOF) mass spectrometry (Brüker, Daltonik GmbH, Leipzig, Germany).[20] 7 bacterial strains from the American Type Culture Collection (ATCC) were also included in the analyses (**Table 1**). These different bacteria were chosen to cover the most commonly encountered bacterial pathogens at the UMCG. Bacteria were cultured on blood agar plates (5% sheep blood, Mediaproducts, Groningen, The Netherlands) for 1-3 days at 37°C.

^{18}F-FDG uptake studies

For ^{18}F-FDG uptake studies, *Streptococcus pneumoniae*, *Enterococcus faecalis* and *Enterococcus faecium* were cultured in Brain-Heart Infusion (BHI), while all other bacteria were cultured in Tryptic Soy Broth (TSB). All bacteria were grown overnight at 37°C under constant agitation (250 RPM), with the exception of *S. pneumoniae* which was grown in standing culture at 5% CO_2. The next day, fresh cultures were prepared by dilution of overnight cultures in 9 mL TSB or BHI, and growth was continued up to an optical density (OD) of 1-5 McFarland units. Heat-killed *Staphylococcus aureus* and *Escherichia coli* were obtained by incubating the respective cultures for 30 min at 99°C. To assess ^{18}F-FDG uptake, the bacterial cultures were incubated with 5-10 megabecquerel (MBq) ^{18}F-FDG dissolved in 0.5 mL NaCl (0.9%) at 37°C for 5 min. Subsequently, 2 mL samples were washed twice by centrifugation and resuspension of the bacterial pellets in phosphate buffered saline (PBS). To image ^{18}F-FDG uptake, the bacteria were pelleted by centrifugation, and four Eppendorf tubes containing bacterial pellets were positioned at the centre of the ring system of a micro-PET (μPET) Focus 220 scanner (Siemens Medical Solutions, TN, US) with the bacterial pellets in the field of view. Images were recorded in 30 min and analysed with the AMIDE software package (Amide's a Medical Imaging Data Examiner). To quantify ^{18}F-FDG uptake, the bacterial pellets were placed in a calibrated gamma-counter (CompuGamma CS1282, LKB-Wallac, Turku, Finland). The radioactivity in each sample was measured, corrected for background and converted into kilobecquerel (kBq). Each ^{18}F-FDG uptake experiment was performed thrice and all quantifications were executed in quadruple with two different clinical isolates per tested bacterial species. Numbers of colony

forming units (CFUs) in different samples were determined in duplicate by resuspension of the bacterial pellets, serial dilution of the resuspended bacteria, and plating on blood agar containing 5% sheep blood. Only in case of *Proteus mirabilis*, MacConkey agar no.3 plates containing crystal violet were used (Mediaproducts, Groningen, The Netherlands). CFUs of bacteria not incubated with ^{18}F-FDG were determined as a control to evaluate the effect of ^{18}F-FDG on bacterial survival.

Table 1. Bacterial strains for ^{18}F-FDG uptake experiments

Strain	Origin or American Type Culture Collection strain number	Date of isolation at UMCG
Citrobacter freundii	clinical isolate clinical isolate	July 2015 November 2015
Enterococcus faecalis	ATCC 29212 clinical isolate	- November 2015
Enterococcus faecium	clinical isolate clinical isolate	July 2015 November 2015
Escherichia coli	ATCC 25922 clinical isolate	- October 2015
Klebsiella pneumoniae	ATCC 700721 clinical isolate	- November 2015
Proteus mirabilis	ATCC 12453 clinical isolate	- October 2015
Pseudomonas aeruginosa	ATCC 27853 clinical isolate	- October 2015
Staphylococcus aureus	clinical isolate clinical isolate	July 2015 October 2015
Staphylococcus epidermidis	ATCC 12228 clinical isolate	- November 2015
Streptococcus pneumoniae	ATCC 49619 clinical isolate	- November 2015
Streptococcus pyogenes	clinical isolate clinical isolate	October 2015 November 2015

Time course analysis of ^{18}F-FDG uptake

Clinical isolates of *S. aureus* and *E. coli* were grown overnight in TSB as indicated above, and the *Bacillus subtilis* type strain 168 (**Table 2**) was grown overnight in Lysogeny Broth (LB) at 37°C under constant agitation (250 RPM). The next day, the bacteria were diluted 1:20 in 12 mL of the respective growth media and grown for ~2.5 h up to an OD of ~2 McFarland (37°C, 250 RPM). Subsequently,

5-7 MBq ^{18}F-FDG (dissolved in 0.5 mL of 0.9% NaCl) was added to the bacterial cultures. Cultures were incubated at 37°C after the addition of ^{18}F-FDG and culture aliquots of 2 mL were withdrawn at 0, 15, 30, 45 and 60 min. To stop ^{18}F-FDG uptake, each culture aliquot was washed twice by centrifugation and resuspension of the bacterial pellets in PBS. Lastly, the bacteria were pelleted by centrifugation and ^{18}F-FDG uptake in the pellets was measured with a calibrated CompuGamma CS1282 gamma-counter. CFUs were determined at t=0, t=30 and t=60 min by resuspension of the pellets, serial dilution and plating on blood agar as described above. Heat-killed *S. aureus* and *E. coli* (30 min, 99°C) served as negative controls. Uptake of ^{18}F-FDG over time was evaluated in duplicate.

Table 2. Laboratory strains used for growth in the presence of FDG

Strain	Genotype	Reference
S. aureus HG001	*rsbU* repaired, *tcaR*	(33)
B. subtilis 168	*trpC2*	Laboratory Collection
B. subtilis QB5435	*trpC2*, *ptsG*::cat, Cm^R	(34)
B. subtilis GP864	*trpC2 ptsI*::Em^R	(35)

Cm^R, Chloramphenicol resistant; Em^R, Erythromycin resistant.

Growth of *S. aureus* and *B. subtilis* in the presence of non-labelled FDG

To assess the toxicity of FDG, the laboratory strain *S. aureus* HG001 and different *B. subtilis* strains (**Table 2**) were grown overnight in TSB or LB, respectively. Where appropriate the media were supplemented with chloramphenicol or erythromycin at a concentration of 5 µg/mL. The overnight cultures were, in triplicate, diluted 1:50 in 100 µL fresh TSB or LB in 96-well microtiter plates, and the plates were incubated for 3 h at 37°C with vigorous agitation (800 RPM). Lastly, each culture was again diluted 1:50 in 100 µL of the respective growth medium supplemented with 2 µg/mL, 20 µg/mL, 200 µg/mL or 2 mg/mL non-radioactive FDG, or without FDG. Cultures were incubated at 37°C in a Biotek synergy 2 plate reader with shaking and the OD at 600 nm (OD600) was recorded at 10 min intervals. Each growth experiment was performed at least twice.

Statistical analyses

Kruskal Wallis and Mann-Whitney U tests were performed using IBM SPSS Statistics 23. P-values of 0.05 or less were considered significant.

Results

In vitro uptake of ^{18}F-FDG

To evaluate whether bacterial pathogens are capable of active uptake of ^{18}F-FDG, a range of different Gram-positive and Gram-negative bacteria including mostly clinical isolates were incubated with ^{18}F-FDG, and uptake was determined with a calibrated gamma-counter. The ^{18}F-FDG PET signals were quantified and the absorbed activity per CFU was determined as shown in **Figure 1** (**A** and **B**). All bacterial isolates showed significant ^{18}F-FDG uptake. No major differences were observed for most of the investigated Gram-positive and Gram-negative bacteria (p=0.60; not shown). Nonetheless, statistically significant differences in ^{18}F-FDG uptake were observed for different bacterial species (p<0.01) as illustrated in **Figure 1**. The Gram-positive bacterium *Streptococcus pyogenes* displayed overall the highest uptake activity per 10^7 CFUs (**Figure 1A** and **B**). *E. coli* and *Citrobacter freundii* showed the highest ^{18}F-FDG uptake amongst the tested Gram-negative species (**Figure 1B**). In contrast, *S. pneumoniae*, *E. faecium* and *P. mirabilis* showed relatively low ^{18}F-FDG uptake, but as shown for *S. pneumoniae* the ^{18}F-FDG uptake was still significantly higher than the negative controls (p=0.01; **Figure 1C**). Importantly, other living bacteria, such as *S. aureus* and *E. coli* accumulated significantly higher ^{18}F-FDG levels than the respective heat-killed bacteria, bacteria incubated in the absence of ^{18}F-FDG, or medium controls (p=0.004).

To evaluate whether bacterial ^{18}F-FDG uptake can also be detected by µPET imaging, the ^{18}F-FDG uptake by several Gram-negative and Gram-positive clinical isolates was qualitatively assessed with a µPET Focus 220 scanner. Indeed, the resulting µPET images clearly show ^{18}F-FDG uptake by the tested bacteria (**Figure 2**). *S. pneumoniae* showed the least uptake activity, which might relate to the high autolytic activity of this bacterium.[21] As expected, little if any ^{18}F-FDG uptake was detectable for heat-killed *S. aureus* and *E. coli*, as was the case for non-incubated bacteria and medium controls. Notably, there were some apparent differences in the relative signals observed in **Figures 1** and **2** for, respectively, the *E. faecium* and *E. faecalis* samples, and for the *S. aureus* and *S. epidermidis* samples. This may relate to the fact that the counting with the calibrated gamma-counter as in **Figure 1** provides quantitative data on ^{18}F-FDG uptake, whereas the µPET scans as in **Figure 2** give semi-quantitative information on ^{18}F-FDG uptake. For example, there may have been some variation in the distribution of the pelleted bacteria in the samples that were imaged by µPET scans. Furthermore, the observed variations may have been due, to some extent, to differing numbers of metabolically active bacteria in the samples respectively used for **Figures 1** and **2**.

To approximate the time needed for uptake of ^{18}F-FDG, time course experiments were performed with *S. aureus* and *E. coli*, two bacterial species showing significant differences in ^{18}F-FDG uptake (**Figure 1**). The results presented in **Figure 3** show indeed significant differences in the rates of uptake by both species, *E. coli* reaching saturation almost instantaneously while ^{18}F-FDG uptake by *S. aureus* was relatively slow. Within 60 min of incubation, *E. coli* absorbed significantly more

^{18}F-FDG than the *S. aureus* ($p<0.001$), while *E. coli* and *S. aureus* both showed higher signals than the respective heat-killed controls ($p<0.01$).

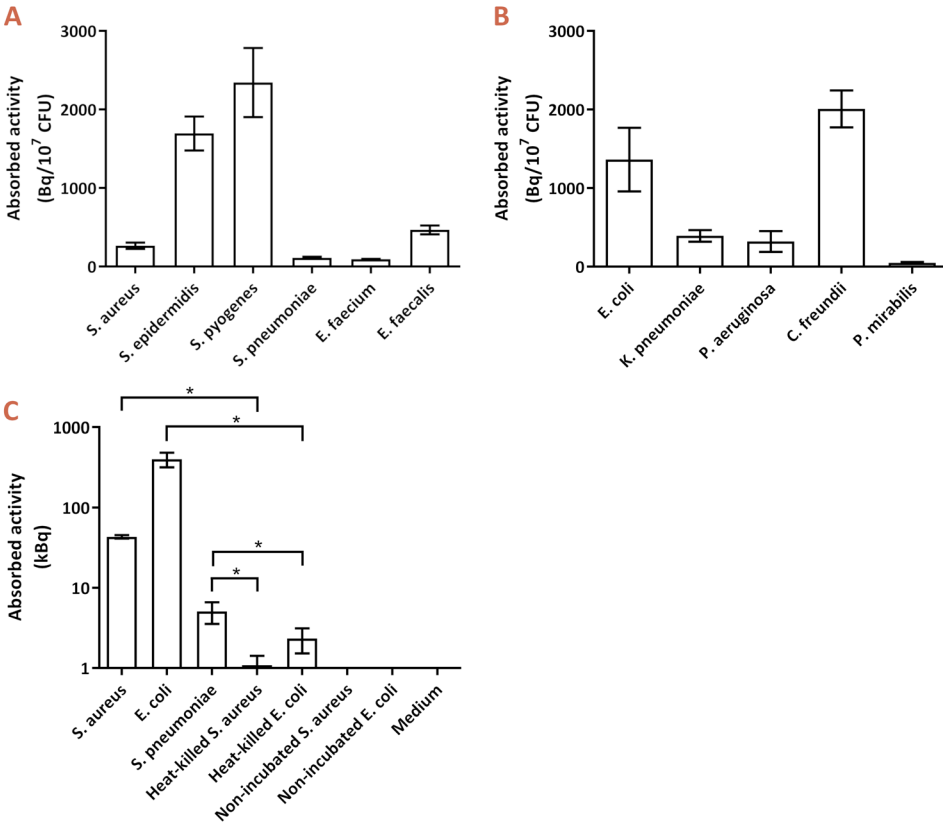

Figure 1. *In vitro* uptake of ^{18}F-FDG by different bacteria. The mean uptake of ^{18}F-FDG by clinical isolates of different Gram-positive (**A**) and Gram-negative (**B**) bacteria was expressed as absorbed activity in Bq/10^7 CFUs. (**C**) Total uptake in kBq of ^{18}F-FDG by *S. aureus*, *E. coli* or *S. pneumoniae* in comparison to heat-killed bacteria, bacteria not incubated with ^{18}F-FDG, and medium controls. The indicated standard deviations include the variations introduced by the use of at least two different isolated per tested species. Note that the detection limit for bacterial species will lie between the non-specifically absorbed activity measured for heat-killed bacteria, such as *E. coli* and *S. aureus*, and the lowest level of ^{18}F-FDG uptake by the living bacteria, such as *S. pneumoniae*. This implies that under the tested conditions, the detection limit is ~2.4 kBq. * $p\leq0.01$. Values represent mean ± SEM (n=8).

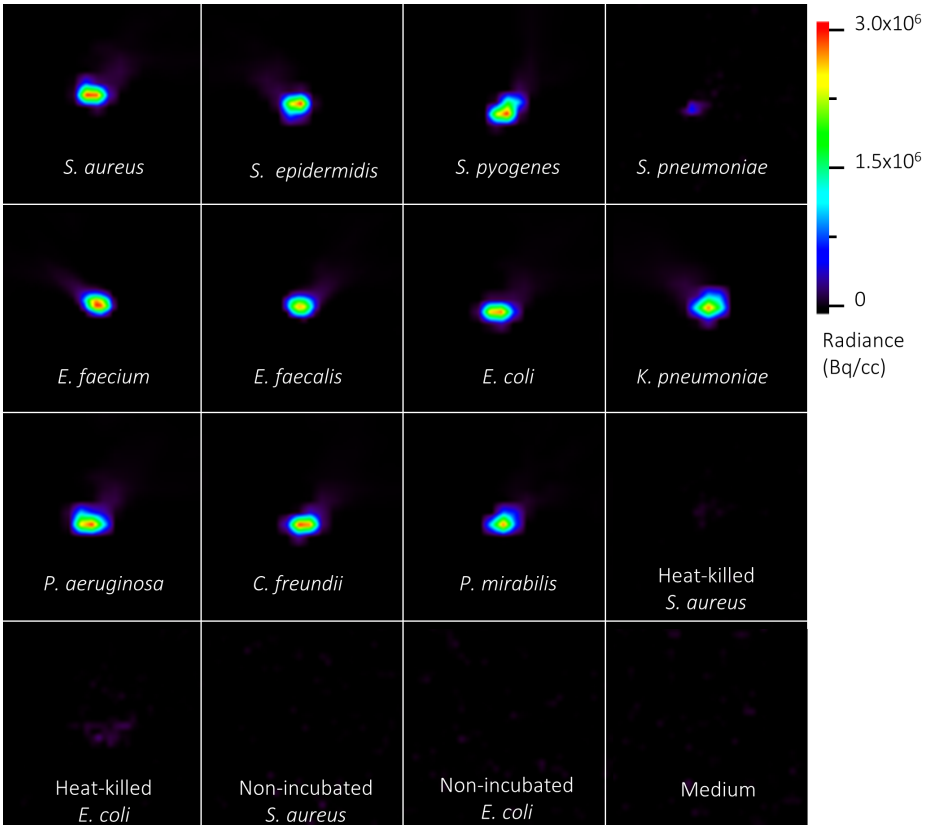

Figure 2. µPET images of ^{18}F-FDG uptake by bacterial isolates. Different clinical bacterial isolates were grown to an OD of 1-5 McFarland units in 9 mL of growth medium, pelleted and resuspended in the same volume at 15 min before the incubation with 0.5 mL of 5-10 MBq ^{18}F-FDG for 5 min. Heat-killed *S. aureus* or *E. coli* were obtained by incubating the respective cultures for 30 min at 99°C. As negative controls, *S. aureus* or *E. coli* cells incubated without added ^{18}F-FDG, or with fresh medium were used. All samples were washed twice in PBS and washed bacterial pellets corresponding to 2 mL culture samples were imaged for 30 min with a µPET scanner for a qualitative evaluation of the bacterial ^{18}F-FDG uptake. The scale bar indicates the colour map range of Radiance in Bq per cubic centimetre (cc).

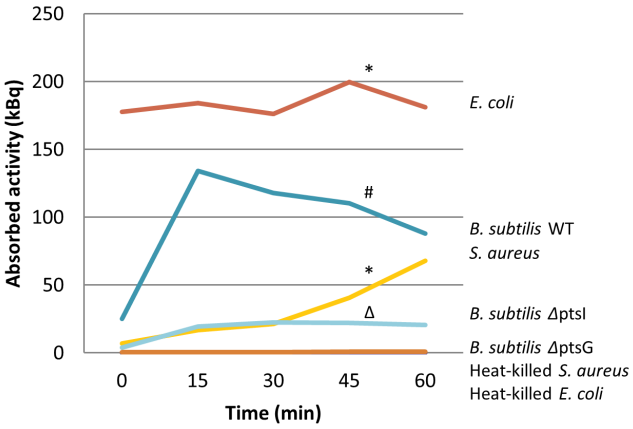

Figure 3. Time course analysis of *in vitro* uptake of ^{18}F-FDG. Mean ^{18}F-FDG uptake was determined over a period of 60 min for clinical isolates of *S. aureus* (yellow) and *E. coli* (red), and for the *B. subtilis* type strain 168 (dark blue) and its *ptsG* (orange) or *ptsI* mutant (light blue) derivatives. Heat-killed bacteria (orange) served as negative controls. Samples were withdrawn at the indicated time points to assess the ^{18}F-FDG uptake. * p<0.01 vs. heat-killed controls; # p<0.001 vs. both mutants; Δ p<0.001 vs. the *ΔptsG* mutant.

Potential mechanism of ^{18}F-FDG uptake

In order to assess the possible mechanism of ^{18}F-FDG uptake, we applied the Gram-positive model bacterium *B. subtilis* for which mutations in the phosphotransferase system (PTS) that facilitates glucose uptake are available.[22] Indeed, *B. subtilis ptsI* and *ptsG* deletion strains displayed a strongly impaired uptake of ^{18}F-FDG compared to the parental wild-type strain *B. subtilis* 168 (p<0.001; **Figure 3**). Of note, the *ptsI* deletion mutant showed a somewhat higher uptake than the *ptsG* deletion mutant (p=<0.001), which is in line with the fact that PtsG is the major glucose transporter,[23] while PtsI is involved in the phosphorylation of internalised glucose making its uptake by PtsG irreversible.[24] These findings show that, at least in *B. subtilis*, ^{18}F-FDG is taken up via the PTS system.

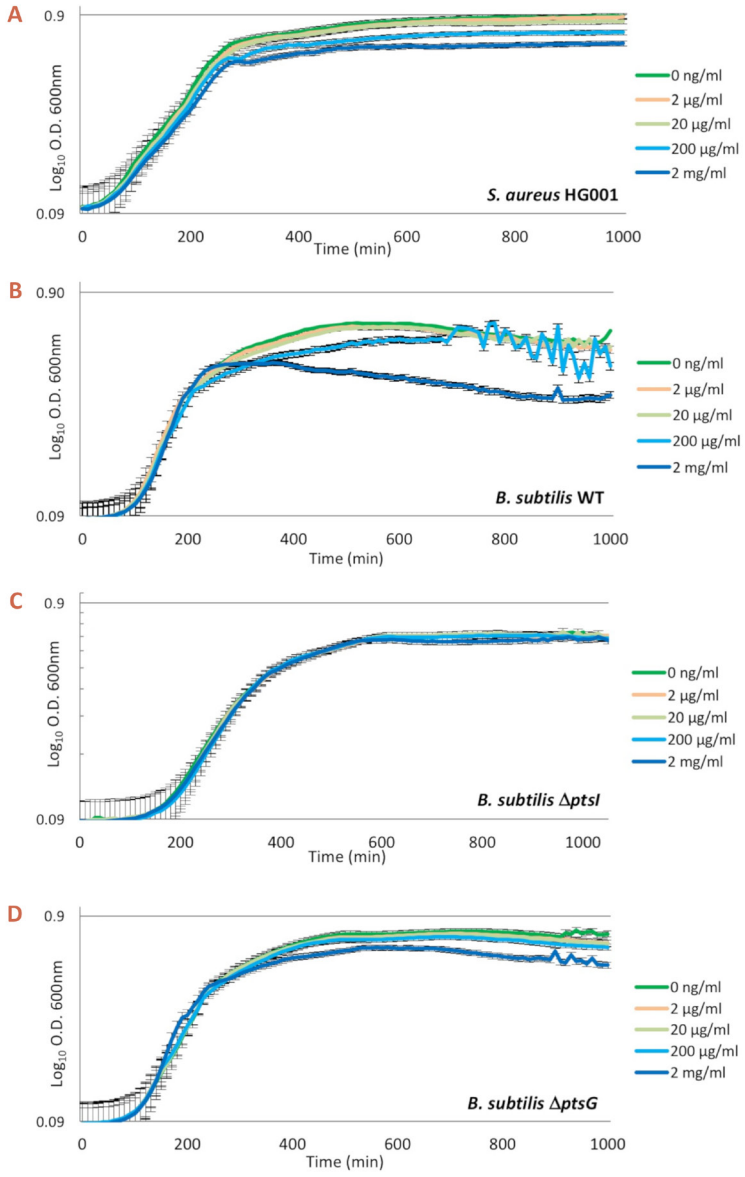

Figure 4. Growth of *S. aureus* and *B. subtilis* in the presence of non-labeled FDG. *S. aureus* HG001 was grown in TSB (**A**), and the *B. subtilis* strains 168 (WT), *ΔptsI* and *ΔptsG* were grown in LB (**B**, **C** and **D**) with increasing concentrations of non-radiolabelled FDG as indicated in colour code. OD600 readings were recorded every 10 min.

FDG-impaired bacterial growth

To test whether FDG could be toxic for bacteria growth experiments were performed with *S. aureus* HG001 and *B. subtilis* 168, where the growth media were supplemented with increasing concentrations of FDG up to 2 mg/mL. As shown in **Figure 4A**, *S. aureus* HG001 reached somewhat lowered OD600 values in the stationary phase when the medium contained 200 µg/mL FDG or more. Similarly, *B. subtilis* reached a lowered optical density in the stationary phase when cultured in the presence of 2 mg/mL FDG (**Figure 4B**). This indicates that FDG is mildly toxic for bacteria, such as *S. aureus* and *B. subtilis*, at high concentrations. To verify this, the *B. subtilis ptsI* and *ptsG* deletion mutants were also cultured in the presence of FDG. The results show that both mutations significantly diminished the growth impairment caused by 2 mg/mL FDG (**Figure 4**, **C** and **D**). Together, these findings show that active FDG uptake may be toxic for bacteria, but only at very high concentrations that will not be reached during ^{18}F-FDG-PET imaging *in vivo*.

Discussion

The current study shows for the first time that clinical isolates of many major Gram-positive and Gram-negative bacterial pathogens can actively take up ^{18}F-FDG. This is consistent with the previous finding of Weinstein *et al.*,[25] who reported that type strains of *E. coli*, *Klebsiella pneumoniae* and *S. aureus* can take up this compound. The combined findings imply that bacterial pathogens may contribute to the signal observed in ^{18}F-FDG-PET imaging of bacterial infections. Furthermore, the observed ^{18}F-FDG uptake was, at least in *B. subtilis*, shown to be facilitated by the PTS system for glucose uptake. Lastly, our present observations show that FDG may be toxic for bacteria but only at very high doses that exceed the physiological levels during ^{18}F-FDG PET imaging about 100- to 1000-fold.

Notably, of all presently tested bacterial species, *S. pyogenes* displayed the highest uptake of ^{18}F-FDG. This bacterium is notorious for causing necrotizing fasciitis, a rapidly progressive infection of deep layers of the skin and subcutaneous tissues, which requires immediate antibiotic therapy and aggressive surgery.[26] The high uptake levels of ^{18}F-FDG suggest that *S. pyogenes* may have been the metabolically most active bacterium under the tested conditions. All other bacteria showed lower ^{18}F-FDG uptake *in vitro*. In view of the fulminant pathology of invasive *S. pyogenes* infections, it is conceivable that this bacterium displays also a high metabolic activity *in vivo*.

In line with the finding that ^{18}F-FDG is actively taken up by the investigated bacteria, the absence of the glucose transporter PtsG abrogated FDG uptake by *B. subtilis*. The absence of PtsI, also known as Enzyme I of the PTS system,[22] had a strong but less drastic negative effect on ^{18}F-FDG uptake suggesting that its contribution to FDG uptake can to some extent be bypassed. Further, our present results show that FDG is toxic for *S. aureus* and *B. subtilis*, but only at high concentrations that are not reached during ^{18}F-FDG PET imaging *in vivo*. Yet, the observed toxicity of FDG is reminiscent of the

toxic effects of 2-DG. In the latter case, the PTS system recognises 2-DG and phosphorylates it into 2-DG-6-phosphate, which is subsequently dephosphorylated by hexose-6-phosphatase. This cycle of 2-DG phosphorylation and de-phosphorylation depletes the bacterial cell of phosphoenolpyruvate and eventually adenosine triphosphate (ATP).[27] Thus, 2-DG has the ability to de-energize bacteria. This may also be the case for FDG, which would explain the observed growth inhibition at high FDG concentrations. Of note, the growth of *B. subtilis ptsG* or *ptsI* deletion mutants was much less affected by FDG than growth of the parental strain, which is consistent with the reduced uptake of ^{18}F-FDG.

Currently, there is ample evidence that ^{18}F-FDG-PET is a very useful diagnostic tool for many infectious indications, including fever of unknown origin, endocarditis, spondylodiscitis, and vascular graft infections.[8,11,12] This approach can help in defining the location and extent of infection, thereby providing guidance for biopsy and for therapy follow-up. In general, the detection limit in the imaging of infections by PET will depend on the sensitivity and resolution of the PET camera, on the volume of bacterial lesion, on the surrounding tissue, and on the target-to-normal tissue (T/N) ratios of radioactivity at sites of infection. Our present study shows that ^{18}F-FDG uptake by infecting bacteria potentially contributes to the overall signal detected by PET imaging of bacterial infections. However, it remains difficult to approximate the contribution of the bacterial ^{18}F-FDG uptake to the total ^{18}F-FDG uptake signal measured during *in vivo* PET imaging of an infection, because the bacterial contribution to the signal will vary depending on the bacterial species that causes the infection, on the metabolic state of the infecting bacteria, and the total number of infecting bacteria. Moreover, the inflammatory status of the infected tissue will impact on the total signal, especially since white blood cell migration may vary depending on the extent of inflammation, and also because inflammation may lead to increased blood flow and vascular permeability. Furthermore, the total signal is likely to depend on the particular body site that is infected. Altogether, this means that, in practice, the relative bacterial contribution to the total ^{18}F-FDG signal will be different for individual patients and for different types of infections. For example, chronic infections can be visualised with ^{18}F-FDG, but the signal contributed by the bacteria themselves may be lower than in acute infections if their metabolic activity is lower, which would result in lower uptake of ^{18}F-FDG. In such cases, an option to improve the bacterial signal could be to start imaging at later time points after tracer injection. Clearly, the conditions *in vivo* are likely to be different compared to the conditions applied in our *in vitro* study. It is therefore presently not possible to make reliable calculations of the detection limit for infections *in vivo*.

Lastly, with ^{18}F-FDG PET it is not possible to differentiate between sterile inflammation and infection. Also, ^{18}F-FDG PET will neither tell us whether bacteria are involved in an infection, nor which bacteria are involved. Specific bacteria-targeted PET tracers are therefore desirable. For example, these could include labelled antibiotics like ^{18}F- or ^{99m}Tc-ciprofloxacin (Infecton®).[6,28–31] A very promising alternative for ^{18}F-FDG may be 2-[^{18}F]-fluorodeoxysorbitol (^{18}F-FDS), since sorbitol is a sugar alcohol that is mainly metabolized by the Gram-negative *Enterobacteriaceae*.[5,25] Another

attractive approach appears to be the detection of bacteria with 6-[^{18}F]-fluoromaltose (^{18}F-FM),[32] because maltose and maltodextrins are metabolizable by all classes of bacteria, in contrast to mammalian cells. Thus, ^{18}F-FM may allow the distinction between bacterial infection and other causes of inflammation. On this basis it is well conceivable that the combined use of ^{18}F-FDS and ^{18}F-FM will facilitate the detection of a wide spectrum of bacteria causing infections. With the aid of both substrates, it should not only be possible to specifically image infecting bacteria over mammalian cells, but also to discriminate infecting Gram-positive and Gram-negative bacteria. The latter would then guide effective antimicrobial therapy. Yet, despite these evident advantages, no clinical studies on infection imaging with ^{18}F-FDS and ^{18}F-FM have thus far been reported.

Conclusion

To date, ^{18}F-FDG is one of the few tracers that may be clinically applied in infection imaging. We now show that this tracer can be taken up by a wide range of commonly encountered bacterial pathogens. We therefore hypothesize that bacterial pathogens may also take up ^{18}F-FDG *in vivo*, thereby contributing to the FDG-PET signal observed in infection imaging. Future experiments are needed to determine the proportion of ^{18}F-FDG that is taken up by infecting bacteria as compared to the ^{18}F-FDG taken up by inflammatory cells. This will unveil the significance of our present findings in the clinical context.

Acknowledgements

We thank Lisanne Braams and Janine Doorduin for technical assistance during the experiments, and Jörg Stülke for providing the *B. subtilis ptsG* and *ptsI* deletion mutants.

Funding statement

RAS was supported by a fellowship from Conacyt. JMvD acknowledges funding from the European Commission, the University of Groningen and the University Medical Center Groningen in the context of the H2020-MSCA-COFUND-2015 Grant Agreements 713482 and 713660. The funders had no role in study design, data collection and analysis, decision to publish, or preparation of the manuscript.

Transparency declarations

The authors declare no conflicts of interest.

Author contributions

MH, JWAS, RAS, AWJMG, GMvD, JMvD, RHJAS, and MvO conceived and designed the experiments. MH, JWAS, and RAS performed the experiments. MH, RAS, JRdJ, JMvD, and MvO analysed the data. HHB, GL, PHE, AWJMG, JMvD, and RHJAS contributed reagents, materials and analysis tools. MH, RAS, HHB, AWJMG, GMvD, JMvD, RHJAS, and MvO wrote the manuscript. All authors have reviewed and approved the final manuscript.

References

1. van Oosten, M. *et al.* Targeted imaging of bacterial infections: advances, hurdles and hopes. *FEMS Microbiol. Rev.* **39**, 892–916 (2015).
2. Laxminarayan, R. *et al.* Antibiotic resistance - the need for global solutions. *Lancet Infect. Dis.* **13**, 1057–1098 (2013).
3. Love, C. & Palestro, C. J. Radionuclide imaging of infection. *J. Nucl. Med. Technol.* **32**, 47–57 (2004).
4. Heuker, M. *et al.* Preclinical studies and prospective clinical applications for bacteria-targeted imaging: the future is bright. *Clin. Transl. Imaging.* **4**, 253–264 (2016).
5. Ordonez, A. A. *et al.* A systematic approach for developing bacteria-specific imaging tracers. *J. Nucl. Med.* **58**, 144–150 (2017).
6. Britton, K. E. *et al.* Imaging bacterial infection with ^{99m}Tc-ciprofloxacin (Infecton). *J. Clin. Pathol.* **55**, 817–823 (2002).
7. Love, C., Tomas, M. B., Tronco, G. G. & Palestro, C. J. FDG PET of infection and inflammation. *Radiographics.* **25**, 1357–1368 (2005).
8. Besson, F. L. *et al.* Contribution of ^{18}F-FDG PET in the diagnostic assessment of fever of unknown origin (FUO): a stratification-based meta-analysis. *Eur. J. Nucl. Med. Mol. Imaging.* **43**, 1887–1895 (2016).
9. Glaudemans, A. W. J. M., Israel, O. & Slart, R. H. J. A. Pitfalls and Limitations of Radionuclide and Hybrid Imaging in Infection and Inflammation. *Semin. Nucl. Med.* **45**, 500–512 (2015).
10. Glaudemans, A. W. J. M. *et al.* The use of ^{18}F-FDG-PET/CT for diagnosis and treatment monitoring of inflammatory and infectious diseases. *Clin. Dev. Immunol.* 623036 (2013).
11. Signore, A. & Glaudemans, A. W. J. M. The molecular imaging approach to image infections and inflammation by nuclear medicine techniques. *Ann. Nucl. Med.* **25**, 681–700 (2011).
12. Bruggink, J. L. M. *et al.* Accuracy of FDG-PET- CT in the diagnostic work-up of vascular prosthetic graft infection. *Eur. J. Vasc. Endovasc. Surg.* **40**, 348–354 (2010).
13. Pysz, M. A., Gambhir, S. S. & Willmann, J. K. Molecular Imaging: Current Status and Emerging Strategies. *Clin. Radiol.* **65**, 500–516 (2010).
14. Garrido, V. *et al. In vivo* monitoring of *Staphylococcus aureus* biofilm infections and antimicrobial therapy by [^{18}F]-fluoro-deoxyglucose-microPET in a mouse model. *Antimicrob. Agents Chemother.* **58**, 6660–6667 (2014).
15. Odekerken, J. C. E., Brans, B. T., Welting, T. J. M. & Walenkamp, G. H. I. M. ^{18}F-FDG microPET imaging differentiates between septic and aseptic wound healing after orthopedic implant placement. *Acta Orthop.* **85**, 305–313 (2014).
16. Odekerken, J. C. E., Walenkamp, G. H. I. M., Brans, B. T., Welting, T. J. M. & Arts, J. J. C. The Longitudinal Assessment of Osteomyelitis Development by Molecular Imaging in a Rabbit Model. *Biomed Res. Int.* 424652 (2014).
17. Keidar, Z., Pirmisashvili, N., Leiderman, M., Nitecki, S. & Israel, O. ^{18}F-FDG uptake in noninfected prosthetic vascular grafts: incidence, patterns, and changes over time. *J. Nucl. Med.* **55**, 392–395 (2014).
18. Keidar, Z., Engel, A., Hoffman, A., Israel, O. & Nitecki, S. Prosthetic Vascular Graft Infection:

The role of ^{18}F-FDG PET/CT. *J. Nucl. Med.* **48**, 1230–1236 (2007).

19. Russell, J. B. & Wells, J. E. The ability of 2-deoxyglucose to promote the lysis of *Streptococcus bovis* JB1 via a mechanism involving cell wall stability. *Curr. Microbiol.* **35**, 299–304 (1997).
20. Veloo, A. C. M., Elgersma, P. E., Friedrich, A. W., Nagy, E. & van Winkelhoff, A. J. The influence of incubation time, sample preparation and exposure to oxygen on the quality of the MALDI-TOF MS spectrum of anaerobic bacteria. *Clin. Microbiol. Infect.* **20**, 1091–1097 (2014).
21. Martner, A., Skovbjerg, S., Paton, J. C. & Wold, A. E. *Streptococcus pneumoniae* autolysis prevents phagocytosis and production of phagocyte-activating cytokines. *Infect. Immun.* **77**, 3826–3837 (2009).
22. Kotrba, P., Inui, M. & Yukawa, H. Bacterial phosphotransferase system (PTS) in carbohydrate uptake and control of carbon metabolism. *J. Biosci. Bioeng.* **92**, 502–517 (2001).
23. Gonzy-Tréboul, G., de Waard, J. H., Zagorec, M. & Postma, P. W. The glucose permease of the phosphotransferase system of *Bacillus subtilis*: evidence for IIGlc and IIIGlc domains. *Mol. Microbiol.* **5**, 1241–1249 (1991).
24. Deutscher, J., Francke, C. & Postma, P. W. How Phosphotransferase System-Related Protein Phosphorylation Regulates Carbohydrate Metabolism in Bacteria. *Microbiol. Mol. Biol. Rev.* **70**, 939–1031 (2006).
25. Weinstein, E. A. *et al.* Imaging *Enterobacteriaceae* infection *in vivo* with ^{18}F-fluorodeoxysorbitol positron emission tomography. *Sci. Transl. Med.* **6**, 1–20 (2014).
26. Darenberg, J. *et al.* Molecular and clinical characteristics of invasive group A streptococcal infection in Sweden. *Clin. Infect. Dis.* **45**, 450–458 (2007).
27. Russell, J. B. & Cook, G. M. Energetics of bacterial growth balance of anabolic and catabolic reactions. *Microbiol. Rev.* **59**, 1–15 (1995).
28. Sarda, L. *et al.* Inability of ^{99m}Tc-Ciprofloxacin Scintigraphy to Discriminate Between Septic and Sterile Osteoarticular Diseases. *J. Nucl. Med.* **44**, 920–926 (2003).
29. Siaens, R. H., Rennen, H. J., Boerman, O. C., Dierckx, R. & Slegers, G. Synthesis and Comparison of ^{99m}Tc-Enrofloxacin and ^{99m}Tc-Ciprofloxacin. *J. Nucl. Med.* **45**, 2088–2094 (2004).
30. Dumarey, N. *et al.* A. Infecton is not specific for bacterial osteo-articular infective pathology. *Eur. J. Nucl. Med.* **29**, 530–535 (2002).
31. Langer, O. *et al. In vitro* and *in vivo* evaluation of [^{18}F]-ciprofloxacin for the imaging of bacterial infections with PET. *Eur. J. Nucl. Med. Mol. Imaging.* **32**, 143–150 (2005).
32. Gowrishankar, G. *et al.* Investigation of 6-[^{18}F]-fluoromaltose as a novel PET tracer for imaging bacterial infection. *PLoS One.* **9**, 6–11 (2014).
33. Herbert, S. *et al.* Repair of global regulators in *Staphylococcus aureus* 8325 and comparative analysis with other clinical isolates. *Infect Immun.* **78**, 2877–2889 (2010).
34. Stülke, J. *et al.* Induction of the *Bacillus subtilis* ptsGHI operon by glucose is controlled by a novel antiterminator, GlcT. *Mol Microbiol.* **25**, 65–78 (1997).
35. Singh, K. *et al.* Carbon catabolite repression in *Bacillus subtilis*: Quantitative analysis of repression exerted by different carbon sources. *J Bacteriol.* **190**, 7275–7284 (2008).

Chapter 4

Non-invasive optical and nuclear imaging of *Staphylococcus*-specific infection with a human monoclonal antibody-based probe

Francisco Romero Pastrana[*], John M. Thompson[*], Marjolein Heuker, Hedzer Hoekstra, Carly A. Dillen, Roger V. Ortines, Alyssa G. Ashbaugh, Julie E. Pickett, Matthijs D. Linssen, Nicholas M. Bernthal, Kevin P. Francis, Girbe Buist, Marleen van Oosten, Gooitzen M. van Dam, Daniel L.J. Thorek, Lloyd S. Miller[#] and Jan Maarten van Dijl[#]

[,#] These authors contributed equally to this work*

Virulence (2018) 1;9(1):262-272

Abstract

Staphylococcus aureus infections are a major threat in healthcare, requiring adequate early-stage diagnosis and treatment. This calls for novel diagnostic tools that allow non-invasive *in vivo* detection of staphylococci. Here we performed a preclinical study to investigate a novel fully-human monoclonal antibody 1D9 that specifically targets the immunodominant staphylococcal antigen A (IsaA). We show that 1D9 binds invariantly to *S. aureus* cells and may further target other staphylococcal species. Importantly, using a human *post-mortem* implant model and an *in vivo* murine skin infection model, preclinical feasibility was demonstrated for 1D9 labelled with the near-infrared fluorophore IRDye800CW to be applied for direct optical imaging of *in vivo S. aureus* infections. Additionally, ^{89}Zirconium-labelled 1D9 could be used for positron emission tomography imaging of an *in vivo S. aureus* thigh infection model. Our findings pave the way towards clinical implementation of targeted imaging of staphylococcal infections using the human monoclonal antibody 1D9.

Keywords: *Staphylococcus aureus; human monoclonal antibody; immunodominant staphylococcal antigen A; IsaA; PET; ^{89}Zr*

Introduction

The rapid and accurate diagnosis of a bacterial infection is important for the initiation of appropriate medical and surgical management. Traditional diagnostic approaches involve microbiological techniques, histologic staining and, more recently, molecular techniques. However, these approaches require sampling of infected tissues, which involves invasive procedures that add cost and potential morbidity, as uninfected tissue or implants are exposed to bacteria from the skin microbiota and surgical environment. Also, culture-based diagnostic approaches are inherently frought with issues of sampling error and contamination. Since current diagnostic tests often take days to deliver results, antibiotic therapy is frequently started empirically, and this can lead to inadequate or incorrect treatment, contributing to worse clinical outcomes. The problems with current diagnosis of infection are particularly relevant for infections caused by *Staphylococcus aureus*, which is responsible for the majority of skin and soft tissue infections, as well as invasive and life-threatening infections, such as cellulitis, pneumonia, osteomyelitis and bacteraemia.[1] *S. aureus* is also a common cause of medical device and implant-related infections, which are exceedingly difficult to treat because the bacteria form biofilms on the foreign materials that inhibit the efficacy of antibiotics. Rapid detection and treatment prior to the seeding of implants and establishment of biofilm is essential. Moreover, the widespread emergence of methicillin-resistant *S. aureus* (MRSA) strains, which are resistant to multiple antibiotics,[2,3] is causing substantial delays in starting adequate antibiotics coverage. This highlights the need for faster, more sensitive and non-invasive diagnostic alternatives than are currently available.

Current non-invasive imaging modalities used to localise infection foci include computed tomography, positron emission tomography (PET) with fluorine-18-fluorodeoxyglucose, and magnetic resonance imaging. However, these approaches cannot accurately differentiate between infected tissue and sterile inflammation. Therefore, there have been intense efforts to develop more targeted imaging techniques by using bacteria-specific tracers, which typically consist of a targeting moiety with affinity for bacteria conjugated to an imaging agent for optical, optoacoustic or PET imaging.[4,5] Promising tracers have combined antibodies, antibiotics, antimicrobial peptides, metabolizable compounds or particular ligands with attached fluorophores or radioisotopes.[4,6–8] However, the vast majority of these tracers has been designed to detect infections caused by a broad spectrum of bacterial species, while relatively few studies have explored species-specific tracers.[9–12]

We have recently provided proof-of-principle for the use of antibiotic-based targeting probes labelled with near-infrared (NIR) fluorophores for optical and optoacoustic imaging, demonstrating preclinical detection of *S. aureus* infections.[5,13] However, antibiotics generally lack the ability to identify specific bacterial species as most have broad affinity, binding indiscriminately to Gram-positive and/or Gram-negative bacteria. Species-specific tracers offer the potential to not only identify the presence of an infection, but to define the causative organism, thereby providing an

actionable diagnosis that could guide targeted antibiotic therapy. This is especially relevant to invasive *S. aureus* infections, such as necrotizing pneumonia and endocarditis, or difficult-to-treat biofilm-related infections. Such targets for staphylococcal-specific imaging might include proteins exposed on the bacterial cell surface.[14–16] A well-conserved surface protein of *S. aureus* is the immunodominant staphylococcal antigen A (IsaA).[17–21] In a previous study, we developed a fully human monoclonal antibody (humAb) against IsaA, which was partially protective against *S. aureus* infections in mouse models.[22] In the present preclinical study we investigated the target specificity of this anti-IsaA humAb, named 1D9, using an extensive panel of different staphylococcal isolates, and explored the feasibility of using 1D9 conjugated with the NIR fluorophore IRDye800CW or the PET tracer ^{89}Zirconium (^{89}Zr) as an *S. aureus*-specific tacer in a human *post-mortem* infection model and in *in vivo* mouse models of *S. aureus* infection.

Materials and methods

Bacterial strains and growth conditions

Bacterial strains are listed in **Supplementary Table S1**. Staphylococci were grown at 37°C in Tryptic Soy Broth (TSB). *Escherichia* coli Xen14 was grown at 37°C in Lysogeny Broth (LB; BD Biosciences, Sparks, MD). *Lactococcus lactis* PA1001 was grown at 30°C in M17 broth (Oxoid Limited, Hampshire, UK) with 2% glucose. Media were supplemented with chloramphenicol for plasmid selection (5 µg/mL for pNG4110 and 10 µg/mL for pLux). Plasmid pLux (pbp2-pro) from *S. aureus* ALC2906[23] was introduced by electroporation into *S. aureus* SH1000 and MS001 as reported.[24,25]

Protein expression, LDS-PAGE and Western blotting

Plasmid pNG4110::*isaA* was constructed by polymerase chain reaction (PCR) amplification of the gene with primers 5'- atatggatccgctgaagtaaacgttgatcaag-3' and 5'-atatgcggccgcttagaatccccaagcacctaaaccttg-3', and subsequent cloning in pNG4110.[26] Production and expression of His_6-tagged IsaA from plasmid pNG4110::*isaA* was performed as described.[26] Bacterial culture supernatants were precipitated with 10% trichloroacetic acid (TCA) and resuspended in lithium dodecyl sulphate (LDS) sample buffer (Life Technologies, Grand Island, NY, USA), cells were disrupted with 0.1 µm glass beads (Biospec Products, Bartlesville, USA) in a Precellys 24 homogeniser (Bertin Technologies, France), and liberated proteins were resuspended in LDS sample buffer. Samples were analysed by LDS-PAGE (NuPAGE gels, Life Technologies) and proteins were visualised by protein staining (Simply Blue Safe Staining, Life Technologies) or by blotting onto Protan nitrocellulose transfer paper (Whatman, Germany) and subsequent immunodetection using mouse anti-His-tag antibodies (Life Technologies) or IRDye800CW-labelled 1D9 antibody. Fluorescent secondary goat anti-human or goat anti-mouse IRDye800CW antibodies were from

LI-COR Biosciences. Antibody binding was visualised using an Odyssey Infrared Imaging System (LI-COR Biosciences, Lincoln, NE, USA).

Antibody production and fluorescence labelling

The human monoclonal antibody 1D9 was produced as described[22] by transient transfection of Expi293F cells (Life Technologies). 1D9 antibodies were isolated by HiTrap Protein A HP column purification (GE Life sciences, Eindhoven, the Netherlands) followed by HiTrap column desalting (GE Life sciences). 1D9 labelling with IRDye800CW (LI-COR Biosciences) was performed as previously described.[27]

Human *post-mortem* implant model

NIR fluorescence imaging of staphylococcal cells in a human *post-mortem* model was performed essentially as previously described.[13]

Mouse model and *in vivo* fluorescence and bioluminescence imaging

Maintenance of C57BL/6 mice and intradermal injection of *S. aureus*, *E. coli* or lipopolysaccharide (LPS) was performed as previously described.[28] *In vivo* fluorescence and bioluminescence imaging was performed with an IVIS Lumina III (PerkinElmer, Alameda, CA, USA) essentially as previously described.[13] Of note, we injected 5 x 10^7 colony forming units (CFUs) of *S. aureus* to provoke intradermal infection, because our previous studies have shown that at least 10^7 CFUs are needed to establish an *S. aureus* infection in our mouse model. Lower numbers of the bacteria will be rapidly cleared by the murine immune system.

Radiolabelling of 1D9 with ^{89}Zr

Mild conjugation was used to modify 1D9 with a radiometal chelate. To antibody in 0.1M HEPES, pH 8.5, three times was added 10 µL of p-SCN-Bn-Deferoxamine (DFO; Macrocyclics, Dallas, TX, USA) in dimethyl sulfoxide (DMSO; 233.3 µM) followed by 30-60 min mixing at room temperature to a final DFO:antibody ratio of 7:1. Unreacted DFO was removed using Amicon Ultra 0.5 mL centrifugal filter 50 kDa (EMD Millipore, Billerica, MA, USA). ^{89}Zr oxalate was obtained from the Mallinckrodt Institute of Radiology, St. Louis, MO. To ^{89}Zr was added an excess of 1 M oxalic acid. 0.1 M Na_2CO_3 was slowly added to a pH of 7-7.5. ^{89}Zr was added to the DFO-conjugated antibody and mixed at room temperature for 40 min. To chelate unbound ^{89}Zr, 50 mM ethylenediaminetetraacetic acid (EDTA), pH 5, was added and removed with Amicon Ultra 0.5 mL centrifugal filters using sterile saline. Instant thin layer chromatography (ITLC) was performed using silica impregnated filter paper (Pall Corporation, New York, NY, USA). ITLC was run in 50 mM EDTA, pH 5, and subsequently imaged and quantified using a Phosphorimager and AutoQuant software (Media Cybernetics, Rockville, MD, USA).

Nuclear and X-ray imaging

The micro-PET R4 system (Concorde Microsystems Inc., Knoxville, TN, USA) was used to acquire PET scans. For all static images, scan time was between 10 and 20 min. Data were sorted into 3D histograms by Fourier rebinning, and transverse images were reconstructed using a maximum *a priori* algorithm to a 128 × 128 × 63 (0.845 mm × 0.845 mm × 1.2115 mm) matrix. Datasets were analysed using ASIPro VM micro-PET software (Siemens Preclinical Solutions, Erlangen, Germany). Volumes of interest were manually defined around areas of bacteria injection and injected activity per gram was calculated. An empirically determined system calibration factor for mice was used to convert voxel count rates to activity concentrations (in µCi per mL of tissue). Figures were generated using Amira (version 5.0; FEI, Hillsboro, OR, USA). Directly after PET scanning, while in the same position, planar images were acquired using the MX-20-DC12 digital X-ray imaging system (Faxitron Bioptics, Tucson, AZ, USA).

Statistical analysis

Fluorescence imaging data were analysed with Prism (GraphPad, La Jolla, CA, USA) and compared using a 1-tailed Student's t-test. Values of $P<0.05$ were considered significant. All PET imaging data are expressed as mean ± SEM. Data were subjected to the Holm-Sidak method, with alpha = 0.05 and the assumption that all rows are sampled from populations with the same scatter using GraphPad Prism. P-values <0.05 were considered significant.

Ethics statement

Post-mortem experiments were conducted according to institutional guidelines with prior approval from the scientific review committee of the Skills Center of the University Medical Center Groningen, the Netherlands. All individuals involved in the human *post-mortem* studies have provided informed written consent for the use of their bodies for scientific research and teaching. All animals were handled in strict accordance with good animal practice as defined in the federal regulations as set forth in the written Assurance of Compliance with PHS Policy to the United States Department of Health and Human Services (Assurance No. A3079-01) and Regulations of the Animal Welfare Act of the United States Department of Agriculture (USDA registration #23-R-0023). All animal work was approved by the Johns Hopkins University Animal Care and Use Committee (ACUC Protocol No. MO15M421) and the animal care program at the Johns Hopkins School of Medicine is fully accredited by the Association for Assessment and Accreditation of Laboratory Animal Care International.

Results and discussion

High target sensitivity of humAb 1D9 for *S. aureus*

A key feature of an effective targeting moiety for the specific detection of an infecting pathogen is the ability to bind to the vast majority of different clinically related isolates. A BLASTP analysis indicated that the *isaA* gene was present in all of the 1912 different *S. aureus* isolates for which sequences are available, with respective IsaA proteins showing at least 98% amino acid sequence identity. In addition, the *isaA* gene was found to be conserved in several other staphylococcal species. When *S. aureus* isolates were excluded from the BLASTP results, significant hits with at least 60% identity at the amino acid sequence level were obtained for *S. epidermidis* (145), *S. argenteus* (6), *S. warneri* (5), *S. schweitzeri* (3), *S. simiae* (2), and *S. haemolyticus* (1). Additional identified staphylococcal species with lower identity scores (<60%) for IsaA included *S. caprae*, *S. delphini*, *S. hominis*, *S. intermedius*, *S. lugdunensis*, *S. microti*, *S. pasteuri*, *S. pseudintermedius*, *S. schleiferi*, *S. schweitzeri*, and *S. simulans*. These findings suggest that the respective species produce IsaA proteins that may be detectable with 1D9. To confirm these results, Western blotting analysis was performed with 1D9. 1D9 detected IsaA production in well-described MRSA strains, including USA300, Mu50, MW2, N315, COL and MRSA252 (**Figure 1A**). IsaA production was also detected with 1D9 in the laboratory strain NCTC8325-4 as well as additional clinical *S. aureus* isolates from the University Medical Center Groningen (isolates A-Y; **Figures 1A**, **B**). Of note, IsaA was always detected in the cell fraction and in most (but not all) growth medium fractions. To control for any off-target binding of 1D9 to different *S. aureus* proteins known to bind to the Fc portion of human IgG1 (i.e., protein A [Spa] and Sbi),[15] cell and medium fractions from *S. aureus* Newman wild-type and *Δspa* or *Δspa Δsbi* mutant derivatives were tested for 1D9 binding. 1D9 bound to IsaA irrespective of the presence of Spa and Sbi (**Figure 1C**). From a test panel of other *Staphylococcus* species, IsaA-specific signals were observed for two out of four *S. epidermidis* isolates, two tested *S. hominis* isolates, as well as an isolate of *S. pettenkoferi* and *S. caprae* (**Figure 1C**). IsaA expression was not detected in *S. lugdunensis*, *S. haemolyticus*, *S. capitis*, *S. warneri* and *S. pasteuri*, nor in *Bacillus subtilis* 168 or *E. coli* DH5α controls (**Figure 1C**). As expected, no IsaA signal was detectable in the cell and growth medium fractions of an *isaA* deletion mutant (**Figure 1D**). Taken together, these findings imply that 1D9 can be used to specifically detect cells of the vast majority of *S. aureus* isolates plus a number of additional clinically-applicable staphylococcal species.

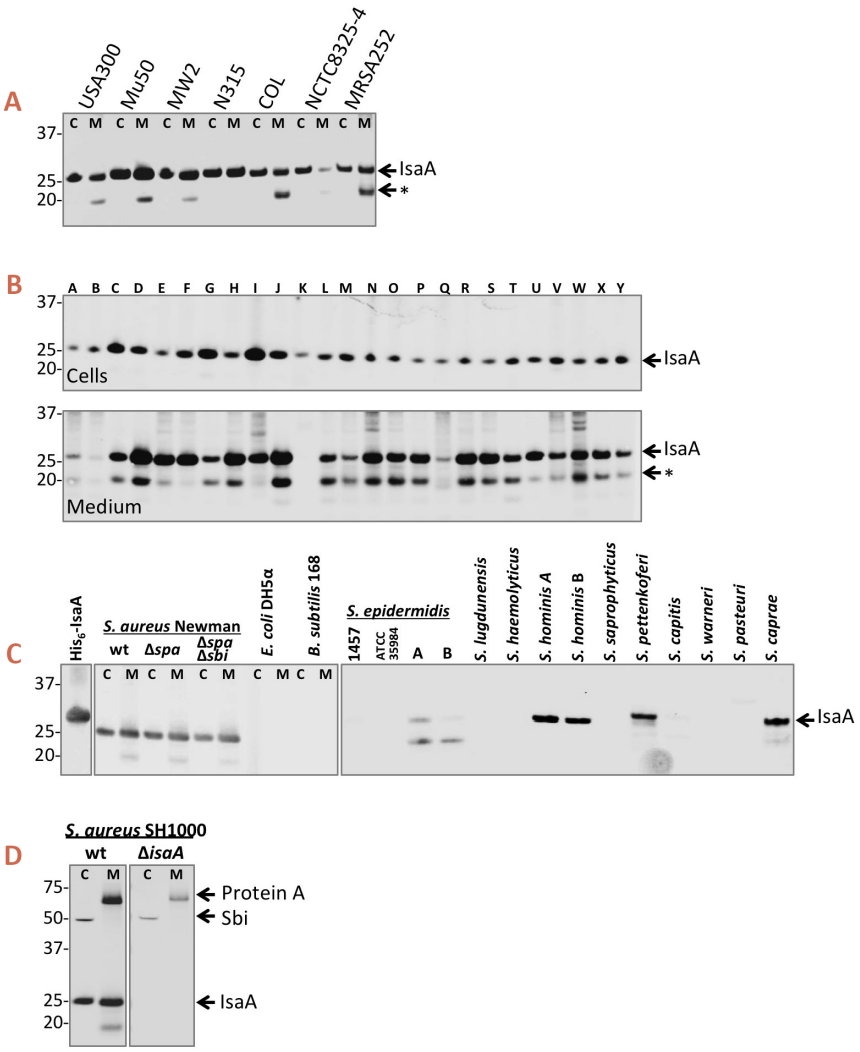

Figure 1. IsaA expression in *S. aureus* and other staphylococcal species. Detection of IsaA production in (**A**) sequenced *S. aureus* strains and (**B**) 25 clinical *S. aureus* isolates (A- Y) by Western blotting and immunodetection with 1D9-800CW. (**C**) Western blotting analysis for IsaA detection in *spa* and *spa sbi* mutants of *S. aureus* Newman, *E. coli* DH5α, *B. subtilis* 168 and several different staphylococcal species. Left panel, immunodetection of IsaA with unlabelled 1D9 and a secondary IRDye800CW-labelled goat anti-human antibody; right panel immunodetection with 1D9-800CW. Purified His_6-IsaA was used as a control. (**D**) Western blotting analysis to verify the absence of IsaA production in *S. aureus* MS001 (*ΔisaA*) using 1D9-800CW for immunodetection. C, cell fraction; M, growth medium fraction. The positions of molecular weight markers are indicated on the left, and the positions of IsaA, an IsaA degradation product (*), Protein A and Sbi are indicated on the right.

Imaging of 1D9-800CW labelled bacteria in a human *post-mortem* implant model

The ability of 1D9 to provide *in vivo* detection of *S. aureus* was first assessed in a *post-mortem* model where Whatman filter paper soaked with bacteria was implanted subdermally on the tibia of a human cadaver with subsequent skin closure.[13] To enable NIR imaging, 1D9 was conjugated to the fluorophore IRDye800CW, and the resulting 1D9-800CW complex was added to wild-type *S. aureus* bacteria. To assess the contribution of IgG-binding proteins Spa and Sbi to the signal, *S. aureus* mutant strains lacking both *spa* and *sbi* (*Δspa Δsbi*) were also probed with 1D9-800CW. We additionally included a *S. aureus* mutant strain lacking *isaA* (*ΔisaA*) and *S. epidermidis* 1457 that are both negative for binding 1D9 (**Figure 1**). All cells incubated with 1D9-800CW were thoroughly washed in phosphate-buffered saline (PBS) and spotted in equal amounts (2.5 x 10^8 CFU) onto a Whatman filter paper. NIR images of the filter paper were recorded prior to and during ~8 mm subdermal implantation in the *post-mortem* model.

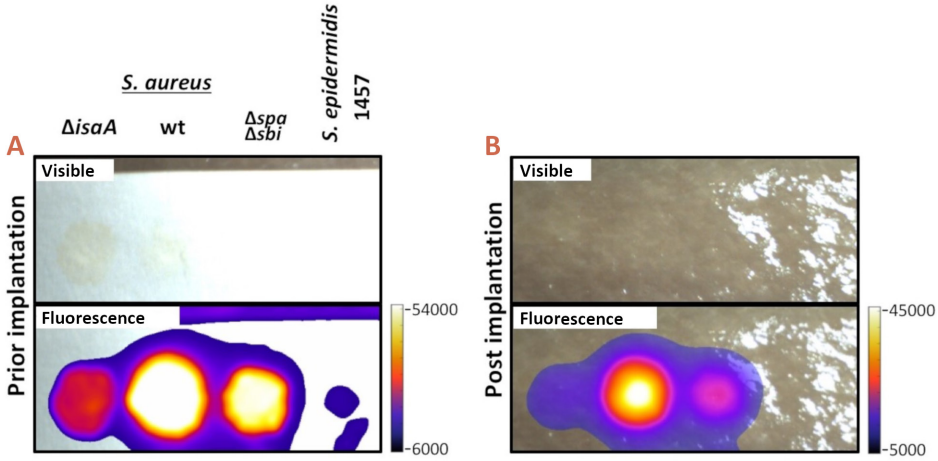

Figure 2. Human *post-mortem* implant model. For NIR fluorescence imaging of staphylococcal cells in a human *post-mortem* model, overnight grown cultures of *S. aureus* MS001 (ΔisaA), *S. aureus* SH1000 (wt), *S. aureus* Newman *Δspa Δsbi* (*Δspa Δsbi*) and *S. epidermidis* 1457 in TSB (5x10^8, CFU) were collected, washed twice with PBS, resuspended in 100 µL of PBS, and incubated with 5 µg of 1D9-800CW. Upon 20 min incubation at room temperature, cells were washed twice with PBS and resuspended in 100 µL of PBS. Of this suspension with fluorescently labelled cells, 50 µL aliquots were spotted on filter paper strips (Whatman), and placed inside sealed plastic wrapping. Visible light and fluorescence images were recorded prior to and during surgical implantation onto the distal tibia of a human *post-mortem* leg. Fluorescence imaging was performed using an intra-operative clinical multispectral fluorescence Explorer Air camera (SurgVision BV). Fluorescence signals were collected 0.5 sec (before implantation) and 0.2 sec (during implantation) with low binning and excitation/emission wavelengths of 740/845 nm.

As shown in **Figure 2**, the strongest NIR signal was observed for wild-type *S. aureus*. A slightly lower signal was observed for the *Δspa Δsbi* double mutant, indicating that 1D9-800CW binding to IgG-binding proteins contributed minimally to the observed signal. In comparison, the signal observed for the *isaA* mutant cells was significantly lower, confirming that Spa and Sbi bind relatively minor amounts of 1D9-800CW compared to IsaA. Minimal signal was detectable for *S. epidermidis* 1457, which is consistent with the Western blotting data in **Figure 1C**. Importantly, the signal from the 1D9-800CW bound to wild-type cells was clearly detectable upon implantation and suturing of the skin, providing proof-of-principle that 1D9 can be used for detection of subdermal *S. aureus* infections in humans.

Non-invasive *in vivo* fluorescence imaging of *S. aureus* infection with 1D9-800CW

To validate the potential use of 1D9-800CW for specific *in vivo* imaging of *S. aureus* infections, a murine skin infection and inflammation model was used. In a first group of mice, opposite flanks of each mouse were inoculated intradermally with a bioluminescent wild-type *S. aureus* SH1000 strain (wt) and the isogenic *isaA* mutant MS001 (*ΔisaA*). In parallel, a group of control mice were inoculated in opposite flanks with bioluminescent *E. coli* Xen14 (*Ec*) and lipopolysaccharide (LPS) to evaluate any off-target accumulation at a site of either an infection caused by a bacterium that does not espress IsaA or sterile inflammation. One day post-inoculation, 2.5 mg/kg 1D9-800CW was administered intravenously. Fluorescence and bioluminescence were recorded one day prior to inoculation (t_{-2}), one hour after inoculation (t_{-1}), immediately before 1D9-800CW administration (t_0), at 2/4/8 h after administration, and daily thereafter (t_{1-7}) (**Figure 3**). From day 1 onwards, significantly higher fluorescence signal was localised in the flanks of mice infected with the wt *S. aureus* strain compared to the *ΔisaA* mutant ($P<0.01$), *E. coli* Xen14 ($P<0.0001$), or LPS ($P<0.001$) (**Figures 3A**, **B**). The significant difference observed for the wt and *ΔisaA S. aureus* strains implies that, similar to the *post-mortem* model (**Figure 2**), 1D9-800CW binds to the IsaA target rather than the IgG Fc-binding proteins Spa and Sbi. Importantly, the stronger fluorescence signals observed for the *S. aureus* isolates compared to the fluorescence signals elicited by *E. coli* Xen14 or LPS show that 1D9-800CW is specific for *S. aureus*, and that *S. aureus* infection overall can be distinguished from other causative infections or LPS-induced sterile inflammation. However, an early peak of fluorescence observed for mice inoculated with LPS indicates that 1D9-800CW does accumulate at early time points at the site of sterile inflammation (**Figure 3B**). This is possibly due to the Enhanced Permeability and Retention (EPR) effect resulting from inflammation, or a higher local density of neutrophils and hence Fc-receptor binding of the 1D9 humAb. This effect was not observed when the mice were inoculated with *E. coli*, suggesting that LPS induced a stronger inflammatory response than *E. coli*. Importantly, the signal became more specific from 2 days onwards. Further, the bioluminescence signals of the three bacterial strains were not significantly different (**Figures 3C**, **D**), showing that differences in fluorescence signal were due to specificity for *S. aureus* rather than the bacterial inoculum.

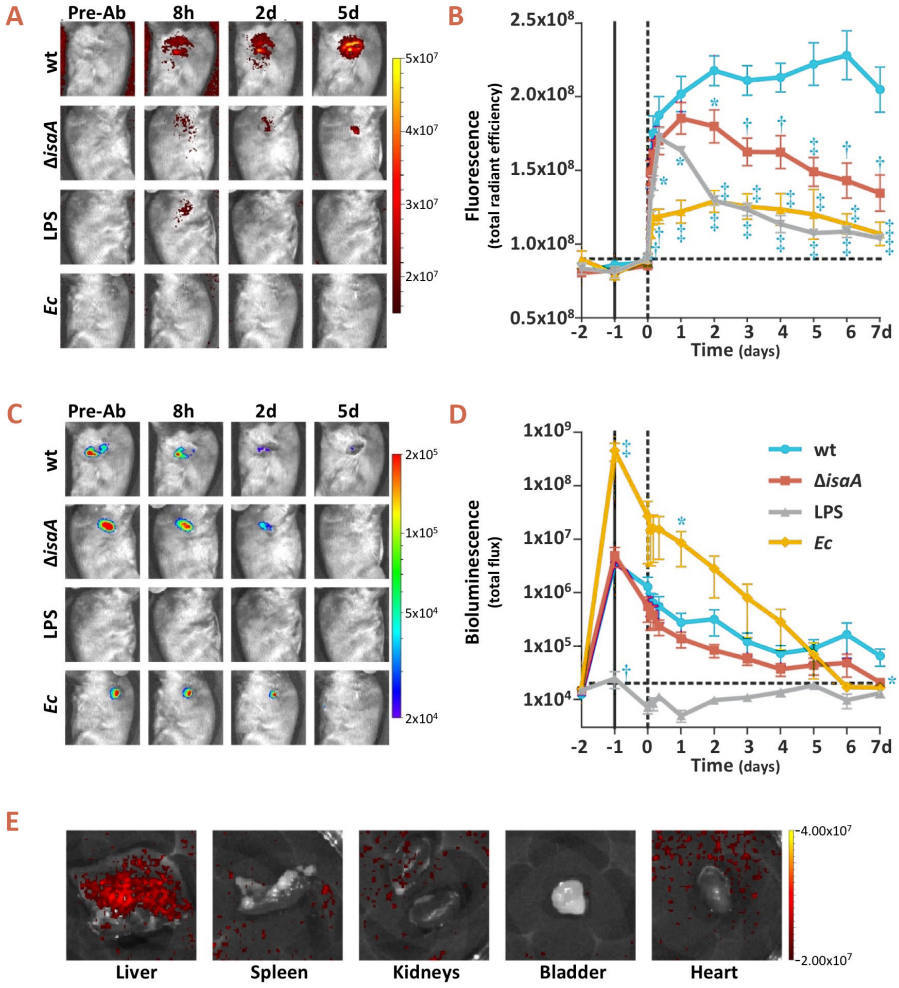

Figure 3. *In vivo* IsaA-specific optical imaging of *S. aureus* infection with 1D9-800CW. Six to eight weeks old C57BL/6 female mice were shaved on the flanks and back, and mid-logarithmic growth phase *S. aureus* SH1000 *lux* (wt) and *ΔisaA S. aureus* MS001 *lux* (5 x 10^7 CFUs in 100 µL of sterile saline) were each injected intradermally into opposite flanks of each mouse (n=7 performed over 3 independent experiments). In a second group of mice, *E. coli* Xen14 (*Ec*; 5 x 10^7 CFUs in 100 µL of sterile saline) and lipopolysaccharide (LPS; 1 mg/kg in 100 µL of sterile saline) were injected intradermal into opposite flanks of each mouse (n=4 performed over 1 experiment). Inoculations were performed on t_{-1}. Control images were recorded 1 day prior to inoculation (t_{-2}). One day post bacterial inoculation (t_0) or 1 h after LPS injection, 1D9-800CW (2.5 mg/kg in 100 µL sterile saline warmed to 37°C) was injected retro-orbitally and images were subsequently recorded at different time points as indicated. The fluorescence (total radiant efficiency [photons/s]/[mW/cm^2]) and bioluminescence signals (total radiance [photons/s]) were measured with a 1.2 × 1.2 cm region of interest (ROI) centered over the site of skin infection/

inflammation. (**A**) NIR fluorescence images of representative mice were collected at 0.5 sec with medium binning and excitation/emission wavelengths of 740/845 nm. (**B**) Mean total radiant efficiency (photons/s)/(mW/cm^2) ± SEM of the *in vivo* fluorescence signals. (**C**) Bioluminescence images of representative mice were collected for 60 sec with medium binning. (**D**) Mean total flux (photons/s) ± SEM (logarithmic scale) of *in vivo* bioluminescence signals. (**E**) Representative NIR fluorescence images of different organs collected on day 2 for assessment of 1D9-800CW accumulation. In panels **B** and **D**, variations are indicated with error bars and statistically significant differences with different symbols for each curve (* = P<0.05; † = P<0.01; ‡ = P<0.001).

Harvested organs on day 2 showed that fluorescence was mostly concentrated in the liver, with no appreciable signals in the spleen, kidneys, bladder or heart (**Figure 3E**), which is consistent with the known clearance of antibodies by the liver. Of note, all bioluminescence signals at sites of infection decreased over time, which could relate to reduced growth, loss of the pLux plasmid that was used to make the bacteria bioluminescence and/or bacterial clearance. For example, we have previously shown that luminescence of the bacteria is significantly reduced once they reach the stationary phase of growth.[13] In contrast, the 1D9 antibody will bind to IsaA irrespective of whether the bacteria are dead or alive. This would explain why a stable signal for 1D9-800CW was observed at time points post-infection where the bioluminescence signal had disappeared. In addition, culturing of infected mouse tissue showed that some *S. aureus* CFU had lost the pLux plasmid (data not shown). Altogether, it seems that the loss of luminescence was probably both related to reduced growth and loss of the pLux plasmid. Yet, it cannot be excluded that a slight decrease in bacterial numbers by immune clearance contributed to the loss of the luminescent signal at the site of infection

Since the above set of experiments involved two groups of mice inoculated in parallel, an independent experiment was performed where opposite flanks of the same mice were inoculated intradermally with a bioluminescent community-acquired MRSA strain (SAP231) and *E. coli* Xen14. In both of these bacterial strains, the *lux* genes for bioluminescence are stably integrated into the chromosome and are thus present in all progeny. Similar to the prior experiment, the fluorescence signals of 1D9-800CW were higher at the site of the *S. aureus* infection compared with the *E. coli* infection (**Figures 4A**, **B**), showing the specificity of 1D9-800CW for *S. aureus*. Likewise, the bioluminescence signals of the infecting bacteria both decreased over time (**Figures 4C**, **D**), suggesting reduced bacterial growth and/or clearance. A noteworthy observation was that the 1D9-800CW signal relating to *S. aureus* infection was highly stable over 7 days, which is in line with the known half-life of IgG1 humAbs of 6-8 days in mice. Since the half-life of IgG1 humAbs in humans is ~3 weeks, our findings imply that this particular probe can be used over several days upon administration, which is a clear advantage for potential clinical applications.

Previously, we have shown that the antibiotic vancomycin labelled with IRDye800CW (i.e. vanco-800CW) also allows for highly specific non-invasive *in vivo* detection of infecting staphylococci. However, vanco-800CW detects a broad spectrum of Gram-positive bacteria.[13] In contrast, a positive signal obtained with 1D9-800CW is diagnostic for potentially virulent staphylococci.

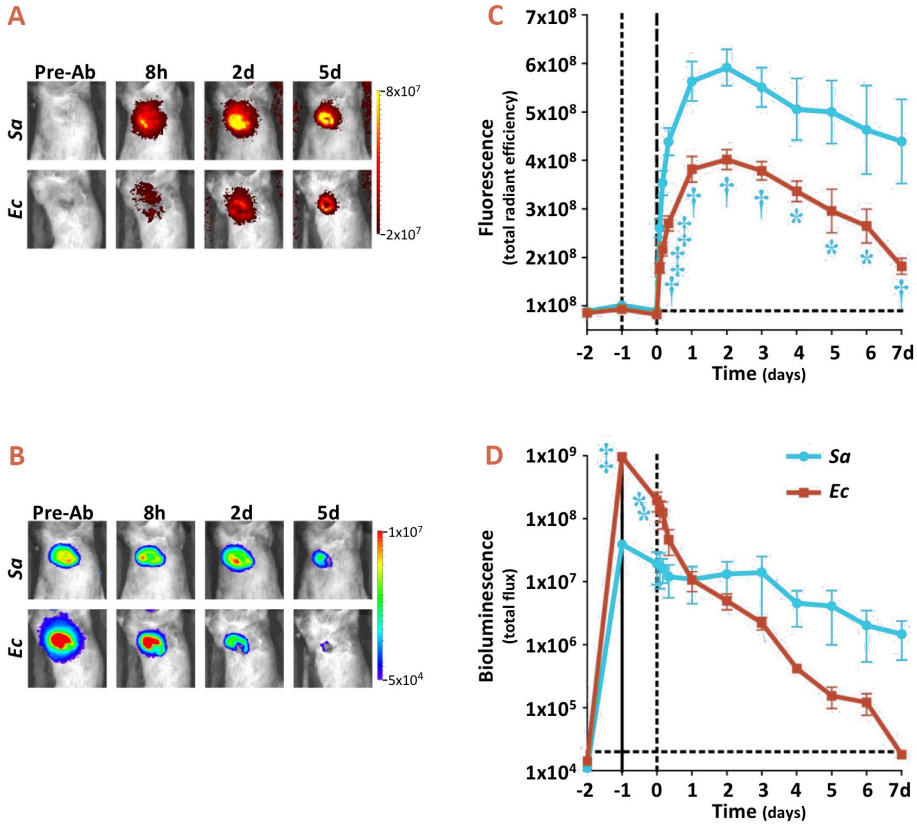

Figure 4. Distinction of *S. aureus* and *E. coli* infection by optical imaging with 1D9-800CW. Mice were inoculated intradermally in opposite flanks with bioluminescent *S. aureus* SAP231 (*Sa*) and *E. coli* Xen14 (*Ec*) as described for **Figure 3**. Images were recorded at different time points pre- and post-intravenous administration of 2.5 mg/kg 1D9-800CW. (**A**) NIR fluorescence images of representative mice were collected with excitation/emission wavelengths of 740/845 nm. (**B**) Mean total radiant efficiency (photons/s)/(mW/cm^2) ± SEM of the *in vivo* fluorescence signals. (**C**) Bioluminescence images of representative mice. (**D**) Mean total flux (photons/s) ± SEM (logarithmic scale) of *in vivo* bioluminescence signals. In panels **B** and **D**, variations are indicated with error bars and statistically significant differences with different symbols for each curve (* = P<0.05; † = P<0.01; ‡ = P<0.001).

Non-invasive *in vivo* PET imaging of *S. aureus* infection with ^{89}Zr-1D9

NIR fluorescence imaging of infection is appealing due to its speed, non-invasiveness and high resolution. In addition, it does not involve the use of radioactive isotopes, which makes it less expensive and more flexible than PET or single-photon emission computed tomography imaging, as well as circumventing the burden of ionizing radiation.[4] Despite these advantages, one major drawback of NIR fluorescence imaging is the limited signal penetration through tissue, which is about 1 cm due to light absorption and scatter.[4] For these reasons, we also explored the possibility of applying 1D9 to whole-body PET imaging to see if this modality would allow the high-sensitivity delineation of deeper-seated infections with clinical significance. Thus, 1D9 was labelled with ^{89}Zr, which has a half-life of 78.4 h. Similar to the experiments shown in **Figure 3A** and **B**, opposite flanks of each mouse were inoculated with wt *S. aureus* SH1000 and the isogenic *isaA* mutant MS001 (*ΔisaA*). At 1 day post-infection, 0.7 mg/kg of ^{89}Zr-1D9 was administered and PET images were recorded on days 3, 5, and 7.

As shown in **Figure 5A** and **B**, ^{89}Zr-1D9 revealed a specific accumulation at the site of infection, with a significantly higher intensity for the infection caused by wild-type *S. aureus* compared to the infection by IsaA-deficient *S. aureus*. Statistically significant differences between the specific and control infections were detected for 3 days. However, due to the limited half-life of ^{89}Zr, imaging was only possible for up to 7 days. Of note, **Figure 5A** shows a strong signal in the body, which is consistent with the data presented in **Figure 3E** where the accumulation of 1D9-800CW in the liver is shown. For potential clinical applications in the future, the known clearance of antibodies by the liver may thus represent a challenge if one wishes to detect specific signals of endocarditis or other infections near high-uptake organs, such as the liver. However, this is likely to represent less of a problem, if any, for the imaging of infections at body sites distant from the liver.

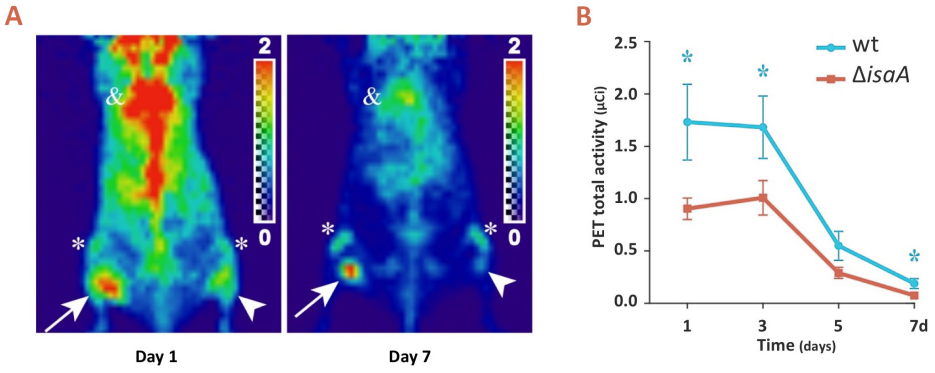

Figure 5. *In vivo* IsaA-specific PET imaging of *S. aureus* infection with ^{89}Zr-1D9. Mice were inoculated intradermally in opposite flanks with either *S. aureus* SH1000 (wt) or *S. aureus* MS001 (*ΔisaA*) as described for **Figure 3** (t_{-1}). One day post inoculation (t_0), 0.7 mg/kg ^{89}Zr-1D9 was administered intravenously and images were

subsequently recorded at different time points as indicated. List-mode data were acquired using a gamma-ray energy window of 350 to 750 keV and a coincidence timing window of 6 ns. PET imaging data were corrected for detector non-uniformity, dead time, random coincidences, and physical decay. For all static images, scan time was between 10 and 20 min. (**A**) PET images of representative mice [arrows = wt infection; arrowheads = *ΔisaA* infection; * = knee joint; & = heart]. (**B**) PET total activity (µCi) at the site of infection. In panel **B**, variations are indicated with error bars and statistically significant differences with an asterisk (* = P<0.05).

Future perspectives

Here we present the humAb 1D9 as a highly specific probe for both fluorescence and PET imaging of staphylococcal infections. The high specificity of 1D9 is demonstrated by longitudinal measurements in mouse infection models with extensive controls, in particular recombinant IsaA-deficient *S. aureus*, the Gram-negative bacterium *E. coli* and purified LPS. Thus, off-target accumulation of 1D9 at sites of inflammation and infection, e.g. due to increased blood flow and vascular permeability, may be ruled out. We consider it important that 1D9 is compatible with PET imaging modalities, because this may permit a faster introduction into the clinic as PET facilities are widely available in hospitals around the globe. Further, our experiments suggest the feasibility of 1D9 applications in optoacoustic imaging, which has a significantly better tissue penetration (>8 cm) than light (~1 cm).[4,5] This relates to the fact that agents used in optoacoustic imaging, like indocyanine green, absorb light of a particular wavelength and subsequently undergo thermo-elastic expansion. In turn, this results in the emission of ultrasonic pressure waves, which have much longer wavelengths than light and higher tissue penetration. Importantly, such ultrasonic signals are detectable with special sensors.

The need for rapid non-invasive modalities for infection imaging is highlighted by recent publications on a variety of probes that, together, allow *in vivo* detection of a broad spectrum of pathogens. For instance, these include probes based on antibiotics,[4,29] maltodextrin,[30] prothrombin,[31] oligonucleotides,[32] the bacteriophage M13,[12,33] and concanavalin A.[34] In this study, the 1D9 probe was evaluated as a novel and alternative antibody-based probe with the highest target specificity for *S. aureus*. 1D9 labelled with the NIR fluorophore IRDye800CW could be used to continuously monitor infecting bacteria over a period of at least 7 days using *in vivo* fluorescence imaging. For the imaging of deeper-seated infections, 1D9 labelled with ^{89}Zr can be used in conjunction with whole-body PET imaging. We therefore conclude that the humAb 1D9 provides new targeted and specific diagnostic imaging tracers for *S. aureus* infections.

Novel diagnostic technologies, especially next-generation DNA sequencing, are becoming increasingly popular tools for the detection of infections. However, next-generation sequencing is probably best-suited for the detection of superficial infections. For detection of deep-seated infections, the invasive sampling that would be required could be dangerous and is subject to

the uncertainties of incorrect sampling and contamination. A potential advantage of using non-invasive imaging in conjunction with a specific monoclonal antibody probe, such as 1D9, is that it may allow the detection of both superficial and deeper seated infections. The latter is particularly the case when the antibody is labelled with a PET tracer, as exemplified in the present study with ^{89}Zr-1D9. Given the increasingly common usage of immunoPET imaging, the application of this tool with microgram amounts of antibody could certainly be justifiable in many cases of infection even though the general use of radioactive labels should be restrained. Importantly, not all possible diagnostic applications of the 1D9 antibody will necessarily require radioactive labels. For instance, it is well-conceivable that a fluorescently labelled antibody, like 1D9-800CW, is suitable to guide surgery through intra-operative imaging of infections as is currently explored in cancer imaging.[4] Further, foci of infection could be detectable by the use of fluorescently labelled antibodies in combination with endoscopy.

Despite the promising results obtained in the present study, the application potential of our humAb 1D9 needs to be assessed in future *ex vivo* or *in vivo* studies. For example, it is currently hard to predict whether the specificity of 1D9 is high enough to discriminate sterile inflammation from infection, especially at early time points after the onset of infection. In addition, it is not yet known how competing circulating antibodies of the host will impact on the efficiency of imaging with labelled 1D9. The latter potential problem can probably be overcome with PET tracers (e.g. ^{89}Zr), since part of the appeal of radioactivity is that low antibody binding can still lead to the emission of a sufficiently strong signal to allow accurate measurements. Another important question relates to the need for parallel diagnostics to detect infections caused by pathogens other than *S. aureus*. In this respect, it would be convenient to have a panel of specific monoclonal antibodies targeting major pathogens, like *Pseudomonas*, *Burkholderia*, or *Acinetobacter*. However, as long as such antibodies are not available for infection imaging, approaches based on the 1D9 antibody could be complemented by other tracers that target a broad range of pathogens. For instance, many Gram-positive bacterial pathogens can be detected *in vivo* with the vancomycin-800CW tracer that we have previously developed.[13] Infections by Gram-negative bacterial pathogens can potentially be imaged by making use of fluorescently labelled maltodextrin,[30] or by radioactively labelled metabolizable compounds, like sorbitol.[4] On the other hand, it would also be very useful to develop an additional humAb that discriminates between MRSA and methicillin-sensitive *S. aureus*, as is underscored by the increasing incidence of MRSA infections world-wide.

Altogether, we conclude that the present study has achieved preclinical proof-of-principle for the use of the 1D9 monoclonal antibody in the *in vivo* imaging of infections caused by *S. aureus*. However, before a clinical study on the possible use of our 1D9 antibody can be justified, further animal studies will be needed to answer the questions how effective the 1D9 antibody will be as a diagnostic tool for deep-seated *S. aureus* infections, and for which clinical indications it is best applied.

Funding

Part of this research was supported by the Top Institute Pharma projects T4-213 and T4-502 (to J.M.v.D), and by the National Institute of Arthritis and Musculoskeletal and Skin Diseases of the U.S. National Institutes of Health grant numbers T32 AR067708 (J.M.T. and J.E.P.) and R01AR069502 (L.S.M.). F.R.P. received a scholarship from CONACyT (169643).

Disclosure of potential conflicts of interest

K.P.F. is an employee of PerkinElmer. All other authors declare no competing financial interests.

Acknowledgments

The authors thank Trishla Sinha and Romano Schreuder for the isolation of staphylococcal strains.

References

1. Tong, S. Y. C., Davis, J. S., Eichenberger, E., Holland, T. L. & Fowler, V. G. *Staphylococcus aureus* infections: Epidemiology, pathophysiology, clinical manifestations, and management. *Clin. Microbiol. Rev.* **28**, 603–661 (2015).
2. Peacock, S. J. & Paterson, G. K. Mechanisms of methicillin resistance in *Staphylococcus aureus*. *Annu. Rev. Biochem.* **84**, 577–601 (2015).
3. Blair, J. M. A., Webber, M. A., Baylay, A. J., Ogbolu, D. O. & Piddock, L. J. V. Molecular mechanisms of antibiotic resistance. *Nat. Rev. Microbiol.* **13**, 42–51 (2015).
4. van Oosten, M. *et al.* Targeted imaging of bacterial infections: advances, hurdles and hopes. *FEMS Microbiol. Rev.* **39**, 892–916 (2015).
5. Wang, Y. *et al.* Preclinical evaluation of photoacoustic imaging as a novel noninvasive approach to detect an orthopaedic implant infection. *J. Am. Acad. Orthop. Surg.* **25**, 7–12 (2017).
6. Ferro-Flores, G., Avila-Rodríguez, M. A. & García-Pérez, F. O. Imaging of bacteria with radiolabeled ubiquicidin by SPECT and PET techniques. *Clin. Transl. Imaging.* **4**, 175–182 (2016).
7. Mills, B., Bradley, M. & Dhaliwal, K. Optical imaging of bacterial infections. *Clin. Transl. Imaging.* **4**, 163–174 (2016).
8. Lazzeri, E. Systematic review of *in vivo* microorganisms imaging with labeled vitamins, bacteriophages and oligomers. *Clin. Transl. Imaging.* **4**, 265–272 (2016).
9. Rubin, R. H. *et al.* Specific and nonspecific imaging of localized Fisher Immunotype 1 *Pseudomonas aeruginosa* infection with radiolabeled monoclonal antibody. *J. Nucl. Med.* **29**, 651–656 (1988).
10. Malpani, B. L., Kadival, G. V. & Samuel, A. M. Radioimmunoscintigraphic approach for the *in vivo* detection of tuberculomas - A preliminary study in a rabbit model. *Int. J. Radiat. Appl. Instrum.* **19**, 45–53 (1992).
11. Lee, J. D. *et al.* Immunoscintigraphy in the detection of tuberculosis with radiolabelled antibody fragment against *Mycobacterium bovis* bacillus Calmette-Guérin: a preliminary study in a rabbit model. *Eur. J. Nucl. Med.* **19**, 1011–5 (1992).
12. Bardhan, N. M., Ghosh, D. & Belcher, A. M. Carbon Nanotubes as *in vivo* Bacterial Probes. *Nat. Commun.* **5**, 4918 (2014).
13. van Oosten, M. *et al.* Real-time *in vivo* imaging of invasive- and biomaterial-associated bacterial infections using fluorescently labelled vancomycin. *Nat. Commun.* **4**, 2584 (2013).
14. Dreisbach, A., van Dijl, J. M. & Buist, G. The cell surface proteome of *Staphylococcus aureus*. *Proteomics.* **11**, 3154–3168 (2011).
15. Foster, T. J., Geoghegan, J. A., Ganesh, V. K. & Höök, M. Adhesion, invasion and evasion: the many functions of the surface proteins of *Staphylococcus aureus. Nat. Rev. Microbiol.* **12**, 46–62 (2014).
16. Olaya-Abril, A., Jiménez-Munguía, I., Gómez-Gascón, L. & Rodríguez-Ortega, M. J. Surfomics: Shaving live organisms for a fast proteomic identification of surface proteins. *J. Proteomics.* **97**, 164–176 (2014).
17. Lorenz, U. *et al.* Human antibody response during sepsis against targets expressed by

methicillin resistant *Staphylococcus aureus*. *FEMS Immunol. Med. Microbiol.* **29**, 145–153 (2000).

18. Sakata, N., Terakubo, S. & Mukai, T. Subcellular location of the soluble lytic transglycosylase homologue in *Staphylococcus aureus*. *Curr. Microbiol.* **50**, 47–51 (2005).
19. Stapleton, M. R. *et al.* Characterization of IsaA and SceD, two putative lytic transglycosylases of *Staphylococcus aureus*. *J. Bacteriol.* **189**, 7316–7325 (2007).
20. Ziebandt, A. K. *et al.* Proteomics uncovers extreme heterogeneity in the *Staphylococcus aureus* exoproteome due to genomic plasticity and variant gene regulation. *Proteomics.* **10**, 1634–1644 (2010).
21. Dreisbach, A. *et al.* Profiling the surfacome of *Staphylococcus aureus*. *Proteomics.* **10**, 3082–3096 (2010).
22. van den Berg, S. *et al.* A human monoclonal antibody targeting the conserved staphylococcal antigen IsaA protects mice against *Staphylococcus aureus* bacteremia. *Int. J. Med. Microbiol.* **305**, 55–64 (2015).
23. Miller, L. S. *et al.* MyD88 mediates neutrophil recruitment initiated by IL-1R but not TLR2 activation in immunity against *Staphylococcus aureus. Immunity.* **24**, 79–91 (2006).
24. Tsompanidou, E. *et al.* The Sortase A Substrates FnbpA, FnbpB, ClfA and ClfB Antagonize Colony Spreading of *Staphylococcus aureus. PLoS One.* **7**, 44646 (2012).
25. Schenk, S. & Laddaga, R. A. Improved method for electroporation of *Staphylococcus aureus. FEMS Microbiol. Lett.* **94**, 133–138 (1992).
26. Neef, J. *et al.* Versatile vector suite for the extracytoplasmic production and purification of heterologous His-tagged proteins in *Lactococcus lactis. Appl. Microbiol. Biotechnol.* **99**, 9037–9048 (2015).
27. ter Weele, E. J. *et al.* Development, preclinical safety, formulation, and stability of clinical grade bevacizumab-800CW, a new near infrared fluorescent imaging agent for first in human use. *Eur. J. Pharm. Biopharm.* **104**, 226–234 (2016).
28. Cho, J. S. *et al.* Neutrophil-derived IL-1β Is Sufficient for Abscess Formation in Immunity against *Staphylococcus aureus* in Mice. *PLoS Pathog.* **8**, 1003047 (2012).
29. Kong, Y. *et al.* Imaging tuberculosis with endogenous β -lactamase reporter enzyme fluorescence in live mice. *Proc. Natl. Acad. Sci. U.S.A.* **107**, 12239–12244 (2010).
30. Ning, X. *et al.* Maltodextrin-based imaging probes detect bacteria *in vivo* with high sensitivity and specificity. *Nat. Mater.* **10**, 602–607 (2011).
31. Panizzi, P. *et al. In vivo* detection of *Staphylococcus aureus* endocarditis by targeting pathogen-specific prothrombin activation. *Nat. Med.* **17**, 1142–1146 (2011).
32. Hernandez, F. J. *et al.* Noninvasive imaging of *Staphylococcus aureus* infections with a nuclease-activated probe. *Nat. Med.* **20**, 301–306 (2014).
33. Bardhan, N. M., Ghosh, D. & Belcher, A. M. M13 Virus based detection of bacterial infections in living hosts. *J. Biophotonics.* **7**, 617–623 (2014).
34. Tang, E. N., Nair, A., Baker, D. W., Hu, W. & Zhou, J. *In vivo* imaging of infection using a bacteria-targeting optical nanoprobe. *J. Biomed. Nanotechnol.* **10**, 856–863 (2014).

Supplementary data

Table S1. Related to bacterial strains and plasmids used in this study

Strains	Relevant phenotype(s) or genotype(s)	Source or reference
B. subtilis 168	trpC2	Laboratory collection
E. coli Xen14	E. coli WS2572 with a stable chromosomal copy of Photorhabdus luminescens lux operon	(1)
E. coli DH5α	λ- ϕ80dlacZΔM15 Δ(lacZYA-argF)U169 recA1 endA hsdR17(rk- mk-)supE44 thi-1 gyrA relA1	Novagen, Madison WI, USA
L. lactis PA1001	MG1363 pepN::nisRK, , ΔacmA ΔhtrA	(2)
S. aureus SH1000	Wild type (rsbU+)	(3)
S. aureus MS001	SH1000 isaA::tet Tcr	(4)
S. aureus SH1000 lux	S. aureus SH1000 pLux(pbp2-pro)	This study
S. aureus MS001 lux	S. aureus MS001 pLux(pbp2-pro)	This study
S. aureus SAP231	NRS384 with integrated P. luminescens lux operon	(5)
S. aureus NCTC8325-4	NCTC8325 cured of ϕ11, ϕ12, and ϕ13	(6)
S. aureus Newman	NCTC 8178 clinical isolate	(7)
S. aureus Newman Δspa	S. aureus Newman spa mutant	(8)
S. aureus Newman Δspa-Δsbi	S. aureus Newman spa sbi mutant	(9)
S. aureus USA300	Community-acquired MRSA isolate	(10)
S. aureus Mu50	Clinical MRSA with complete annotated sequence	(11)
S. aureus MW2	Community-acquired MRSA, USA400	(12)
S. aureus N315	Hospital-acquired MRSA	(11)
S. aureus COL	MRSA clinical isolate	(13)
S. aureus MRSA252	UK hospital-acquired MRSA	(14)
S. capitis	UMCG-MolBac collection	This study
S. caprae	UMCG-MolBac collection	This study
S. epidermidis ATCC 35984	Slime-producing strain, catheter-associated sepsis	(15)
S. epidermidis1457	Biofilm-positive laboratory strain	(16)
S. epidermidis A	UMCG-MolBac collection	This study
S. epidermidis B	UMCG-MolBac collection	This study
S. haemolyticus	UMCG-MolBac collection	This study
S. hominis A	UMCG-MolBac collection	This study
S. hominis B	UMCG-MolBac collection	This study
S. lugdunensis	UMCG-MolBac collection	This study
S. pasteuri	UMCG-MolBac collection	This study
S. pettenkoferi	UMCG-MolBac collection	This study
S. saprophyticus	UMCG-MolBac collection	This study
S. warneri	UMCG-MolBac collection	This study
Plasmids	**Relevant phenotype(s) or genotype(s)**	**Source or reference**
pLux(pbp2-pro)	pSK236 containing penicillin-binding protein 2 (pbp2) promoter fused to the modified luxABCDE from Photorhabdus luminescens	(17)
pNG4110	pNG400 containing his6, BamHI/NotI cloning sites	(18)
pNG4110::isaA	pNG4110 containing S. aureus NCTC8325-4 isaA (30-233a)	This study

his_6, 6 Histidine-tag; [a] position of amino acid residues (AA) in *isaA* sequence of *S. aureus* NCTC8325 (YP_501340)

References

1. Rocchetta, H. L. *et al.* Validation of a noninvasive, real-time imaging technology using bioluminescent *Escherichia coli* in the neutropenic mouse thigh model of infection. *Antimicrob. Agents Chemother.* **45**, 129–137 (2001).
2. Bosma, T. *et al.* Novel surface display system for proteins on non-genetically modified gram-positive bacteria. *Appl. Environ. Microbiol.* **72**, 880–889 (2006).
3. Horsburgh, M. J. *et al.* δb modulates virulence determinant expression and stress resistance: Characterization of a functional rsbU strain derived from *Staphylococcus aureus* 8325-4. *J. Bacteriol.* **184**, 5457–5467 (2002).
4. Stapleton, M. R. *et al.* Characterization of IsaA and SceD, two putative lytic transglycosylases of *Staphylococcus aureus*. *J. Bacteriol.* **189**, 7316–7325 (2007).
5. Plaut, R. D., Mocca, C. P., Prabhakara, R., Merkel, T. J. & Stibitz, S. Stably Luminescent *Staphylococcus aureus* Clinical Strains for Use in Bioluminescent Imaging. *PLoS One.* **8**, 1–6 (2013).
6. Peng, H. L., Novick, R. P., Kreiswirth, B., Kornblum, J. & Schlievert, P. Cloning, Characterization, and Sequencing of Accessory Gene Regulator (agr) in *Staphylococcus aureus*. *J. Bacteriol.* **170**, 4365–4372 (1988).
7. Duthie, E. S. & Lorenz, L. L. Staphylococcal coagulase; mode of action and antigenicity. *J. Gen. Microbiol.* **6**, 95–107 (1952).
8. Patel, A. H., Nowlan, P., Weavers, E. D. & Foster, T. Virulence of protein A-deficient and alpha-toxin-deficient mutants of *Staphylococcus aureus* isolated by allele replacement. *Infect. Immun.* **55**, 3103–3110 (1987).
9. Sibbald, M. J. J. B. *et al.* Synthetic effects of secG and secY2 mutations on exoproteome biogenesis in *Staphylococcus aureus*. *J. Bacteriol.* **192**, 3788–3800 (2010).
10. McDougal, L. K. *et al.* Pulsed-Field Gel Electrophoresis Typing of Oxacillin-Resistant *Staphylococcus aureus* Isolates from the United States: Establishing a National Database. *J. Clin. Microbiol.* **41**, 5113–5120 (2003).
11. Kuroda, M. *et al.* Whole genome sequencing of meticillin-resistant *Staphylococcus aureus*. *Lancet.* **357**, 1225–1240 (2001).
12. Naimi, T. S. *et al.* Epidemiology and clonality of community-acquired methicilin-resistant *Staphylococcus aureus* in Minnesota, 1996-1998. *Clin. Infect. Dis.* **33**, 990–996 (2001).
13. Shafer, W. M. & Landolo, J. J. Genetics of staphylococcal enterotoxin B in methicillin-resistant isolates of *Staphylococcus aureus*. *Infect. Immun.* **25**, 902–911 (1979).
14. Holden, M. T. G. *et al.* Complete genomes of two clinical *Staphylococcus aureus strains*: Evidence for the evolution of virulence and drug resistance. *Proc. Natl. Acad. Sci.* U.S.A. **101**, 9786–9791 (2004).
15. Christensen, G. D., Simpson, W. A., Bisno, A. L. & Beachey, E. H. Adherence of slime-producing strains of *Staphylococcus epidermidis* to smooth surfaces. *Infect. Immun.* **37**, 318–326 (1982).
16. Mack, D., Siemssen, N. & Laufs, R. Parallel induction by glucose of adherence and a polysaccharide antigen specific for plastic-adherent *Staphylococcus epidermidis*: Evidence for functional relation to intercellular adhesion. *Infect. Immun.* **60**, 2048–2057 (1992).

17. Miller, L. S. *et al.* MyD88 mediates neutrophil recruitment initiated by IL-1R but not TLR2 activation in immunity against *Staphylococcus aureus. Immunity.* **24**, 79–91 (2006).

18. Neef, J. *et al.* Versatile vector suite for the extracytoplasmic production and purification of heterologous His-tagged proteins in *Lactococcus lactis. Appl. Microbiol. Biotechnol.* **99**, 9037–9048 (2015).

Chapter 5

Ex vivo tracer efficacy in optical imaging of *Staphylococcus aureus* nuclease activity

Colin W.K. Rosman, Francisco Romero Pastrana, Girbe Buist, Marjolein Heuker, Marleen van Oosten, James O. McNamara, Gooitzen M. van Dam and Jan Maarten van Dijl

Scientific Reports (2018) 8(1):1305

Abstract

The key to effective treatment of bacterial infections is a swift and reliable diagnosis. Current clinical standards of bacterial diagnosis are slow and laborious. There are several imaging modalities that can detect infectious diseases, but none can distinguish between bacterial infection and sterile inflammation. Novel tracers, such as smart-activatable fluorescent probes, represent a promising development that allow fast and specific testing without the use of ionizing radiation. Previously, a smart-activatable probe was developed which is based on the enzymatic activity of the micrococcal nuclease as produced specifically by *Staphylococcus aureus*. In the present study, the function of this probe was validated. Practical applicability in terms of sensitivity was assessed by incubation of the probe with 26 clinical *S. aureus* isolates, and probe specificity was verified by incubation with 30 clinical isolates and laboratory strains of various bacterial pathogens. The results show that the nuclease-specific probe was activated by all tested *S. aureus* isolates and laboratory strains with a threshold of ~10^6–10^7 cells/mL. Moreover, the probe was activated by certain opportunistic staphylococci. We therefore propose that the studied nuclease probe represents a significant step forward to address the need for a rapid, practical, and precise method to detect infections caused by *S. aureus*.

Keywords: *smart-activatable probe; nuclease; fluorescence imaging; Staphylococcus aureus*

Introduction

Bacterial infections are a serious clinical problem in all fields of modern medicine. *Staphylococcus aureus* is one of the largest contributors to in-hospital infections, causing 19.5% of all surgical site infections (SSIs), 14.6% of all Intensive Care Unit (ICU)-acquired pneumonia episodes and 10.1% of all ICU-acquired bloodstream infections in the European Union.[1] Particularly, the rapid acquisition of resistance and the ability to form biofilms makes this pathogen dangerous. Especially methicillin-resistant *S. aureus* (MRSA) is very hard to treat. In 2014, 46.4% of all *S. aureus* associated ICU-acquired infections were caused by MRSA.[1] Common sites of infection with *S. aureus* are catheters, prosthetic devices and SSIs.[2] Biomaterial-associated infections, e.g. of prosthetic devices, and SSIs are especially difficult to treat once biofilm formation has started. Moreover, *S. aureus* is a major cause of many focal bacterial infections, such as osteomyelitis,[3] septic arthritis[4] and pyomyositis.[5] The fact that these patients are often old, morbid and stationary, makes the treatment of these infections even more challenging.

The current standard to diagnose infectious diseases is based on sample collection by, respectively, performing a biopsy or swabbing the affected area, and subsequent culture of these samples. A major downside of this approach is the amount of time and labour it takes to reach a reliable diagnosis.[6,7] Moreover, the different diagnostic techniques are prone to false-negative results.[8] Importantly, focal bacterial infections can be life-threatening, while current diagnostic procedures typically take hours to days, which gives rise to higher hospital costs and patient dissatisfaction. Other ways of detecting infections are the use of anatomical imaging modalities, such as ultrasound, computed tomography (CT) or magnetic resonance imaging (MRI), or functional imaging modalities, such as positron emission tomography (PET), single photon emission computed tomography (SPECT) or scintigraphy.[9,10] These techniques allow detection of infection in the whole body and are non-invasive. However, none of these imaging modalities can discriminate bacterial infection from a sterile inflammation, nor can they give any information about the causative pathogen.[11–14]

In recent years, multiple researchers have proposed techniques to improve imaging modalities for diagnosing infectious diseases by using a wide array of probes and suggesting new imaging approaches.[15] Promising new imaging techniques are fluorescence imaging and photoacoustic tomography (PAT).[16] These techniques do not require any form of ionizing radiation like CT, MRI, PET, SPECT and scintigraphy. Furthermore, they can be used relatively easily in the operating theatre. The main advantage of PAT is that the optical scattering is bypassed by using soundwaves.[15] However, before this imaging method can be used in the clinic, both the PAT capabilities and probe functionality have to be improved.[17]

To be able to distinguish between sterile inflammation and bacterial infection, various probes have been designed that specifically target bacteria. Examples are tracers linked to antibiotics, such as vancomycin,[18] or sugars that are solely metabolized by bacteria, such as sorbitol[19] and maltose.[20,21] These types of tracers do not allow identification of a specific pathogen, but give an indication

of the group of bacteria causing the infection. An even more specific approach involves the use of fluorescently labelled antibodies or nanobodies. In general, it takes approximately 4-6 days for antibodies to reach the optimal target to normal tissue (T/N) ratio, which makes the use of antibodies less practical when rapid diagnosis is needed.[22] Researchers have developed nanobodies that reach the optimal T/N ratio in several hours to overcome this problem.[23] First results look promising, though much more extensive research is needed to safeguard the function after binding to imaging agents and reduce clearance.[23]

Another highly innovative development is based on smart-activatable probes. After activation, these probes emit a different signal from their default state. By determining the T/N ratio, the accuracy of the measurements can be vastly improved.[24,25] Degradative enzymes are optimal targets for this type of probes. A promising enzyme is the micrococcal nuclease, which is a deoxyribonucleic acid (DNA)-degrading enzyme of which many different bacteria express their own, type-specific version.[26] In particular, Hernandez *et al.* have reported a nuclease-activated probe that reacted specifically to staphylococcal nuclease.[27] This so called 'TT-probe' consisted of a fluorophore and a quencher that are connected by a short, 11-base, oligonucleotide. Specifically, the TT-probe used fluorescein amidite (FAM) as a fluorophore, 2 deoxythymidine nucleotides flanked by several 2′-O-methyl modified nucleotides as oligonucleotide and the ZEN and Iowa Black RQ quenchers of Integrated DNA Technologies (IDT). For *in vivo* experiments the FAM was replaced by the fluorophore Cy5.5. The latter probe allowed the detection of a focal *S. aureus* infection within 1 hour *in vitro* and 1-2 hours in mice.

The present study was aimed at validating the function and determining the potential for clinical application of the nuclease-activated P2&3 TT-probe. The P2&3 TT-probe is a derivative of the original TT-probe[27] in which the unmodified TT dinucleotide is placed at nucleotide positions 2 and 3 of the 11-nucleotide-long oligonucleotide (versus positions 5 and 6 in the original TT-probe). This probe derivative was found to yield greater sensitivity for micrococcal nuclease of *S. aureus* than the original TT-probe (McNamara lab, unpublished data). In this study, we focused on the verification of the working mechanism, probe stability in human blood, sensitivity and specificity in a clinical setting.

Materials and methods

Bacterial lab strains and clinical isolates

The *S. aureus* Newman nuclease mutants were a gift from Alexander Horswill, PhD, Department of Microbiology, Roy J. and Lucille A. Carver College of Medicine, University of Iowa, USA. The clinical strains were collected at the diagnostic laboratory of the Department of Medical Microbiology at the University Medical Center Groningen (UMCG) and treated anonymously to ensure patient privacy. Clinical *S. aureus* isolates A/Y (n=25) were collected in a previous study.[28] Isolate Z (n=1) was

collected later. The other clinical strains are presented as species with a number to differentiate between independent isolates of the same bacterial species. These include *Staphylococcus epidermidis* (epi 1-6), *Staphylococcus hominis* (hom 1-3), *Staphylococcus haemolyticus* (haem 1-2), *Staphylococcus pasteuri* (pas 1-2), *Staphylococcus warneri* (war 1-2), *Staphylococcus saprophyticus* (sap 1-2), *Staphylococcus lugdunensis* (lug 1-2), *Staphylococcus capitis* (capi 1-2), *Staphylococcus caprae* (caprae), *Staphylococcus pettenkoferi* (pet) and *Streptococcus pyogenes* (pyo). The laboratory strains used in this study include *Bacillus subtilis* 168, *S. aureus* Newman,[29] *S. aureus* RN4220, *Escherichia coli* DH5α, *S. epidermidis* American type culture collection (ATCC) 35984 and *S. epidermidis* 1457.

Bacterial growth conditions

All bacteria were cultured by plating on a blood agar (BA) with 5% sheep blood (Media Products B.V., Groningen, the Netherlands) and incubated overnight at 37°C. The following day, one colony was resuspended in a round bottom 96-well plate with 200 µL growth medium. *B. subtilis* and *E. coli* were grown in Lysogeny Broth (LB; BD Biosciences, Sparks, MD). All other bacteria were grown in Tryptic Soy Broth (TSB; BD Biosciences, Sparks, MD). After inoculation, the 96-well plate was incubated for 1 hour at 37°C under constant agitation (800 RPM).

Nuclease-probe and assay

The nuclease-activated P2&3 TT-probe was developed at the McNamara lab of the Department of Internal Medicine of the Roy J. and Lucille A. Carver College of Medicine at the University of Iowa, USA, as previously described.[27] The probe was synthesised and high performance liquid chromatography (HPLC) purified by Integrated DNA Technologies (IDT) of Coralville, IA. The probe consists of the following sequence: 5′-FAM-mU T T mU mU mU mU mU mU mU-ZEN-RQ-3′, where FAM is fluorescein amidite, mU is 2′-O-methyl modified U, T is unmodified deoxythymidine, ZEN is the ZEN quencher and RQ is the Iowa Black RQ quencher. The lyophilised probe was dissolved in 10 mM Tris-hydrochloride (Tris-HCl) pH 8.0, 1 mM ethylenediaminetetraacetic acid (EDTA) to a final concentration of 500 µM, and stored at -20°C. For nuclease assays, 9 µL of 10mM Tris-HCl pH 9.0, 10 mM calcium chloride ($CaCl_2$) was added to 1 µL 500 µM probe to yield the probe working stock. For reactions, 1 µL probe working stock was added to 9 µL substrate. Growth medium with added P2&3 TT-probe was considered as negative control. For the positive controls, 1 µL purified nuclease (10 U/mL) was added to the growth medium. The reactions were incubated for 1 hour at 37°C. Subsequently, 290 µL of 10 mM Tris-HCl pH 9.0, 10 mM EDTA was added to stop the activity of the micrococcal nuclease by binding the free Ca^{2+} ions which are needed for nuclease activity. 95 µL of each stopped reaction was transferred in triplicate to a flat bottomed 96-well plate and fluorescence (fluorescein isothiocyanate; FITC) was measured using a Biotek synergy 2.0 plate reader unless stated otherwise. Optics position was set at 'bottom' and the sensitivity at 35.

Secreted and cell wall-bound nuclease assay

To determine the effect of secreted and cell wall-bound nuclease on the nuclease probe activation, three varieties of *S. aureus* Newman strains were used, namely the wild-type strain, a *Δnuc* mutant and a *Δnuc Δnuc2* double mutant. The expression of the *nuc* and *nuc2* genes leads to, respectively, the secretion of active nuclease and the expression of a cell wall-bound nuclease.[30] Probe incubated in TSB served as negative control. Probe incubated in TSB with purified recombinant nuclease served as positive control. Recombinant micrococcal nuclease was purified from *Lactococcus lactis* as previously described.[31]

Blood interference assay

To determine the effect of whole blood and plasma on the probe, the probe was suspended in either plasma or whole blood. Blood was donated by a healthy volunteer and stored in a BD Vacutainer® Blood Collection Sodium Citrate Tube, 0.105M/3.2%. Plasma was obtained by centrifuging the blood for 1 min at 14000 RPM and, thereafter, extracting the plasma. From each blood or plasma suspension with probe, two samples were withdrawn. One sample was incubated with purified nuclease and the other sample without. Probe incubated in phosphate buffered saline (PBS) served as a negative control and was used to correct for background interference. Probe incubated in PBS with purified nuclease served as positive control. After terminating the reaction, nuclease activity in the suspension was measured in triplicate as described above.

Sensitivity, specificity and bacterial growth assays

To determine the sensitivity and specificity of the probe, 1 colony forming unit (CFU) of each bacterial strain was incubated with the nuclease probe per assay and subsequently imaged. Incubations were performed in triplicate. Negative controls were included in the analysis by incubating the probe in growth medium, while for positive controls purified nuclease was added to the TSB or LB. Fluorescence was measured as described above.

To observe the nuclease activity in diverse growth phases of *S. aureus*, four different strains (resp. *S. aureus* Newman, *S. aureus* Newman *Δnuc* and isolates X and U), were cultured overnight in TSB and subsequently washed thrice with PBS. Optical density (OD) was measured at 600 nm and all strains were resuspended in TSB or Roswell Park Memorial Institute medium (RPMI) 1640, to an OD (OD600) of 0.0001. RPMI 1640 medium was supplemented with 2 mM glutamine (GE Healthcare/PAA, Little Chalfont, United Kingdom). After 0, 3, 6, 12, and 24 h of incubation, CFUs were determined through serial dilution and plating in triplicate. Samples were collected and stored at -80°C for subsequent nuclease activity measurements. This experiment was performed thrice.

Statistical analyses

Except where stated otherwise all experiments were performed in triplicate. Mean fluorescence of each well was measured and corrected for background by subtracting the mean fluorescence

levels of negative controls (i.e. blood, plasma or medium with the P2&3 TT-probe). Thereafter, the normalized fluorescence was calculated by dividing the respective fluorescence signal by the positive control (i.e. P2&3 TT-probe in blood, plasma or medium). All P-values were calculated using a Student's t-test in IBM SPSS statistics 22. P-values of <0.05 were considered significant.

Ethical approval

The Independent Ethics Committee of the Foundation 'Evaluation of Ethics in Biomedical Research' (Assen, the Netherlands), approved the protocol for blood donations from healthy volunteers. This protocol is registered by QPS Groningen (code 04132-CS011). All volunteers provided their written informed consent. The study was performed with adherence to the guidelines of the Declaration of Helsinki and local regulations, and all samples were anonymised.

Results

Probe activation by secreted nuclease

To evaluate whether secreted and cell wall-bound nuclease have an effect on the P2&3 TT-probe activation, the probe was incubated with three different *S. aureus* Newman strains, namely the wild-type, a *Δnuc* mutant and a *Δnuc Δnuc2* double mutant. The fluorescence was determined with a Biotek synergy 2.0 plate reader, corrected for the background and normalized. As shown in **Figure 1**, probe activation was almost solely dependent on secreted nuclease. Incubation of the *S. aureus* Newman wild-type strain with the P2&3 TT-probe resulted in a mean fluorescence intensity of 1.115 (SD 0.448), whereas incubation of the *Δnuc* mutant and the *Δnuc Δnuc2* double mutant strains resulted in mean fluorescence intensities of respectively 0.0421 (SD 0.088) and -0.251 (SD 0.038). Both nuclease mutants showed statistically different probe activation levels compared to the wild-type strain (P<0.0001). No statistical difference was observed between both mutants.

Probe stability in human blood and plasma

In order to assess whether blood or plasma has an effect on probe activation, nuclease assay experiments were performed with human blood or plasma. The measured fluorescence was corrected for the background and normalized based on the positive control. **Figure 2** shows that incubation of the P2&3 TT-probe in human blood or plasma alone did not result in probe activation. In contrast, incubation of the probe in human blood or plasma with added purified nuclease resulted in activation of the probe. Incubation of plasma without nuclease resulted in a fluorescence intensity of 0.076 (SD 0.000) compared to plasma with nuclease, which resulted in a fluorescence intensity of 0.969 (SD 0.015; P<0.0001). Similar results are shown for the experiments with human blood without nuclease (a fluorescence intensity of 0.035, SD 0.002), in comparison with human blood including nuclease (a fluorescence intensity of 0.436, SD 0.058; P<0.0001). Importantly, a

significant difference in P2&3 TT-probe activation between incubations of plasma and blood with nuclease was observed (P<0.0001). The lower fluorescence intensity of activated probe in blood can be explained by the fact that there is an overlap in the absorption spectrum of haemoglobin and the emission spectrum of the fluorophore FITC.

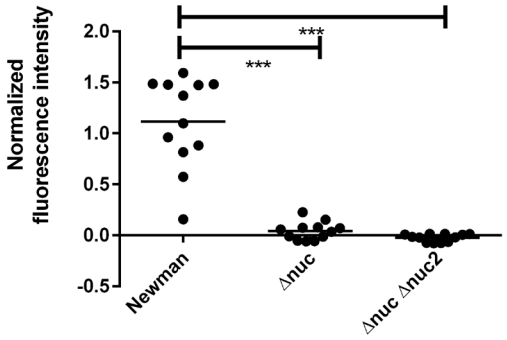

Figure 1. Probe activation by secreted or cell wall-bound nuclease. P2&3 TT-probe activation by *S. aureus* Newman (Newman), the *S. aureus* Newman *Δnuc* mutant (*Δnuc*), which lacks the *nuc* gene that is responsible for the secretion of active nuclease, and the *S. aureus* Newman *Δnuc Δnuc2* double mutant (*Δnuc Δnuc2*). The *nuc2* gene leads to the expression of cell wall-bound nuclease. The horizontal line represents the mean fluorescence detected. *** indicates P<0.0001.

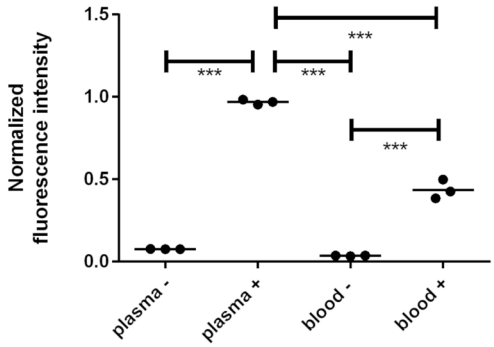

Figure 2. Normalized fluorescence intensity after probe incubation in human blood and plasma. Nuclease was respectively added (+) or omitted (-) in the the assay. The horizontal line represents the mean fluorescence detected. *** indicates P<0.0001.

Sensitivity of the nuclease probe

26 clinical *S. aureus* isolates were incubated with the P2&3 TT-probe in triplicate. The fluorescence signal was corrected for the background and normalized based on the positive control. The mean normalized fluorescence intensity of all clinical isolates was 0.86 (SD 0.43). The cut-off for a positive reaction was set at 43% of the positive control signal. This cut-off point represents the mean activation minus one standard deviation and covers all tested *S. aureus* strains (**Figure 3**). Of note, a large heterogeneity in probe activation was detected. This corresponds with the heterogeneity observed in nuclease production as documented in a previous study where the exoproteomes of 25 of the presently tested clinical *S. aureus* isolates were characterised.[28]

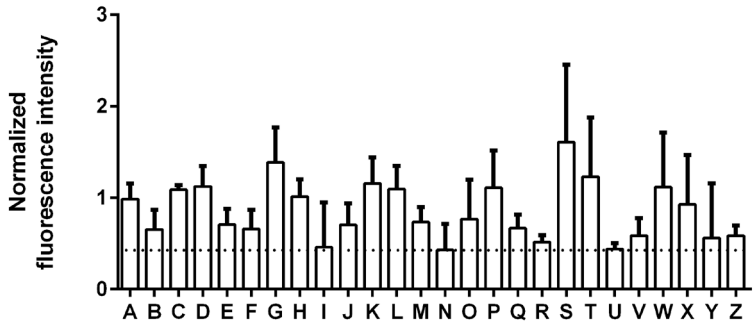

Figure 3. Normalized fluorescence intensity after incubation of clinical *S. aureus* isolates. The letters A-Z indicate the different clinical *S. aureus* isolates used for the nuclease assay. The dotted horizontal line represents the positive cut-off value, which exemplifies the mean activation minus one standard deviation, and is set at 43%. Values represent mean + SD.

For validation of the P2&3 TT-probe activation by different amounts of bacteria or by bacteria grown to different growth stages, we measured the nuclease activity of four different *S. aureus* strains over time. These strains included *S. aureus* Newman wild-type, the nuclease-deficient *Δnuc* mutant, and the clinical isolates X and U. The two clinical isolates were chosen, because of their differing nuclease production levels. Isolate X is a high-level nuclease producer, whereas isolate U is a low-level producer of the nuclease enzyme. All bacteria were grown in both, TSB and RPMI medium. Of note, the RPMI 1640 was used to grow *S. aureus*, because the global gene expression patterns of *S. aureus* cells grown in RPMI or human plasma were recently shown to be highly similar.[32] At T=0, 3, 6, 12, and 24 hours, the CFUs per mL and nuclease activity were measured (**Figure 4**). All strains grew more abundantly in TSB than in RPMI medium. As shown in **Figure 4**, the wild-type Newman strain showed an increase in nuclease activity upon entering the stationary growth phase, while

no nuclease activity was detectable for the isogenic *Δnuc* mutant. As expected, isolate X showed significant nuclease production in the late exponential and stationary growth phases (**Figure 4C**). In contrast, isolate U showed significant nuclease activity during growth in TSB, but it did not show any nuclease activity whilst growing in RPMI medium (**Figure 4D**). With exception of this specific condition, and the nuclease deficient mutant, all strains activated the probe above the threshold at 10^6-10^7 CFU/mL, regardless of the growth medium used.

Essentially the same results were obtained when the nuclease activity in the samples was measured with the so-called poly T-probe (**Supplementary Figure S1**). This poly T-probe consists of the same fluorophore and quencher as the P2&3 TT-probe, but the connecting oligonucleotide consists of 11 unmodified thymine bases.[33] This results in a higher sensitivity for nuclease activity which enables detection of the lower level of nuclease in isolate U when it is grown in RPMI, but lowers the specificity to staphylococcal nuclease as the poly T-probe can be degraded by many different endonucleases.[27]

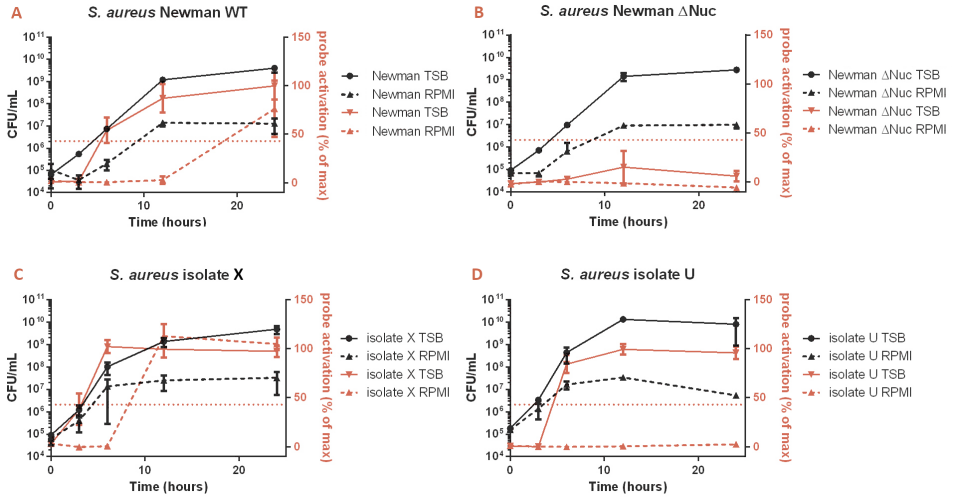

Figure 4. Activation of the P2&3 TT-probe by *S. aureus* at different growth phases. Diverse isolates of *S. aureus* were grown over time in TSB or RPMI medium. The strains included were (**A**) *S. aureus* Newman wild-type; (**B**) a nuclease deficient *S. aureus* mutant (*Δnuc*); (**C**) *S. aureus* clinical isolate X;[28] and (**D**), *S. aureus* clinical isolate U.[28] CFUs/mL and nuclease activity were measured at T=0, 3, 6, 12 and 24 hours. The black graphs represent the bacterial growth density in CFU/mL, while the red graphs represent the probe activation as a percentage of the maximum activation. Data represent mean ± SD of the triplicate fluorescence measurements.

Specificity of the nuclease probe

To verify the specificity of the P2&3 TT-probe, 30 different bacterial laboratory and clinical strains of various species were incubated and fluorescence emission was measured. These strains included two *S. aureus* laboratory strains (Newman and RN4220), four non-*S.aureus* laboratory strains (i.e. *B. subtilis* 168, *E. coli* DH5α, *S. epidermidis* ATCC 35984 and *S. epidermidis* 1457), and a total of 24 clinical isolates of 12 different bacterial species as described above. Abiding by the cut-off point that was previously determined, eight bacterial isolates tested positive for nuclease activity. These included *S. aureus* Newman, *S. aureus* RN4220, *S. lugdunensis* 1 and 2, *S. caprae*, *S. capitis* 1 and 2, and *B. subtilis* 168 (**Figure 5A**). The 22 other strains tested negative with values lower than the cuto-ff point of 43% (**Figure 5B**).

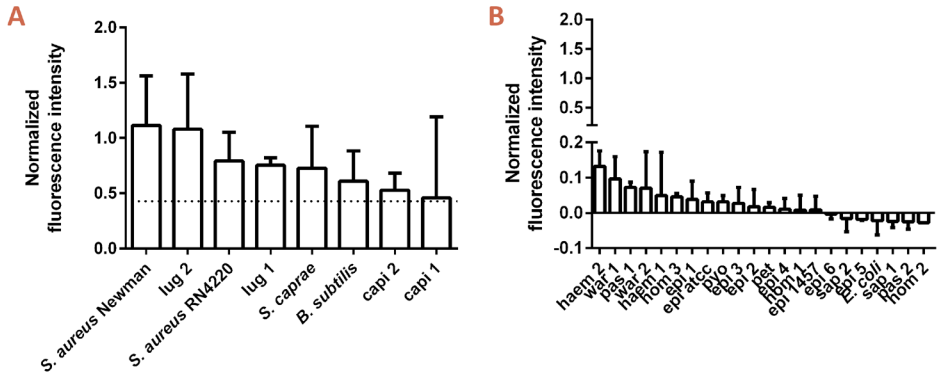

Figure 5. P2&3 TT-probe activiation by different bacterial species. (**A**) Normalized fluorescence intensity upon P2&3 TT-probe activation of all strains that tested positive. The horizontal line represents the positive cut-off value of 43%. (**B**) Normalized fluorescence intensity of strains that tested negative upon P2&3 TT-probe administration. Values represent mean + SD.

Discussion

The objective of this research was to validate the function of the nuclease-activated P2&3 TT-probe, an optimised version of the probe described by Hernandez *et al.*,[27] and to assess its *ex vivo* efficacy in optical imaging of *S. aureus* infections. All incubations were done in 1 hour, demonstrating the swiftness of the process and the potential for a fast and accurate diagnosis of infections caused by *S. aureus*. As expected, the P2&3 TT-probe was consistently activated by secreted nuclease of a variety of clinical *S. aureus* isolates. Apart from *S. aureus*, incubation with four other staphylococcal

species also resulted in activation of the probe.

The P2&3 TT-probe proved to be stable and maintained its function in both, human blood and plasma. However, the signal strength was much lower in human blood than observed in plasma. This might be explained by the overlap of the FITC label emission spectrum (521 nm) and the absorption spectrum of hemoglobin.[34] Nevertheless, *in vitro* absorption of the P2&3 TT-probe's fluorescence does not have to pose a problem, as long as the normalization standard is subject to the same degree of absorption. For *in vivo* use, or use in an assay that includes haemoglobin, a different fluorophore will have to be used. For example, imaging *in vivo* with a Cy5 fluorophore instead of FITC was already established by Hernandez *et al.*[27]

The clinical *S. aureus* isolates tested are representative for the diversity of *S. aureus* that can be encountered in a clinical setting, in our case at the UMCG. Our results thus show that the P2&3 TT-probe is an effective tool to detect the presence of such different *S. aureus* isolates. The signal strength observed in the different *S. aureus* incubations showed a great heterogeneity, as was to be expected based on previous proteome analyses that had shown variety in the levels of nuclease produced by different clinical *S. aureus* isolates.[28] This heterogeneity implies that nuclease production, and therefore probe activation, is likely to be different for every *S. aureus* strain.

Three of the four non-*S. aureus* species that tested positive are regarded as harmless, being soil bacteria (*B. subtilis*) and non-pathogenic human commensals (*S. capitis* and *S. caprae*). The fourth bacterium that tested positive is *S. lugdunensis*. This species is regarded as a true pathogen and has been implicated in infections reminiscent of *S. aureus* infections.[35] Activation of the TT-probe by *S. lugdunensis* was also reported by Hernandez *et al.*[27] We note that Hernandez *et al.* and Brakstad *et al.* found relatively lower levels of nuclease activity produced by *S. lugdunensis*,[27] *S. capitis*[36] and *S. caprae*[36] as compared to *S. aureus*. As most of the signals in the positives of **Figure 5A** are essentially saturated, it is difficult to derive relative levels of nuclease activity from these samples. Our results are thus not inconsistent with these previous reports. Of note, all tested bacterial species that can cause infection gave a positive signal with the probe, while bacterial species that produce non-micrococcal nucleases did not activate the probe. This indicates that the tested P2&3 TT-probe has a high application potential in a clinical-diagnostic setting. One concern could be that mutations in the nuclease-encoding gene could cause a diagnostic resistance. To date, there has been no large investigation on the possible occurrence of nuclease-deficient *S. aureus* in the clinic. However, nuclease plays an important role in *S. aureus* biofilm dynamics and has been widely used as a specific marker for *S. aureus*. Thus, it seems unlikely that spontaneous nuclease mutations will occur. Two other conceivable complications are (i) that it is not precisely known how nuclease production is influenced by random mutations that can be encountered in a clinical setting, or (ii) what influence different growth conditions may have on nuclease production. The lack of P2&3 TT-probe activation by the clinical *S. aureus* isolate U grown in RMPI medium is an example of the latter possibility. Here, it should be noted that isolate U is the clinical isolate with the lowest nuclease

production levels in our collection.

Altogether, our present observations support the view that smart-activatable probes are a promising development towards rapid, robust, sensitive and specific diagnostic and imaging tools. Importantly, the presently studied P2&3 TT-probe allows for specific *in vitro* imaging of nucleases produced by pathogenic staphylococci without the use of ionizing radiation. Future use of this probe could be in clinical diagnostic tools or in the context of an imaging modality. Clinical applications may include the identification of *S. aureus* on patient material (like skin or body fluids), material that has been in contact with patients (like bandages, prosthetics or catheters) or even *in vivo* imaging during and after surgery. Additional research will be needed to investigate all possible future applications.

Competing interests

The authors declare no competing financial interests.

Author contributions statement

CWKR, FRP, GB, MH, MvO, JOM and JMvD conceived and designed the experiments. CWKR and FRP planned and performed the experiments. JOM supplied the probe. CWKR, FRP, GMvD and JMvD wrote the manuscript. All authors have reviewed and approved the manuscript.

References

1. European Centre for Disease Prevention and Control. Annual epidemiological report 2014. Antimicrobial resistance and healthcare-associated infections. Available from: http://ecdc.europa.eu/en/publications/Publications/antimicrobial-resistance-annual-epidemiological-report.pdf (2015). [Accessed 25th May 2016].
2. Carnicer-Pont, D. *et al.* Risk factors for hospital-acquired methicillin-resistant *Staphylococcus aureus* bacteraemia: A case-control study. *Epidemiol. Infect.* **134**, 1169–1173 (2006).
3. Carek, P. J., Dickerson, L. M. & Sack, J. L. Diagnosis and Management of Osteomyelitis. *Am. Fam. Physician.* **63**, 2413–2420 (2001).
4. Clerc, O., Prod'hom, G., Greub, G., Zanetti, G. & Senn, L. Adult native septic arthritis: A review of 10 years of experience and lessons for empirical antibiotic therapy. *J. Antimicrob. Chemother.* **66**, 1168–1173 (2011).
5. Agarwal, V., Chauhan, S. & Gupta, R. K. Pyomyositis. *Neuroimaging Clin. N. Am.* **21**, 975–983 (2011).
6. Davies, C. E. *et al.* A prospective study of the microbiology of chronic venous leg ulcers to reevaluate the clinical predictive value of tissue biopsies and swabs. *Wound Repair Regen.* **15**, 17–22 (2007).
7. Lipsky, B. A. *et al.* Expert opinion on the management of infections in the diabetic foot. *Diabetes. Metab. Res. Rev.* **28**, 163–178 (2012).
8. Gardner, S. E. *et al.* Diagnostic validity of three swab techniques for identifying chronic wound infection. *Wound Repair Regen.* **14**, 548–557 (2006).
9. van Oosten, M. *et al.* Targeted imaging of bacterial infections: advances, hurdles and hopes. *FEMS Microbiol. Rev.* **39**, 892–916 (2015).
10. Glaudemans, A. W. J. M., Slart, R. H. J. A., van Dijl, J. M., van Oosten, M. & van Dam, G. M. Molecular imaging of infectious and inflammatory diseases: A terra incognita. *J. Nucl. Med.* **56**, 659–661 (2015).
11. Love, C. & Palestro, C. J. Radionuclide imaging of infection. *J. Nucl. Med. Technol.* **32**, 47–57 (2004).
12. Love, C., Tomas, M. B., Tronco, G. G. & Palestro, C. J. FDG PET of infection and inflammation. *Radiographics.* **25**, 1357–1368 (2005).
13. Strobel, K. & Stumpe, K. D. M. PET/CT in musculoskeletal infection. *Semin. Musculoskelet. Radiol.* **11**, 353–364 (2007).
14. Sarda, L. *et al.* Inability of ^{99m}Tc-Ciprofloxacin Scintigraphy to Discriminate Between Septic and Sterile Osteoarticular Diseases. *J. Nucl. Med.* **44**, 920–926 (2003).
15. Heuker, M. *et al.* Preclinical studies and prospective clinical applications for bacteria-targeted imaging: the future is bright. *Clin. Transl. Imaging.* **4**, 253–264 (2016).
16. Wang, Y. *et al.* Preclinical evaluation of photoacoustic imaging as a novel noninvasive approach to detect an orthopaedic implant infection. *J. Am. Acad. Orthop. Surg.* **25**, 7–12 (2017).
17. Nie, L. & Chen, X. Structural and functional photoacoustic molecular tomography aided by emerging contrast agents. *Chem. Soc. Rev.* **43**, 7132–7170 (2014).
18. van Oosten, M. *et al.* Real-time *in vivo* imaging of invasive- and biomaterial-associated

bacterial infections using fluorescently labelled vancomycin. *Nat. Commun.* **4**, 2584 (2013).

19. Weinstein, E. A. *et al.* Imaging *Enterobacteriaceae* infection *in vivo* with ^{18}F-fluorodeoxysorbitol positron emission tomography. *Sci. Transl. Med.* **6**, 259 (2014).
20. Namavari, M., Gowrishankar, G., Hoehne, A., Jouannot, E. & Gambhir, S. S. Synthesis of [^{18}F]-labelled Maltose Derivatives as PET Tracers for Imaging Bacterial Infection. *Mol. Imaging Biol.* **17**, 168–176 (2015).
21. Gowrishankar, G. *et al.* Investigation of 6-[^{18}F]-fluoromaltose as a novel PET tracer for imaging bacterial infection. *PLoS One.* **9**, 107951 (2014).
22. Rubin, R. H. *et al.* Specific and nonspecific imaging of localized Fisher Immunotype 1 *Pseudomonas aeruginosa* infection with radiolabeled monoclonal antibody. *J. Nucl. Med.* **29**, 651–656 (1988).
23. Chakravarty, R., Goel, S. & Cai, W. Nanobody: The 'magic bullet' for molecular imaging? *Theranostics.* **4**, 386–398 (2014).
24. Elias, D. R., Thorek, D. L. J., Chen, A. K., Czupryna, J. & Tsourkas, A. *In vivo* imaging of cancer biomarkers using activatable molecular probes. *Cancer Biomarkers.* **4**, 287–305 (2008).
25. Savariar, E. N. *et al.* Real-time *in vivo* molecular detection of primary tumors and metastases with radiometric activatable cell-penetrating peptides. *Cancer Res.* **73**, 855–864 (2013).
26. Yang, W. Nucleases: Diversity of Structure, Function and Mechanism. *Quarterly reviews of biophysics.* **1**, 1-93 (2011).
27. Hernandez, F. J. *et al.* Noninvasive imaging of *Staphylococcus aureus* infections with a nuclease-activated probe. *Nat. Med.* **20**, 301–306 (2014).
28. Ziebandt, A. K. *et al.* Proteomics uncovers extreme heterogeneity in the *Staphylococcus aureus* exoproteome due to genomic plasticity and variant gene regulation. *Proteomics.* **10**, 1634–1644 (2010).
29. Duthie, E. S. & Lorenz, L. L. Staphylococcal coagulase; mode of action and antigenicity. *J. Gen. Microbiol.* **6**, 95–107 (1952).
30. Dreisbach, A. *et al.* Profiling the surfacome of *Staphylococcus aureus*. *Proteomics.* **10**, 3082–3096 (2010).
31. Neef, J., Koedijk, D. G. A. M., Bosma, T., van Dijl, J. M. & Buist, G. Efficient production of secreted staphylococcal antigens in a non-lysing and proteolytically reduced *Lactococcus lactis* strain. *Appl. Microbiol. Biotechnol.* **98**, 10131–10141 (2014).
32. Mäder, U. *et al. Staphylococcus aureus* Transcriptome Architecture: From Laboratory to Infection-Mimicking Conditions. *PLoS Genet.* **12**, 1–32 (2016).
33. Burghardt, E. L. *et al.* Rapid, culture-free detection of *Staphylococcus aureus* bacteremia. *PLoS One.* **11**, 1–17 (2016).
34. Weissleder, R. & Ntziachristos, V. Shedding light onto live molecular targets. *Nat. Med.* **9**, 123–128 (2003).
35. Herchline, T. E. & Ayers, L. W. Occurrence of *Staphylococcus lugdunensis* in consecutive clinical cultures and relationship of isolation to infection. *J. Clin. Microbiol.* **29**, 419–421 (1991).
36. Brakstad, O. G., Maeland, J. A. & Chesneau, O. Comparison of tests designed to identify *Staphylococcus aureus* thermostable nuclease. *APMIS.* **103**, 219–224 (1995).

Supplementary data

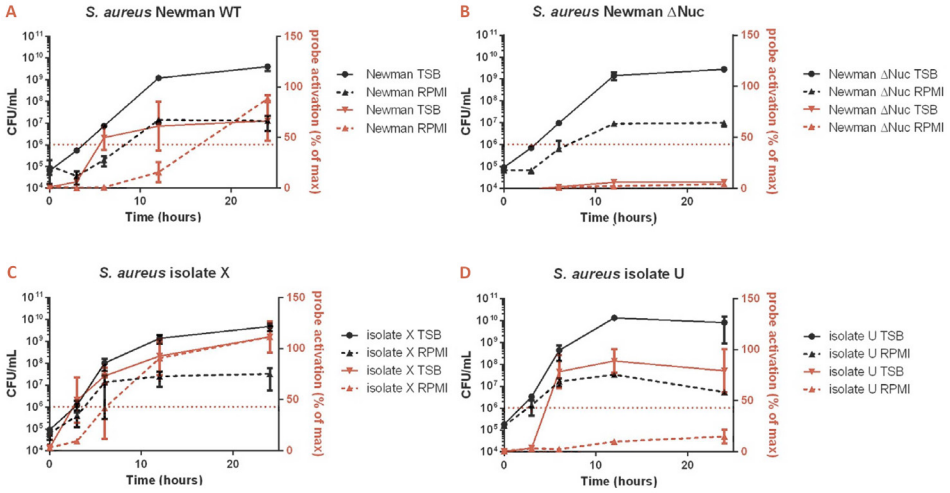

Figure S1. Activation of the poly T-probe by *S. aureus* at different growth phases. The poly T-probe consists of the same fluorophore and quencher as the P2&3 TT-probe, but the connecting oligonucleotide consists of 11 thymine bases. This results in a higher sensitivity for nuclease activity, but lowers the specificity to micrococcal nuclease as this probe can be degraded by many different endonucleases.[27] The experiment was conducted using the same samples that were used for measurements with the P2&3 TT-probe in **Figure 4**. The strains included were (**A**) *S. aureus* Newman wild-type; (**B**) a nuclease deficient *S. aureus* mutant (*Δnuc*); (**C**) *S. aureus* clinical isolate X;[28] and (**D**), *S. aureus* clinical isolate U.[28] CFUs/mL and nuclease activity were measured at T=0, 3, 6, 12 and 24 hours. The black graphs represent the bacterial growth density in CFU/mL, while the red graphs represent the probe activation as a percentage of the maximum activation. Data represent mean ± SD of the triplicate fluorescence measurements.

Chapter 6

The smart-activatable P2&3 TT-probe allows accurate, fast, and highly sensitive detection of *Staphylococcus aureus* in clinical blood culture samples

Marina López-Álvarez, Marjolein Heuker*, Jorrit W.A. Schoenmakers*, Gooitzen M. van Dam, James O. McNamara, Jan Maarten van Dijl and Marleen van Oosten

** Both authors contributed equally to this work*

Scientific Reports (2020) 5;10(1):19216

Abstract

Staphylococcus aureus bacteraemia (SAB) is associated with high mortality and morbidity rates. Yet, there is currently no adequate diagnostic test for early and rapid diagnosis of SAB. Therefore, this study was aimed at exploring the potential for clinical implementation of a nuclease-activatable fluorescent probe for early diagnosis of SAB. To this end, clinical blood culture samples from patients with bloodstream infections were incubated for 1 hour with the "smart"-activatable P2&3 TT-probe, the total assay time being less than 2 hours. Cleavage of this probe by the secreted *S. aureus* enzyme micrococcal nuclease results in emission of a readily detectable fluorescence signal. Incubation of *S. aureus*-positive blood culture samples with the P2&3 TT-probe resulted in 50-fold higher fluorescence intensity levels than incubation with culture-negative samples. Moreover, incubation of the probe with non-*S. aureus*-positive blood cultures yielded essentially background fluorescence intensity levels for cultures with Gram-negative bacteria, and only ~3.5-fold increased fluorescence intensity levels over background for cultures with non-*S. aureus* Gram-positive bacteria. Importantly, the measured fluorescence intensities were dose-dependent, and a positive signal was clearly detectable for *S. aureus*-positive blood cultures with bacterial loads as low as ~7,000 colony-forming units/mL. Thus, the nuclease-activatable P2&3 TT-probe distinguishes clinical *S. aureus*-positive blood cultures from non-*S. aureus*-positive blood cultures and culture-negative blood, accurately, rapidly and with high sensitivity. We conclude that this probe may enhance the diagnosis of SAB.

Keywords: *bacteraemia; blood culture; Staphylococcus; SAB; tracer; nuclease*

Introduction

Bloodstream infections (BSIs) are serious clinical conditions with high rates of morbidity and mortality.[1–3] *Staphylococcus aureus* is the leading cause of nosocomial bacteraemia and the second most frequent cause of community-acquired bacteraemia.[4] Despite the availability of appropriate antibiotics, annual mortality rates for *S. aureus* bacteraemia (SAB) remain high with ~2 to 10 deaths per 100,000 population.[5,6] Currently, the low bacterial loads in blood of bacteraemia patients delay accurate diagnosis of SAB and appropriate antimicrobial therapy.[4,7] About 18% of the patients with SAB have circulating bacteria at titres of less than 0.04 colony-forming units (CFUs) per mL of blood.[8] In ~25% of the SAB cases, bacterial titres range between 1-10 CFU/mL, but they may reach over 100 CFU/mL in severe bacteraemia cases.[7–9]

The current diagnosis of bacteraemia relies on blood culture methods that take days. Therefore, initial treatment of patients with suspected bacteraemia is based on empiric infection management with broad-spectrum antibiotics, while traditional culture methods are performed to identify the causative organism.[4] As a consequence of the resulting use of broad-spectrum antibiotics, multi-drug-resistant bacteria are more likely to emerge, complicating treatment and leading to worse outcomes. Moreover, initial treatment can be wrong if a *S. aureus* infection is not suspected.

A highly promising molecular detection approach for rapid and culture-independent detection of *S. aureus* infections is based on enzymatic activity of micrococcal nuclease (MN), a protein also referred to as staphylococcal nuclease (SNase) or thermonuclease (TNase), which is specifically and invariably secreted by *S. aureus*.[10–15] The signal-amplifying ability of MN and its relative abundance provide a very sensitive means of detecting *S. aureus*, possibly enabling diagnosis of SAB in hours instead of days.[4]

The present study was aimed at validating the potential for clinical implementation of a nuclease-activatable fluorescent probe named P2&3 TT for diagnosis of SAB. Of note, in addition to MN, *S. aureus* produces a second nuclease (Nuc2), a surface-bound nuclease that exhibits substantially less activity than MN.[13,16,17] Upon specific cleavage of this probe by the secreted MN, it emits a readily detectable fluorescence signal.[12,13] Here we report that the P2&3 TT-probe can distinguish clinical *S. aureus*-positive blood cultures from clinical non-*S. aureus*-positive blood cultures and culture-negative blood, rapidly and with high sensitivity.

Methods

Nuclease-activatable P2&3 TT-probe

The structure of the nuclease-activatable P2&3 TT-probe was previously described.[4,13] In short, it consists of an oligonucleotide comprising 2'- O-methyl modified uridines flanking a pair of unmodified deoxythymidines, which is coupled to fluorescein amidite on the 5'-end and the ZEN

and Iowa Black RQ quenchers on the 3'-end. For the present study, it was synthesised and purified by Integrated deoxyribonucleic acid (DNA) Technologies, Inc. (IDT; Coralville, IA). The lyophilised probe was dissolved in 10 mM Tris-hydrochloride (Tris-HCl) pH 8.0, 1 mM ethylenediaminetetraacetic acid (EDTA) to a final concentration of 391.6 µM and stored at -80°C. For the assay, 1 µL of probe was diluted in 9 µL of 10 mM Tris-HCl pH 9.0, 10 mM calcium chloride ($CaCl_2$) to yield a working stock of 39.16 µM.[13]

Blood culture samples

Clinical blood cultures generated in BD Bactec bottles (Becton, Dickinson and Company, USA) were collected from the department of Medical Microbiology (University Medical Center Groningen; UMCG) after one to two weeks of culturing and storage. All blood culture samples were incubated until marked positive by a BD BACTEC FX Blood Culture System, or until unloaded as culture-negative after 4-7 days. Each blood sample was sub-cultured in parallel according to standard procedures to verify the microbiological diagnosis by plating and matrix-assisted laser desorption/ionization time-of-flight (MALDI-TOF) mass spectrometry.

Blood samples from healthy volunteers

Blood from healthy volunteers was collected in BD Vacutainer Heparin tubes to perform sensitivity assays on the day of the experiment. These blood samples were also used to prepare dilutions of infected-blood cultures to assess the sensitivity of the P2&3 TT-probe.

Determination of bacterial titres

To determine CFUs, serially diluted blood cultures were plated on blood agar media immediately prior to carrying out the nuclease assays, and the respective plates were incubated overnight at 37°C.

Detection of micrococcal nuclease activity in blood

Blood culture samples prior or after dilution with blood from healthy volunteers were supplemented with $CaCl_2$ (10 µM), heated to 90°C for 20 min, and centrifuged for 10 min (16,000 RPM, room temperature). 10 µL of the supernatant were incubated with the P2&3 TT-probe for 1 h at 37°C.[4] Then, 290 µL of the stop solution (10 mM Tris-HCl pH 9.0, 10 mM EDTA) was added to stop activity of the micrococcal nuclease. The stop solution works by restraining the free Ca^{2+} ions needed for activity of the nuclease. Afterwards, 95 µL aliquots of each stopped reaction sample were transferred in triplicate to a flat-bottomed transparent 96-well plate and fluorescence was measured in a Biotek Synergy 2.0 plate reader (BioTek Instruments, Inc., USA). Fluorescence was measured with filters optimal for fluorescein isothiocyanate (FITC), excitation was set at 480 nm and emission at 520 nm, with optics position at "bottom". All measurements were carried out in triplicate at 37°C without shaking.

Statistical analyses

In each experiment, unless stated otherwise, mean fluorescence levels of background controls (e.g., blood without the P2&3 TT-probe) were subtracted from the signal of the measured condition and divided by the signal of the P2&3 TT-probe in buffer to calculate a target-to-background (T/B) signal. The blood was divided into four equal volumes, 1 mL each, of which two were incubated with the probe and two were incubated in parallel without probe. All fluorescence measurements were made in triplicate. All p-values were calculated using a one-way ANOVA in GraphPad Prism 8.1.0. P-values <0.05 were considered significant.

Ethical approval

Permission for this study was obtained via the Medical Ethical Review Board Committee of the UMCG (permission number METc2017/098). The study was performed with adherence to the guidelines of the Declaration of Helsinki and local regulations, and all patient samples were treated pseudo-anonymously. Of note, during the present study period, patients admitted to the UMCG complied with hospital guidelines in an opt-out research consent procedure. Consequently, individual written consent was not required for inclusion of their diagnostic waste materials in our study, as consent was given through this opt-out practise unless stated otherwise in the medical file. Blood donations from healthy volunteers were collected with approval of the medical ethics committee of the UMCG (approval number METc 2016/621). All blood donations were obtained after written informed consent from all volunteers, in accordance to the Helsinki Guidelines and local regulations, and all the samples were anonymised.

Results

Evaluation of the P2&3 TT-probe in blood culture samples

To test whether the P2&3 TT-probe allows the direct detection of *S. aureus* in blood cultures of SAB patients, 17 blood cultures, identified as *S. aureus*-positive with conventional culture-based methods, were spiked with calcium chloride, heat-treated and centrifuged. Notably, the heat treatment was previously shown to increase the detection sensitivity of MN by several orders of magnitude through the inactivation of potential MN inhibitory antibodies in human serum.[4] The supernatants were then incubated with the probe at a concentration of 3.9 µM. Indeed, probe activation was observed in all 17 cases as shown in **Figure 1**. In contrast, incubation of the probe with culture-negative blood (n=7) or non-*S. aureus*-positive blood cultures (n=32) did not result in probe activation and, consequently, only marginal fluorescence was detected. The differences in fluorescence signals obtained upon probe incubation with *S. aureus*-positive blood cultures compared to *S. aureus*-negative blood cultures containing other Gram-positive bacteria (p=0.0006)

or Gram-negative bacteria (p<0.0001), or compared to culture-negative blood (p<0.0001) were statistically significant (**Figure 1**).

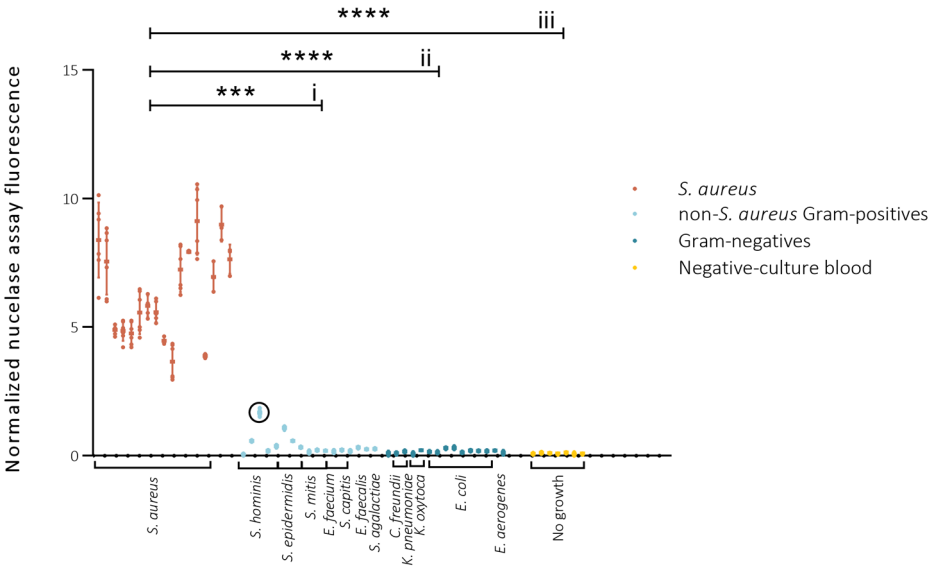

Figure 1. Evaluation of the P2&3 TT-probe in blood cultures. Nuclease activity assays were carried out with blood culture samples from: patients with negative-culture outcomes (n=7, yellow), and patients with positive blood culture outcomes for non-*S. aureus* pathogens including both Gram-positive bacteria (n=17, light blue) and Gram-negative bacteria (n=15, dark blue), or *S. aureus* (n=17, red) (probe concentration 3.9 µM). The detected pathogens are indicated. After correction for the background based on subtraction of the fluorescence value of each blood sample without the probe, fluorescence values were normalized to the average fluorescence values of the probe signal in buffer. Variations in nuclease activity in the different blood samples are indicated by dots. Of note, a *S. hominis*-infected blood culture co-infected with *S. saprophyticus* and *S. epidermidis* is marked with a circle. The fluorescence intensity of this sample (1.67, SD 0.16) is higher than expected based on the T/B value for *S. hominis*. Possibly, this sample contained also a minor undetected fraction of *S. aureus*, or the detected *S. hominis*, *S. epidermidis* or *S. saprophyticus* secreted a nuclease that can cleave the probe. To test statistical significance, the nuclease activity measured in *S. aureus*-positive blood culture samples was compared with that in blood cultures testing positive for Gram-positive non-*S. aureus bacteria* (i), Gram-negative bacteria (ii), or negative blood culture samples (iii). **** Indicates P<0.0001, *** indicates P=0.0006 (Kruskal-Wallis GraphPad Prism 8.0.1).

To calculate T/B ratios, for each investigated blood culture sample the background fluorescence of the sample without probe was subtracted from the fluorescence measured for the sample incubated with probe. Next, the resulting background-corrected fluorescence value of the sample was normalized by dividing it by the signal of the P2&3 TT-probe in buffer. This showed that probe incubation in *S. aureus*-positive blood culture samples resulted in an average normalized fluorescence intensity of 6.08 (SD 2.03), whereas this number was 0.12 (SD 0.09) for culture-negative blood culture samples. Probe incubation in non-*S. aureus*-positive blood cultures yielded an average normalized fluorescence intensity of 0.17 (SD 0.08) for Gram-negative bacteria and 0.42 (SD 0.41) for non-staphylococcal Gram-positive bacteria. Probe incubation with blood cultures positive for other *Staphylococcus* species resulted in average normalized fluorescence intensities of 0.63 (SD 0.59) for *Staphylococcus hominis*, 0.67 (SD 0.34) for *Staphylococcus epidermidis*, and 0.19 (SD 0.04) for *Staphylococcus capitis* (**Figure 2**).

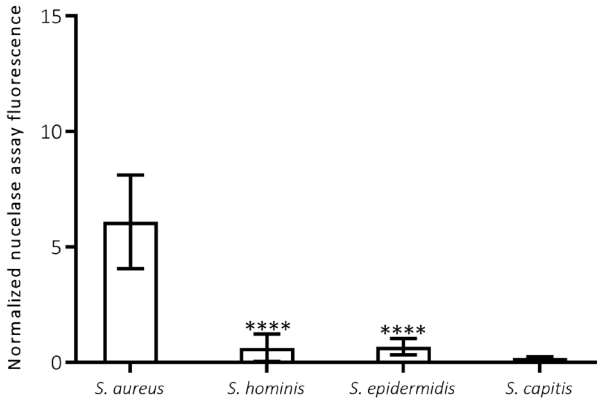

Figure 2. Nuclease activity in blood cultures of *Staphylococcus* species. Average nuclease activity in blood cultures of *S. aureus*, *S. hominis*, *S. epidermidis* and *S. capitis*. 10 µL of blood culture supernatant was incubated with the P2&3 TT-probe for 1 hour at 37˚C and fluorescence was measured and corrected as previously indicated. **** Indicates P<0.0001. (Brown-Forsythe and Welch GraphPad Prism 8.0.1).

Evaluation of P2&3 TT-probe sensitivity for *S. aureus* detection in blood

Considering the strong performance of the probe in blood cultures, we next evaluated its potential in detecting *S. aureus* directly in patient blood samples. An *S. aureus*-positive blood culture was step-wise diluted in healthy donor blood to simulate *S. aureus*-positive, uncultured blood. We spiked the sample with calcium chloride, heated and incubated the heat-treated sample supernatants with

3.9 µM probe. CFU counting was performed in parallel to determine the input bacterial loads. As expected, the highest fluorescence intensity was observed with undiluted *S. aureus*-positive blood culture, but with as much as 104-fold dilution corresponding to ~7,000 CFU/mL, a fluorescence signal that was clearly distinguishable from the control signal of the corresponding *S. epidermidis*-positive blood cultur dilution was obtained (**Figure 3**).

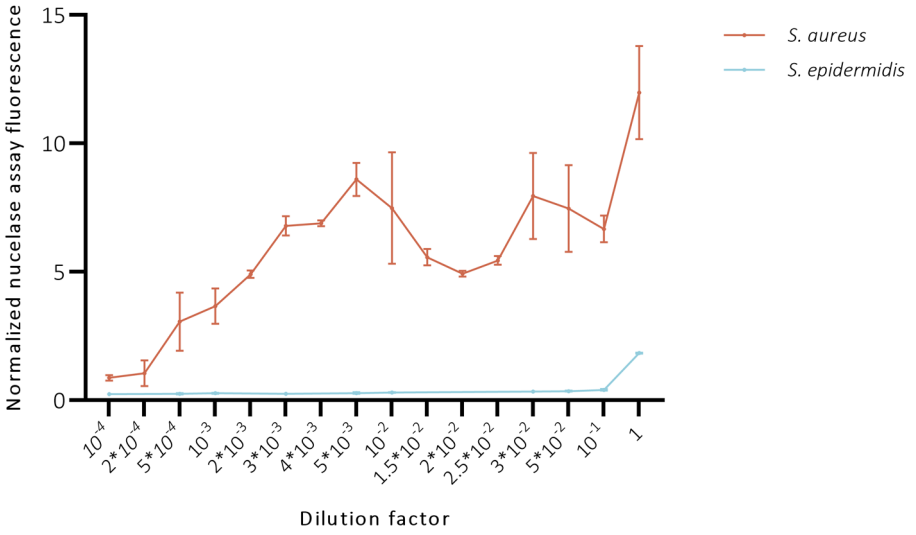

Figure 3. Evaluation of the P2&3 TT-probe in blood cultures diluted with blood from healthy volunteers. Nuclease activity assays were carried out with dilutions from *S. aureus* and *S. epidermidis*-positive blood cultures (**Figure 1**) (probe concentration 3.9 µM). The initial amount of bacteria in the blood cultures (corresponding to dilution factor 1) was 7.1 x10^7 CFU/mL and 2.16 x10^9 CFU/mL for *S. aureus* and *S. epidermidis* respectively. After the correction for the background based on the subtraction of the fluorescence value of each blood sample without the probe, fluorescence values were normalized to the average fluorescence values of the probe signal in buffer.

Lastly, to determine whether *S. aureus*-positive blood could be identified with lower concentrations of P2&3 TT-probe, we incubated two SAB blood culture samples with step-wise reduced P2&3 TT-probe concentrations. This resulted in step-wise reduction of the fluorescence signal, which was still clearly detectable at probe concentrations of ~0.5 µM (**Figure 4A**). In parallel, we investigated whether a substantially lowered *S. aureus* load would be detectable with the P2&3 TT-probe at different concentrations. *S. aureus*-positive cultured blood was 10^4-fold diluted with blood from healthy volunteers and incubated with different concentrations of probe. For the 10^4-fold diluted

S. aureus-positive blood sample, the probe used at the standard concentration of 3.9 µM still gave a clear fluorescence signal that could be distinguished from that of the *S. epidermidis* control. However, this signal was strongly enhanced by using higher probe concentrations, which was tested for a maximum final probe concentration of 39.1 µM (**Figure 4B**). From these sensitivity studies which, together, involved three different *S. aureus*-positive blood cultures with triplicate measurements for each of the three biological replicates (**Figures 3** and **4**), we conclude that the P2&3 TT-probe can enable rapid and precise diagnosis of SAB.

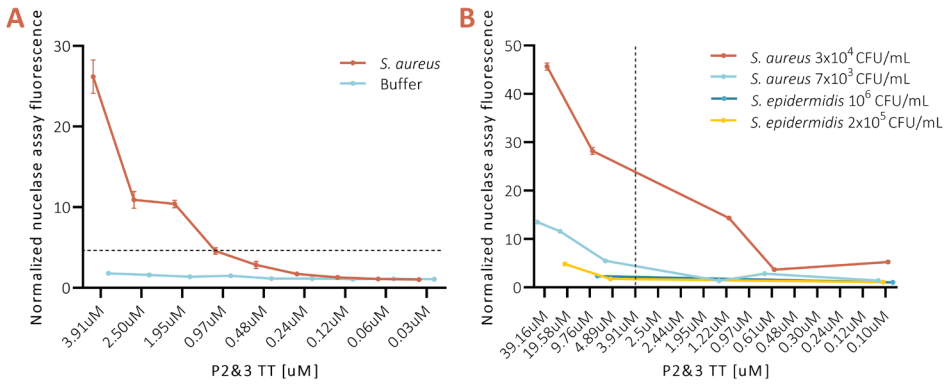

Figure 4. Sensitivity of the P2&3 TT-probe. P2&3 TT-probe was diluted in buffer and incubated at 37˚C for 1 hour (**A**) in blood cultures from SAB patients, or (**B**) in blood cultures diluted with blood from healthy volunteers. Subsequently, fluorescence was measured. Error bars indicate standard deviations of triplicate measurements. The horizontal line represents fluorescence signal considered as positive for *S. aureus* based on the results presented in **Figure 1**. The vertical line represents the probe concentration selected as optimal for SAB blood culture. Normalization of the fluorescence measurements was done by dividing each fluorescence measurement by the signal of each blood sample without the P2&3 TT-probe.

Discussion

Considering the high risk of BSIs for patients, a point-of-care test that provides reliable diagnoses within minutes would be ideal. Unfortunately, current diagnostic methods take much longer, ranging between one to seven days, or more. This delayed diagnosis results in poorer outcome for patients. The empirical broad-spectrum antimicrobial therapy initiated when BSI is suspected can exhibit side-effects and is prone to elicit antibiotic resistance.[18] In worst case, empirical antimicrobial therapy does not cover the causative micro-organism, potentially leading to death of the patient. These concerns are particularly relevant for SAB, because of the high *S. aureus* virulence.[13,19]

Since the previously developed P2&3 TT-probe may offer significantly faster SAB detection,[13] this validation study aimed at assessing its sensitivity and specificity using clinical blood culture samples. Here we demonstrate recovery of active MN from *S. aureus*-positive blood cultures. We specifically detect this enzyme with the P2&3 TT-probe, even after 10^4-fold dilution of cultures prior to probe incubation (corresponding to ~7,000 CFU/mL). Accordingly, we conclude that the detection of SAB with the P2&3 TT-probe is at least 10^4-fold more sensitive than the sensitivity achieved by diagnostic culturing based on the detection of CO_2 as implemented in the BD BACTEC blood culture system (BACTEC Fluorescent Series User's Manual).[16] Of note, this will generally apply to SAB since the P2&3 TT-probe, under presently applied assay conditions, is unlikely to detect BSIs caused by organisms other than *S. aureus*. Further, the nuclease assay takes less than 2 hours and is inexpensive. Methods currently in common use require plating on agar media and incubating until colonies are formed, taking a minimum of 12-14 hours.[1]

Our data support the notion that the P2&3 TT-probe assay can provide the needed specificity for rapid *S. aureus* identification. However, we cannot exclude the possibility that rare infections (e.g. caused by uncommon coagulase-negative staphylococci such as *S. argenteus*, *S. hyicus*, *S. intermedius*, and *S. schweitzeri*) may yield false positive results since they were not encountered in our proof-of-concept study.[20–22] Based on its time-to-result, P2&3 TT-probe-based detection of *S. aureus* provides the means to expedite identification of *S. aureus* bacteraemia by at least several hours versus current methods in common use. As a standalone assay that is specific for a single bloodstream pathogen, this assay will not replace current methods which detect pathogens regardless of their species. Rather, we envision its use as a complementary tool to current methods (e.g. mass spectrometry- and polymerase chain reaction (PCR)-based identification of culture isolates) that provides more rapid identification of the most impactful bacterial bloodstream pathogen.

Lastly, in the present experimental set-up, we have sampled blood culture bottles which, for ethical reasons, was done once culture-positive signals were obtained, or when blood samples tested negative after 4-7 days of culturing. Since CO_2 production during blood culturing is detected with fluorescent tracers in some blood culture devices, it is well conceivable that next-generation MN-activatable probes can be directly implemented in diagnostic blood culture systems. We conclude that MN-activatable probes, like the P2&3 TT-probe can enable rapid and precise diagnosis of SAB.

Transparency declaration

JOM is founder and CEO of Nuclease Probe Technologies Inc., and he holds patents on oligonucleotide-based nuclease-activatable probes for detection of bacterial nucleases. GMvD is CEO, founder and shareholder of AxelaRx / TRACER group, CSO AxelaRx Biosciences Inc. The other authors have no conflicts of interest to disclose.

Funding

ML-A is funded by Marie Skłodowska-Curie Actions grant number 713660 PRONKJEWAIL.

Acknowledgements

We thank Francis Cavallo for helpful discussions.

Contributions

ML-A, MH, JWAS GMvD, JOM, JMvD and MvO conceived the study. JOM, JMvD and MvO supplied materials. ML-A performed the experiments. ML-A, JMVD and MvO wrote the manuscript. All authors reviewed and approved the manuscript.

References

1. Peker, N., Couto, N., Sinha, B. & Rossen, J. W. Diagnosis of bloodstream infections from positive blood cultures and directly from blood samples: recent developments in molecular approaches. *Clin. Microbiol. Infect.* **24**, 944–955 (2018).
2. Bearman, G. M. L. & Wenzel, R. P. Bacteremias: a leading cause of death. *Arch. Med. Res.* **36**, 646–659 (2005).
3. Wisplinghoff, H. *et al.* Nosocomial bloodstream infections in US hospitals: Analysis of 24,179 cases from a prospective nationwide surveillance study. *Clin. Infect. Dis.* **39**, 309–317 (2004).
4. Burghardt, E. L. *et al.* Rapid, culture-free detection of *Staphylococcus aureus* bacteremia. *PLoS One.* **11**, 1–17 (2016).
5. van Hal, S. J. *et al.* Predictors of mortality in *Staphylococcus aureus* bacteremia. *Clin. Microbiol. Rev.* **25**, 362–386 (2012).
6. Braquet, P. *et al.* Factors associated with 12 week case-fatality in *Staphylococcus aureus* bacteraemia: a prospective cohort study. *Clin. Microbiol. Infect.* **22**, 948.e1-948.e7 (2016).
7. Yagupsky, P. & Nolte, F. S. Quantitative aspects of septicemia. *Clin. Microbiol. Rev.* **3**, 269–279 (1990).
8. Jonsson, B., Nyberg, A. & Henning, C. Theoretical aspects of detection of bacteraemia as a function of the volume of blood cultured. *APMIS.* **101**, 595–601 (1993).
9. Henry, N. K. *et al.* Microbiological and clinical evaluation of the Isolator lysis-centrifugation blood culture tube. *J. Clin. Microbiol.* **17**, 864–869 (1983).
10. Ziebandt, A. K. et al. Proteomics uncovers extreme heterogeneity in the *Staphylococcus aureus* exoproteome due to genomic plasticity and variant gene regulation. *Proteomics.* **10**, 1634–1644 (2010).
11. Sibbald, M. J. J. B. *et al.* Mapping the Pathways to Staphylococcal Pathogenesis by Comparative Secretomics. *Microbiol. Mol. Biol. Rev.* **70**, 755–788 (2006).
12. Hernandez, F. J. *et al.* Noninvasive imaging of *Staphylococcus aureus* infections with a nuclease-activated probe. *Nat. Med.* **20**, 301–306 (2014).
13. Rosman, C. W. K. *et al. Ex Vivo* Tracer Efficacy in Optical Imaging of *Staphylococcus Aureus* Nuclease Activity. *Sci. Rep.* **8**, 1–8 (2018).
14. Brakstad, O. G., Maeland, J. A. & Chesneau, O. Comparison of tests designed to identify *Staphylococcus aureus* thermostable nuclease. *APMIS.* **103**, 219–224 (1995).
15. Heins, J. N., Suriano, J. R., Taniuchi, H. & Anfinsen, C. B. Characterization of a nuclease produced by *Staphylococcus aureus*. *J. Biol. Chem.* **242**, 1016–1020 (1967).
16. Hu, Y. *et al.* Characterization and comparative analysis of a second thermonuclease from *Staphylococcus aureus. Microbiol. Res.* **168**, 174–182 (2013).
17. Kiedrowski, M. R. *et al. Staphylococcus aureus* Nuc2 is a functional, surface-attached extracellular nuclease. *PLoS One.* **9**, 95574 (2014).
18. Trecarichi, E. M., Cauda, R. & Tumbarello, M. Detecting risk and predicting patient mortality in patients with extended-spectrum-lactamase-producing *Enterobacteriaceae* bloodstream infections. *Future Microbiol.* **7**, 1173–1189

(2012).

19. Lesens, O. *et al.* Positive surveillance blood culture is a predictive factor for secondary metastatic infection in patients with *Staphylococcus aureus* bacteraemia. *J. Infect.* **48**, 245–252 (2004).
20. Chesneau, O. & El Solh, N. Primary structure and biological features of a thermostable nuclease isolated from *Staphylococcus hyicus*. *Gene.* **145**, 41–47 (1994).
21. Chesneau, O. & El Solh, N. Nucleotide sequence of a nuc gene encoding the thermonuclease of *Staphylococcus intermedius. Nucleic Acids Res.* **20**, 5232 (1992).
22. Schaumburg, F. *et al.* Characterization of a novel thermostable nuclease homolog (NucM) in a highly divergent *Staphylococcus aureus* clade. *J. Clin. Microbiol.* **52**, 4036–4038 (2014).

Chapter 7

Bacteria-targeted fluorescence imaging for visualisation of fracture-related infections in orthopaedic trauma surgery

Marjolein Heuker[†], Marina López-Álvarez[†], Klaas A. Sjollema, Gooitzen M. van Dam, Jan Maarten van Dijl, Frank F.A. IJpma[‡] and Marleen van Oosten[‡]

[†,‡]These authors contributed equally to this work

Under revision for publication in European Journal of Nuclear Medicine and Molecular Imaging

Abstract

Purpose: Fracture-related infection (FRI) is a serious complication in orthopaedic trauma surgery worldwide. Especially the distinction of infection from sterile inflammation and detection of low-grade infection are highly challenging. The aim of the present study was to explore the use of bacteria-targeted fluorescence imaging for enhanced detection of FRI on osteosynthesis devices as a step-up towards real-time image-guided trauma surgery.

Methods: Extracted osteosynthesis devices from 12 patients, who needed revision surgery after fracture treatment, were treated with a near-infrared fluorescent tracer composed of the antibiotic vancomycin and the fluorophore IRDye800CW (i.e. vanco-800CW). Subsequently, the devices were imaged macro- and microscopically. The fluorescence signals were directly correlated to bacterial growth upon replica plating of the extracted devices on blood agar, and to the results of microbiological culturing.

Results: Importantly, compared to culturing, the bacteria-targeted fluorescence imaging of extracted osteosynthesis devices with vanco-800CW allows for prompt diagnosis reducing the time-to-result from days to less than 30 min. Moreover, bacteria-targeted imaging will provide surgeons with real-time visual information on the presence and extent of infection.

Conclusion: Here we present the first clinical application of fluorescence imaging for detection of FRI. We conclude that imaging with vanco-800CW allows early, accurate and real-time visual diagnostic information of FRI in the clinical setting, even in case of low-grade infections.

Keywords: *fluorescence imaging; bone fracture; trauma; bacteria; infection; vancomycin*

Introduction

Fracture-related infection (FRI) is a devastating complication after bone fracture treatment, resulting in severe patient morbidity and loss of quality of life. FRIs can be differentiated in 1) acute infections with clear signs of infection caused by highly pathogenic bacteria, and 2) low-grade infections caused by less pathogenic bacteria. Low-grade infections often lack specific clinical symptoms, which complicates their diagnosis. Treatment of FRI usually consists of revision surgery, including debridement and removal of infected bone and osteosynthesis devices (e.g. plates, nails and screws), combined with long-term antibiotic therapy.[1,2] During surgery, samples are collected for culture to verify infections, and identify causative micro-organisms for specific antibiotic therapy.[2–4] A major challenge is the distinction between non-infected and infected areas during surgery, especially in case of low-grade infections. Surgeons rely on tactile and visual information to establish whether and to what extent wound areas are affected by the suspected infection. Further, a definitive pre-operative diagnosis of FRI is often not possible in case of low-grade infections due to the absence of clinical symptoms. In particular, the results from diagnostic modalities, such as white blood cell scintigraphy, fluorodeoxyglucose positron emission tomography (FDG-PET), or magnetic resonance imaging (MRI) are often inconclusive.[3,5,6] Therefore, a diagnostic imaging tool enabling early, accurate and real-time visualisation of the infecting bacteria themselves, rather than inflammatory responses elicited by the infection, would provide a solution to this clinical problem.

Bacteria-targeted optical (i.e. fluorescence) imaging is an upcoming clinical imaging technique with great potential for the visualisation of infections.[7] In particular, a conjugate of the antibiotic vancomycin and the near-infrared fluorophore IRDye800CW (i.e. vanco-800CW) was previously identified as an effective bacteria-targeted optical tracer in preclinical infection imaging studies.[8,9] Like vancomycin, vanco-800CW specifically targets the Gram-positive bacterial cell wall. Since FRIs are mostly caused by Gram-positive bacteria, such as *Staphylococcus aureus*, vanco-800CW seems particularly suited as a bacteria-targeted optical tracer for real-time diagnosis of FRI. Moreover, vanco-800CW efficiently binds Gram-positive bacterial biofilms encountered in FRI.[10]

The present study was aimed at investigating whether vanco-800CW allows discrimination between infected and non-infected osteosynthesis devices, and whether it can be applied to visualise bacterial biofilms in clinical practice. To this end, we investigated osteosynthesis devices from 12 patients, who needed revision surgery and extraction of plates and/or screws after fracture treatment.

Materials and methods

Fluorescence imaging of extracted osteosynthesis devices

Osteosynthesis devices extracted from 12 trauma patients were included in this study. During surgery, the removed plates were divided in two by using nippers. One half of the plate was

used for fluorescence imaging, the other half was used for regular diagnostics (described in the following section). A number of extracted screws, all retrieved from the same surgical site, were used for regular microbial diagnostics, and some for fluorescence imaging. Upon extraction, the osteosynthesis devices of 12 patients were washed with phosphate-buffered saline (PBS), and incubated with vancomycin-IRDye800CW (vanco-800CW; 0.14 nmol mL-1; Li-COR Biosciences, Nebraska, USA) for 15 min at 37°C. Subsequently, the incubated devices were washed twice with PBS to remove unbound vanco-800CW and imaged in the near-infrared range with an IVIS Lumina II imaging system (Emission filter ICG, Excitation 710 nm, Exposure times 1-10 s; PerkinElmer Inc., USA) and an intra-operative Explorer Air camera coupled to a closed-field imaging box (Vault; Exposure times 100-200 ms; SurgVision B.V. Groningen, NL). Microscopic imaging was performed with a two-photon confocal laser scanning microscope (objective 5x/0.16, filters 500-550/575-610, wavelength 850 nm, Zeiss LSM 7MP) using vancomycin-BODIPY™ FL as a tracer (Thermo Fisher Scientific, USA). Of note, the use of a two-photon microscope was appropriate due to the shape and size of the materials tested (plates and screws) in order to have enough distance between the sample and objective. The fluorescence imaging workflow of extracted osteosynthesis devices is schematically represented in **Figure 1**.

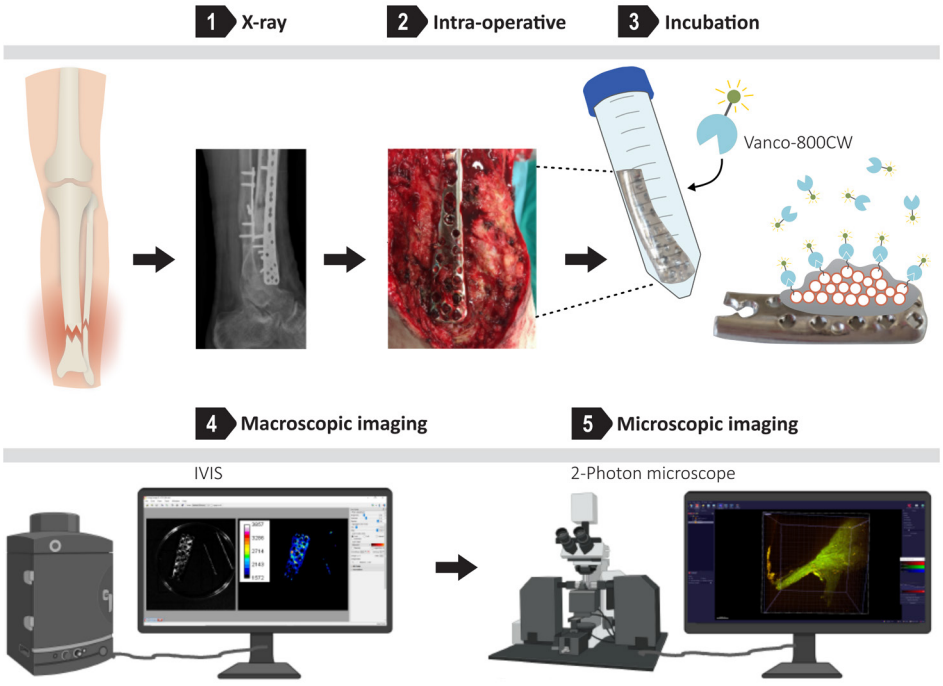

Figure 1. Schematic overview of the fluorescence imaging workflow. Osteosynthesis devices extracted during surgery were washed with PBS and incubated with vanco-800CW (0.14 nmol/mL) for 15 min at 37°C. Subsequently, the incubated devices were washed twice with PBS to remove unbound vanco-800CW and imaged macroscopically with an IVIS Lumina II imaging system and an intra-operative Explorer Air camera coupled to a closed-field imaging box (Vault). For some osteosynthesis devices additional microscopic imaging was performed with a two-photon confocal laser scanning microscope using vancomycin-BODIPY™ FL as a tracer. This figure is created with BioRender.com.

Sonication and cultivation of extracted osteosynthesis devices

The presence of micro-organisms on extracted osteosynthesis devices and collected tissues was independently investigated at the diagnostic microbiology laboratory of the University Medical Center Groningen (UMCG). Sonication of extracted osteosynthesis devices was performed as described by Trampuz *et al.*,[11] with subsequent culturing of the sonicate on aerobic blood agar, chocolate agar, anaerobic blood agar and in blood culture bottles (BD BACTECTM) as liquid culture. The decision whether osteosynthesis devices and/or tissues were infected was taken by the medical team, including a trauma surgeon, infectious disease specialist and a clinical microbiologist according to the standard protocol.

Data analysis

Macroscopic fluorescence images were analysed using ImageJ (National Institutes of Health, Maryland, USA) and Living Image 4.7.3 (PerkinElmer Inc, USA) software. Microscopic images were analysed using Imaris 9.5.0 software. Regions of interest (ROIs) were drawn around the stained osteosynthesis devices after which the fluorescence signal was quantified. The background signal was quantified by drawing ROIs in uncontaminated biomaterials. To determine target-to-background (T/B) ratios, ROIs were divided by the average background fluorescence.

Ethical approval

Only surplus osteosynthesis devices that were considered unnecessary for clinical diagnosis were used for the present bacteria-targeted imaging with vanco-800CW in accordance with the permission obtained from the Medical Ethical Review Board of the UMCG (permission number METc 2016/481). All experiments were performed with adherence to the guidelines of the Declaration of Helsinki and local regulations. Patient data were used pseudo-anonymously based on informed consent.

Results

The investigated patient cohort consisted of 12 patients, who underwent revision surgery in the UMCG between January 2018 and August 2019 to extract osteosynthesis devices after bone fracture treatment. Patients were operated upon clinical suspicion of FRI (i.e. redness, swelling, persistent wound-leakage, non-union, plate breakage; n = 8; **Figure S1**) or for removal of osteosynthesis devices for mechanical reasons (n = 4; culture-negative controls; **Figure S2**). The extracted osteosynthesis devices were treated with vanco-800CW and imaged macro- and microscopically as schematically represented in **Figure 1**. Evaluation of the imaging results obtained with the osteosynthesis devices from all 12 patients included in the present proof-of-principle study with vanco-800CW allowed a clear distinction of infected and non-infected devices, as was independently verified by microbiological culturing. Moreover, no true false-positives or false-negatives were identified (**Figures S1, S2**). This is illustrated with two clinical cases of bacteria-targeted fluorescence imaging with vanco-800CW. Importantly, these cases demonstrate the first clinical application of bacteria-targeted fluorescence imaging.

Bacteria-targeted imaging in an infected non-union of a tibial fracture

A first clinical example of successful bacteria-targeted fluorescence imaging with vanco-800CW in a clinical setting was obtained for a patient with tibial non-union accompanied with acute FRI (**Figure 2**). In this case, a 51-year-old man suffered a lower leg fracture for which he was initially treated with a cast. After 7 months, barely any fracture healing of the tibia had occurred and therefore operative debridement of the non-union site, followed by a cancellous bone graft and tibial plate fixation was performed. The post-operative course was complicated by FRI, characterised by wound dehiscence and eventually an exposed implant (**Figure 2A**, **B**). Therefore, the infected plate and screws had to be removed. The plate was surrounded by debris and minimal cloudy seroma (**Figure 2C**).

Figures 2C and **2D** respectively show the tibial plate *in situ*, upon macroscopic analysis after extraction and 15 min incubation with vanco-800CW. The latter revealed a clear fluorescence signal with a patchy distribution, while control osteosynthesis devices of a confirmed infection-negative patient emitted no fluorescence signals (**Figures 2E-G**; **Figure S1**, patient 11; **Figure S2**, patient 10). Moreover, a bacterial biofilm stained with vanco-BODIPY™ FL was clearly visualised by two-photon microscopy, demonstrating the high binding specificity of vancomycin-based tracers (**Figure 2H**, **I**; for Video, see supplementary data, **Movie S1**). Sonication of extracted biomaterials and subsequent microbiological culturing identified *Corynebacterium tuberculostearicum*, *Staphylococcus aureus* and *Staphylococcus epidermidis* as causative agents of the infection

Detection of low-grade FRI with vanco-800CW

The high sensitivity and specificity of bacteria-targeted optical imaging with vanco-800CW is supported by a second case, where a patient with a fracture-related low-grade infection of the

femur presented no clinical symptoms of infection prior surgery (**Figure 3A**). The X-ray showed a non-union of a femoral fracture with a broken plate (**Figure 3B**). During surgery, no signs of bacterial infection were observed (**Figure 3C**, **D**, **F**). Nonetheless, clear fluorescence signals were detectable upon 15 min incubation of the extracted plate and screws with vanco-800CW (**Figure 3E**, **G**, **I**). Moreover, the fluorescence signals were directly correlated to bacterial growth upon replica plating of the extracted screws on blood agar (**Figure 3H-J**). Microbiological culturing revealed that osteosynthesis devices of this patient carried *Cutibacterium* (*Propionibacterium*) *acnes*..

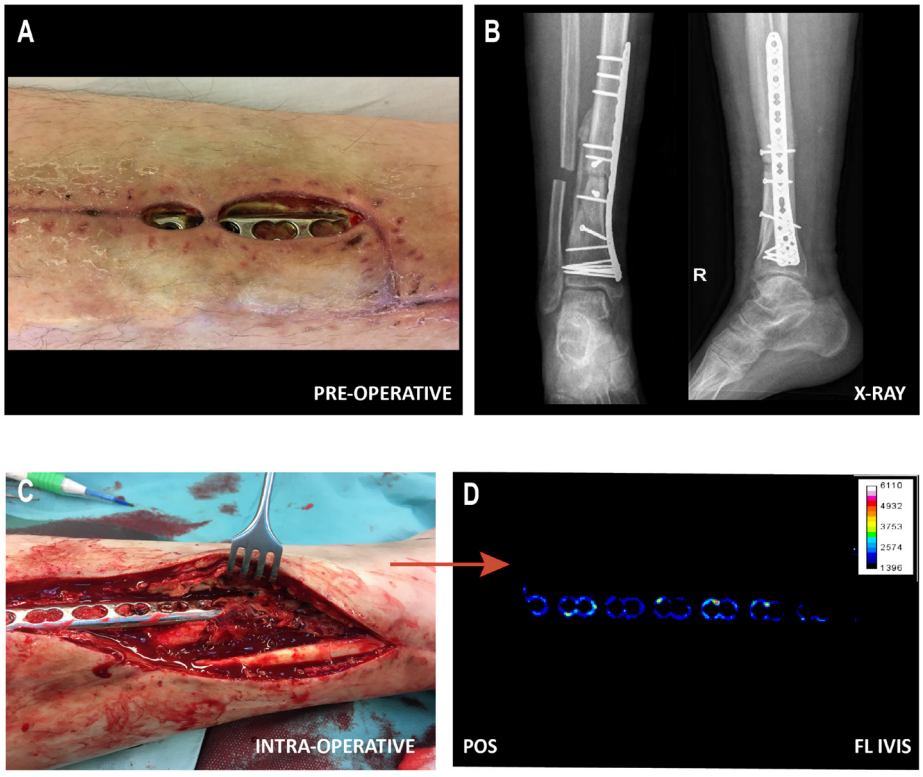

Figure 2. Bacteria-targeted imaging with fluorescently labelled vancomycin of a fracture-related lower leg implant infection. Images relate to patient 11 unless indicated otherwise. **A**. Pre-operative clinical presentation with wound dehiscence and an exposed plate of the lower leg. **B**. X-ray of the delayed union of a crural fracture with tibial plate fixation. **C**. Intra-operative image showing the infected tibial plate prior extraction. **D**. Macroscopic fluorescence image (FL IVIS) of the extracted plate upon staining with vanco-800CW.

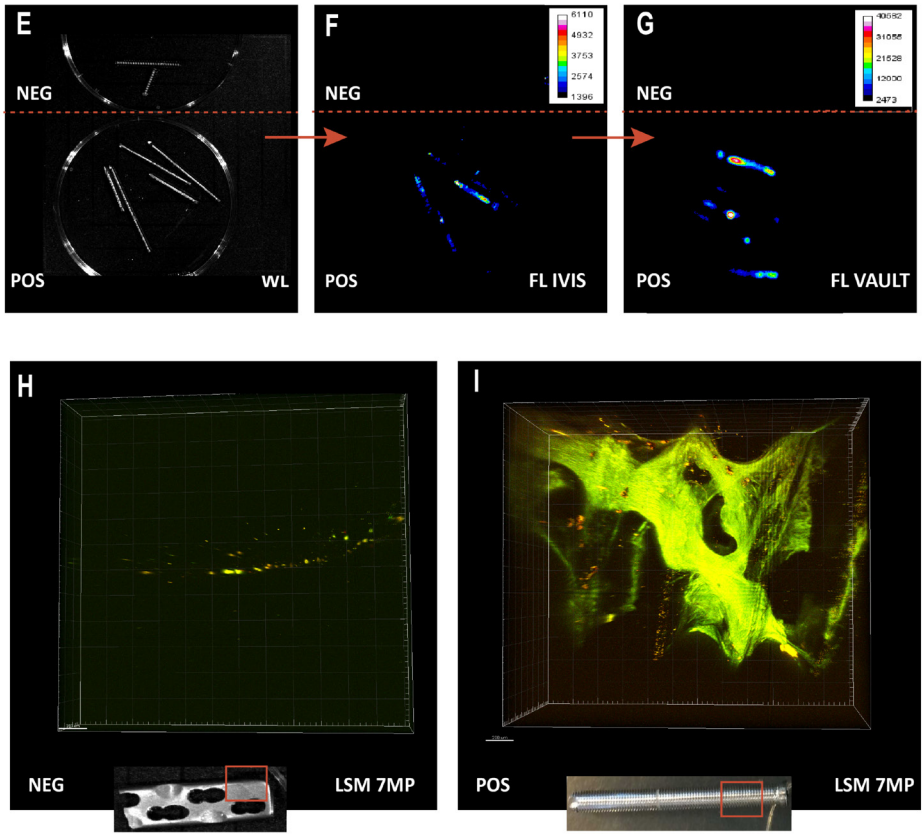

E. White light (WL) image of both infected (POS) and confirmed culture-negative (NEG) extracted screws. Note that the culture-negative screws were obtained from a different patient (patient 10; **Figure S2**), but imaged simultaneously with infected screws of patient 11. **F**,**G**. Fluorescence images of the screws presented in **E** upon staining with vanco-800CW performed with two different imaging devices, respectively an IVIS Lumina II (**F**. PerkinElmer Inc., USA; Excitation 710 nm; Emission filter ICG, Exposure time 10 s) and an intra-operative camera (**G**. Explorer Air coupled to a closed-field imaging box [Vault], SurgVision B.V. Groningen, NL; Exposure times 100-200 ms). **H**,**I**. Microscopic image of a negative control (**H**) and infected screw (**I**) upon staining with vancomycin-BODIPY™ FL showing the biofilm dimensions. Microscopy was performed with a two-photon confocal laser scanning microscope (Zeiss LSM 7MP). Images were analysed with ImageJ, Living Image 4.7.3 and Imaris 9.5.0 software.

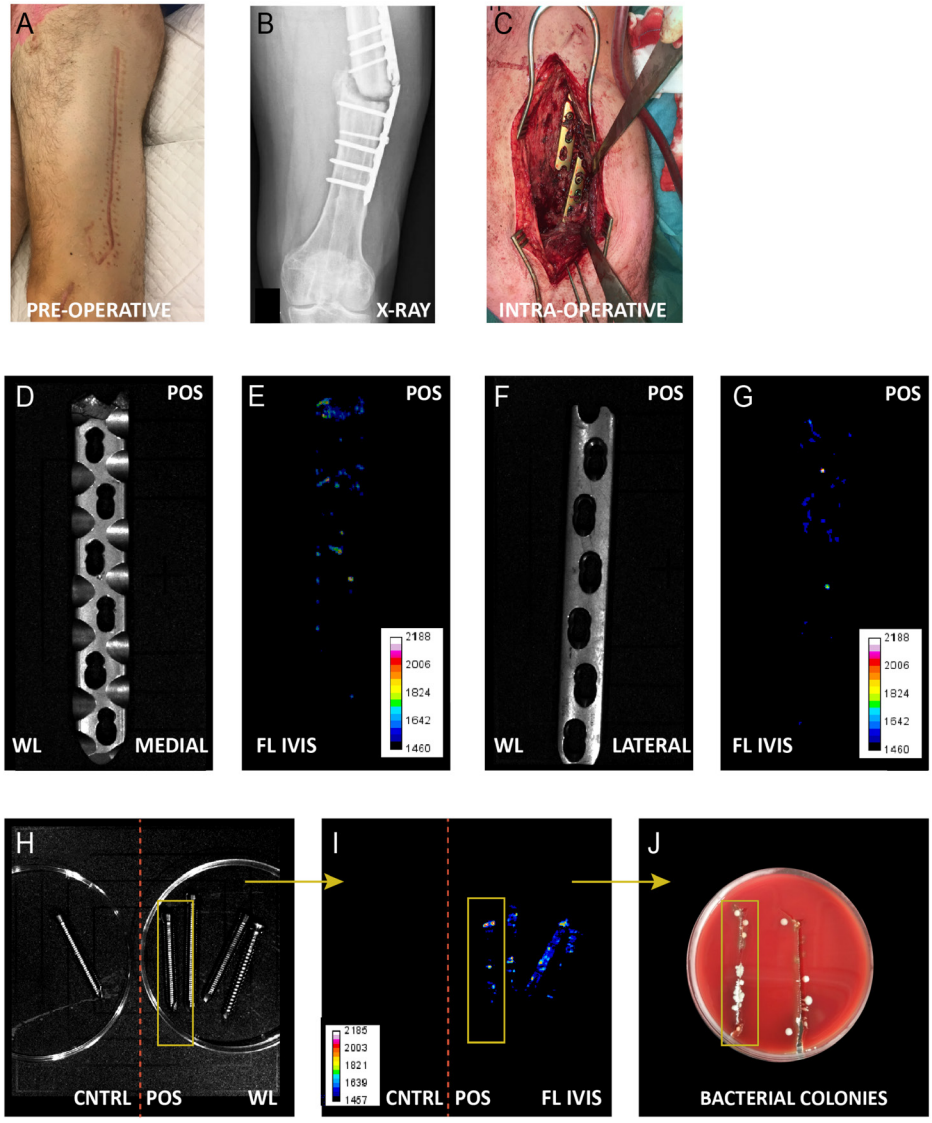

Figure 3. Bacteria-targeted fluorescence imaging and corresponding microbiological culturing of a fracture-related femur infection. Images relate to patient 5. **A**. Pre-operative clinical presentation with no signs of infection at the lateral thigh. **B**. X-ray of a non-union of a femoral fracture with a broken plate. **C**. Intra-operative image showing no signs of infection (e.g. no fluid, abscesses or diseased bone around the broken implant). **D-G**. Macroscopic white-light (WL) images of the back- and front sides of the extracted plate (**D**,**F**) with corresponding fluorescence images (**E**,**G**. IVIS Lumina II; Excitation 710 nm; Emission filter ICG, Exposure time 10 s). **H**,**I**. WL image (**H**) and corresponding fluorescence image (**I**) of suspected infected (POS) and new negative control

(CNTRL) screws (IVIS Lumina II; Excitation 710 nm; Emission filter ICG, Exposure time 10 s). **I**,**J**. Correlation between fluorescence images (**I**) with bacterial colonies on a blood agar plate (**J**). Images were analysed with ImageJ and Living Image 4.7.3 software.

Discussion

The present clinical investigation shows that detection of bacterial growth on osteosynthesis devices by optical imaging with vanco-800CW is highly specific, sensitive, fast and feasible in the clinical setting. On the contrary, the current diagnosis of FRI relies heavily on culture-based methods that may take several days. Hence, patients with suspected FRI are often treated empirically with revision surgery and broad-spectrum antibiotics until the causative organism(s) have been identified. Here we show that imaging of potentially infected osteosynthesis devices with vanco-800CW reduces the time-to-result from days to less than 30 min. This implies that bacteria-targeted fluorescence imaging may significantly enhance intra-operative clinical decision-making regarding empirical antibiotic treatment, extensive debridement, the choice between one- and two-stage revision surgery, or implant exchange.[12] A possible limitation of the fluorescence imaging approach with vanco-800CW is that it cannot replace current diagnostic procedures, because it does not identify the causative agents of FRI and the associated antibiotic resistances. Hence, we regard optical imaging with vanco-800CW as a complementary tool to the current diagnostic methods for prompt visualisation of an infection. Ideally, a definitive diagnosis of the causative agent is needed to direct antibiotic treatment, which may be achieved in the future by the use of multiple tracers next to vanco-800CW, i.e. targeting Gram-negative bacteria, or specific bacterial species.

Based on the present results, we envisage that intra-operative topical application of vanco-800CW, incubation and rinsing off excess and unbound tracer during surgery may provide surgeons with real-time visual information on the presence and extent of infection. Here it is noteworthy that imaging can be performed with doses of vanco-800CW that are ~20-40-fold below the minimal inhibitory concentration (MIC) of vancomycin for staphylococci (https://eucast.org/clinical_breakpoints/).[8,10] Thus, the results of routine diagnostic procedures and culturing will not be affected by the imaging procedure. Another clear advantage of vanco-800CW is its fluorescence in the near-infrared range, which minimizes interference by tissue auto-fluorescence.[6,10,13,14] In our study, an IVIS imaging system and an intra-operative camera coupled to a closed-field imaging box were used to detect the emitted fluorescence signal. The latter camera system is already in use for surgical applications in the operating theatre.[15,16] Yet, prior to any intra-operative application of vanco-800CW, it will be necessary to assess its safety, although vancomycin[17] and the IRDye800CW fluorophore have separately been approved for clinical implementation.[18,19] A second limitation of vanco-800CW is that it will probably not detect FRI caused by Gram-negative bacteria, because vancomycin shows

the highest specificity for Gram-positive bacterial cell walls. However, Gram-negative bacteria cause ~30% of all cases,[20] which implies that vanco-800CW will allow a correct diagnosis of FRI in most cases, a view that is supported by the present results.

Altogether, we conclude that bacteria-targeted optical imaging with vanco-800CW provides new perspectives in the fight against FRI. This technique allows early, accurate and real-time diagnosis of FRI in the clinical setting, even in case of low-grade infections. Moreover, our findings suggest that bacteria-targeted imaging may serve as a highly sensitive tool for rapid detection of implant infections, ranging from osteosynthesis devices to surgical meshes, stents, prosthetic valves and vascular grafts.

Acknowledgments

We thank Pieter Jan Steinkamp for help with the image analysis, the department of Biomedical Engineering at the UMCG, in particular Jelmer Sjollema, for access to the IVIS Lumina II, and Ed de Jong for excellent technical assistance.

Declarations

Funding

ML-A was funded by Marie Skłodowska-Curie Actions grant number 713660 PRONKJEWAIL. MH was funded by the Graduate School of Medical Sciences of the University of Groningen.

Conflict of interest

GMvD is consultant for OncoNano Medicine Inc. and CEO, founder and shareholder of the AxelaRx/TRACER BV group. The other authors have no conflicts of interest to disclose.

Availability of data and material

All data are provided with the manuscript, except data that identify the included patients. Vanco-800CW was purchased from Li-COR Biosciences, Nebraska, USA.

Author contributions

ML-A, MH, GMvD, JMvD, FFAIJ, and MvO conceived the study. JMvD, FFAIJ and MvO supplied materials. ML-A and MH performed the experiments. ML-A and KAS performed the microscopy. ML-A, MH, JMvD, FFAIJ and MvO wrote the manuscript. All authors reviewed and approved the manuscript.

Ethical approval

Permission for this study was granted by the local Medical Ethical Review Board (Medisch Ethische Toetsingscommissie; METc; number 2016/481) for the use of surplus osteosynthesis devices and clinical data, that would not interfere with the diagnostic process. The research was performed with adherence to the guidelines of the Declaration of Helsinki.

Consent to participate

Patients gave informed consent, which included the use of pseudo-anonymised data and samples for the purpose of research and publication.

Consent for publication

All authors have read the manuscript and agree with its publication.

References

1. Engelsman, A. F. *et al.* The risk of biomaterial-associated infection after revision surgery due to an experimental primary implant infection. *Biofouling.* **26**, 761–767 (2010).
2. Morgenstern, M. *et al.* Diagnostic challenges and future perspectives in fracture-related infection. *Injury.* **49**, S83–S90 (2018).
3. Govaert, G. A. M. *et al.* Diagnosing Fracture-Related Infection: Current Concepts and Recommendations. *J. Orthop. Trauma.* **34**, 8–17 (2020).
4. Metsemakers, W. J. *et al.* Fracture-related infection: A consensus on definition from an international expert group. *Injury.* **49**, 505–510 (2018).
5. Ordonez, A. A. *et al.* Molecular imaging of bacterial infections: Overcoming the barriers to clinical translation. *Sci. Transl. Med.* **508**, 8251 (2019).
6. van Oosten, M. *et al.* Targeted imaging of bacterial infections: advances, hurdles and hopes. *FEMS Microbiol. Rev.* **39**, 892–916 (2015).
7. Heuker, M. *et al.* Preclinical studies and prospective clinical applications for bacteria-targeted imaging: the future is bright. *Clin. Transl. Imaging.* **4**, 253–264 (2016).
8. Reeßing, F. *et al.* A Facile and reproducible synthesis of near-infrared fluorescent conjugates with small targeting molecules for microbial infection imaging. *ACS Omega.* **5**, 22071–22080 (2020).
9. van Oosten, M. *et al.* Real-time *in vivo* imaging of invasive- and biomaterial-associated bacterial infections using fluorescently labelled vancomycin. *Nat. Commun.* **4**, 2584 (2013).
10. Schoenmakers, J. W. A. *et al.* Image-guided *in situ* detection of bacterial biofilms in a human prosthetic knee infection model: a feasibility study for clinical diagnosis of prosthetic joint infections. *Eur. J. Nucl. Med. Mol. Imaging.* **48**, 757-767 (2020).
11. Trampuz, A. & Zimmerli, W. Diagnosis and treatment of infections associated with fracture-fixation devices. *Injury.* **37**, 59–66 (2006).
12. Voskuil, F. J. *et al.* Exploiting metabolic acidosis in solid cancers using a tumor-agnostic pH-activatable nanoprobe for fluorescence-guided surgery. *Nat. Commun.* **11**, 1–10 (2020).
13. Joshi, B. P. & Wang, T. D. Targeted Optical Imaging Agents in Cancer: Focus on Clinical Applications. *Contrast Media Mol. Imaging.* **2018**, 2015237 (2018).
14. Mills, B., Bradley, M. & Dhaliwal, K. Optical imaging of bacterial infections. *Clin. Transl. Imaging.* **4**, 163–174 (2016).
15. Steinkamp, P. J. *et al.* Fluorescence-guided visualization of soft tissue sarcomas by targeting vascular endothelial growth factor-A: a phase 1 single-center clinical trial. *J. Nucl. Med.* **62**, 342–347 (2021).
16. van Dam, G. M. *et al.* Intraoperative tumor-specific fluorescence imaging in ovarian cancer by folate receptor-α targeting: first in-human results. *Nat. Med.* **17**, 1315–1319 (2011).
17. Rubinstein, E. & Keynan, Y. Vancomycin revisited - 60 years later. *Front. Public Heal.* **2**, 1–7 (2014).
18. de Jongh, S. J. *et al.* Back-Table Fluorescence-Guided Imaging for Circumferential Resection Margin Evaluation Using Bevacizumab-800CW in Patients with Locally Advanced Rectal Cancer.

J. Nucl. Med. **61**, 655–661 (2020).

19. Voskuil, F. J. *et al.* Fluorescence-guided imaging for resection margin evaluation in head and neck cancer patients using cetuximab-800CW: A quantitative dose-escalation study. *Theranostics.* **10**, 3994–4005 (2020).
20. Maleb, A. *et al.* Bacteriological aspects of chronic osteoarticular infections in adults: The influence of the osteosynthesis material. *BMC Res. Notes.* **10**, 635 (2017).

Supplementary data

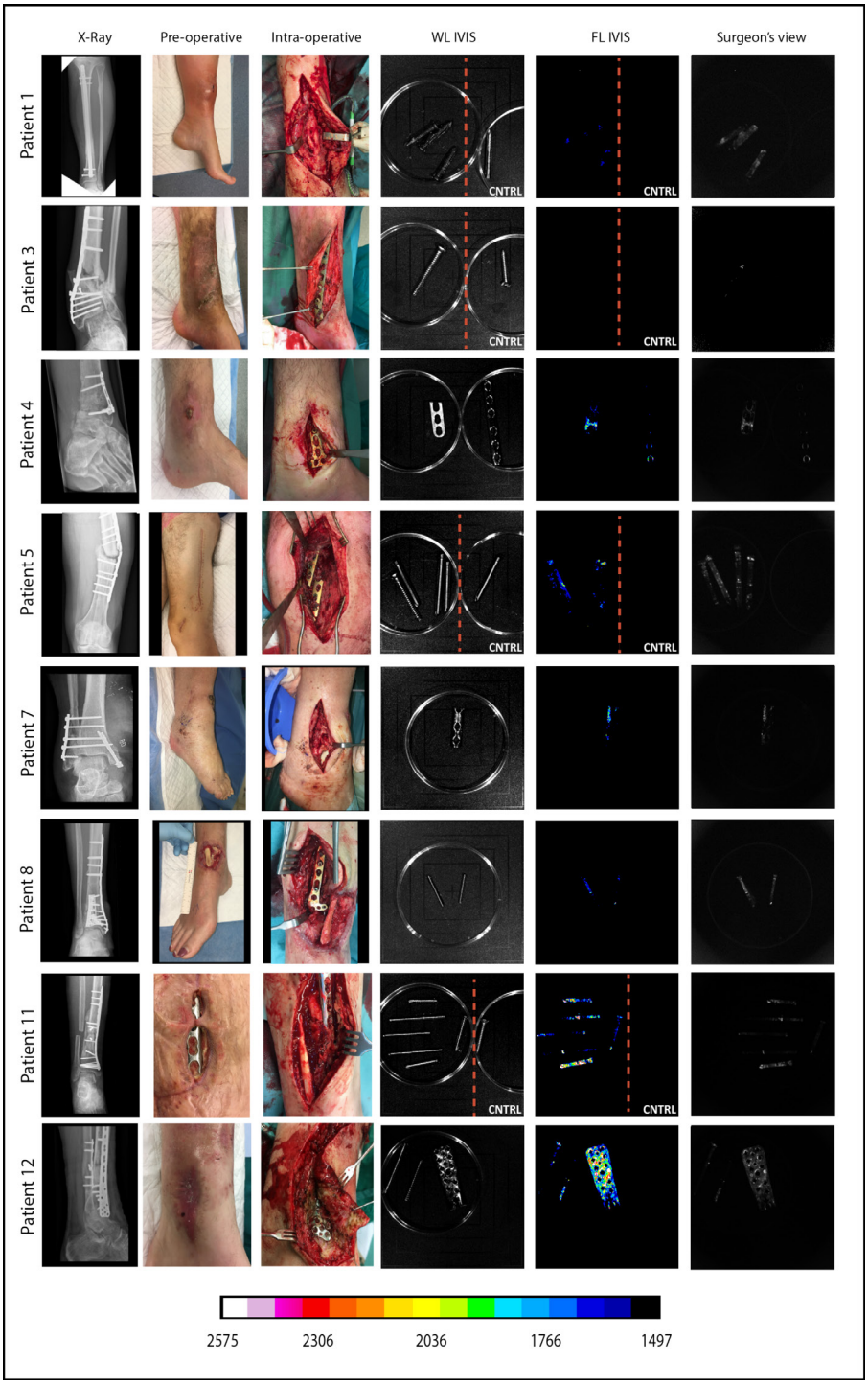

Figure S1. Bacteria-targeted fluorescence imaging of extracted osteosynthesis devices from patients with microbiologically confirmed fracture-related infections. Corresponding X-ray, pre-operative, intra-operative, white light (WL IVIS) and fluorescence (FL IVIS) images (IVIS Lumina II imaging system, PerkinElmer Inc., USA; Excitation 710 nm; Emission filter ICG, Exposure time 10 sec) of 8 patients and their extracted osteosynthesis devices with a microbiologically confirmed fracture-related infection (FRI) after surgery. The right column shows the raw images as can be viewed by the surgeon (Surgeon's view). The presence of micro-organisms on extracted osteosynthesis devices was investigated by culturing in the diagnostic microbiology laboratory of the University Medical Center Groningen, independently from the bacteria-targeted imaging with vanco-800CW. **Patient 1**. *Diagnosis:* FRI after intramedullary nailing of a crural fracture. *Clinical signs:* local redness and swelling with elevated inflammation markers (C-reactive protein 347 mg/L). *Surgery:* removal of the nail, local debridement of the pretibial abscess and cavitary defect of the tibia. *Culture:* low growth density of *Streptococcus anginosus* (Gram-positive). *Imaging:* positive, however, weak signal due to a low bacterial density. **Patient 3**. Diagnosis: infected non-union of the distal tibia with plate breakage. *Clinical signs:* scar tissue on the medial side of the lower leg with some redness. *Surgery:* removal of the broken plate and screws, debridement and washout of the non-union site, temporary antibiotic cement spacer (Masquelet procedure) and application of an external fixator. *Culture: Enterobacter cloacae* (Gram-negative) and *Staphylococcus epidermidis* (Gram-positive) both in very low densities. *Imaging:* positive, however, weak signal due to low Gram-positive bacterial density. **Patient 4**. *Diagnosis:* FRI after multiple operations of a comminuted distal tibial fracture. *Clinical signs:* redness and fistula at the medial malleolus. *Surgery:* excision of the fistula, removal of osteosynthesis devices, local debridement and washout. *Culture: Acinetobacter radioresistens* (Gram-negative), *Citrobacter koseri* (Gram-negative), *Corynebacterium aurimucosum* (Gram-positive), *Corynebacterium jeikeium* (Gram-positive), *Dermabacter hominis* (Gram-positive), *Staphylococcus haemolyticus* (Gram-positive). *Imaging:* positive. **Patient 5**. *Diagnosis:* infected non-union of the left femur with a plate breakage. *Clinical signs:* no clinical signs of infection at the lateral thigh. *Surgery:* removal of the osteosynthesis devices, debridement of the non-union site and reosteosynthesis with an intramedullary nail. *Culture: Cutibacterium* (*Propionibacterium*) *acnes* (Gram-positive). *Imaging:* positive. Note that these data are also shown in **Figure 3** of the main manuscript. **Patient 7**. *Diagnosis:* FRI after osteosynthesis of a Gustillo grade 3 complicated ankle fracture. *Clinical signs:* pain, swelling, redness, septic arthritis, elevated inflammation markers (CRP 280 mg/L). *Surgery:* removal of the osteosynthesis devices, washout of the ankle joint, reosteosynthesis of the medial malleolus. *Culture: Staphylococcus aureus* (Gram-positive). *Imaging:* positive. **Patient 8**. *Diagnosis:* FRI after osteosynthesis of a distal tibial fracture. *Clinical signs:* wound dehiscence with partially exposed plate. *Surgery:* removal of ventral plate and washout of the wound. *Culture: Enterococcus faecalis* (Gram-positive) and *Staphylococcus aureus* (Gram-positive). *Imaging:* positive. **Patient 11**. *Diagnosis:* infected non-union of a crural fracture. *Clinical signs:* wound dehiscence and exposed implant. *Surgery:* removal of infected osteosynthesis devices and a washout of the non-union site. *Culture: Staphylococcus aureus* (Gram-positive). *Imaging:* positive. Note that these data are also presented in **Figure 2** of the main manuscript. **Patient 12**. *Diagnosis:* infected non-union of the distal tibia. *Clinical signs:* local redness, swelling around the scar on the medial malleolus. *Surgery:* removal of plates and screws, debridement of the non-union, temporary antibiotic cement spacer (Masquelet procedure), soft tissue coverage with a latissimus dorsi flap. *Culture: Enterococcus faecalis* (Gram-positive), *Staphylococcus capitis* (Gram-positive) and *Staphylococcus epidermidis* (Gram-positive). *Imaging:* positive. Images were analysed with ImageJ and Living Image 4.7.3 software.

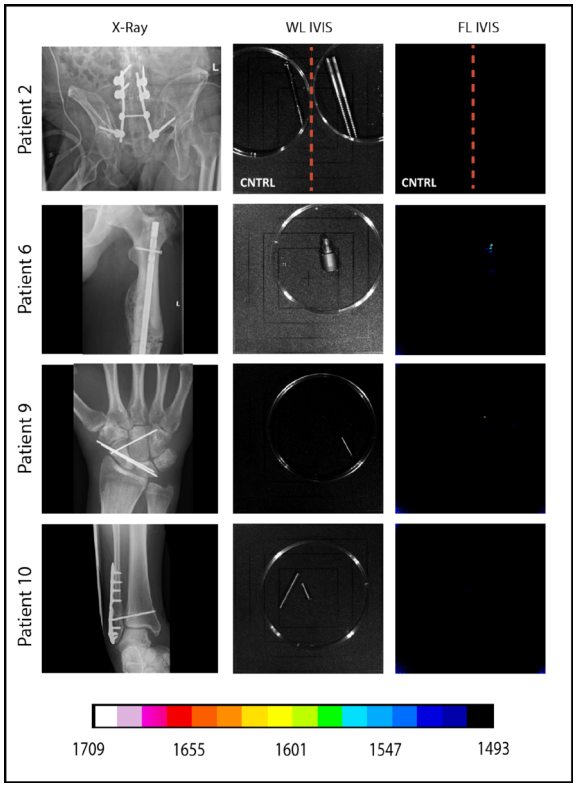

Figure S2. Bacteria-targeted fluorescence imaging of four confirmed culture-negative osteosynthesis devices. Corresponding X-ray, white light (WL IVIS) and fluorescence (FL IVIS) images (IVIS Lumina II imaging system, PerkinElmer Inc., USA; Excitation 710 nm; Emission filter ICG, Exposure time 10 sec) of four patients without detectable implant infections. The absence of micro-organisms on extracted osteosynthesis devices was concluded based on culturing in the diagnostic microbiology laboratory of our hospital, independently from the bacteria-targeted imaging with vanco-800CW. None of the patients showed clinical symptoms of inflammation and all imaging results of extracted osteosynthesis devices incubated with vanco-800CW were negative. **Patient 2**. Extracted lumbo-pelvic fixation device due to lower back pain. **Patient 6**. Removed endcap of a femur nail during exchange nailing for a non-union of a femoral fracture. **Patient 9**. Routinely removed K-wires of the right wrist after treatment of carpal injuries. **Patient 10**. Routinely removed lag screw after open reduction internal fixation of a Weber C ankle fracture. Images were analysed with ImageJ and Living Image 4.7.3 software.

Movie S1. Microscopic fluorescence imaging of an extracted screw from patient 5 with microbiologically confirmed fracture-related infection

Scan me!

Chapter 8

Image-guided *in situ* detection of bacterial biofilms in a human prosthetic knee infection model: A feasibility study for clinical diagnosis of prosthetic joint infections

Jorrit W. A. Schoenmakers, Marjolein Heuker*, Marina López-Álvarez*, Wouter B. Nagengast, Gooitzen M. van Dam, Jan Maarten van Dijl, Paul C. Jutte and Marleen van Oosten

** Both authors contributed equally to this work*

European Journal of Nuclear Medicine and Molecular Imaging (2020) 48(3):757-767

Abstract

Purpose: Due to an increased human life expectancy, the need to replace arthritic or dysfunctional joints by prosthetics is higher than ever before. Prosthetic joints are unfortunately inherently susceptible to bacterial infection accompanied by biofilm formation. Accurate and rapid diagnosis is vital to increase therapeutic success. Yet, established diagnostic modalities cannot directly detect bacterial biofilms on prostheses. Therefore, the present study was aimed at investigating whether arthroscopic optical imaging can accurately detect bacterial biofilms on prosthetic joints.

Methods: Here, we applied a conjugate of the antibiotic vancomycin and the near-infrared fluorophore IRDye800CW, in short vanco-800CW, in combination with arthroscopic optical imaging to target and visualise biofilms on infected prostheses.

Results: We show in a human *post-mortem* prosthetic knee infection model that a staphylococcal biofilm is accurately detected in real-time and distinguished from sterile sections in high-resolution. In addition, we demonstrate that biofilms associated with the clinically most relevant bacterial species can be detected using vanco-800CW.

Conclusion: The presented image-guided arthroscopic approach provides direct visual diagnostic information and facilitates immediate appropriate treatment selection.

Keywords: *infection imaging; prosthetic joint; biofilm; optical tracer; fluorescence*

Introduction

Human life expectancy is presently higher than ever before. The need for biomaterials to replace arthritic or dysfunctional body parts by prosthetics has, therefore, never been greater.[1] Total joint replacement with a prosthesis is nowadays the most performed substitute, which usually contributes to an enhanced quality of life. Approximately two percent of the patients, however, experience device failure in the form of a bacterial infection of the prosthesis and adjacent tissue.[2] These prosthetic joint infections (PJIs) are dreaded complications. They are difficult to diagnose, can manifest at any time after arthroplasty and usually require multiple surgeries and a prolonged course of antibiotic treatment.[3–5] The economic impact of PJIs is accordingly significant with yearly estimated treatment costs exceeding 1.5 billion dollars in the United States alone.[2]

Implanted biomaterials are highly susceptible to infection due to biofilm formation on the prosthetic surface. A bacterial biofilm is a sessile community of bacteria surrounded by a matrix of extracellular polymeric substances (EPS).[6] The matrix, which is produced by the bacteria, acts as a structural network. It captures and disseminates nutrients and functions as a barrier for the host immune system and antibiotics. These properties make the eradication of bacterial biofilms challenging. Moreover, the bacterial tolerance to therapeutic interventions increases as the biofilm matures.[7] This calls for innovative diagnostic tools that allow their early detection.

Established diagnostic modalities for PJIs, such as blood tests, analysis of synovial fluid, culturing, biopsies and imaging all have their pros and cons in detecting infection, but no test is 100% accurate for PJI.[8–10] As a result, the diagnosis often remains unclear, whereas the proper therapeutic approach is uncertain. One factor that consistently plays a role in biomaterial-associated infection, however, is bacterial biofilm formation. Up to date, there are no diagnostic procedures capable of *in vivo* detection of bacterial biofilm on a (total) joint prosthesis.

Targeted fluorescence (i.e. optical) imaging (TFLI) has great potential for the *in vivo* detection of bacterial infections.[11] It relies on the administration of a tracer that consists of an exogenous fluorophore conjugated to a bacteria-targeting molecular probe. After administration of the tracer, a sensitive optical camera readily detects the fluorescence emission at the infection site and converts this into an image on a screen. This allows for high-resolution, low-cost imaging in real-time. A promising tracer is vanco-800CW, which is a conjugate of the antibiotic vancomycin and the near-infrared (NIR) fluorophore IRDye800CW (**Figure 1**).[12] Vanco-800CW is particularly suitable for the detection of PJIs as vancomycin targets the cell wall of Gram-positive (GP) bacteria. Bacteria belonging to this class are the most frequently encountered causative agents of biomaterial-associated infections.[8] Previously, our team has demonstrated that this tracer can be successfully applied to detect a range of planktonic GP bacteria, to detect staphylococcal infections in mice, and to image an infected implant through several millimetres of human skin.[12]

The present proof-of-principle study was aimed at evaluating the possible use of vanco-800CW for detection of PJIs. A human *post-mortem* prosthetic knee infection model was used to assess

the clinical feasibility of detecting bacterial biofilms through TFLI. An arthroscopic approach was chosen for imaging the bacterial biofilms directly intra-articularly on the implanted prosthesis. In addition to the arthroscopy, an *in vitro* experiment was performed to verify that vanco-800CW is a suitable tracer for the detection and imaging of a representative panel of clinical PJI-causing bacterial isolates.

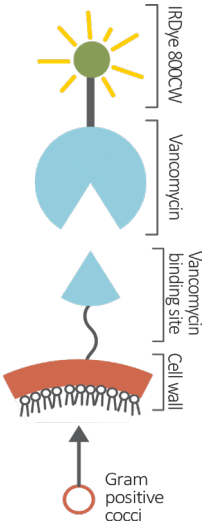

Figure 1. Schematic representation of vanco-800CW and its binding to the bacterial cell wall. The fluorescent tracer vanco-800CW is a conjugate of the antibiotic vancomycin and the near-infrared fluorophore IRDye800CW. It binds to the D-Ala-d-Ala moieties of N-acetylmuramic acid and N-acetylglucosamine peptides in the cell wall of Gram-positive bacteria.[12]

Materials and methods

Human *post-mortem* experiments

The *post-mortem* experiments were performed in duplicate, using the legs of two human cadavers, where each leg was used only once. Both individuals had provided written informed consent for the *post-mortem* use of their bodies for scientific research. All *post-mortem* experiments were conducted in accordance with the applicable law ("Wet op de Lijkbezorging", Art 18, lid 1 and 19, BWBR0005009), and institutional guidelines of the University Medical Center Groningen (UMCG).

Biofilm formation on the lateral part of a knee prosthesis

Before implantation in human cadaver knee joints, cobalt-chrome knee prostheses (size 5 triathlon femoral component, Stryker®, USA) were coated with a biofilm of *Staphylococcus epidermidis*. To this end, the *S. epidermidis* American Type Culture Collection (ATCC) strain 35984 was cultured overnight in 10 mL Tryptic Soy Broth (TSB) at 37°C. 1 mL of the *S. epidermidis* culture with an optical density at 600 nm (OD600) of 0.1 was transferred to a sterile container with 199 mL TSB, 5% glucose and 4% sodium chloride (NaCl). Next, a knee prosthesis was incubated in the suspension with the lateral segment submerged. Accordingly, in this standing culture system, biofilm formation would only occur at the submerged lateral prosthetic region. This allowed for distinction during the arthroscopy between parts with biofilm (lateral side) or without biofilm (medial side). The prosthesis was biofilm-coated in 4 days at 37°C. During this period, medium was manually refreshed once per day by removing 199 mL of suspension and replacing it by 199 mL of fresh TSB with 5% glucose and 4% NaCl.

Formation of a biofilm matrix of EPS on the knee prosthesis was verified by growing the biofilms in the presence of 0.2 mg/mL or 20 mg/mL Congo Red stain (Sigma-Aldrich, Germany) for 4 days at 37°C as described above.[13] Subsequently, the prosthesis was washed twice with phosphate-buffered saline (PBS) and incubated for 30 min with Congo Red (0.004 mg/mL). Lastly, the prosthesis was washed twice with PBS to remove any unbound stain. Images of the stained biofilm on the prosthesis were recorded with a photographic camera.

Total knee arthroplasty

The human cadaver knee joint was disinfected and draped. A longitudinal midline incision anterior of the knee joint was made, the joint was opened in a medial parapatellar fashion to gain access to the knee, and the patella was everted laterally. Subsequently, the knee joint was placed in 90 degrees of flexion. The distal femoral bone cuts were performed using an oscillating saw to allow accurate placement of the femoral component of the prosthesis. A biofilm-coated prosthesis (as described above) was implanted on the distal femur (**Figure 2**). Suturing of the soft tissues was performed in a double layer technique to allow for watertight closure (Ethilon 3-0, Ethicon Somerville, NJ, USA).

Imaging procedures and incubation with vanco-800CW

The knee was placed in 90 degrees of flexion. An intra-articular portal was made by a small incision of 1 cm lateral to the lateral border of the patella tendon in the soft spot just distal to the pole of the patella. An arthroscope (Arthrex, Naples Florida, USA) connected to a saline irrigation pressure pump was placed inside the knee joint cavity. Physiological saline solution ('saline') was pumped into the joint for distention. The prosthesis was then imaged with a white-light and NIR light camera (SurgVision Explorer Custom, Netherlands) with a fluorescence fiber attached to it (Schoelly Fiberoptic GmbH, Germany) as a control prior to the injection of vanco-800CW. The saline was sucked out of the knee with the irrigation system after this first round of imaging.

After imaging, the knee was placed in full extension and 20 mL of vanco-800CW dissolved in saline (0.07 nmol/mL, LI-COR Biosciences, Nebraska, USA) was injected into the knee joint cavity (**Figure 3-1**). The joint was then manually flexed and extended five times to ensure an even dispersion of the tracer. After a 15 min incubation period in extension, the knee joint cavity was thoroughly flushed with the arthroscope irrigation system with 2 L saline to remove all unbound tracer as well as any planktonic bacteria that could potentially be present (**Figure 3-2**). Thereafter, the imaging procedure was repeated (**Figure 3-3**).

Figure 2. Image from the anterior side of the biofilm-coated prosthesis after implantation in the left knee of a human cadaver. The lateral part of the prosthesis was biofilm-coated with *S. epidermidis*, whereas the medial part was essentially sterile.

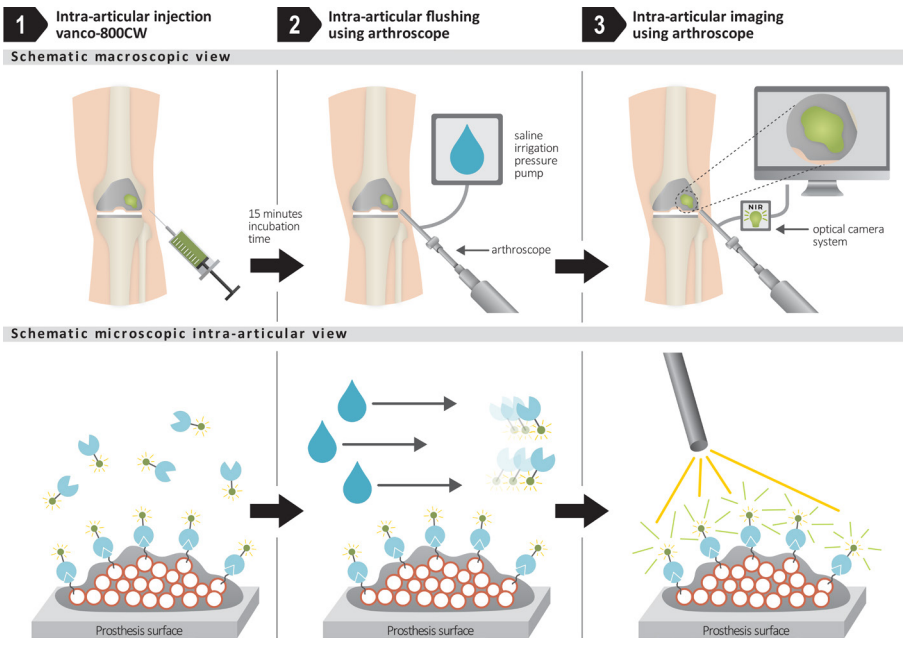

Figure 3. Schematic overview of arthroscopic biofilm imaging using vanco-800CW. (**1**) Vanco-800CW is injected intra-articularly, where it binds to the cell wall of biofilm-resident Gram-positive bacteria. (**2**) By arthroscopically flushing the joint with physiological saline solution, unbound vanco-800CW is removed. As a consequence, this tracer is solely retained in areas where it is bound to Gram-positive bacteria in the biofilm. (**3**) The joint is arthroscopically imaged in the near-infrared range. Fluorescence of vanco-800CW bound to bacteria in the biofilm is visualised on a screen. A video showing the procedure is provided as supplemental **Movie S1**.

TFLI of biofilms of clinical bacterial isolates using vanco-800CW

A representative panel of commonly encountered PJI-causing bacterial pathogens, both GP and Gram-negative (GN), was collected from the diagnostic laboratory of the Department of Medical Microbiology at the UMCG. All clinical isolates were retrieved from sonicated infected biomaterials from patients. Ethical approval for the collection of patient samples was obtained from the medical ethical committee at the UMCG (METC 2017/526). Biofilms of these strains, plus a biofilm of the *S. epidermidis* ATCC 35984 strain (used in the *post-mortem* experiments), were formed on cobalt-chrome discs (diameter 2.5 cm) in 4 days following the same inoculation and standing culture protocol as described for the *post-mortem* experiments above. These biomaterials, plus one sterile control containing no biofilm, were incubated with vanco-800CW (0.07 nmol/mL) and washed twice with PBS. White-light and NIR images were recorded using a fluorescence camera (SurgVision Explorer Air, Netherlands). The formation of EPS in the *S. epidermidis* biofilm was assessed by staining with Congo Red as described above.[13] The stained and imaged biomaterials were sonicated after which serial dilutions of the sonication-fluid were made. Samples were plated on blood agar plates (5% sheep blood, Mediaproducts B.V., the Netherlands) and numbers of colony forming units (CFUs) were determined. The experiment was performed in duplicate.

Fluorescence microscopy of *S. epidermidis* biofilms

S. epidermidis ATCC 38984 was grown overnight at 37°C in TSB using a shaking incubator. Subsequently, the bacteria were diluted in TSB supplemented with 5% glucose and 4% NaCl to a final OD600 of 0.1, and incubated in a 12-well microtiter plate containing 18 mm chemically resistant borosilicate glass coverslips for microscopy (Paul Marienfeld GmbH, Germany). After 48 h of incubation, the coverslips were incubated for 15 min with vancomycin at 0.5, 1, 2, 4 or 8 mg/L final concentration, or without vancomycin. Subsequently, the coverslips were washed once with PBS, incubated with 0.07 nmol/mL of vancomycin-BODIPY™ FL (vanco-BODIPY) for 15 min (Thermo Fisher Scientific, USA), washed once with PBS to remove any unbound tracer, and fixed with 4% paraformaldehyde. Finally, the coverslips were mounted on microscopy slides. Image acquisition was performed with a Leica TCS SP8X microscope.

Data analysis

Fluorescence images of the *post-mortem* experiments and the biofilm experiments with clinical bacterial isolates were analysed using the ImageJ software package (National Institutes of Health, Maryland, US). The detection limit for the fluorescence signal was set at the lowest value at which biofilm signals were visually easily discernible from the negative control signal at biofilm-free sites. For the fluorescence assay, regions of interest (ROIs) were drawn around fluorescent biofilm-coated regions on the biomaterials after which the software quantified the fluorescence signal. The background fluorescence was quantified by drawing a ROI off-target in a background area of the same image. To determine the target-to-background (T/B) ratio, ROIs were divided by the background fluorescence. Graphs were plotted using GraphPad Prism 8.1.1 (GraphPad Software, California, USA). The fluorescence microscopy images recorded to assess competition of the antibiotic vancomycin with vanco-BODIPY for binding to *S. epidermidis* ATCC 38984 were processed using Imaris 9.5.0 software (Oxford Instruments, United Kingdom).

Results

Human *post-mortem* experiment

To assess the formation of genuine *S. epidermidis* biofilms on cobalt-chrome biomaterials, we investigated the presence of EPS by staining the bacteria that had adhered to discs and knee prostheses with Congo Red.[13] This showed that after 4 days of culturing, *S. epidermidis* had indeed formed EPS-containing biofilms on these biomaterials (**Figure 4**).

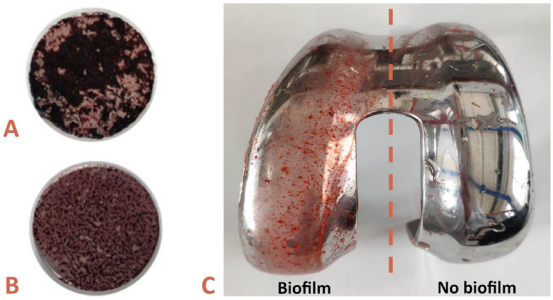

Figure 4. *S. epidermidis* biofilms stained with Congo Red. *S. epidermidis* biofilms were grown in 4 days on cobalt-chrome discs in the presence of 20 mg/mL (**A**) or 0.2 mg/mL (**B**) Congo Red. The *S. epidermidis* biofilm on the cobalt-chrome knee prosthesis, formed after 4 days of culturing, was stained for 30 min with 0.004 mg/mL Congo Red (**C**). Red staining of the biofilms marks the presence of extracellular polymeric substances (EPS).

The clinical feasibility of detecting bacterial biofilms through TFLI was evaluated by total knee arthroplasty with prostheses coated with (unstained) *S. epidermidis* biofilms on the lateral part, and subsequent arthroscopy. Arthroscopic images captured by the white-light camera revealed the spatial distribution of the *S. epidermidis* biofilm on the lateral part of the prosthesis (**Figure 5C**, red dotted line). At the uncoated medial part of the prosthesis, no biofilm was visible (**Figure 5A**). Prior to the administration of vanco-800CW, no NIR fluorescence signal was detectable at both the lateral and the medial side of the prosthesis compared to the background. Upon incubation with vanco-800CW and subsequent washing with saline, the recorded NIR images revealed a strong fluorescence signal emitted from the biofilm-coated lateral part of the prosthesis (**Figure 5D**), whereas the uncoated medial part showed no fluorescence signal, comparable to the background (**Figure 5B**). Co-localisation revealed a high degree of overlap between the white-light camera image and the fluorescence image (**Figure 5C**, **D**).

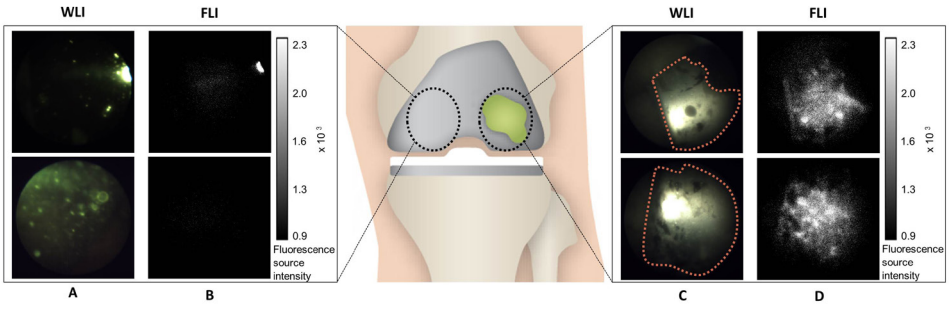

Figure 5. Fluorescence arthroscopic imaging of bacterial biofilms in a human *post-mortem* knee implant model. The green stain represents a *S. epidermidis* biofilm, applied *in vitro* prior to arthroplasty. Images were obtained after 15 min incubation with vanco-800CW and subsequent washing with saline. (**A**) White-light image (WLI) of the uncoated biofilm-free part of the prosthesis. (**B**) Corresponding near-infrared fluorescence image (FLI) of the uncoated part of the prosthesis. The bar on the right marks the corresponding fluorescence signal intensity. The bright spot in the upper image is caused by white light reflection on the implant. (**C**) WLI of the biofilm-coated part of the prosthesis. The biofilm-coated areas are highlighted by the red dotted lines. (**D**) Corresponding near-infrared FLI of the biofilm-coated part of the prosthesis. The bar on the right marks the corresponding fluorescence signal intensity. Settings for fluorescence measurements: exposure 200 ms, gain 300.

Close-up images of the biofilms captured with the white-light camera and the NIR fluorescence camera were subsequently compared. Minor interruptions in the biofilm of only several millimetres wide (**Figure 6A**) were detectable with the white-light camera. These shapes could easily be recognised by the NIR fluorescence camera (**Figure 6B**), providing proof-of-principle that vanco-

800CW and arthroscopic optical imaging can be applied for high-resolution visualisation of bacterial biofilms on infected prostheses.

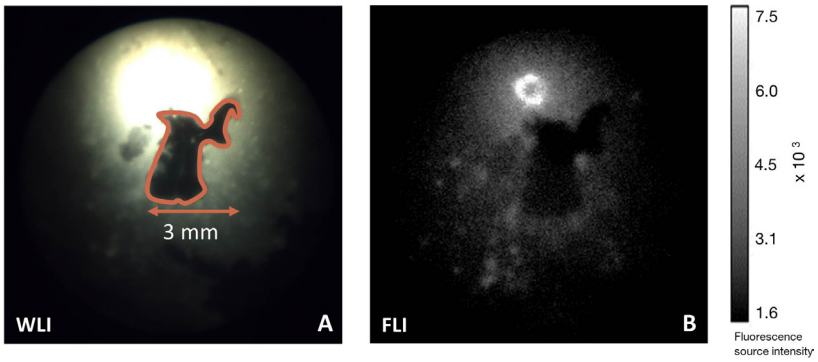

Figure 6. Close-up arthroscopic image of a *S. epidermidis* biofilm in a human *post-mortem* prosthetic knee model. Images were obtained after 15 min incubation with vanco-800CW and subsequent washing with saline. (**A**) White-light image (WLI) of the biofilm. There is a 3-millimeter wide interruption in the biofilm-coated part where biofilm is missing, which is highlighted by the red line. The bright spot above the highlighted area is caused by white light reflection on the implant. (**B**) Near-infrared fluorescence image (FLI) of the biofilm. The bar on the right marks the corresponding fluorescence signal intensity. Note the absence of fluorescence signal at the biofilm-free part of the prosthesis, which correlates with the zone highlighted by the red line in panel **A**. Settings for fluorescence measurements: exposure 800 ms, gain 300.

TFLI to detect biofilms of clinical bacterial isolates using vanco-800CW

A representative panel of 14 clinical bacterial isolates was collected and used to grow *in vitro* biofilms on cobalt-chrome discs. The panel consisted of *Staphylococcus aureus* (2 isolates, GP), *S. epidermidis* (2 isolates, GP), *Staphylococcus lugdunensis* (2 isolates, GP), *Staphylococcus caprae* (2 isolates, GP), *Enterococcus faecalis* (2 isolates, GP), *Escherichia coli* (2 isolates, GN), and *Pseudomonas aeruginosa* (2 isolates, GN). In addition, biofilms of the *S. epidermidis* ATCC 35984 strain were grown on duplicate disks for control. Results of the subsequent biofilm imaging are shown in **Figure 7** (note that per strain only one image is shown). The biofilms of all GP bacterial isolates emitted a strong fluorescence signal (well above 1.0 x 10^4 fluorescence units). In contrast, the GN bacterial isolates emitted a substantially lower fluorescence signal (0.5 - 1.0 x 10^3 fluorescence units), as was to be expected because vancomycin particularly targets GP bacteria. The fluorescence signal detectable for the sterile controls was comparable to the background (<0.5 x 10^3 fluorescence units). After sonication and plating of the sonicates, the CFUs measured for the GP isolates (median: 1.9 x 10^9) were comparable to the CFUs measured for the GN strains (median: 3.5 x 10^8; see **Supplementary**

Table S1 for the CFU counts and fluorescence measurements per ROI per species). Calculated average T/B ratios per species are shown in **Figure 8**. All the GP strains showed a substantially higher T/B ratio (range 14.2 – 56.5, median: 31.8) than the GN strains (range 3.2 – 3.5, median 3.4). The T/B ratios for the sterile biomaterials were 1, meaning that the sterile control presented the same fluorescence intensity as the unstained background.

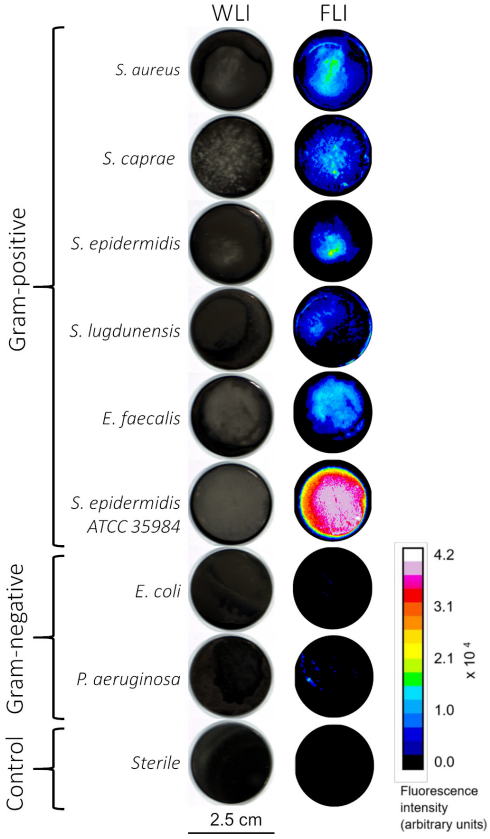

Figure 7. White-light images (WLI) and fluorescence images (FLI) of bacterial biofilms on cobalt-chrome biomaterials after treatment with vanco-800CW. The bacterial isolates were derived by sonication of infected prostheses with the exception of the *S. epidermidis* ATCC 35984 strain, which was also used in the *post-mortem* experiments. Images were obtained after 15 min incubation with vanco-800CW and subsequent washing with PBS. Of note, the *S. epidermidis* ATCC 35984 strain is known for its ability to rapidly form thick biofilms.[14] Consequently, the biofilms formed by the ATCC 35984 strain were thicker and bound more vanco-800CW than those formed by the clinical isolates. The bar on the right marks the correspondence of colour in the FLI to fluorescence signal intensity. Settings for fluorescence measurements: exposure 25 ms, gain 300.

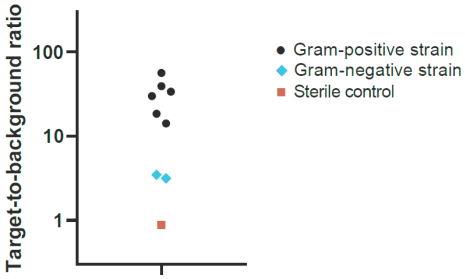

Figure 8. Average target-to-background (T/B) ratios for bacterial biofilms stained with vanco-800CW. Bacterial strains used to grow duplicate biofilms on cobalt-chrome biomaterials were derived by sonication of infected prostheses as described for **Figure 7**. Upon staining of the biofilms with vanco-800CW, the average T/B ratios were determined for each strain. The Gram-positive bacterial strains included clinical isolates of *S. aureus*, *S. epidermidis*, *S. lugdunensis*, *S. caprae* and *E. faecalis*, as well as the *S. epidermidis* ATCC 35984 strain. The Gram-negative bacterial strains included clinical *E. coli* and *P. aeruginosa* isolates. Fluorescence signals were quantified with ImageJ software.

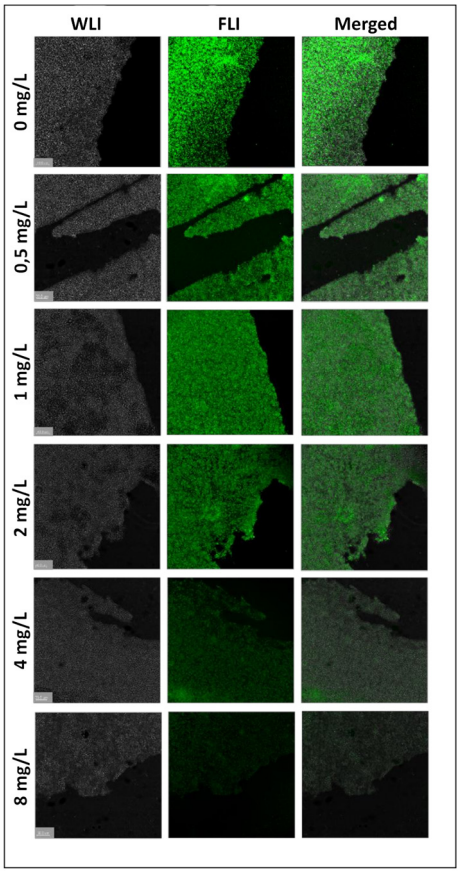

Figure 9. Competitive inhibition of *S. epidermidis* biofilm staining with fluorescent vancomycin by increasing concentrations of unlabelled vancomycin. *S. epidermidis* biofilms were grown on microscopy coverslips. The biofilms were incubated for 15 min with different concentrations of unlabelled vancomycin (up to 8 mg/L; shown on the left), or without vancomycin. After washing with PBS, the biofilms were stained with vanco-BODIPY for 15 min. White-light (WLI) and fluorescence images (FLI) were recorded with a Leica TCS SP8X microscope (magnification 40x).

Competitive inhibition of *S. epidermidis* biofilm staining with fluorescent vancomycin by unlabelled vancomycin

To ascertain that the observed staining of GP bacterial biofilms by the fluorescently labelled vancomycin was vancomycin-specific, we performed a blocking experiment with unlabelled vancomycin. To this end, *S. epidermidis* biofilms grown on microscopy coverslips were treated with unlabelled vancomycin prior to the incubation with fluorescently labelled vancomycin and fluorescence microscopy. In this case we used vanco-BODIPY instead of vanco-800CW, as vanco-BODIPY was more suitable for high-resolution fluorescence microscopy of biofilms in our set-up. The results of the fluorescence microscopy analyses are shown in **Figure 9**. Indeed, pre-treatment of the biofilms with vancomycin at concentrations higher than 2 mg/L resulted in a gradual decrease of biofilm staining by vanco-BODIPY. This shows that the observed labelling with fluorescent vancomycin derivatives is vancomycin-specific.

Discussion

In this proof-of-principle study, we show that arthroscopic detection and real-time imaging of bacterial biofilms on a human knee prosthesis is feasible with vanco-800CW. In addition, we demonstrate that this tracer is highly effective in tracking biofilms formed by representative clinical GP bacterial isolates. As current diagnostic modalities for the detection of PJIs often yield inconclusive results, successful treatment can be hampered and lead to an increased patient- and healthcare burden. Therefore, the development of fast and accurate novel bacteria-targeting diagnostic modalities is desirable. The potential advantages of arthroscopic TFLI in comparison with present diagnostic modalities for PJIs are considerable. The presently shown ability of TFLI to detect and image bacterial biofilms *in situ* on a prosthesis, both in high-resolution and in real-time, are aspects that mark this technology's exceptional potential for clinical implementation.

Especially in oncological research, pioneering clinical studies have demonstrated the benefits of TFLI guided detection of cancer, surveillance biopsies and surgical resection.[15,16] To date, infection imaging with TFLI has never been done in patients, but has proven extremely promising *in vitro* and *in vivo*.[11] Due to recent (technical) advances concerning fluorophores, targeting molecules and

optical camera systems, the first-in-man studies exploiting TFLI in infection imaging are expected within the next few years according to Mills *et al.*[17] Moreover, fluorescently-labelled antimicrobial peptides and antibiotics, such as vanco-800CW, are likely to be the first tracers used in clinical practice. Before clinical introduction, vanco-800CW awaits toxicity testing and good manufacturing practices to ensure its safety. In this respect, it is noteworthy that vancomycin and the IRDye800CW have, as separate molecules, already been approved for clinical implementation. Importantly, as imaging is performed with an extremely low dose of vanco-800CW (0.07 nmol/mL), which is ~20- to 40-fold below the minimal inhibitory concentration (MIC) of vancomycin for staphylococci (https://eucast.org/clinical_breakpoints/), the possible side effects associated with vancomycin and a rapid selection for antimicrobial resistance are unlikely.[11] Consistent with this view, we observed thus far no effects of the tracer at these concentrations on culture results. We consider it therefore also unlikely that the described imaging approach could interfere with subsequent routine culturing. Furthermore, as vanco-800CW fluoresces in the NIR range, interfering tissue auto-fluorescence is minimal.[18] Indeed, in our human cadaver model, there was relatively little auto-fluorescence detectable. This has also been shown in live animal models[12] and oncologic TLFI studies where IRDye800CW was used.[15]

Due to the characteristics of fluorophores and camera systems, TFLI is currently mainly suitable for imaging of superficial targets and intra-operative or endoscopic approaches. The NIR imaging system used in the present *post-mortem* experiment was, for example, designed for wide-field endoscopy and clinically implemented in the Gastroenterology and Hepatology department of our hospital.[19] Our present study is the first in its kind that combines TFLI with arthroscopy. Importantly, by imaging the prosthesis intra-articular at the prosthetic surface, less fluorescence signal is lost compared to non-invasive imaging outside the knee joint. Accordingly, increased sensitivity and resolution in the detection of infection can be achieved.[20] This is underpinned by the observation that minor interruptions in the biofilm could arthroscopically be visualised with the fluorescence camera at submillimetre resolution (**Figure 6**) during the *post-mortem* experiments.

In the clinic, around 60-70% of PJIs are caused by *S. aureus*, coagulase-negative staphylococci, streptococci and enterococci, which are all GP bacteria, while less than 10% are caused by aerobic GN bacteria.[8] Judged by these percentages, vanco-800CW is suitable for the detection of PJIs in the majority of cases. This view is underscored by the finding that biomaterials coated with GP bacterial biofilms could, after treatment with vanco-800CW, all be easily discriminated from the tested GN bacteria and controls. The measured T/B ratios further showed that the GP bacterial strains with bound vanco-800CW emit fluorescence to a much higher level than the GN strains compared to the background. This finding is consistent with the notion that vanco-800CW is preferentially bound by GP bacteria.[11] The binding specificity of the fluorescently labelled vancomycin was further reinforced by the observed competitive inhibition of biofilm labelling through the pre-treatment of an *S. epidermidis* biofilm with non-labelled vancomycin at increasing concentrations. Observing that low amounts of vanco-800CW were also bound by the GN bacterial biofilms was surprising, but

this finding can possibly be explained by the fact that peptidoglycan, the target for vanco-800CW, may not be fully covered in all instances by the GN bacterial outer membranes. This applies, for example, to dead bacteria. Whether this represents sufficient vanco-800CW accumulation to detect GN bacterial biofilms in a clinical context is yet to be explored. However, based on our findings, we anticipate that arthroscopic TFLI with vanco-800CW will have a much lower sensitivity for the detection of GN bacteria involved in PJI than for GP bacteria. Importantly, this potential limitation of the presently explored arthroscopic imaging approach can be overcome by multispectral arthroscopic imaging with multiple simultaneously applied tracers that target different microbial species, including GN bacteria. Considering that empirical antibiotic therapy may be less frequently needed, the direct diagnostic approach based on arthroscopic optical imaging is likely to result in better therapeutic regimens while, at the same time, less antimicrobial resistance may be elicited.[21] Some other limitations of this study need to be considered. Firstly, to reliably assess whether a prosthesis is infected, it also has to be scanned at spots were imaging is difficult. This mostly concerns the edges of the prosthesis and the prosthesis-bone interface. The imaging fiber used in the present experiment was not ideal for monitoring these spots due to a restricted manoeuvrability of the tip. This will also apply to the imaging of other joints, for example hip prostheses, where arthroscopy is even more challenging. These practical restrictions still need to be addressed before clinical implementation can be considered. Secondly, careful selection of patients who might benefit from arthroscopic TFLI is important, as arthroscopy is a minimally invasive procedure and may also put patients at risk for new infections. Nonetheless, the risks of causing new infections though arthroscopy, mainly through the transfer of skin flora to the joint cavity, are estimated as very low (<1%).[22] Thirdly, the results of this study show that vanco-800CW is capable of detecting a representative panel of bacterial species *in vitro*. However, in the presented *post-mortem* arthroplasty experiments only a *S. epidermidis* strain was used. The reliability of this tool for the detection of other bacterial species is therefore yet to be established and such experiments might include bacteria incapable of biofilm formation as negative controls. Finally, our *in vitro* method of biofilm formation on the prosthesis, in a laboratory setting with excess nutrients and controlled environmental conditions, does probably not fully resemble biofilms as they appear *in vivo* in patients. Nonetheless, we demonstrated the presence of EPS in the *in vitro* grown biofilms with Congo Red, which is proof of their authenticity.[23] However, biofilms grown in a laboratory setting with excess nutrients and controlled environmental conditions will be different from the ones that develop in patients. In addition, the arthroscopy experiments were conducted in a *post-mortem* setting, which undoubtedly presents differences with the actual *in vivo* situation. It will therefore be important to extend our proof-of-principle studies to *in vivo* arthroscopy in PJI animal models,[24] and to examine whether vanco-800CW is capable of detecting real patient derived biofilms (*ex vivo*) on infected biomaterials.

Conclusion

This proof-of-principle study shows for a human prosthetic *post-mortem* infection model that arthroscopic detection and imaging of PJIs caused by GP bacteria is feasible with vanco-800CW. Its ability to directly and rapidly detect bacterial biofilms makes it stand out in comparison to other currently applied diagnostic approaches in clinical microbiology. This view is underpinned by the affinity of vanco-800CW for biofilms of a representative panel of clinically relevant bacterial species associated with biomaterial infections. We therefore believe that the here presented novel diagnostic modality holds great promise for clinical implementation with the exciting perspective of accurate and fast *in situ* diagnosis of PJIs

Acknowledgements

We thank Sip Zwerver and Richard Koster for their expert technical support, and Studio Apenzaken, in particular Peter Groot and Kevin Harkema, for designing and making the video.

Declarations

Funding

ML-A received funding from CEU MSCI-ITN grant 713660 (Pronkjewail). Funding for the other authors was provided by their employers.

Conflicts of interest

GMvD is CSO of TRACER™. The other authors declare neither financial nor non-financial conflicts of interest.

Ethical approval

The *post-mortem* experiments on human cadavers were approved by the authorised staff of the Department of Anatomy and Medical Physiology of the UMCG, and conducted according to the applicable law (“Wet op de Lijkbezorging”, Art 18, lid 1 and 19, BWBR0005009) and institutional guidelines of the UMCG. Ethical approval for the collection of microbiological patient samples was obtained from the medical ethical committee at the UMCG (METC 2017/526).

Consent to participate

For experiments on human cadavers, the respective individuals had provided written informed consent for the use of their bodies for scientific research and education in the context of the "body donation programme" at UMCG.

Consent for publication

All authors have read the manuscript and agree with its publication.

References

1. Kurtz, S., Ong, K., Lau, E., Mowat, F. & Halpern, M. Projections of primary and revision hip and knee arthroplasty in the United States from 2005 to 2030. *J. Bone Jt. Surg.* **89**, 780–785 (2007).
2. Kurtz, S. M., Lau, E., Watson, H., Schmier, J. K. & Parvizi, J. Economic burden of periprosthetic joint infection in the united states. *J. Arthroplasty.* **27**, 61–65 (2012).
3. Osmon, D. R. *et al.* Diagnosis and management of prosthetic joint infection: Clinical practice guidelines by the infectious diseases Society of America. *Clin. Infect. Dis.* **56**, 1–25 (2013).
4. Murdoch, D. R. *et al.* Infection of orthopedic prostheses after *Staphylococcus aureus* bacteremia. *Clin. Infect. Dis.* **32**, 647–649 (2001).
5. Darouiche, R. O. Treatment of infections associated with surgical implants. *N. Engl. J. Med.* **350**, 1422–1429 (2004).
6. Donlan, R. M. & Costerton, J. W. Biofilms: Survival mechanisms of clinically relevant microorganisms. *Clin. Microbiol. Rev.* **15**, 167–193 (2002).
7. Stewart, P. S. Antimicrobial Tolerance in Biofilms. *Microbiol. Spectr.* **3**, 1–30 (2015).
8. Tande, A. J. & Patel, R. Prosthetic joint infection. *Clin. Microbiol. Rev.* **27**, 302–345 (2014).
9. Gomez-Urena, E. O., Tande, A. J., Osmon, D. R. & Berbari, E. F. Diagnosis of Prosthetic Joint Infection: Cultures, Biomarker and Criteria. *Infect. Dis. Clin. North Am.* **31**, 219–235 (2017).
10. Beam, E. & Osmon, D. Prosthetic Joint Infection Update. *Infect. Dis. Clin. North Am.* **32**, 843–859 (2018).
11. van Oosten, M. *et al.* Targeted imaging of bacterial infections: advances, hurdles and hopes. *FEMS Microbiol. Rev.* **39**, 892–916 (2015).
12. van Oosten, M. *et al.* Real-time *in vivo* imaging of invasive- and biomaterial-associated bacterial infections using fluorescently labelled vancomycin. *Nat. Commun.* **4**, 2584 (2013).
13. Kaiser, T. D. L. *et al.* Modification of the Congo red agar method to detect biofilm production by *Staphylococcus epidermidis*. *Diagn. Microbiol. Infect. Dis.* **75**, 235–239 (2013).
14. Malhotra, R., Dhawan, B., Garg, B., Shankar, V. & Nag, T. C. A Comparison of Bacterial Adhesion and Biofilm Formation on Commonly Used Orthopaedic Metal Implant Materials: An *In vitro* Study. *Indian J. Orthop.* **53**, 148–153 (2019).
15. Joshi, B. P. & Wang, T. D. Targeted Optical Imaging Agents in Cancer: Focus on Clinical Applications. *Contrast Media Mol. Imaging.* 2015237 (2018).
16. Keereweer, S. *et al*. Optical image-guided cancer surgery: Challenges and limitations. *Clin. Cancer Res.* **19**, 3745–3754 (2013).
17. Mills, B., Bradley, M. & Dhaliwal, K. Optical imaging of bacterial infections. *Clin. Transl Imaging*. **4**, 163–174 (2016).
18. Frangioni, J. V. *In vivo* near-infrared fluorescence imaging. *Curr. Opin. Chem. Biol.* **7**, 626–634 (2003).
19. Nagengast, W. B. *et al.* Near-infrared fluorescence molecular endoscopy detects dysplastic oesophageal lesions using topical and systemic tracer of vascular endothelial growth factor A. *Gut.* **68**, 7–10 (2019).
20. Ntziachristos, V. Going deeper than microscopy:

the optical imaging frontier in biology. *Nat. Methods.* **7**, 603–614 (2010).

21. Beceiro, A., Tomás, M. & Bou, G. Antimicrobial resistance and virulence: A successful or deleterious association in the bacterial world? *Clin. Microbiol. Rev.* **26**, 185–230 (2013).
22. Bauer, T., Boisrenoult, P. & Jenny, J. Y. Post-arthroscopy septic arthritis: Current data and practical recommendations. *Orthop. Traumatol. Surg. Res.* **101**, 347–350 (2015).
23. Freeman, D. J., Falkiner, F. R. & Keane, C. T. New method for detecting slime production by coagulase negative staphylococci. *J. Clin. Pathol.* **42**, 872–874 (1989).
24. Miller, R. J. *et al. In Vivo* Bioluminescence Imaging in a Rabbit Model of Orthopaedic Implant Associated Infection to Monitor Efficacy of an Antibiotic-Releasing Coating. *J. Bone Jt. Surg.* **101**, e12 (2019).

Supplementary data

Table S1. Colony forming units, fluorescence source intensities and target-to-background (T/B) ratios per bacterial strain

Bacterial strain	Average colony forming units	Average fluorescence source intensity per ROI	Average fluorescence background intensity per ROI	T/B ratio
S. aureus	6.61×10^8	4429	254.5	18.42
S. caprae	2.22×10^{10}	9733.5	254.5	36.28
S. epidermidis	1.70×10^9	3962	276	14.15
S. lugdunensis	1.99×10^9	9510.5	273	33.69
E. faecalis	5.03×10^9	7767.5	255.5	29.97
S. epidermidis ATCC 35984	1.75×10^7	15759.5	219.5	56.5
E. coli	3.24×10^8	962.5	267.5	3.48
P. aeruginosa	3.52×10^8	859	267.5	3.15
Sterile	0	220.5	261	0.86

14 bacterial strains were analysed, which were retrieved from sonicated infected prostheses. The samples consisted of *S. aureus* (2 samples, Gram-positive (GP)), *S. epidermidis* (2 samples, GP), *S. lugdunensis* (2 samples, GP), *S. caprae* (2 samples, GP), *E. faecalis* (2 samples, GP), *E. coli* (2 samples, Gram-negative (GN)), and *P. aeruginosa* (2 samples, GN). Samples, plus 2 sterile biomaterials as controls, were treated with vanco-800CW. Fluorescence images were recorded using the SurgVision Explorer Air (settings for fluorescence measurements: fluorescence exposure 25 ms, fluorescence gain 300; SurgVision, the Netherlands). The biomaterials were sonicated after which serial dilutions of the sonication-fluid were made. Samples were plated on blood agar plates (5% sheep blood) and numbers of colony forming units (CFUs) were determined. Data was analysed using ImageJ software (National Institutes of Health, Maryland, US). Regions of interest (ROIs) were drawn around the biomaterials after which the fluorescence signal was quantified. The background signal was quantified by drawing a ROI off-target in the background of the same image. To determine target-to-background (T/B) ratios, ROIs were divided by the background fluorescence. It should be noted that CFU counting after sonication is a semi-quantitative method, and that the yield after sonication can vary per bacterial species. Therefore, it is not possible to directly link a fluorescence signal to the respective CFU count. Nonetheless, the present data imply that comparable biofilms of GP and GN bacterial species were formed in the present experiments, whereas only the GP biofilms were detected with vanco-800CW.

Movie S1. Targeted optical arthroscopy to detect bacterial biofilm

The supplemental **Movie S1** provides a theoretical and practical overview of the image-guided *in situ* detection of bacterial biofilms in a human prosthetic knee infection model.

Chapter 9

Ex vivo visualisation of bacterial infection and pulmonary microbiological colonisation in resected human and porcine lungs using targeted optical endomicroscopy

Marjolein Heuker[*], Usma Koser[*], Caroline van de Wauwer, Michiel E. Erasmus, Wim Timens Gooitzen M. Van Dam, Wouter B. Nagengast, Adam D.L. Marshall, Kev Dhaliwal, Jan Maarten van Dijl[#], Erik A.M. Verschuuren[#] and Marleen van Oosten[#]

[,#] These authors contributed equally to this work*

To be submitted

Abstract

Respiratory failure and infections are a leading cause of death, which imposes a clinical need for fast and precise bedside diagnostic modalities. The present study was aimed at evaluating the value of fluorescence-targeted probe-based confocal laser endomicroscopy (pCLE) for the detection of micro-organisms in the alveolar space. To this end, we applied two distinct microbe-specific tracers in the imaging of 19 diseased human resected lung specimens using an *ex vivo* ventilation model. Diagnoses based on visual inspection of recorded images and computational image analysis was benchmarked against the outcomes of microbiological culture and pathology tests. The results demonstrate the feasibility to detect pneumonia and microbial colonisation of the human distal lung, even when the gold-standard of microbiological culturing fails. Further, we propose that fluorescence-targeted pCLE during *ex vivo* lung perfusion (EVLP) can provide valuable, objective information, which may serve to optimise and accept borderline organs for transplantation. Altogether, the present study implies that fluorescence-targeted pCLE is a promising bedside diagnostic tool for pulmonary medicine.

Keywords: *pneumonia; bacteria; probe-based confocal imaging (pCLE); fluorescence/optical imaging; ex vivo lung perfusion (EVLP)*

Introduction

Pneumonia is a frequently occurring infection that has remained a leading cause of death.[1] It is one of the most common reasons for being admitted into level 3 care and the administration of intensive therapy. In critically unwell patients the risk of an acquired pneumonia not only increases mortality, but it also increases length of stay and treatment and, thereby, the financial burden on healthcare systems. Unfortunately, delineating the underlying aetiology and identifying definitive pneumonia in general intensive care unit (ICU) patients can be challenging. Currently, clinicians rely on clinical signs and symptoms, radiography and microbiology culture results to reach a diagnosis. However, radiographic imaging is often non-specific, as it is unable to distinguish the varying differentials of pulmonary infiltration. Moreover, it often takes several days before a micro-organism can be identified from microbiological culture and a definitive diagnosis is established in the best case scenario. Unfortunately, generating a representative culture is challenging, with limitations towards sensitivity and specificity. As a consequence, empirical broad-spectrum antimicrobial therapy is usually started prior to identification of the causative micro-organisms, which in turn potentiates the global antimicrobial resistance challenge.[2,3] Therefore, developing and optimising novel approaches for rapid and accurate diagnostics, which allow optimal and targeted treatment, may help decrease the time to therapy, morbidity, mortality, and economic burden, and improve antimicrobial stewardship thus reducing potential antimicrobial resistance.

A promising tool to diagnose pneumonia, which enables greater accuracy in clinical decision making and optimisation of antimicrobial management, is probe-based confocal laser endomicroscopy (pCLE).[4,5] Complementary to wide-field images obtained during bronchoscopy, cellular and subcellular optical imaging can be performed via pCLE. pCLE utilises a laser focusing at a specific depth and, due to the pinhole confocal aperture, only light from that plane is refocused and reflected back, which results in optimal resolution. In addition, the probe can travel distally beyond the bronchoscope. This allows imaging of the alveolar space, and provides so-called optical biopsies that are essentially based on the specific auto-fluorescence of the imaged tissue. Importantly, by combining targeted optical molecular imaging with pCLE (i.e. fluorescence-targeted pCLE), it is possible to directly visualise infectious micro-organisms in the distal respiratory tract and diagnose pneumonia.[6]

Optical bacteria-targeted imaging is a branch of molecular imaging that utilises fluorescence techniques and provides a rapid, at point method, to identify a potential target micro-organism.[2,3,7] This has the benefit of reducing time to targeted treatment and the capacity for therapeutic response monitoring. Antimicrobial peptides were previously researched as targeting molecules for imaging. For instance, the peptide ubiquicidin (UBI) binds to a wide panel of Gram-positive and Gram-negative bacteria as well as fungi, and radio-labelled derivatives have been tested for infection imaging in patients.[3] UBI conjugated with the fluorophore 7-nitrobenz-2-oxa-1,3-diazole (NBD), here referred to as BAC 1, has shown good signal-to-noise ratios and minimal degradation in

previous studies.[6,8] In particular, BAC 1 was used to detect bacteria in explant lungs of cystic fibrosis (CF) patients.[9] Another recently explored tracer, BAC 2, is based on the antibiotic colistin (polymyxin E) conjugated to NBD. This tracer binds specifically to lipopolysaccharide (LPS), present in the Gram-negative bacterial cell envelope. Recently, Akram and colleagues have successfully demonstrated the use of BAC 2 to detect clinically relevant bacterial loads in the distal alveolar space in unwell and mechanically ventilated ICU patients.[10]

In addition to the diagnosis of pneumonia, fluorescence-targeted pCLE seems also applicable in the field of lung transplantation to investigate and differentiate inflammatory and infective pulmonary aetiologies. Lung transplantation has significantly transformed life expectancy for patients with endstage pulmonary conditions including, CF and chronic obstructive pulmonary disease (COPD).[11] However, donor lung procurement struggles to meet the demand of patients suffering from respiratory failure and in 2020, this has further compounded due to the COVID-19 pandemic. Unfortunately, in up to 40% of cases, donor lungs are disapproved for transplant use, even though they would have likely been suitable for transplant.[12,13] In this context, *ex vivo* lung perfusion (EVLP) and resource management has revolutionised transplantation medicine by allowing the assessment and optimisation of borderline lungs, thereby increasing the donor organ pool by up to 20%.[14] A variety of clinical and research techniques is presently utilised to assess the viability of these lungs. However, molecular information of the alveolar space is lacking, including tissue degradation, inflammation, infection and bacterial colonisation. This crucial information could be provided by fluorescence-targeted pCLE to aid the transplant team's assessment in lung selection.

The present study was designed to assess the performance of fluorescence-targeted pCLE in the alveolar space of resected human lungs using the BAC 1 and BAC 2 tracers. In particular, we have investigated whether a real-time, load-dependent relationship of bacterial recognition and signal is feasible. To explore the potential clinical relevance and sensitivity of fluorescence-targeted pCLE, we used a broad spectrum of resected lung materials reflecting different pathologies and bacterial loads. In particular, we sought to establish whether fluorescence-targeted pCLE could potentially aid the assessment of donor lungs for EVLP.

Methods and experimental procedures

Proof-of-principle: ventilated and infected porcine lungs

As a conceptual study, we tested our set-up on a large animal *ex vivo* lung. A day prior to experimental procedure, clinical isolates of *Staphyloccocus epidermidis* (Gram-positive) and *Escherichia coli* (Gram-negative) were grown overnight in tryptic soy broth (TSB) at 37°C under constant agitation (250 RPM). The following day, bacteria were diluted 1:20 in 10 mL of TSB and grown in comparable circumstances for ~2.5h up to an optical density of ~2 McFarland. Lungs from a pig destined for slaughter were obtained and transported on ice in order to commence the experimental procedure

on *ex vivo* intubation and ventilation. The porcine lungs were infected by injection of 2-5 mL of bacterial culture (respectively *S. epidermidis* or *E. coli*) per pulmonary segment, and imaged as described in the sections below.

Resected human lungs and lobes

From April 2018 to August 2019, resected lungs from patients undergoing lung transplant, lobes of lungs resected for malignancy, and one donor lung rejected after EVLP for lung oedema, were collected from patients who were operated on the Cardiothoracic Surgery department of the University Medical Center Groningen (UMCG), the Netherlands. All lung specimens were collected within hours of surgical resection and moved to an approved clinical area in order to perform the imaging procedure.

***Ex vivo* imaging procedure**

Lung specimens were intubated with size 6-8 endotracheal tube (Shiley™, USA) and placed on a ventilator unit (Oxylog® 3000, Dräger Medical Systems, Lübeck, Germany). Some small specimens (i.e. lobes) were not ventilated due to practical reasons. The procedures were performed at room temperature using estimated ventilation pressure values and a respiratory rate of 10-14 per min. Bronchoscopic examination was performed to assess the general anatomy and gauge accessibility of endobronchial segmental anatomy (Ambu® aScope™ 7 regular 5.0/2.2, Denmark). A fiber (Cellvizio® AlveoFlex™, Mauna Kea Technologies, France) was inserted via the working channel of the bronchoscope and baseline imaging was performed (without tracer). pCLE images were recorded, capturing at 8 frames/s with a field of view of ~602 µm by 602 µm, with lateral resolution of 5 µm and an axial resolution of 15 µm. Imaging was undertaken with a 1.4 mm diameter AlveoFlex, using a 488 nm laser excitation source with constant laser power. Following capturing of baseline images, microdoses (0.0315 µmol in 2 mL) of either BAC 1[6,9] or BAC 2[10] was administered via the working channel of the bronchoscope and imaging procedure was immediately repeated. **Figure 1** shows a schematic representation of the imaging procedure.

Sample collection, culture and microbiological identification

Samples collected from the patients and resected lung specimens included sputum prior to surgery, bronchoalveolar lavage (BAL), and 'protected endobronchial brush samples' of the resected specimens after experimental imaging procedure. BAL samples were collected using a single-use bronchoscope and a sterile Milli-Q water ~10-20 mL wash to enable a result of ~5 mL sampling from the endobronchial segment. Protected brush (Cellebrity™, Boston Scientific, USA) samples were taken in the selected area prior to a lavage and were directly stored in 1 mL phosphate buffered saline (PBS). Following the procedure, BAL samples were centrifuged at 3,000 RPM in 15 mL sample tubes at 4°C for 10 min. The resultant cell pellet was concentrated to a final volume of 1 mL PBS.

Microbiological culture was performed with the appropriate culture media. This included Sabouraud dextrose (SAB), chocolate (CHOC), MacConkey, blood agar (BA) and colistin oxolinic-acid blood agar (COB) plates, incubated at 37°C on CO_2 and O_2 incubators for 2 or 5 days. The numbers of colonyforming units (CFUs) was documented. Only 1-2 CFU(s) of clinically likely contaminants were not considered as a positive culture. Determination was performed by matrix-assisted laser desorption/ionization time-of-flight (MALDI-TOF; Bruker, USA) mass spectrometry.

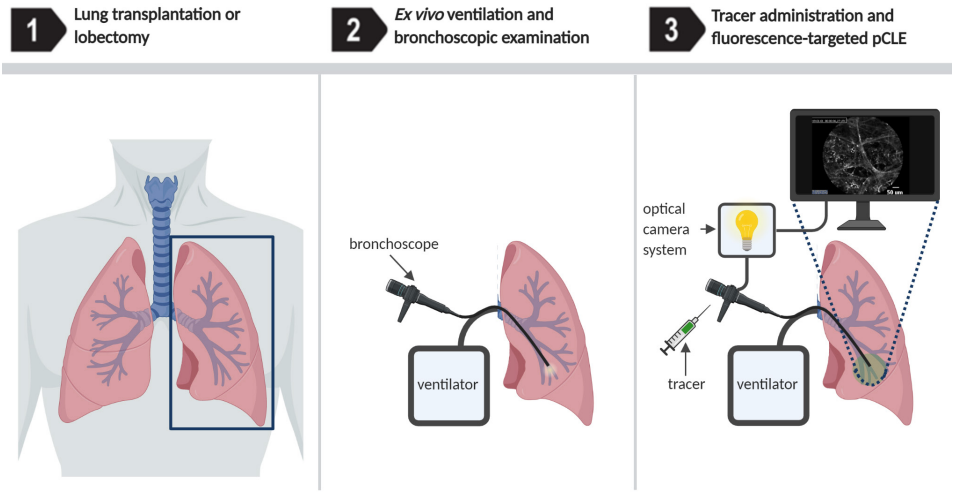

Figure 1. Schematic overview of the fluorescence imaging methodology. Resected lung specimens after lung transplantation or lobectomy were intubated and ventilated *ex vivo*. Subsequently, bronchoscopic examination was performed. Tracer, respectively BAC 1 or BAC 2, was administered and imaging was performed with the Cellvizio probe based confocal laser endomicroscopic imaging system. This figure is created with BioRender.com.

Image analysis

Spot detection filters incorporating 'Laplacian of Gaussian' (Log) and 'difference of Gaussian' (Dog) were used to define areas of positive fluorescence over background.[15,16] Recently described algorithms for spot detection (fluorescent bacteria) using Log and Dog filters were used in this study via Matlab R2018b (The MathWorks Inc, USA).[10] Frame-by-frame blinded, scrutiny was performed of each video. Frames with artefact, blurring, fluid bubbles and false increased fluorescence due to anatomical presence of blood vessels were excluded. Algorithm analysis was performed and the number of spots detected was then converted into numerical values in files. If specimen videos were deemed to include an excess of poor quality images, they were removed from the overall analysis as described above.

Data collection

Demographic and clinical information was obtained via the electronic health record system (Electronic Patient Dossier; EPD) of the UMCG. Several demographic characteristics, patient comorbidities, surgical information, microbiological, pathology and radiographical results were collected

Statistical analysis

The values of each anatomical group were represented in median and interquartile ranges. P-values were calculated by Kruskal-Wallis or Mann-Whitney U tests in Graphpad Prism 8.1.0 (Graphpad Software, USA). A p-value of <0.05 was considered the cut-off for statistical significance.

Ethics

Permission for this study was granted by the local Medical Ethical Review Board (Medisch Ethische Toetsingscommissie; METc; number 2017/219) for the use of clinical data and material (sputum and resected lung tissue) that would not impede the clinical treatment or diagnostic process. Patients gave written, informed consent, which included the use of pseudo-anonymised data and samples for the purpose of research and publication. All collected data was treated pseudo-anonymously and in adherence with the Declaration of Helsinki (adapted version Fortaleza, Brazil, 2013).

Results and discussion

The present study was aimed at investigating the feasibility of using microbe-targeted tracers in pCLE in order to visualise bacteria in the alveolar space of human lung specimens. Importantly, *ex vivo* alveolar fluorescence-targeted pCLE was thus far only performed in CF end-stage explanted lungs, where bacterial loads are high.[9] However, this technology was not explored in resected lungs from other end-stage diseases to ascertain bacterial colonisation levels.

Proof-of-principle: porcine *ex vivo* lung model

A porcine proof-of-principle model was set-up in order to establish a working method for testing both the BAC 1 and 2 tracers by using Gram-positive (*S. epidermidis*) and Gram-negative (*E. coli*) bacteria that were introduced in specified segments of the lung. The infected segments were imaged along with bacteria-naïve segments in order to make a comparison for both visual and software-based spot detection. **Figure 2** shows an example of the pCLE images recorded, where panel **A** shows a bacteria-naïve segment without tracer, and panel **B** a pCLE image of a bacteria-naïve segment with BAC 2. Panel **C** shows *S. epidermidis* following BAC 1 application that led to clearly elevated fluorescence. Likewise, panel **D** shows a pCLE image of *E. coli* following BAC 2 application that led to readily detectable fluorescent spots.

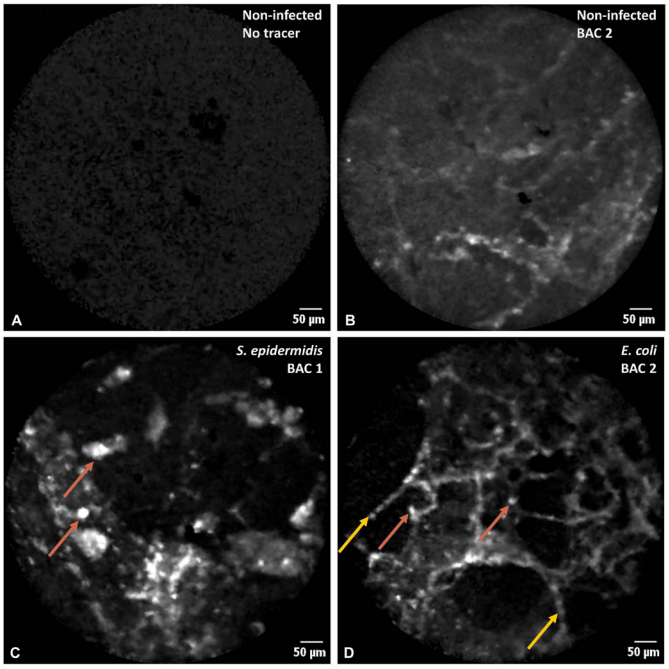

Figure 2. Porcine alveolar pCLE images in infected and non-infected pulmonary segments. A) Represents a non-infected segment without tracer with no evidence of fluorescence. **B**) Shows a non-infected segment with BAC 2. **C**) Shows fluorescence with BAC 1 when administered in a bronchial segment infected with *S. epidermidis*. Finally, **D**) shows fluorescence with BAC 2 administration in an *E. coli* infected segment. (The red arrows indicate fluorescently labelled bacteria and the yellow arrows indicate elastin). pCLE = probe-based confocal laser endomicroscopy. BAC 1 = ubiquicidin conjugated to fluorophore 7-nitrobenz-2-oxa-1,3-diazole (NBD). BAC 2 = antibiotic colistin (polymyxin E) conjugated to NBD.

Case characteristics and demographics

In this study, 19 resected individual human lung cases were imaged. A total of three cases were excluded as the resultant imaging files were of poor quality, or displayed increased cellularity or artefact. The surgical procedures performed, demographic information and aetiologies for the cases are listed in **Table 1**. One EVLP lung specimen (n = 1) was included following disapproval for transplantation on the basis of clinical suspicion of infection.

Table 1. Case characteristics and clinical information

Case	Type of Surgery	Gender	Age	Aetiology	Smoker
1	Lobectomy RML	F	55	Renal cancer, metastasis	Never
3	Open bi-lobectomy RUL RML	M	67	Lung cancer	Not known
4	Lobectomy RUL	F	76	Lung cancer	Ex-smoker
5	Bilateral lung transplant	F	62	COPD	Ex-smoker
6	EVLP	Not disclosed	Not disclosed	Not disclosed	Not disclosed
7	Bilateral lung transplant	F	59	COPD, fibrosis, bronchiectasis	Ex-smoker
8	Open lobectomy RLL	M	74	Lung cancer	Not known
10	Open lobectomy RUL	M	70	Lung cancer	Current
11	Bilateral lung transplant	M	64	CPFE, emphysema	Current
13	RUL lobectomy	F	71	Lung cancer	Current
14	Bilateral lung transplant	M	57	COPD, Alpha-1-antitrypsin	Never
15	Bilateral lung transplant	M	54	COPD	Never
16	Bilateral lung transplant	F	11	Cystic fibrosis	Never
17	Bilateral lung transplant	F	25	Idiopathic pulmonary hypertension	Never
18	Bilateral lung transplant	M	26	Cystic fibrosis	Never
19	Bilateral lung transplant	M	44	Cystic fibrosis	Never

Case demographic details for all explants included in the analysis. Male (M), female (F), right upper lobe (RUL), right middle lobe (RML), right lower lobe (RLL), *ex vivo* lung perfusion (EVLP), chronic obstructive pulmonary disease (COPD), combined pulmonary fibrosis and emphysema (CPFE). Video-assisted thoracic surgery was performed for the lobectomies unless stated otherwise (open).

Micro-organism identification

Control cases were deemed non-infected based on negative culture results and clinical investigations. Infected cases were classified as such based on culture results, clinical examination and diagnostic information. Specifically, the pathology results of case 1 showed granulomatous organising pneumonia, although microbiological culture results were negative. In addition, case 6 concerned a lung from a failed EVLP where, on tactile examination, the lung parenchyma was considered oedematous. Moreover, the lung was poorly compliant with ventilation. Although the respective culture results were negative, pathology on the contralateral lung proved positive for inflammation in keeping with acute pneumonia. Consequently, cases 1 and 6 were added to the infected cases. **Table 2** summarises the culture results of those cases that tested positive for the presence of bacteria and fungi. Cases not listed in **Table 2** showed no growth or only 1-2 CFU(s) upon culturing, which was most likely due to contamination of the respective cultures.

***Ex vivo* image analysis of human explant lungs: overview**

To evaluate the feasibility of micro-organism detection in the alveolar space of diseased resected lungs, pCLE images from pre- and post-tracer administration were visually compared with microbiological culture and standardised software analysis. The blinded analysis of the pCLE videos was performed by two independent researchers. The median spot detection in baseline images (pre-tracer) in non-infected (control) versus infected and/or colonised cases showed that there was a difference in fluorescence values between the baseline images. This disparity meant that an overall grouped analysis and comparison was not possible and from herein individual, intra-case analysis was performed.

Table 3a summarises the imaging results of the control (non-infected) cases. In cases 4, 5, 7, 10 and 14, we observed a minimal increase in spots detected by the image analysis software. This correlated with no visual fluorescent spot detection and no growth upon microbiological culture. **Table 3b** summarises the imaging results for all explants with positive microbiological culture or suspected clinical infection. In the majority of cases, when there was evidence of microbiological culture this correlated with overall visual (by eye) detection of fluorescent spots on pCLE. A more detailed segmental software analysis and clinical radiology and pathology information is presented as Supplementary Data (**Table S1a** and **S1b**). Of note, we found in some cases the visual detection of fluorescent spots by the operator more consistent than the increase in numerical values as detected by software-based image analysis. However, this can be explained by particular clinical aspects in the respective cases, as discussed below.

Table 2. Microbiological information

Case	Pre-operative sputum culture of patient	Micro- organisms cultured upon imaging		
		Gram-positive bacteria	Gram-negative bacteria	Yeast/Fungi
11	*Staphylococcus aureus*	*Actinomyces odontolyticus;* *Corynebacterium accolens;* *Rothia mucilaginosa;* *Staphylococcus aureus;* *Staphylococcus epidermidis;* *Streptococcus species*	*Neisseria perflava*	-
15	*Klebsiella pneumoniae;* *Staphylococcus aureus*	*Rothia dentacoriosa;* *Staphylococcus and* *Streptococcus species*	*Haemophilus sputorum;* *Neisseria subflava;* *Sphingomonas paucimobilis*	-
16	*Pseudomonas aeruginosa;* *yeasts*	*Staphylococcus aureus;* *Staphylococcus epidermidis*	*Escherichia coli;* *Pseudomonas aeruginosa*	*Aspergillus fumigatus;* *Candida species*
17	*Staphylococcus aureus*	-	-	-
18	*Haemophilus influenzae;* *Proteus mirabilis;* *Staphylococcus aureus*		*Escherichia coli;* *Haemophilus influenza;* *Proteus mirabilis;* *Pseudomonas aeruginosa*	*Aspergillus fumigatus;* *Candida species*
19	*Pseudomonas aeruginosa*	*Staphylococcus aureus;* *Staphylococcus epidermidis*	*Haemophilus influenza;* *Pseudomonas aeruginosa*	*Aspergillus fumigatus;* *Candida species*

Explant specimens showing culture growth of microbe(s) are detailed per case. Cases not listed showed no microbiological growth. Pre-operative sputum cultures were those documented within the 2 months prior to surgery. Patients received only ceftazidim at the start of surgery.

Table 3a. Imaging results of non-infected cases

Case	Tracer used	Change in spots detected (software)	Overall visual observation/comments
3	BAC 1 BAC 2	↑ 39 ↑ 4	Bacterial signal -/-
4	BAC 2	↓ 3	Bacterial signal -/-
5	BAC 2	↑ 7	Bacterial signal -/-
7	BAC 2	↓ 1	Bacterial signal -/-
8	BAC 1 BAC 2	↑ 14 ↑ 28	Bacterial signal -/- Increased general background autofluorescence
10	BAC 2	↓ 5	Bacterial signal -/-
13	BAC 1 BAC 2	↓ 19 ↑ 15	Bacterial signal -/-
14	BAC 1 BAC 2	↑ 10 ↑ 12	Bacterial signal -/-
17	BAC 1 BAC 2	↑ 34 ↓ 3	Bacterial signal +/- Low signal in some videos, corresponding to a low volume colonisation

Values represent the median increase or decrease in fluorescent spots detected. The arrows represent respectively an increase (↑) or decrease (↓) in the numbers of detected spots. Bacterial signal is defined as negative (-/-); moderate (+/-) or positive (+/+). All cases showed no bacterial growth upon microbiological culturing.

Ex vivo image analysis of culture-positive human explant lungs

For the positive cases, the majority of visualised bacterial signal corresponded with the microbial culture and software analyses. In **Figure 3**, we display representative data for case 16, where different anatomical regions were imaged. The areas imaged in the left lung's upper lobe (LUL) illustrate a median rise of 50 spots with BAC 1, while the images of the left lower lobe (LLL) illustrate a median rise of 20 spots with BAC 2 ($p < 0.0001$). In the right lower lobe (RLL), an increase of 35 spots was detected from baseline following BAC 2 administration ($p < 0.0001$). The corresponding pCLE images as observed by the operator correlated with the above software analysis. More detailed results for all the imaged segments are listed in **Table S1b**, and the corresponding videos are presented in the Supplementary Data (**Movies S1-S4.1**).

Table 3b. Imaging results of infected and/or colonised cases

Case	Tracer used	Change in spots detected (software)	Overall visual observation/comments
1	BAC 1 BAC 2	↑ 16 ↑ 57	Bacterial signal -/-
6	BAC 2	↑ 32	Bacterial signal -/-
11	BAC 1 BAC 2	↑ 15 ↑ 14	Bacterial signal -/-
15	BAC 1 BAC 2	↑ 6 ↑ 10	Bacterial signal -/-
16	BAC 1 BAC 2	↑ 17 ↓ 5	Bacterial signal -/- Increased general background autofluorescence
18	BAC 1 BAC 2	↑ 12 ↑ 12	Bacterial signal -/-
19	BAC 1 BAC 2	↑ 17 ↑ 29	Bacterial signal +/- Low signal in some videos, corresponding to a low volume colonisation

Values represent the median increase or decrease in fluorescent spots detected. The arrows represent respectively an increase (↑) or decrease (↓) in the numbers of detected of spots. Bacterial signal is defined as negative (-/-); moderate (+/-) or positive (+/+). Microbiological culture is defined as no bacterial growth (-) or bacterial growth (+).

Of note, in some of the recorded images there was an apparent mismatch between the numbers of detected spots by visual inspection and image analysis software as illustrated for cases 16 and 18 (**Table S1b**). In all cases, the visual detection of bacterial spots, as illustrated in **Figure 4**, was fully consistent with the results from microbiological culture and/or pathology. Nonetheless, image analysis software suggested a decrease in the numbers of spots detected with BAC 2 (82 spots) compared to the baseline (87 spots). Similarly, in case 18, the median number of spots detected by the image analysis software suggested a minimal increase in the numbers of detectable spots upon administration of BAC 1, despite the clear visualisation of high numbers of fluorescent bacterial spots (**Figure 5A-B**). Importantly, also in this case the visual detection of bacteria with BAC 1 was confirmed by microbiological culturing (**Table 2**).

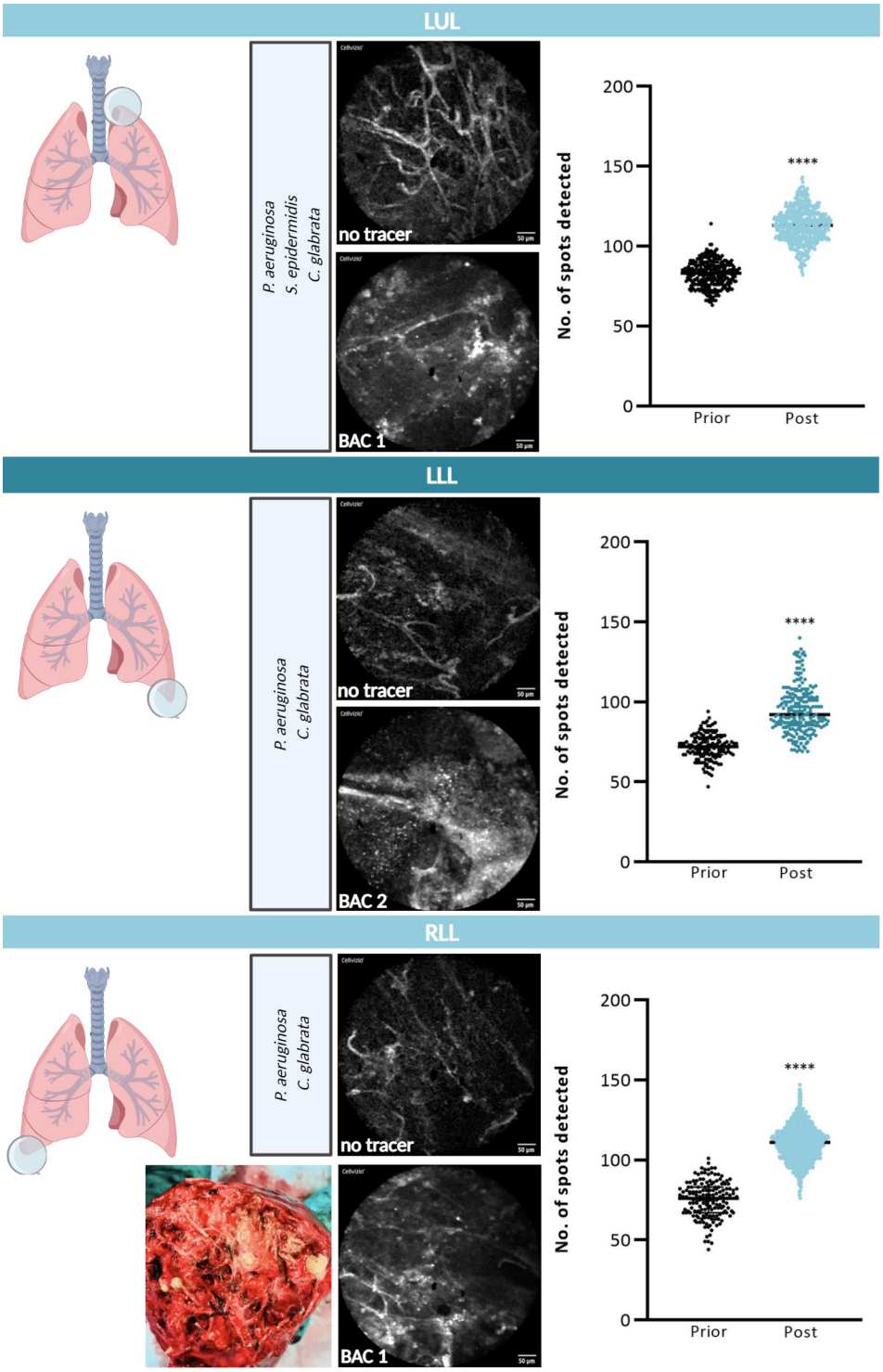
LUL
P. aeruginosa
S. epidermidis
C. glabrata
no tracer
BAC 1
No. of spots detected
200
150
100
50
0
****
Prior
Post
LLL
P. aeruginosa
C. glabrata
no tracer
BAC 2
No. of spots detected
200
150
100
50
0
****
Prior
Post
RLL
P. aeruginosa
C. glabrata
no tracer
BAC 1
No. of spots detected
200
150
100
50
0
****
Prior
Post

Figure 3. Summary illustration of explant case 16. Individual results of the anatomical segments, i.e. the left upper lobe (LUL) and the right and left lower lobes (RLL and LLL, respectively) are presented for case 16. Mixed micro-organism cultures are indicated for the imaged anatomical regions. The bottom left photograph shows a cross-section of the RLL with evidence of pustulating, suppurative and destructive disease due to end-stage cystic fibrosis. Dot plots on the right represent the data from baseline images prior administration of fluorescent tracer (black spots), or following the administration of BAC 1 (light blue spots) or BAC 2 (dark blue spots). Each individual dot represents the fluorescent bacterial spots detected in a single recorded frame. Data are presented as median (IQR; interquartile range). ****P < 0.0001. pCLE = probe-based confocal laser endomicroscopy. BAC 1 = ubiquicidin conjugated to fluorophore 7-nitrobenz-2-oxa-1,3-diazole (NBD). BAC 2 = antibiotic colistin (polymyxin E) conjugated to NBD. This figure is created with BioRender.com.

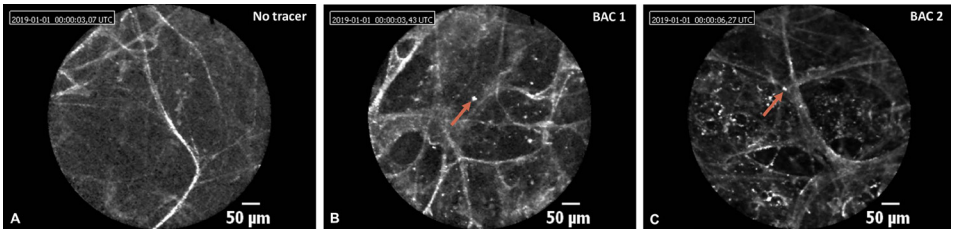

Figure 4. pCLE alveolar images of explant case 16. A) Baseline fluorescence prior to tracer administration in the left lower lobe. **B**) Fluorescence recorded in the left lower lobe following BAC 1 administration. **C**) Fluorescence recorded in the right lower lobe following BAC 2 administration. Microbial cultures from these anatomical segments, revealed the presence of both Gram-positive and Gram-negative bacterial species (**Table 2**). The red arrows mark individual bacterial spots. pCLE = probe-based confocal laser endomicroscopy. BAC 1 = ubiquicidin conjugated to fluorophore 7-nitrobenz-2-oxa-1,3-diazole (NBD). BAC 2 = antibiotic colistin (polymyxin E) conjugated to NBD.

The above-mentioned CF cases (case 16, 18 and 19) show colonisation by different organisms (**Table 2**). Nonetheless, these patients did not present clinical signs of active infection. CF patients are often subject to cycles of antibiotic therapy prior to lung transplantation, and they must clinically be in the right condition for major surgery. Importantly, pneumonia is an unlikely pre-operative complication in patients who are about to undergo lung transplantation and, accordingly, the moderate rise in bacterial signal was consistent with our expectations. This does probably explain why lower numbers of bacterial spots where detected in our present study compared to a previous study where pneumonia was imaged.[10] Furthermore, in select bronchial segments of cases 18 and 19, there was overgrowth of *Proteus* spp. Previous work with BAC 2 has shown that signal was not detected for this bacterial species, which relates to their intrinsic colistin resistance and may

explain at least in part why fewer spots were detected despite the culture positive results.[10] In this context, one also needs to bear in mind that, apart from differing target specificities, the imaging characteristics of the BAC 1 and BAC 2 tracers will differ. This relates to the fact that BAC 1 is based on a tribranched molecule conjugated with three NBD moieties, whereas BAC 2 is a conjugate that contains only a single NBD moiety. It should further be noted that the explant tissue from cases 16 and 18 had significant disease with extensive fibrotic and cystic structural change. This rendered the ventilation challenging with atelectasis and pustulating disease resulting in significant background fluorescence. As a consequence, the image analysis software may have had some difficulties in discriminating bacterial signal from background auto-fluorescence. Of importance, this will be of less relevance for the clinical translation of this tool, since lungs with this disease extent would not be imaged in a clinical settling.

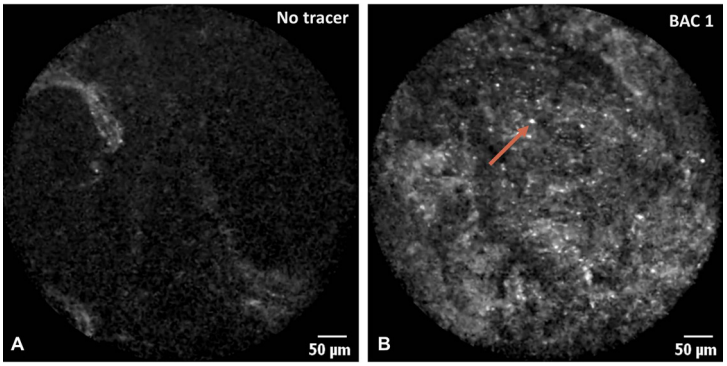

Figure 5. pCLE alveolar images of explant case 18. A) Fluorescence image of the right upper lobe prior tracer administration. **B**) Fluorescence image of the same area following topical administration of BAC 1. The red arrow indicate an individual bacterial spot. pCLE = probe-based confocal laser endomicroscopy. BAC 1 = ubiquicidin conjugated to fluorophore 7-nitrobenz-2-oxa-1,3-diazole (NBD).

Ex vivo image analysis of culture-negative human explant lungs

In eight of eleven culture-negative explant lungs, there was no visualisation of bacterial signals, which is in keeping with the culture results as exemplified in **Figure 6**.

Overall, we noticed also for the culture-negative cases some discrepancies between the numbers of visual spots and the numbers of spots reported by the image analysis software. For example, following tracer administration a median spot increase was reported by the software in cases 3 and 8, whereas this increase was not observed visually. The latter was consistent with the subsequent culture-negative test results (**Table 3a**). This implies that the human eye is presently still better able to discern differences in spot intensities in the recorded video frames than the applied image

analysis software, and that a next step in the translation of this infection imaging technology will require the advent of sophisticated machine-learning and artificial intelligence techniques. In addition, the implementation of tracers that fluoresce in the near-infrared range would minimize the interference by background auto-fluorescence.[7,17–19]

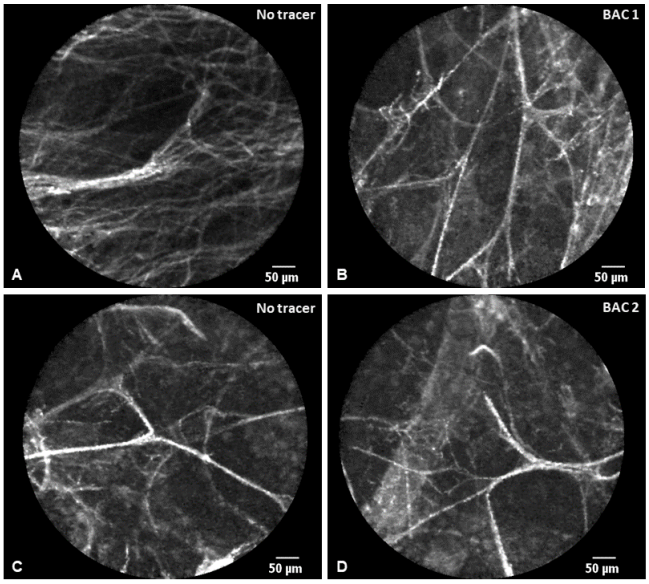

Figure 6. pCLE alveolar images of case 8. Explant case 8; no microbiological growth (**Table 2**). **A**) Right lower lobe (RLL) pre-tracer, and **B**) following topical administration of BAC 1. **C**) RLL pre-tracer and **D**) following BAC 2. No visual evidence of fluorescent spots above background is seen in all 4 images. pCLE = probe-based confocal laser endomicroscopy. BAC 1 = ubiquicidin conjugated to fluorophore 7-nitrobenz-2-oxa-1,3-diazole (NBD). BAC 2 = antibiotic colistin (polymyxin E) conjugated to NBD.

Added value of *ex vivo* image analysis: detection of bacteria in some culture-negative human explant lungs

In three culture-negative cases, namely 1, 6 and 17, bacterial signal was detected visually and with image analysis software. Case 1 concerned the right middle lobe after lobectomy, which showed some positive as well as negative fluorescence areas for BAC 2 (**Figure 7**). Although culture results remained negative, pathology results proved positive for a local pneumonia (**Table S1b**). Moreover, imaging analysis software showed a high increase of BAC 2 signal, corresponding to the presence of a Gram-negative bacterial species.

In addition, case 6, the post-EVLP specimen, tested bacterial culture negative, while tactile examination by the surgeon and pathology results from the contralateral lung showed clear evidence of pneumonia (**Table S1b**). Unfortunately, imaging was not possible in all segments of the left lung of case 6, as there was parenchymal damage during the procedure rendering ventilation and inflation of the lung challenging. Nonetheless, fluorescent spots were clearly observed with BAC 2 following imaging of the lingula, which corresponded to a median rise of 32 spots from baseline imaging using the image analysis software ($p < 0.0001$) (**Figure 8A**). **Figure 8B-D** shows alveolar images of pCLE pre- and post- tracer administration with clear fluorescent spots visualised. Corresponding pCLE videos are presented in the Supplementary Data (**Movie S5**, no tracer and **S5.1**, with BAC 2). These real-time observations are in keeping with a pneumonic infection.[10]

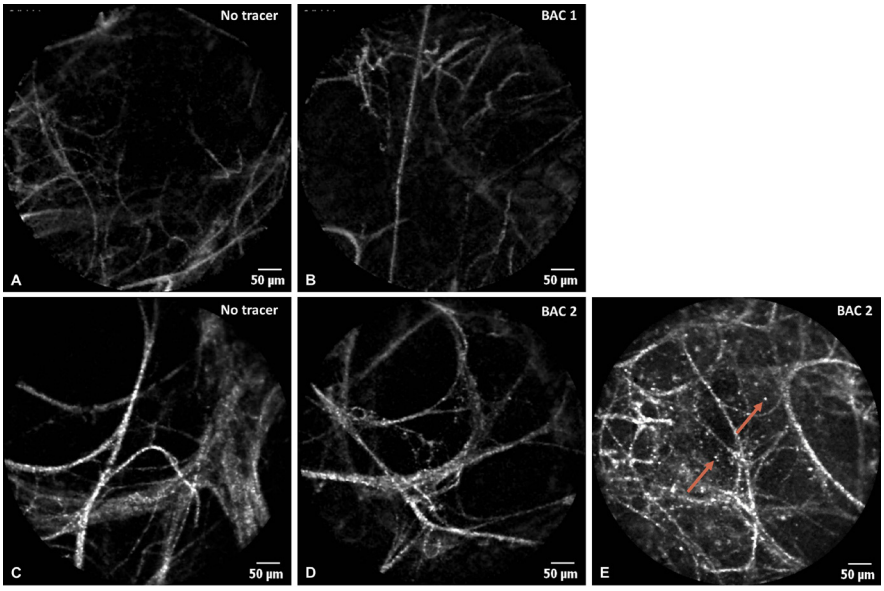

Figure 7. pCLE alveolar images of culture-negative case 1. Pathology results showed local pneumonia. **A**) Right middle lobe (RML) lateral side pre-tracer and **B**) following topical administration of BAC 1. **C**) The RML medial side pre-tracer and **D**, **E**) following BAC 2. The red arrows indicate fluorescently labelled bacteria. pCLE = probe-based confocal laser endomicroscopy. BAC 1 = ubiquicidin conjugated to fluorophore 7-nitrobenz-2-oxa-1,3-diazole (NBD). BAC 2 = antibiotic colistin (polymyxin E) conjugated to NBD.

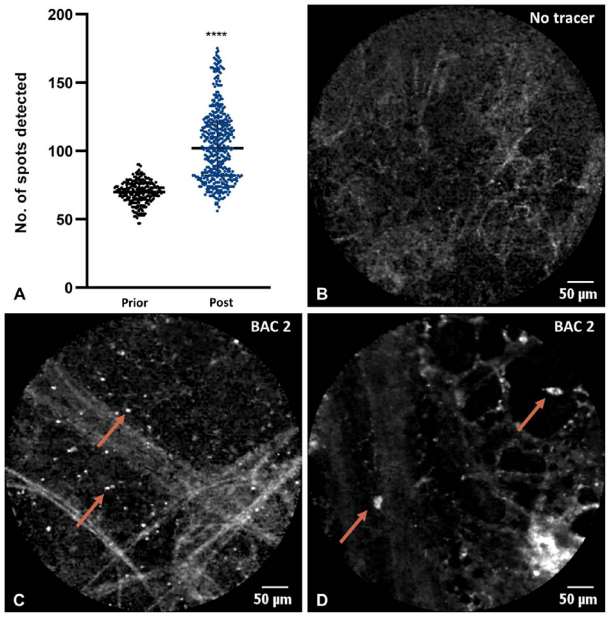

Figure 8. Graphical and pCLE alveolar images of explant case 6. A) The dot plot represents the collated results from all anatomical segments recorded at baseline, pre-tracer (black spots) and following BAC 2 insertion (blue spots). Each individual dot represents the numerical value of fluorescent bacterial spots detected in a single recorded frame. Data is presented as median (IQR; interquartile range). ****P < 0.0001. **B**) pCLE alveolar images pre-tracer and **C**-**D**) following topical administration of BAC 2. There is clear visualisation of fluorescent spots representing bacteria in the distal lung. The red arrows indicate fluorescently labelled bacteria. pCLE = probe-based confocal laser endomicroscopy. BAC 2 = antibiotic colistin (polymyxin E) conjugated to fluorophore 7-nitrobenz-2-oxa-1,3-diazole (NBD).

In case 17, a low bacterial signal was observed visually in some videos, which is in line with the moderate increase in spots detected by the image analysis software and potentially corresponds to a low volume colonisation. Nevertheless, the culture results were negative. This suggests that the imaged bacteria were unable to grow under the standard culture conditions used in this study, or that the pre-operative administration of ceftazidim had inhibited their growth. In fact, this may also explain the imaging of bacteria in the culture-negative cases 1 and 6.

Conclusion

Altogether, the present study implies that fluorescence-targeted pCLE is a promising bedside diagnostic tool for pulmonary medicine. In particular, we show that fluorescence-targeted pCLE allows the detection of microbial colonisation and infection of the distal lung, also in cases where the gold-standard diagnostic procedure of microbiological culture fails. Further, we show that fluorescence-targeted pCLE can provide valuable, objective information, beyond that gained from clinical inspection and assessment. This imaging modality may, thus, serve to optimise and accept borderline organs for transplantation. The real-time visualisation of lung-resident micro-organisms with different tracers could also allow direct targeted therapy during EVLP to reduce complications in the recipient patient. Even though some hurdles relating to the computational image analysis still need to be taken, we conclude that fluorescence-targeted pCLE may become a valuable asset in pulmonary medicine in general, and lung transplantation in particular.

Acknowledgements

Firstly, we would like to thank the many patients, who gave consent for this research to be conducted and the staff of the Cardiothoracic Surgery department for invaluable support. We thank the EPSRC IRC Proteus team in Edinburgh for bacterial tracer supply, methods and data analysis algorithms. We thank the cardiothoracic student team and specially J.E. van Zanden, who led this team, for communicating the availability of resected lungs. We thank the clinical skills centre at the UMCG, in particular S. Zwerver and R. Koster for providing equipment and hosting the experiments.

Funding

U.K. was supported by CEC MSCA-ITN grant 713660 (Pronkjewail) and the De Cock foundation. M.H. was funded by the Graduate School of Medical Sciences of the University of Groningen. A.M. was supported by Warrens Wish. K.D. was supported by Engineering and Physical Sciences Research Council (EPSRC, United Kingdom) Interdisciplinary Research Collaboration grant EP/K03197X/1 and the Department of Health and the Wellcome Trust through the Health Innovation Challenge Fund (HICF). Funding Reference Number: 0510-069. This research received no other specific grants from funding agencies in public, commercial, or not-for-profit sectors. Funding for the other authors was provided by their employers.

Author contributions

U.K. and M.H. contributed to the literature search, design of the study, experimental work, analysis and interpretation of the data and manuscript writing. M.E., W.T., G.M.v.D., A.D.L.M., K.D., W.B.N., J.M.v.D., E.A.M.V., and M.v.O. supplied materials and methods. M.E, C.v.D.W. and E.A.M.V. were central to identifying patients. U.K., M.H., M.v.O. and J.M.v.D. wrote the manuscript. All authors reviewed and approved the manuscript.

Competing interests

G.M. van Dam is CEO of TRACER™ Europe BV and CSO of AxelaRx Biosciences Inc. K. Dhaliwal has a shareholding in Edinburgh Molecular Imaging Ltd. The other authors declare neither financial nor non-financial conflicts of interest.

References

1. Mizgerd, J. Acute lower respiratory tract infection. *N. Engl. J. Med.* **358**, 716–727 (2008).
2. Heuker, M. *et al.* Preclinical studies and prospective clinical applications for bacteria-targeted imaging: the future is bright. *Clin. Transl. Imaging.* **4**, 253–264 (2016).
3. van Oosten, M. *et al.* Targeted imaging of bacterial infections: advances, hurdles and hopes. *FEMS Microbiol. Rev.* **39**, 892–916 (2015).
4. Thiberville, L. *et al. In vivo* imaging of the bronchial wall microstructure using fibered confocal fluorescence microscopy. *Am. J. Respir. Crit. Care Med.* **175**, 22–31 (2007).
5. Yserbyt, J., Dooms, C., Decramer, M. & Verleden, G. M. Probe-based confocal laser endomicroscopy of the respiratory tract: A data consistency analysis. *Respir. Med.* **107**, 1234–1240 (2013).
6. Akram, A. R. *et al.* A labelled-ubiquicidin antimicrobial peptide for immediate *in situ* optical detection of live bacteria in human alveolar lung tissue. *Chem. Sci.* **6**, 6971–6979 (2015).
7. Mills, B., Bradley, M. & Dhaliwal, K. Optical imaging of bacterial infections. *Clin. Transl. Imaging.* **4**, 163–174 (2016).
8. Gunasekaran, R. *et al.* Exploratory Use of Fluorescent SmartProbes for the Rapid Detection of Microbial Isolates Causing Corneal Ulcer. *Am. J. Ophthalmol.* **219**, 341–350 (2020).
9. Akram, A. R. *et al.* Enhanced avidity from a multivalent fluorescent antimicrobial peptide enables pathogen detection in a human lung model. *Sci. Rep.* **9**, 8422 (2019).
10. Akram, A. R. *et al. In situ* identification of Gram-negative bacteria in human lungs using a topical fluorescent peptide targeting lipid A. *Sci. Transl. Med.* **464**, 0033 (2018).
11. Venuta, F. & van Raemdonck, D. History of lung transplantation. *J. Thorac. Dis.* **9**, 5458–5471 (2017).
12. Makdisi, G., Makdisi, T., Jarmi, T. & Caldeira, C. C. *Ex vivo* lung perfusion review of a revolutionary technology. *Ann. Transl. Med.* **5**, 1–7 (2017).
13. Ware, L. B. *et al.* Assessment of lungs rejected for transplantation and implications for donor selection. *Lancet.* **360**, 619–620 (2002).
14. Tane, S., Noda, K. & Shigemura, N. *Ex Vivo* Lung Perfusion: A Key Tool for Translational Science in the Lungs. *Chest.* **151**, 1220–1228 (2017).
15. Kong, H., Akakin, H. C. & Sarma, S. E. A generalized laplacian of gaussian filter for blob detection and its applications. *IEEE Trans. Cybern.* **43**, 1719–1733 (2013).
16. Xu, Y., Wu, T., Gao, F., Charlton, J. R. & Bennett, K. M. Improved small blob detection in 3D images using jointly constrained deep learning and Hessian analysis. *Sci. Rep.* **10**, 326 (2020).
17. van Dam, G. M. *et al.* Intraoperative tumor-specific fluorescence imaging in ovarian cancer by folate receptor-α targeting: first in-human results. *Nat. Med.* **17**, 1315–1319 (2011).
18. van Oosten, M. *et al.* Real-time *in vivo* imaging of invasive- and biomaterial-associated bacterial infections using fluorescently labelled vancomycin. *Nat. Commun.* **4**, 2584 (2013).
19. Zoller, S. D. *et al.* Multimodal imaging guides surgical management in a preclinical spinal implant infection model. *JCI Insight.* **4**, 1–13 (2019).

Supplementary data

Movie S1. and **S1.1.** Case 16 (CF) left upper lobe no tracer (**S1.**) and BAC 1 (**S1.1.**).
Movie S2. and **S2.1.** Case 16 (CF) left lower lobe no tracer (**S2.**) and BAC 2 (**S2.1.**).
Movie S3. and **S3.1.** Case 16 (CF) right lower lobe no tracer (**S3.**) and BAC 1 (**S3.1.**).
Movie S4. and **S4.1.** Case 19 (CF) left lower lobe no tracer (**S4.**) and BAC 2 (**S4.1.**).
Movie S5. and **S5.1.** Case 6 (EVLP) lingula no tracer (**S5.**) and BAC 2 (**S5.1.**).

Scan me!

Table S1a. Detailed imaging results of non-infected cases

Case	Anatomical site	NP software	BAC 1 software	BAC 2 software	Radiology	Pathology
3	RML/RUL	86 (71-118)	125 (115-135)	90 (82-102)	RUL mass	Squamous cell carcinoma
4	RUL	136 (126-145)	x	133 (116-145)	Right hilar mass	Squamous cell carcinoma
5	RML/RUL	114 (100-126)	X	121 (108-129)	Severe emphysema, left upper lobe fibrotic change	Changes in keeping with COPD
7	R+L Collated	84 (58-106)	X	83 (73-92)	RUL, bi-basal bronchiectasis and fibrosis	Emphysema
8	RLL	92 (76-102)	106 (93-121)	120 (99-137)	Right basal mass, LLL bronchiectasis	Adenocarcinoma
10	RUL	63 (58-69)	x	58 (51-63)	Right apical mass	Adenocarcinoma
13	RUL	117 (101-129)	98 (93-105)	132 (122-145)	RUL mass	Adenocarcinoma
14	R+L Collated	98 (84-120)	108 (100-115)	110 (100-121)	Extensive bullous emphysema	Extensive emphysema
17	Left Lung	73 (61-89)	107 (94-166)	70 (64-75)	Interstitial lung changes in keeping with NSIP pattern	Fibrosis

Values represent median (IQR; interquartile range). Right upper lobe (RUL), right middle lobe (RML), right lower lobe (RLL), left lower lobe (LLL), right (R), left (L), no probe (NP), non-specific interstitial pneumonia (NSIP), chronic obstructive pulmonary disease (COPD).

Table S1b. Detailed imaging results of infected and/or colonised cases

Case	Anatomical site	NP software	BAC 1 software	BAC 2 software	Radiology	Pathology
1	RML	65 (47-85)	81 (68-93)	122 (85-137)	RML pulmonary mass	Granulomatous organising pneumonia and bronchiectasis
6	LUL/lingula	70 (64-76)	x	102 (82-121)	Evidence of inflammatory change in RUL and RML	Inflammatory change and pneumonia
11	RUL apical	95 (62-107)	x	112 (105-121)	Bilateral extensive fibrotic change	Emphysema and severe fibrosis
	RLL basal	109 (96-126)	112 (102-117)	x		
	RML	84 (85-100)	x	108 (98-117)		
	LLL basal	89 (84-94)	108 (97-119)	x		
	LUL	115 (107-121)	x	131 (121-144)		
	LUL anterior	123 (116-130)	133 (121-146)	x		
	Collated	**103 (89-118)**	**118 (107-131)**	**117 (107-129)**		
15	RML medial	104 (98-110)	x	141 (135-147)	Large volume emphysema and bronchiectasis	Emphysema and bronchiectasis
	RLL basal posterior	125 (120-132)	111 (105-119)	x		
	RUL anterior	108 (102-114)	x	123 (112-133)		
	RUL posterior	114 (107-120)	110 (104-115)	x		
	RUL apical	117 (110-125)	x	121 (115-128)		
	LLL basal lateral	101 (94-108)	x	114 (107-121)		
	LLL basal apical	117 (111-123)	125 (119-133)	x		
	LUL anterior	115 (109-120)	123 (115-129)	x		
	Lingula	108 (102-115)	x	115 (97-133)		
	Collated	**113 (106-121)**	**119 (112-128)**	**123 (111-135)**		
16	RUL anterior	81 (76-87)	x	81 (76-87)	Cystic bronchiectasis with extensive inflammatory changes and destruction	CF changes
	RML lateral	88 (81-94)	90 (84-97)	x		
	RML medial	89 (81-95)	x	82 (71-90)		
	RLL basal	76 (67-83)	111 (103-118)	x		
	LUL apical	83 (76-88)	133 (105-120)	x		
	LUL anterior	112 (104-120)	x	82 (73-89)		
	LLL lateral	72 (67-78)	x	92 (85-103)		
	Lingula	84 (78-90)	75 (68-82)	x		
	Collated	**87 (79-107)**	**104 (89-115)**	**82 (72-90)**		
18	RUL apical	55 (49-59)	71 (60-82)	x	Bilateral bronchiectatic change, greatest at the LUL	CF changes
	LLL basal	61 (56-66)	x	69 (63-75)		
	LUL	95 (89-101)	x	78 (72-85)		
	Collated	**60 (52-70)**	**72 (62-84)**	**72 (65-79)**		
19	LLL lateral	70 (60-76)	72 (62-83)	x	Extensive bilateral bronchiectatic change	No pathological investigation was performed
	LLL anteromedial	61 (51-75)	x	90 (76-113)		
	LLL posterior	93 (84-107)	114 (103-122)	115 (104-126)		
	RML medial	71 (54-89)	x	82 (73-91)		
	RUL apical	104 (99-113)	109 (103-119)	113 (96-130)		
	RLL	87 (73-112)	x	129 (119-139)		
	Collated	**70 (58-79)**	**87 (73-120)**	**99 (82-120)**		

Values represent median (IQR; interquartile range). Right upper lobe (RUL), right middle lobe (RML), right lower lobe (RLL), left upper lobe (LUL), left lower lobe (LLL), no probe (NP), cystic fibrosis (CF).

Chapter 10

Summary, discussion and conclusion

Summary

Infectious diseases have always been a major threat to human health and, despite major advances in medicine and the development of potent antimicrobial agents, this is still true today. In 2017, bacterial infections caused globally more than 8 million deaths and they were responsible for most morbidity among the human diseases.[1] Despite advanced diagnostic technologies for typing and detection of pathogens, diagnosis of bacterial infections is unfortunately rarely straightforward and often it is time-consuming to identify the causative agent.[2] Moreover, current anatomical and functional imaging modalities are insufficiently capable of distinguishing bacterial infection from sterile inflammation.[3–6] As a consequence, the treatment of infections may be delayed or ineffective. Therefore, novel fast and accurate diagnostic techniques to detect and identify bacterial pathogens are urgently needed.

Bacteria-targeted fluorescence imaging is a promising diagnostic approach with the potential to improve diagnosis for different infectious diseases.[6,7] This thesis presents an overview of currently used infection imaging techniques with a focus on positron emission tomography (PET) and newly designed bacteria-specific fluorescence imaging approaches to diagnose different infectious diseases. **Chapter 1** describes the general introduction, the diagnostic challenges and the outline of this thesis.

Chapter 2 is a literature review on bacteria-targeted radionuclide-mediated and fluorescence imaging. In the past years, target selection has mainly been focused on antibiotics and antimicrobial peptides.[1] Although radiolabelled bacteria-targeted tracers seem promising, many tracers may not be ideal candidates for bacteria-specific imaging in patients. For example, the advanced radiolabelled antibiotic ciprofloxacin (^{99m}Techneticum-ciprofloxacin; ^{99m}Tc-ciprofloxacin; Infection©) was not able to reliably differentiate infection from sterile inflammation. Other promising imaging agents are based on bacteria-specific metabolizable compounds such as 6-[^{18}F]-fluoromaltose (^{18}F-FM) and 2-[^{18}F]-fluoro-deoxy-sorbitol (^{18}F-FDS). It is believed that these metabolizable compounds have high potential for the clinical translation of bacteria-targeted imaging. A relatively new and upcoming imaging technique is bacteria-targeted imaging based on fluorescence. Several studies have shown promising results in animal infection models where different bacteria-targeted tracers were used. One of these promising tracers is based on the antibiotic vancomycin coupled to the near-infrared (NIR) fluorophore IRDye800CW (in short vanco-800CW). Importantly, vanco-800CW allowed the specific detection of *Staphylococcus aureus* over sterile inflammation or a Gram-negative bacterial infection *in vivo*. Overall, novel imaging modalities are highly needed to accurately and quickly diagnose bacterial infections. In this regard, bacteria-targeted imaging is an attractive option, due to its specificity and ease of detection. Clearly, a rapid and accurate diagnosis is crucial for the effective treatment of a vast number of infectious diseases. Even though it remains uncertain which particular tracers will ultimately prove to be most appropriate for clinical use, it can

be anticipated that some of the tracers and respective imaging techniques described in Chapter 2 will be implemented in routine clinical diagnostic procedures.

Chapter 3 is focused on the clinically used radionuclide-mediated infection imaging modality PET. Fluorine-18-fluorodeoxyglucose (^{18}F-FDG) combined with PET imaging can be used to detect infection and inflammation, and it is especially useful in tracking down the cause of fever of unkown origin.[4,8] This non-specific infection imaging technique is based on the glucose uptake by cells involved in the inflammatory process and, therefore, it does not readily distinguish between bacterial infection and sterile inflammation.[9] In Chapter 3, the intriguing question is answered whether infecting bacteria accumulate ^{18}F-FDG and potentially contribute to the signal detected by ^{18}F-FDG-PET infection imaging. A wide range of frequently encountered bacterial pathogens did indeed show active uptake of ^{18}F-FDG *in vitro*. Accordingly, it seems plausible that these pathogens also accumulate ^{18}F-FDG and contribute to the ^{18}F-FDG-PET signal in human. Of all tested bacteria, *Streptococcus pyogenes* displayed the highest uptake of ^{18}F-FDG. However, some infections caused by this bacterium, especially necrotizing fasciitis, require immediate antibiotic therapy and aggressive surgery. This emphasizes the need for faster, preferably real-time, bacteria-targeted imaging that cannot be achieved with ^{18}F-FDG-PET.

With the overarching objective to explore the possibilities for bacteria-specific infection imaging, the research described in **Chapters 4** to **6** addressed the targeted detection of staphylococcal infections. In particular, *S. aureus* is responsible for the majority of skin and soft tissue infections, but can also cause other severe infectious diseases, such as osteomyelitis and bacteraemia.[10] A previously developed fully human monoclonal antibody (1D9) against the immunodominant staphylococcal antigen A (Isa A)[11] was coupled to the NIR fluorophore IRDye800CW for fluorescence imaging, or ^{89}Zirconium for PET (**Chapter 4**). Here, specific targeting of *S. aureus* was demonstrated, both in a human *post-mortem* infection model and in an *in vivo* murine skin infection model. Although the results seem promising for both the fluorescence and PET imaging, further research will be needed to evaluate the effectiveness of the human monoclonal antibody 1D9 to target deep-seated infections.

Chapter 5 describes a smart-activatable tracer that responds to the enzymatic activity of a micrococcal nuclease that is specifically secreted by *S. aureus*. This tracer consists of a fluorophore and a quencher, and it has the favourable characteristic to only emit a fluorescence signal when it is cleaved by nuclease activity. Of note, the investigated tracer was a derivative of a previously described nuclease-activated tracer[12] with enhanced sensitivity for the micrococcal nuclease. Therefore, the investigation was focused on the new tracer's sensitivity, specificity and stability in human blood and plasma. Subsequently, **Chapter 6** gives a glimpse of the future clinical implementation of this nuclease-activated tracer in diagnosing early and accurate *S. aureus* bloodstream infections.

The research presented in the last sections of this thesis (**Chapters 7** to **9**) was aimed at exploring new clinical applications for bacteria-targeted fluorescence imaging. The first step to reach this aim is shown in **Chapter 7**, where successful *ex vivo* fluorescence imaging of clinical bacterial biofilms on osteosynthesis devices with vanco-800CW is described. In fact, the bacteria-targeted fluorescence imaging with vanco-800CW allowed a correct diagnosis of FRIs in less than 30 min, which represents a remarkable increase in the time to result compared to the standard microbiological diagnosis. It can be anticipated that, for patients with fracture-related infections (FRIs), *in vivo* fluorescence-guided surgery may be of even greater value, since it can provide surgeons with real-time visual information on the infected tissue and materials, allowing them to spare the non-infected surrounding tissue.

In **Chapter 8**, the feasibility of fluorescence-guided arthroscopic imaging of prosthetic joint infections (PJIs) is presented for the first time in a human *post-mortem* knee infection model. Also in this setting, the fluorescent vanco-800CW tracer allowed accurate real-time detection of a staphylococcal biofilm. Moreover, it was shown that the fluorescently labelled vancomycin has affinity for biofilms of most Gram-positive bacteria, which are the causative agents in the majority of PJIs. Therefore, this application holds great promise for future clinical implementation.

Lastly, fluorescence-targeted imaging of bacterial colonisation and infection in the human distal lung is presented in **Chapter 9**. By combining probe-based confocal laser endomicroscopy with microbe-targeted fluorescence imaging, micro-organisms were visualised in the alveolar space of human resected lung specimens. Importantly, fluorescence-targeted imaging was shown to be of added value in the detection of micro-organisms, even in cases where the gold standard of microbiological culture failed.

Discussion

Future diagnostic perspectives

Bacteria-targeted imaging is an attractive diagnostic modality, which is of upcoming interest these days. This technique can pinpoint infections more specifically than the currently used anatomical and functional imaging modalities. Although bacteria-targeted imaging is still in its infancy, the development of specific tracers and various imaging modalities described in this thesis demonstrates the potential benefits for diagnosing several infectious diseases. In addition, this technology may also be of great value for monitoring the treatment response and patient follow-up in the clinical practice. Notwithstanding the promising results obtained, more research and further development of new targeting molecules and imaging agents is needed to improve the imaging sensitivity. Translation of tracers into clinical use would be easiest for those molecules that have shown to be non-toxic for patients, such as the antibiotic vancomycin and the NIR fluorophore IRDye800CW.[13] Other aspects of bacteria-targeted infection imaging that need further development relate to the

computer-aided image analysis through sophisticated machine-learning and artificial intelligence approaches for enhanced detection of abnormal patterns. This will allow a more accurate distinction between infected areas and normal structures.

Over the past years, much experience has been gained in fluorescence-targeted imaging in the field of oncology and surgery.[14–19] Using fluorescence-guided surgery, tumour spots of <1 mm were visualised in patients with ovarian cancer.[20] Likewise, in the field of infectious diseases, intra-operative bacteria-targeted fluorescence imaging might be able to accurately visualise the extent and borders of infection. For example, in fulminant infectious diseases, such as the afore-mentioned necrotizing fasciitis, a more precise resection of infected tissue would potentially improve patient outcome.

It is believed that bacteria-targeted fluorescence imaging allows for an early and accurate bedside diagnosis in different infectious diseases, such as pneumonia or biomaterial-associated infections (**Chapters 7**, **8** and **9**). However, a major drawback of fluorescence imaging is its limited penetration depth, which makes this technique mainly suitable for surface and endoscopic imaging. Another promising real-time imaging technique that allows detection of appropriate tracers at a tissue depth of several centimetres is optoacoustic imaging.[21] The optoacoustic imaging modality is based on the absorption of light by photo-absorbing molecules, followed by thermo-elastic expansion, which results in the emission of ultrasound waves.[22–24] This new imaging approach holds great promise for the enhanced diagnosis of deeper-seated infections in patients.

Most investigated imaging approaches described in this thesis involve the use of a single tracer. It is, however, very well conceivable that the use of multiple tracers targeting different micro-organisms and multi-spectral imaging will allow a precise identification of the causative agent. For instance, the *Staphylococcus*-specific antibody 1D9 or the nuclease-specific smart activatable tracer described in **Chapters 4**, **5** and **6** could be complemented by other species-specific tracers. However, as long as these tracers are not yet available, Gram-positive and Gram-negative bacterial pathogens could be visualised, respectively, with vanco-800CW and the colistin (polymyxin E)-based tracer described in **Chapters 7**, **8** and **9**.[13,25,26] In this respect, it would be even more desirable to develop targeting molecules that are able to discriminate between antibiotic resistant and non-resistant micro-organisms. In particular, smart-activatable tracers, such as the nuclease-activated tracer described in **Chapters 5** and **6** of this thesis, that allow for greater target-to-background ratios, would be well suited for this purpose. To further improve imaging techniques for the detection of infectious agents, multi-modality imaging with tracers that emit both a fluorescence signal and a second signal based on for example radionuclides or MRI contrast agents, would allow for pre-operative localisation of deep-seated infections and intra-operative guidance.[27,28] Feasibility of this concept was shown for the *Staphylococcus*-specific antibody 1D9 as demonstrated in a recent study by Zoller *et al.*, where this antibody was dual-labelled with a NIR fluorophore and ^{89}Zirconium.[29]

Future therapeutic perspectives

Besides bacteria-targeted imaging for diagnosing infectious diseases, a bacteria-targeted therapeutic approach could improve the treatment of infections. In particular, a potential therapeutic approach based on targeted photodynamic therapy (PDT) appears highly attractive.[30–39] Bacteria-targeted PDT is based on the excitation of a photo-sensitive molecule, a photosensitizer, resulting in both an optical signal and the generation of reactive oxygen species that specifically kill the targeted micro-organism. Targeted PDT against *S. aureus* was recently described *in vivo* and in a human *post-mortem* model with a so called theragnostic agent, based on the *Staphylococcus*-specific antibody presented in **Chapter 4** of this thesis.[40] This specific theragnostic agent is able to disrupt biofilms, and it is therefore highly promising for the treatment of biomaterial-associated infections. Theoretically, once a biofilm gets disrupted, bacteria will become more susceptible for antibiotic treatment, which will improve eradication of the infecting micro-organisms.

Besides the treatment of biomaterial-associated infections, bacteria-targeted PDT could potentially be of great value for the treatment of many different infectious diseases. For example, as highlighted in **Chapter 9**, targeted treatment in donor lungs, in an *ex vivo* lung perfusion setting, could be of help to prevent pneumonia in the recipient in the future. In principle, bacteria-targeted therapy could aid in the cleaning-up of organs prior to transplantation. Whether this is a realistic option needs to be assessed through further research.

Conclusion

Altogether, this thesis describes the possible use of bacteria-targeted imaging in the diagnosis of different infectious diseases with focus on bloodsteam infections, biomaterial-associated infections and pneumonia. Bacteria-targeted fluorescence imaging is fast and feasible, and has a high potential to aid in the accurate diagnosis of infections, which will be of great benefit for patients. Moreover, this relatively new imaging technique will most likely allow for the intra-operative direct detection of infecting micro-organisms. As described in this thesis, different bacteria-targeted tracers are promising candidates for clinical implementation. Future studies are needed to translate these tracers and the respective imaging modalities into the clinical setting. However, already now it can be foreseen that reinforcement of the here presented diagnostic approaches with optoacoustic imaging, multi-spectral or multi-modality imaging, and targeted therapy is likely to empower the fight against infectious diseases.

References

1. Ordonez, A. A. *et al.* Molecular imaging of bacterial infections: Overcoming the barriers to clinical translation. *Sci. Transl. Med.* **508**, 8251 (2019).
2. Sabat, A. J. *et al.* Overview of molecular typing methods for outbreak detection and epidemiological surveillance. *Eurosurveillance.* **18**, 1–15 (2013).
3. Love, C. & Palestro, C. J. Radionuclide imaging of infection. *J. Nucl. Med. Technol.* **32**, 47–57 (2004).
4. Love, C., Tomas, M. B., Tronco, G. G. & Palestro, C. J. FDG PET of infection and inflammation. *Radiographics.* **25**, 1357–1368 (2005).
5. Strobel, K. & Stumpe, K. D. M. PET/CT in musculoskeletal infection. *Semin. Musculoskelet. Radiol.* **11**, 353–364 (2007).
6. van Oosten, M. *et al.* Targeted imaging of bacterial infections: advances, hurdles and hopes. *FEMS Microbiol. Rev.* **39**, 892–916 (2015).
7. Mills, B., Bradley, M. & Dhaliwal, K. Optical imaging of bacterial infections. *Clin. Transl. Imaging.* **4**, 163–174 (2016).
8. Besson, F. L. *et al.* Contribution of ^{18}F-FDG PET in the diagnostic assessment of fever of unknown origin (FUO): a stratification-based meta-analysis. *Eur. J. Nucl. Med. Mol. Imaging.* **43**, 1887–1895 (2016).
9. Glaudemans, A. W. J. M., Israel, O. & Slart, R. H. J. A. Pitfalls and Limitations of Radionuclide and Hybrid Imaging in Infection and Inflammation. *Semin. Nucl. Med.* **45**, 500–512 (2015).
10. Tong, S. Y. C., Davis, J. S., Eichenberger, E., Holland, T. L. & Fowler, V. G. *Staphylococcus aureus* infections: Epidemiology, pathophysiology, clinical manifestations, and management. *Clin. Microbiol. Rev.* **28**, 603–661 (2015).
11. van den Berg, S. *et al.* A human monoclonal antibody targeting the conserved staphylococcal antigen IsaA protects mice against *Staphylococcus aureus* bacteremia. *Int. J. Med. Microbiol.* **305**, 55–64 (2015).
12. Hernandez, F. J. *et al.* Noninvasive imaging of *Staphylococcus aureus* infections with a nuclease-activated probe. *Nat. Med.* **20**, 301–306 (2014).
13. van Oosten, M. *et al.* Real-time *in vivo* imaging of invasive- and biomaterial-associated bacterial infections using fluorescently labelled vancomycin. *Nat. Commun.* **4**, 2584 (2013).
14. van Dam, G. M. *et al.* Intraoperative tumor-specific fluorescence imaging in ovarian cancer by folate receptor-α targeting: First in-human results. *Nat. Med.* **17**, 1315–1319 (2011).
15. de Jongh, S. J. *et al.* Back-Table Fluorescence-Guided Imaging for Circumferential Resection Margin Evaluation Using Bevacizumab-800CW in Patients with Locally Advanced Rectal Cancer. *J. Nucl. Med.* **61**, 655–661 (2020).
16. Voskuil, F. J. *et al.* Fluorescence-guided imaging for resection margin evaluation in head and neck cancer patients using cetuximab-800CW: A quantitative dose-escalation study. *Theranostics.* **10**, 3994–4005 (2020).
17. Voskuil, F. J. *et al.* Exploiting metabolic acidosis in solid cancers using a tumor-agnostic pH-activatable nanoprobe for fluorescence-guided surgery. *Nat. Commun.* **11**, 1–10 (2020).
18. Joshi, B. P. & Wang, T. D. Targeted Optical Imaging Agents in Cancer: Focus on Clinical Applications. *Contrast Media Mol. Imaging.*

2018, 2015237 (2018).

19. Steinkamp, P. J. *et al.* Fluorescence-guided visualization of soft tissue sarcomas by targeting vascular endothelial growth factor-A: a phase 1 single-center clinical trial. *J. Nucl. Med.* **62**, 120.245696 (2020).
20. Terwisscha van Scheltinga, A. G. T. *et al.* Intraoperative near-infrared fluorescence tumor imaging with vascular endothelial growth factor and human epidermal growth factor receptor 2 targeting antibodies. *J. Nucl. Med.* **52**, 1778–1785 (2011).
21. Ntziachristos, V. Going deeper than microscopy: the optical imaging frontier in biology. *Nat. Methods.* **7**, 603–614 (2010).
22. Ntziachristos, V. & Razansky, D. Molecular imaging by means of multispectral optoacoustic tomography (MSOT). *Chem. Rev.* **110**, 2783–2794 (2010).
23. Neuschmelting, V. *et al.* Performance of a Multispectral Optoacoustic Tomography (MSOT) System equipped with 2D vs. 3D Handheld Probes for Potential Clinical Translation. *Photoacoustics.* **4**, 1–10 (2016).
24. Taruttis, A. & Ntziachristos, V. Advances in real-time multispectral optoacoustic imaging and its applications. *Nat. Photonics.* **9**, 219–227 (2015).
25. Akram, A. R. *et al. In situ* identification of Gram-negative bacteria in human lungs using a topical fluorescent peptide targeting lipid A. *Sci. Transl. Med.* **10**, 0033 (2018).
26. Gunasekaran, R. *et al.* Exploratory Use of Fluorescent SmartProbes for the Rapid Detection of Microbial Isolates Causing Corneal Ulcer. *Am. J. Ophthalmol.* **219**, 341–350 (2020).
27. Azhdarinia, A., Ghosh, P., Ghosh, S., Wilganowski, N. & Sevick-Muraca, E. M. Dual-labeling strategies for nuclear and fluorescence molecular imaging: A review and analysis. *Mol. Imaging Biol.* **14**, 261–276 (2012).
28. Ding, N. *et al.* Folate receptor-targeted fluorescent paramagnetic bimodal liposomes for tumor imaging. *Int. J. Nanomedicine.* **6**, 2513–2520 (2011).
29. Zoller, S. D. *et al.* Multimodal imaging guides surgical management in a preclinical spinal implant infection model. *JCI Insight.* **4**, 1–13 (2019).
30. Ragàs, X. *et al.* Cationic porphycenes as potential photosensitizers for antimicrobial photodynamic therapy. *J Med Chem.* **53**, 7796–7803 (2010).
31. Bhatti, M. *et al.* Antibody-targeted lethal photosensitization of *Porphyromonas gingivalis*. *Antimicrob. Agents Chemother.* **44**, 2615–2618 (2000).
32. Demidova, T. N. & Hamblin, M. R. Photodynamic therapy targeted to pathogens. *Int. J. Immunopathol. Pharmacol.* **17**, 245–254 (2004).
33. Dosselli, R. *et al.* Synthesis, characterization, and photoinduced antibacterial activity of porphyrin-type photosensitizers conjugated to the antimicrobial peptide apidaecin 1b. *J. Med. Chem.* **56**, 1052–1063 (2013).
34. Suci, P., Kang, S., Gmür, R., Douglas, T. & Young, M. Targeted delivery of a photosensitizer to *Aggregatibacter actinomycetemcomitans* biofilm. *Antimicrob. Agents Chemother.* **54**, 2489–2496 (2010).
35. Embleton, M. L., Nair, S. P., Cookson, B. D. & Wilson, M. Selective lethal photosensitization of methicillin-resistant *Staphylococcus aureus* using an IgG-in (IV) chlorin e6 conjugate. *J. Antimicrob. Chemother.* **50**, 857–864 (2002).

36. Embleton, M. L., Nair, S. P., Cookson, B. D. & Wilson, M. Antibody-directed photodynamic therapy of methicillin-resistant *Staphylococcus aureus*. *Microb. Drug Resist.* **10**, 92–97 (2004).

37. Embleton, M. L. *et al.* Development of a novel targeting system for lethal photosensitization of antibiotic-resistant strains of *Staphylococcus aureus*. *Antimicrob. Agents Chemother.* **49**, 3690–3696 (2005).

38. Kim, G., Karbaschi, M., Cooke, M. & Gaitas, A. Light-based methods for whole blood bacterial inactivation enabled by a recirculating flow system. *Photochem. Photobiol.* **94**, 744–751 (2018).

39. Wang, K. K. *et al.* Target-oriented photofunctional nanoparticles (TOPFNs) for selective photodynamic inactivation of Methicillin-resistant *Staphylococcus aureus* (MRSA). *J. Photochem. Photobiol. B Biol.* **183**, 184–190 (2018).

40. Bispo, M. *et al.* Fighting *Staphylococcus aureus* infections with light and photo-immunoconjugates. *JCI Insight.* **22**, 139512 (2020).

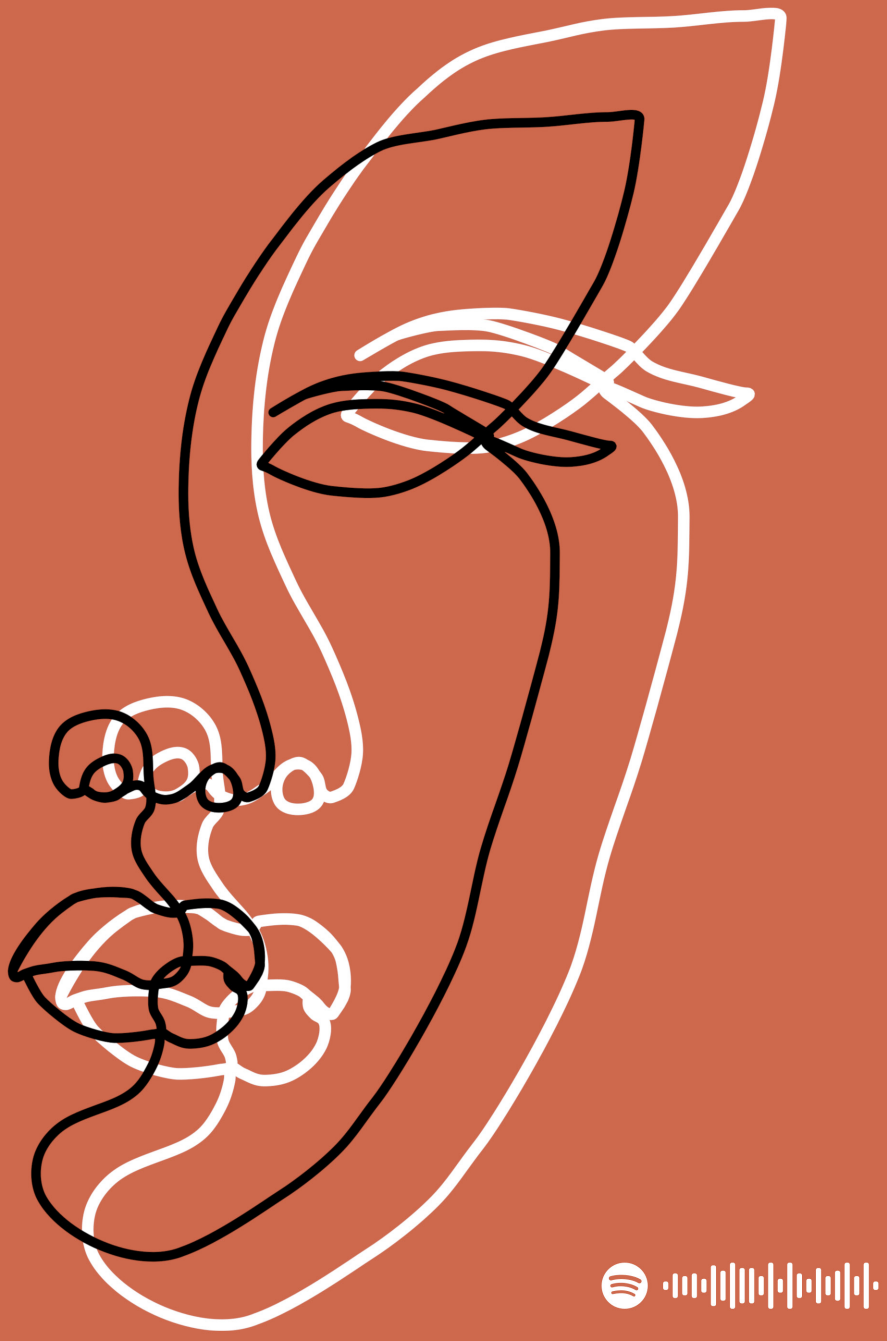

Chapter 11

Nederlandse samenvatting

(Dutch summary)

Introductie

Bacteriële infecties

Infectieziekten zijn sinds mensenheugenis een grote bedreiging voor de menselijke gezondheid. Ondanks de grote vooruitgang in de geneeskunde en de ontwikkeling van antimicrobiële middelen, is dit tegenwoordig nog steeds het geval. In 2017 veroorzaakten bacteriële infecties wereldwijd meer dan 8 miljoen doden en waren zij verantwoordelijk voor de grootste morbiditeit bij de mens.[1] De incidentie van bacteriële infecties neemt toe als gevolg van een toenemende vergrijzing en geavanceerde medische technologieën, waaronder het gebruik van geïmplanteerde kunstmaterialen en orgaantransplantaties. Daarnaast is er een snelle toename van resistente bacteriën, die ongevoelig zijn voor antibiotica, waardoor bacteriële infecties steeds moeilijker te behandelen zijn.[1-3] Een snelle en adequate diagnose van de (bacteriële) ziekteverwekker is van cruciaal belang voor een gerichte behandeling en resulteert uiteindelijk in een betere prognose voor de patiënt. In principe kunnen micro-organismen alle delen en functies van een menselijk lichaam infecteren en verstoren. Er zijn dan ook talloze verschillende infectieziekten bekend. In het onderzoek dat beschreven is in dit proefschrift staan drie specifieke bacteriële infectieziekten centraal, namelijk bloedbaaninfecties, kunstmateriaal-gerelateerde infecties en longontsteking (de zogenaamde pneumonie).

Klinische uitdagingen bij het diagnosticeren van infecties

Ondanks geavanceerde diagnostische technologieën voor het typeren en detecteren van pathogenen, is de diagnose van bacteriële infecties helaas niet altijd eenvoudig. De klinische diagnose 'infectie' wordt momenteel gesteld op basis van een combinatie van klinische kenmerken en symptomen, infectieparameters in het bloed, microbiologische kweken van lichaamsmaterialen en beeldvorming met niet-specifieke technieken zoals 'computed tomography' (CT), 'magnetic resonance imaging' (MRI), echografie, 'positron emission tomography' (PET), 'single-photon emission computed tomography' (SPECT) en scintigrafie. De genoemde verschillende beeldvormende technieken zijn echter niet in staat om specifiek een bacteriële infectie van een steriele inflammatie of andere infectie (bijvoorbeeld een virale of schimmelinfectie) te onderscheiden.[2,4-6] Microbiologische kweken of moleculaire detectietechnieken zijn bovendien nodig om het veroorzakende micro-organisme te kunnen identificeren. Dit diagnostische proces duurt echter vaak uren tot dagen, waarbij intussen met een empirische behandeling met breed-spectrum antibiotica wordt gestart.[7] Bovendien is het soms niet mogelijk om geschikte biopten of kweekmateriaal te verkrijgen, waardoor het stellen van de juiste diagnose zeer uitdagend kan zijn. Als gevolg hiervan kan de behandeling van infecties worden vertraagd of er wordt een suboptimale therapie ingesteld. Er is daarom dringend behoefte aan een snelle en nauwkeurige techniek om bacteriële ziekteverwekkers op te sporen en te identificeren. Een snelle detectie van bacteriën is nodig om antibiotische therapie te optimaliseren,

bijwerkingen te beperken en bovendien medische kosten te verlagen. Daarnaast helpt een doelgerichte behandeling met de juiste antibiotica de selectie en verspreiding van resistente micro-organismen te voorkomen.

Nieuwe diagnostische beeldvormende technieken

In de kliniek is een gevoelige en specifieke beeldvormingstechniek die snel en betrouwbaar is en die direct de detectie van infecterende bacteriën mogelijk maakt, zeer wenselijk. De bovengenoemde huidige beeldvormende technieken (d.w.z. anatomische beeldvormende technieken, zoals CT, MRI en echografie, en functionele beeldvormende technieken, zoals PET, SPECT en scintigrafie) voldoen helaas niet aan deze eisen. Een belangrijk nadeel van de huidige beeldvormingstechnieken is het onvermogen om bacteriële infecties betrouwbaar te onderscheiden van andere oorzaken van inflammatie, zoals bijvoorbeeld maligniteiten, of van fysiologische processen zoals wondgenezing. Derhalve is een nieuwe beeldvormingstechniek, die een snelle en nauwkeurige, directe detectie van infecterende micro-organismen mogelijk maakt van groot belang in de klinische praktijk. Idealiter verschaft deze nieuwe techniek zelfs specifieke informatie over de verwekker en het resistentiepatroon.

Fluorescentie-beeldvorming

Fluorescentie (optische)-beeldvorming is een elegante beeldvormingstechniek die zich de laatste jaren snel ontwikkelt. Het principe van fluorescentie-beeldvorming is gebaseerd op de excitatie van een fluorescerend molecuul (een zogeheten fluorofoor) door middel van licht met een bepaalde golflengte. De elektronen van de fluorofoor worden geëxciteerd en wanneer deze elektronen vervolgens terugkeren naar hun grondtoestand, wordt licht uitgezonden met een net iets langere golflengte. Dit licht kan worden gedetecteerd met een speciale fluorescentiecamera. Menselijk weefsel is van nature autofluorescent, wat voornamelijk detecteerbaar is in het zichtbare spectrum (400-600 nm). Het is van belang dat fluoroforen sterke signalen uitzenden, zodat het signaal van de fluorofoor kan worden onderscheiden van de autofluorescentie van het omliggende weefsel. Fluoroforen die signalen uitzenden in het nabij-infrarode spectrum (700-1000 nm) zijn het best detecteerbaar, met een maximale weefsel-penetratie, terwijl de autofluorescentie in het nabij-infrarode spectrum minimaal is.[8] Fluorescentie-beeldvorming heeft een aantal voordelige eigenschappen: een hoge resolutie, het is minimaal invasief, de afwezigheid van radioactieve straling en de mogelijkheid om *real-time* beeldvorming te verrichten.[8] Vanwege de beperkte penetratiediepte van ~1 cm in weefsel, bij gebruik van fluoroforen in het nabij-infrarode spectum, en zelfs minder voor fluoroforen met kortere golflengtes, is deze beeldvormingstechniek met name geschikt voor oppervlakte- en endoscopische beeldvorming.[9]

Bacterie-gerichte beeldvorming

Bacterie-gerichte beeldvorming is gebaseerd op een 'targeting'-molecuul (bijvoorbeeld een antilichaam, antibioticum of antimicrobieel eiwit), dat specifiek bindt aan bacteriën of andere micro-organismen, gekoppeld aan een beeldvormingsmolecuul zoals een radionuclide of fluorofoor. Middels bacterie-gerichte beeldvorming is het niet alleen mogelijk om de locatie van een infectie te visualiseren, maar ook om een specifiek micro-organisme identificeren.[2,3] Doelgerichte fluorescentie-beeldvorming van bacteriële infecties heeft diverse veelbelovende toepassingen, waaronder de mogelijkheid tot intra-operatieve *real-time* beeldvorming, beeldvorming van infecties middels artroscopie of bronchoscopie, of *ex vivo* diagnostische beeldvorming van infecties. Daarmee biedt doelgerichte fluorescentie-beeldvorming de mogelijkheid om als 'rode vlag' te dienen voor het identificeren van infecterende micro-organismen.

Samenvatting van dit proefschrift

Bacterie-gerichte beeldvorming is een veelbelovende techniek die de diagnose van verschillende infectieziekten kan verbeteren.[2,3] In dit proefschrift wordt een overzicht gegeven over de huidige beeldvormingstechnieken voor infectieziekten. Daarnaast is het onderzoek gericht op nieuw ontwikkelde bacterie-specifieke fluorescentie-beeldvorming om verschillende infectieziekten te diagnosticeren. **Hoofdstuk 1** beschrijft de achtergronden van het onderzoek, de uitdagingen voor het stellen van infectiediagnoses en de algehele strekking van dit proefschrift.

Hoofdstuk 2 beschrijft een literatuuronderzoek naar bacterie-gerichte radionuclide- en fluorescentie-gemedieerde beeldvorming. In de afgelopen jaren heeft 'target'-selectie met name plaatsgevonden middels antibiotica en antimicrobiële eiwitten.[1] Hoewel radioactief gelabelde bacterie-gerichte beeldvormingsmoleculen (zogeheten tracers) veelbelovend lijken voor het diagnosticeren van infectieziekten, zijn veel tracers niet geschikt voor bacterie-specifieke beeldvorming in patiënten. Het uitgebreid bestudeerde radioactief gelabelde antibioticum ciprofloxacine (^{99m}Techneticum-ciprofloxacine; ^{99m}Tc-ciprofloxacine; Infection©) was bijvoorbeeld niet geschikt om een betrouwbaar onderscheid te maken tussen een infectie en een steriele inflammatie. Andere veelbelovende tracers zijn gebaseerd op verbindingen die specifiek gemetaboliseerd worden door bacteriën, zoals 6-fluor-18-fluoromaltose (^{18}F-FM) en 2-[^{18}F]-fluoro-deoxy-sorbitol (^{18}F-FDS). Het wordt verwacht dat deze metaboliseerbare tracers een grote rol gaan spelen in de klinische translatie van bacterie-gerichte beeldvorming. Een relatief nieuwe en opkomende beeldvormingstechniek is bacterie-gerichte beeldvorming op basis van fluorescentie. Verschillende onderzoeken hebben veelbelovende resultaten laten zien in dierinfectiemodellen, waarbij verschillende bacterie-gerichte tracers werden gebruikt. Eén van deze veelbelovende tracers is gebaseerd op het antibioticum vancomycine, gekoppeld aan de nabij-infrarode fluorofoor

IRDye800CW (afgekort vanco-800CW). Belangrijk is dat vanco-800CW de specifieke detectie van *Staphylococcus aureus* mogelijk maakte in vergelijking met een steriele ontsteking of een Gram-negatieve bacteriële infectie *in vivo*. Over het algemeen zijn nieuwe beeldvormingsmodaliteiten hard nodig om bacteriële infecties nauwkeurig en snel te diagnosticeren. In dit opzicht is bacterie-gerichte beeldvorming een aantrekkelijke optie, vanwege de specificiteit en het gemak van deze beeldvormingstechniek. Het is duidelijk dat een snelle en nauwkeurige diagnose cruciaal is voor de effectieve behandeling van een groot aantal infectieziekten. Hoewel het onzeker blijft welke specifieke tracers uiteindelijk het meest geschikt zullen blijken voor klinisch gebruik, kan verwacht worden dat sommige van de tracers en respectievelijke beeldvormende technieken beschreven in Hoofdstuk 2 zullen worden geïmplementeerd in routinematige klinische diagnostische procedures.

Hoofdstuk 3 is gericht op de klinisch toegepaste, radionuclide-gemedieerde beeldvormingstechniek PET. ^{18}F-fluorodeoxyglucose (^{18}F-FDG) kan worden gebruikt om infectie en inflammatie op te sporen en is met name nuttig bij het opsporen van de oorzaak van koorts zonder focus.[5,10] Deze niet-bacterie-specifieke beeldvormingstechniek is gebaseerd op de glucoseopname door cellen die betrokken zijn bij het ontstekingsproces. Derhalve is het niet gemakkelijk om onderscheid te maken tussen een bacteriële infectie en een steriele ontsteking.[11] In Hoofdstuk 3 wordt de intrigerende vraag beantwoord of infecterende bacteriën ^{18}F-FDG accumuleren en mogelijk bijdragen aan het signaal dat wordt gedetecteerd middels ^{18}F-FDG-PET-beeldvorming. Een breed scala van veel voorkomende bacteriële pathogenen toonde inderdaad een actieve opname van ^{18}F-FDG *in vitro*. Het lijkt daarmee aannemelijk dat deze bacteriële pathogenen ook ^{18}F-FDG accumuleren en bijdragen aan het ^{18}F-FDG-PET-signaal in de mens. Van alle geteste bacteriën toonde *Streptococcus pyogenes* de hoogste opname van ^{18}F-FDG. Sommige infecties die door deze bacterie worden veroorzaakt, met name fasciïtis necroticans, vereisen onmiddellijk antibiotische therapie en agressieve chirurgie. Dit benadrukt de behoefte aan een snelle, bij voorkeur *real-time*, bacterie-gerichte beeldvorming, hetgeen niet kan worden bereikt met ^{18}F-FDG-PET.

Met het overkoepelende doel om de mogelijkheden voor bacterie-specifieke infectiebeeldvorming te analyseren, is het onderzoek beschreven in de **Hoofdstukken 4** tot en met **6** gericht op de specifieke detectie van stafylokokkeninfecties. *S. aureus* is verantwoordelijk voor de meeste infecties van de huid en weke delen, maar kan ook andere ernstige infectieziekten veroorzaken, zoals osteomyelitis, een bacteriëmie of zelfs sepsis.[12] Een specifieke tracer voor de detectie van stafylokokken is gebaseerd op een eerder ontwikkeld humaan monoklonaal antilichaam (1D9) tegen het immunodominante stafylokokkenantigeen A (Isa A).[13] Dit antilichaam is gekoppeld aan de nabij-infrarode fluorofoor IRDye800CW voor fluorescentie-beeldvorming of aan ^{89}Zirconium voor PET-beeldvorming (**Hoofdstuk 4**). In dit hoofdstuk wordt de specifieke detectie van *S. aureus* aangetoond, zowel in een humaan *post-mortem* infectiemodel als in een *in vivo* huidinfectiemodel in muizen. Hoewel de resultaten veelbelovend lijken voor zowel de fluorescentie- als PET-

beeldvorming, zal verder onderzoek nodig zijn om de effectiviteit van het monoklonale antilichaam 1D9 te evalueren om dieper gelegen infecties op te sporen.
Hoofdstuk 5 beschrijft een zogeheten 'slim-te-activeren' tracer die reageert op de enzymatische activiteit van een microkokken-nuclease, dat specifiek wordt uitgescheiden door *S. aureus*. Deze tracer bestaat uit een fluorofoor en een licht-absorberend molecuul (een zogenaamde quencher) en heeft de eigenschap om alleen een fluorescent signaal uit te zenden wanneer de quencher van de fluorofoor wordt gescheiden door het nuclease-enzym. De onderzochte tracer is een afgeleide van een eerder beschreven door nuclease-geactiveerde tracer,[14] maar met een verhoogde gevoeligheid voor microkokken-nuclease. Om deze reden is het onderzoek gericht op de gevoeligheid, de specificiteit en de stabiliteit van deze nieuwe tracer in humaan bloed en plasma uitgevoerd. Vervolgens beschrijft **Hoofdstuk 6** de toekomstige klinische implementatie van deze door nuclease-geactiveerde tracer bij het nauwkeurig diagnosticeren van een vroege *S. aureus* bacteriëmie.

Het onderzoek dat beschreven wordt in het laatste deel van dit proefschrift (**Hoofdstukken 7** tot en met **9**) was gericht op het verkennen van nieuwe klinische toepassingen voor bacterie-gerichte fluorescentie-beeldvorming. De eerste stap om dit doel te bereiken wordt uitgelicht in **Hoofdstuk 7**, waar succesvolle *ex vivo* fluorescentie-beeldvorming van klinische bacteriële biofilms op osteosynthese-materiaal met vanco-800CW wordt beschreven. Middels bacterie-gerichte fluorescentie-beeldvorming met vanco-800CW is het mogelijk om in minder dan 30 minuten een correcte diagnose te stellen van fractuur-gerelateerde infecties. Dit is een aanzienlijke verbetering qua tijdsduur tot de diagnose in vergelijking met de standaard microbiologische technieken. Verwacht mag worden dat voor patiënten met fractuur-gerelateerde infecties *in vivo* intra-operatieve fluorescentie-geleide chirurgie zelfs van nog grotere waarde kan zijn, aangezien het de chirurg van *real-time* visuele informatie kan voorzien over het geïnfecteerde weefsel en de geïnfecteerde materialen. Bacterie-gerichte fluorescentie-beeldvorming kan bijdragen aan het vaststellen in hoeverre een infectie zich uitstrekt, hetgeen kan leiden tot preciezere en radicale resectie, waarbij niet-geïnfecteerd materiaal en omliggend weefsel kan worden gespaard.
In **Hoofdstuk 8** wordt fluorescentie-geleide artroscopie van een gewrichtsprothese-infectie voor het eerst gepresenteerd in een humaan *post-mortem* knie-infectiemodel. Ook in deze setting maakt de fluorescente vanco-800CW tracer nauwkeurige *real-time* detectie van een stafylokokken biofilm mogelijk. Bovendien is aangetoond dat het fluorescent gelabelde vancomycine affiniteit heeft voor biofilms van de meeste Gram-positieve bacteriën. Deze groep micro-organismen is de veroorzaker van het merendeel van de gewrichtsprothese-infecties. Een toekomstige klinische implementatie van deze techniek met vanco-800CW lijkt dan ook veelbelovend.
Tot slot wordt doelgerichte fluorescentie-beeldvorming van bacteriële kolonisatie en infectie in de distale long gepresenteerd in **Hoofdstuk 9**. Micro-organismen in de alveolaire ruimte van humane gereseceerde longen of longkwabben kunnen worden gevisualiseerd middels het combineren

van sonde-gebaseerde confocale laser-endomicroscopie en bacterie-gerichte fluorescentie-beeldvorming. Belangrijk is dat doelgerichte fluorescentie-beeldvorming een meerwaarde blijkt te hebben voor de detectie van micro-organismen, zeker in gevallen waarin de gouden standaard van microbiologische kweken uitdagend is.

Discussie

Toekomstperspectieven voor diagnostiek

Bacterie-gerichte beeldvorming is een aantrekkelijke diagnostische techniek, die zich momenteel snel ontwikkelt. Middels deze techniek kunnen infecties specifieker gelokaliseerd worden dan met de huidig gebruikte anatomische en functionele beeldvormingstechnieken. Hoewel bacterie-gerichte beeldvorming nog in de kinderschoenen staat, toont de ontwikkeling van specifieke tracers en verschillende beeldvormingsmodaliteiten beschreven in dit proefschrift de potentiële voordelen voor het diagnosticeren van verschillende infectieziekten. Bovendien kan deze technologie van grote waarde zijn voor het evalueren van de behandelrespons en de follow-up van de patiënt in de klinische praktijk. Ondanks de veelbelovende resultaten is er meer onderzoek nodig, inclusief verdere ontwikkeling van nieuwe 'targeting'-moleculen en beeldvormende middelen, om de beeldvormingsgevoeligheid te verbeteren. De klinische translatie van tracers zou het gemakkelijkst zijn voor moleculen, waarvan is aangetoond dat ze niet-toxisch zijn voor patiënten, zoals het klinisch goedgekeurde antibioticum vancomycine en de nabij-infrarode fluorofoor IRDye800CW.[15] Andere aspecten van bacterie-gerichte infectie-beeldvorming die verder moeten worden ontwikkeld, hebben betrekking op de computerondersteunde beeldanalyse door middel van geavanceerde 'machine-learning' en kunstmatige intelligentie voor een verbeterde detectie van abnormale patronen. Hierdoor kan een nauwkeuriger onderscheid worden gemaakt tussen geïnfecteerde gebieden en normale, niet-geïnfecteerde structuren.

In de afgelopen jaren is veel ervaring opgedaan met doelgerichte fluorescentie-beeldvorming op het gebied van de oncologie en de chirurgie.[16-21] Met behulp van fluorescentie-geleide chirurgie werden tumorvlekken van <1 mm zichtbaar bij patiënten met eierstokkanker.[22] Intra-operatieve bacterie-gerichte fluorescentie-beeldvorming kan hoogstwaarschijnlijk op dezelfde wijze nauwkeurig de omvang en de grenzen van een infectie in beeld brengen. Bijvoorbeeld bij snel optredende infectieziekten, zoals de eerder genoemde necrotiserende fasciitis, zou een nauwkeuriger resectie van geïnfecteerd weefsel waarschijnlijk de uitkomst van de patiënt verbeteren.

Bacterie-gerichte fluorescentie-beeldvorming maakt een vroege en nauwkeurige diagnose aan het bed aannemelijk bij verschillende infectieziekten, zoals een pneumonie of kunstmateriaal-gerelateerde infecties (**Hoofdstukken 7**, **8** en **9**). Een groot nadeel van fluorescentie-beeldvorming is echter de beperkte penetratiediepte van het signaal, waardoor deze techniek vooral geschikt is voor oppervlakte- en endoscopische beeldvorming. Een andere veelbelovende *real-time*

beeldvormingstechniek, waarmee geschikte tracers op een weefseldiepte van enkele centimeters kunnen worden gedetecteerd, is opto-akoestische beeldvorming.[23] De opto-akoestische beeldvormingstechniek is gebaseerd op de absorptie van licht door foto-absorberende moleculen, gevolgd door thermo-elastische expansie, resulterend in de emissie van ultrasone geluidsgolven.[24–26] Deze nieuwe beeldvormingstechniek is veelbelovend voor een betere diagnose van dieper gelegen infecties bij patiënten.

De meeste onderzochte beeldvormende technieken die in dit proefschrift worden beschreven, maken gebruik van een enkele tracer. Het is echter goed denkbaar dat het gebruik van meerdere tracers, die zich richten op verschillende micro-organismen, en multispectrale beeldvorming, een nauwkeurige identificatie van ziekverwekkers mogelijk maakt. Het stafylokokken-specifieke antilichaam 1D9 of de nuclease-specifieke 'slim-te-activeren' tracer, beschreven in de **Hoofdstukken 4**, **5** en **6**, kunnen bijvoorbeeld worden aangevuld met andere soortspecifieke tracers. Zolang deze tracers nog niet beschikbaar zijn, kunnen Gram-positieve en Gram-negatieve bacteriële pathogenen worden gevisualiseerd met respectievelijk vanco-800CW en de op colistine (polymyxine E) gebaseerde tracer beschreven in de **Hoofdstukken 7**, **8** en **9**.[15,27,28] Het zou zelfs nog wenselijker zijn om doelgerichte moleculen te ontwikkelen die in staat zijn om onderscheid te maken tussen antibiotica-resistente en niet-resistente micro-organismen. Met name 'slim-te-activeren' tracers, zoals de nuclease-geactiveerde tracer beschreven in **Hoofdstukken 5** en **6** van dit proefschrift, zouden hiervoor geschikt zijn, omdat bij deze techniek een grotere 'target-to-background' ratio haalbaar is. Een hogere ratio is wenselijk aangezien dit leidt tot een sterkere signaal-ruisverhouding. Om beeldvormingstechnieken voor de detectie van infectieziekten verder te verbeteren kunnen tracers dusdanig ontworpen worden dat zij zowel een fluorescent signaal als een tweede signaal uitzenden op basis van bijvoorbeeld een radionuclide of MRI-contrastmiddel. Een dergelijk hybride tracer voor beeldvorming gebaseerd op meerdere modaliteiten zou zowel pre-operatieve lokalisatie van diepgelegen infecties mogelijk maken als intra-operatieve begeleiding.[29,30] Het principe van dit concept is recent aangetoond voor het stafylokokken-specifieke antilichaam 1D9, waarbij dit antilichaam dubbel gelabeld was met een nabij-infrarode fluorofoor en ^{89}Zirconium.[31]

Toekomstperspectieven voor behandeling

Naast bacterie-gerichte beeldvorming voor het diagnosticeren van infectieziekten, zou een bacterie-gerichte therapeutische aanpak de behandeling van infecties nog verder kunnen verbeteren. Met name een anti-bacteriële behandeling op basis van doelgerichte foto-dynamische therapie lijkt zeer aantrekkelijk.[32-41] Bacterie-gerichte foto-dynamische therapie is gebaseerd op de excitatie van een lichtgevoelig molecuul, een zogeheten fotosensibilisator, wat resulteert in zowel een fluorescent signaal als in het genereren van reactieve zuurstofmoleculen die specifiek het beoogde micro-organisme doden. Gerichte foto-dynamische therapie tegen *S. aureus* is recentelijk *in vivo* en in een humaan *post-mortem* model beschreven met een zogenaamd theragnostische tracer, gebaseerd op het stafylokokken-specifieke antilichaam gepresenteerd in **Hoofdstuk 4** van dit

proefschrift.[42] Deze op 1D9 gebaseerde theragnostische tracer is in staat om bacteriële biofilms te verstoren en is zodoende veelbelovend voor de behandeling van kunstmateriaal-gerelateerde infecties. Theoretisch zullen bacteriën, zodra een biofilm verstoord raakt, bereikbaar worden voor antibiotische behandeling, wat de eradicatie van de infecterende micro-organismen zal bevorderen. Bacterie-gerichte therapie kan, naast kunstmateriaal-gerelateerde infecties, van grote waarde zijn voor de behandeling van veel verschillende infectieziekten. Zoals benadrukt in **Hoofdstuk 9** zou gerichte behandeling in donor longen, in een *ex vivo* longperfusie-setting, kunnen helpen om een pneumonie bij de ontvanger in de toekomst te voorkomen. Bacterie-gerichte therapie kan wellicht ook helpen bij het behandelen van andere organen voorafgaand aan de transplantatie. Desalniettemin zal nader onderzoek moeten worden verricht om te evalueren of dit een realistische optie is.

Conclusie

Dit proefschrift beschrijft het gebruik van bacterie-gerichte beeldvorming bij de diagnose van verschillende infectieziekten, met de nadruk op bloedbaaninfecties, kunstmateriaal-gerelateerde infecties en pneumonie. Bacterie-gerichte fluorescentie-beeldvorming is snel, haalbaar en veelbelovend voor een nauwkeurige diagnose van infectieziekten, hetgeen van groot belang is voor de patiënt. Bovendien zal deze betrekkelijk nieuwe beeldvormingstechniek hoogstwaarschijnlijk de intra-operatieve *real-time* detectie van infecterende micro-organismen mogelijk maken. Zoals beschreven in dit proefschrift, zijn verschillende bacterie-gerichte tracers veelbelovende kandidaten voor klinische implementatie. Verdere studies zijn echter nodig om deze tracers en de respectievelijke beeldvormingstechnieken te vertalen naar de klinische setting. Het gebruik van de in dit proefschrift beschreven diagnostische beeldvormende technieken, samen met opto-akoestische, multispectrale of multimodale beeldvorming en doelgerichte therapie zal bijdragen aan de strijd tegen infectieziekten.

References

1. Ordonez, A. A. *et al.* Molecular imaging of bacterial infections: Overcoming the barriers to clinical translation. *Sci. Transl. Med.* **508**, 8251 (2019).
2. van Oosten, M. *et al.* Targeted imaging of bacterial infections: advances, hurdles and hopes. *FEMS Microbiol. Rev.* **39**, 892–916 (2015).
3. Mills, B., Bradley, M. & Dhaliwal, K. Optical imaging of bacterial infections. *Clin. Transl. Imaging.* **4**, 163–174 (2016).
4. Love, C. & Palestro, C. J. Radionuclide imaging of infection. *J. Nucl. Med. Technol.* **32**, 47–57 (2004).
5. Love, C., Tomas, M. B., Tronco, G. G. & Palestro, C. J. FDG PET of infection and inflammation. *Radiographics*. **25**, 1357–1368 (2005).
6. Strobel, K. & Stumpe, K. D. M. PET/CT in musculoskeletal infection. *Semin. Musculoskelet. Radiol.* **11**, 353–364 (2007).
7. Sabat, A. J. *et al.* Overview of molecular typing methods for outbreak detection and epidemiological surveillance. *Eurosurveillance.* **18**, 1–15 (2013).
8. Luo, S., Zhang, E., Su, Y., Cheng, T. & Shi, C. A review of NIR dyes in cancer targeting and imaging. *Biomaterials.* **32**, 7127–7138 (2011).
9. Pleijhuis, R. G. *et al.* Near-infrared fluorescence (NIRF) imaging in breast-conserving surgery: Assessing intraoperative techniques in tissue-simulating breast phantoms. *Eur. J. Surg. Oncol.* **37**, 32–39 (2011).
10. Besson, F. L. *et al.* Contribution of ^{18}F-FDG PET in the diagnostic assessment of fever of unknown origin (FUO): a stratification-based meta-analysis. *Eur. J. Nucl. Med. Mol. Imaging.* **43**, 1887–1895 (2016).
11. Glaudemans, A. W. J. M., Israel, O. & Slart, R. H. J. A. Pitfalls and Limitations of Radionuclide and Hybrid Imaging in Infection and Inflammation. *Semin. Nucl. Med.* **45**, 500–512 (2015).
12. Tong, S. Y. C., Davis, J. S., Eichenberger, E., Holland, T. L. & Fowler, V. G. *Staphylococcus aureus* infections: Epidemiology, pathophysiology, clinical manifestations, and management. *Clin. Microbiol. Rev.* **28**, 603–661 (2015).
13. van den Berg, S. *et al.* A human monoclonal antibody targeting the conserved staphylococcal antigen IsaA protects mice against *Staphylococcus aureus* bacteremia. *Int. J. Med. Microbiol.* **305**, 55–64 (2015).
14. Hernandez, F. J. *et al.* Noninvasive imaging of *Staphylococcus aureus* infections with a nuclease-activated probe. *Nat. Med.* **20**, 301–306 (2014).
15. van Oosten, M. *et al.* Real-time *in vivo* imaging of invasive- and biomaterial-associated bacterial infections using fluorescently labelled vancomycin. *Nat. Commun.* **4**, 2584 (2013).
16. van Dam, G. M. *et al.* Intraoperative tumor-specific fluorescence imaging in ovarian cancer by folate receptor-α targeting: First in-human results. *Nat. Med.* **17**, 1315–1319 (2011).
17. de Jongh, S. J. *et al.* Back-Table Fluorescence-Guided Imaging for Circumferential Resection Margin Evaluation Using Bevacizumab-800CW in Patients with Locally Advanced Rectal Cancer. *J. Nucl. Med.* **61**, 655–661 (2020).
18. Voskuil, F. J. *et al.* Fluorescence-guided imaging for resection margin evaluation in head and neck cancer patients using cetuximab-

800CW: A quantitative dose-escalation study. *Theranostics.* **10**, 3994–4005 (2020).

19. Voskuil, F. J. *et al.* Exploiting metabolic acidosis in solid cancers using a tumor-agnostic pH-activatable nanoprobe for fluorescence-guided surgery. *Nat. Commun.* **11**, 1–10 (2020).
20. Joshi, B. P. & Wang, T. D. Targeted Optical Imaging Agents in Cancer: Focus on Clinical Applications. *Contrast Media Mol. Imaging.* **2018**, 2015237 (2018).
21. Steinkamp, P. J. *et al.* Fluorescence-guided visualization of soft tissue sarcomas by targeting vascular endothelial growth factor-A: a phase 1 single-center clinical trial. *J. Nucl. Med.* **62**, 120.245696 (2020).
22. Terwisscha van Scheltinga, A. G. T. *et al.* Intraoperative near-infrared fluorescence tumor imaging with vascular endothelial growth factor and human epidermal growth factor receptor 2 targeting antibodies. *J. Nucl. Med.* **52**, 1778–1785 (2011).
23. Ntziachristos, V. Going deeper than microscopy: the optical imaging frontier in biology. *Nat. Methods.* **7**, 603–614 (2010).
24. Ntziachristos, V. & Razansky, D. Molecular imaging by means of multispectral optoacoustic tomography (MSOT). *Chem. Rev.* **110**, 2783–2794 (2010).
25. Neuschmelting, V. *et al.* Performance of a Multispectral Optoacoustic Tomography (MSOT) System equipped with 2D vs. 3D Handheld Probes for Potential Clinical Translation. *Photoacoustics.* **4**, 1–10 (2016).
26. Taruttis, A. & Ntziachristos, V. Advances in real-time multispectral optoacoustic imaging and its applications. *Nat. Photonics.* **9**, 219–227 (2015).
27. Akram, A. R. *et al. In situ* identification of Gram-negative bacteria in human lungs using a topical fluorescent peptide targeting lipid A. Sci. *Transl. Med.* **10**, 0033 (2018).
28. Gunasekaran, R. *et al.* Exploratory Use of Fluorescent Smart Probes for the Rapid Detection of Microbial Isolates Causing Corneal Ulcer. *Am. J. Ophthalmol.* **219**, 341–350 (2020).
29. Azhdarinia, A., Ghosh, P., Ghosh, S., Wilganowski, N. & Sevick-Muraca, E. M. Dual-labeling strategies for nuclear and fluorescence molecular imaging: A review and analysis. *Mol. Imaging Biol.* **14**, 261–276 (2012).
30. Ding, N. *et al.* Folate receptor-targeted fluorescent paramagnetic bimodal liposomes for tumor imaging. *Int. J. Nanomedicine.* **6**, 2513–2520 (2011).
31. Zoller, S. D. *et al.* Multimodal imaging guides surgical management in a preclinical spinal implant infection model. *JCI Insight.* **4**, 1–13 (2019).
32. Ragàs, X. *et al.* Cationic porphycenes as potential photosensitizers for antimicrobial photodynamic therapy. *J Med Chem.* **53**, 7796–7803 (2010).
33. Bhatti, M. *et al.* Antibody-targeted lethal photosensitization of *Porphyromonas gingivalis*. *Antimicrob. Agents Chemother.* **44**, 2615–2618 (2000).
34. Demidova, T. N. & Hamblin, M. R. Photodynamic therapy targeted to pathogens. *Int. J. Immunopathol. Pharmacol.* **17**, 245–254 (2004).
35. Dosselli, R. *et al.* Synthesis, characterization, and photoinduced antibacterial activity of porphyrin-type photosensitizers conjugated to the antimicrobial peptide apidaecin 1b. *J. Med. Chem.* **56**, 1052–1063 (2013).
36. Suci, P., Kang, S., Gmür, R., Douglas, T. & Young, M. Targeted delivery of a photosensitizer to

Aggregatibacter actinomycetemcomitans biofilm. *Antimicrob. Agents Chemother.* **54**, 2489–2496 (2010).

37. Embleton, M. L., Nair, S. P., Cookson, B. D. & Wilson, M. Selective lethal photosensitization of methicillin-resistant *Staphylococcus aureus* using an IgG-in (IV) chlorin e6 conjugate. *J. Antimicrob. Chemother.* **50**, 857–864 (2002).
38. Embleton, M. L., Nair, S. P., Cookson, B. D. & Wilson, M. Antibody-directed photodynamic therapy of methicillin-resistant *Staphylococcus aureus*. *Microb. Drug Resist.* **10**, 92–97 (2004).
39. Embleton, M. L. *et al.* Development of a novel targeting system for lethal photosensitization of antibiotic-resistant strains of *Staphylococcus aureus*. *Antimicrob. Agents Chemother.* **49**, 3690–3696 (2005).
40. Kim, G., Karbaschi, M., Cooke, M. & Gaitas, A. Light-based methods for whole blood bacterial inactivation enabled by a recirculating flow system. *Photochem. Photobiol.* **94**, 744–751 (2018).
41. Wang, K. K. *et al.* Target-oriented photofunctional nanoparticles (TOPFNs) for selective photodynamic inactivation of Methicillin-resistant *Staphylococcus aureus* (MRSA). *J. Photochem. Photobiol. B Biol.* **183**, 184–190 (2018).
42. Bispo, M. *et al.* Fighting *Staphylococcus aureus* infections with light and photo-immunoconjugates. *JCI Insight.* **22**, 139512 (2020).

Chapter 12

List of abbreviations *(Afkortingenlijst)*

Biography *(Biografie)*

List of publications *(Publicatielijst)*

Acknowledgements *(Dankwoord)*

List of abbreviations *(Afkortingenlijst)*

A

ACUC	animal care and use committee
AIDS	acquired immune deficiency syndrome
ATCC	American type culture collection
ATP	adenosine triphosphate, energy carrying molecule

B

BA	blood agar, culture medium
BAC 1	optical tracer based on ubiquicidin
BAC 2	optical tracer based on colistin (polymyxin E)
BAL	bronchoalveolar lavage
BHI	Brain-Heart Infusion, growth medium
BLA	activatable β-lactamase-targeted optical tracer
BSI(s)	bloodstream infection(s)
B. subtilis	*Bacillus subtilis*

C

C	cell fraction
°C	degree Celcius
$CaCl_2$	calcium chloride
capi	*Staphylococcus capitis*
caprae	*Staphylococcus caprae*
cc	cubic centimetre
CCD	charge-coupled device (cameras)
CEF	techneticum-99m labelled ceftriaxone
CF	cystic fibrosis
C. freundii	*Citrobacter freundii*
CFU(s)	colony forming unit(s)
CHOC	chocolate, culture medium
CIP	techneticum-99m or fluorine-18 labelled ciprofloxacin
cm	centimetre
cm^2	cubic centimetre
Cm^R	chloramphenicol resistant
CNTRL	negative control
CO_2	carbon dioxide
COB	colistin oxolinic-acid blood agar, culture medium

COPD	chronic obstructive pulmonary disease
CPFE	combined pulmonary fibrosis and emphysema
CSF	cerebrospinal fluid
CT	computed tomography

D

1D9	fully-human monoclonal antibody that specifically targets the immunodominant staphylococcal antigen A
1D9-800CW	1D9-IRDye800CW, optical tracer
2-DG	2-deoxy-glucose
DFO	deferoxamine
DMSO	dimethyl sulfoxide
DNA	deoxyribonucleic acid, carrier of genetic information
Dog	difference of Gaussian, spot detection filter

E

Ec	*Escherichia coli*
E. coli	*Escherichia coli*
EDTA	ethylenediaminetetraacetic acid
E. faecalis	*Enterococcus faecalis*
E. faecium	*Enterococcus faecium*
e.g.	for example (Latin: *exempli gratia*)
Em^R	erythromycin resistant
EPD	electronic patient dossier
epi	*Staphylococcus epidermidis*
EPR	enhanced permeability and retention
EPS	extracellular polymeric substances
et al.	and others (Latin: *et alii*)
EVLP	*ex vivo* lung perfusion

F

F	female
^{18}F	fluorine-18, unstable radioactive isotope of fluorine
FAM	fluorescein amidite, fluorophore
(^{18}F)-FDG	(^{18}F)-fluorodeoxyglucose, radiolabelled glucose
(^{18}F)-FDG-PET	(^{18}F)-fluorodeoxyglucose positron emission tomography
(^{18}F)-FDG-PET/CT	(^{18}F)-fluorodeoxyglucose positron emission tomography with low dose computed tomography

^{18}F-FDS	2-[^{18}F]-fluoro-deoxy-sorbitol, radiolabelled sorbitol
^{18}F-FM	6-[^{18}F]-fluoromaltose, radiolabelled maltose
FIAU	1-(2-deoxy-2-fluoro-β-D-arabino-furanosyl)-5-iodouracil, radionuclide-mediated tracer based on the nucleoside analogue fialuridine
FITC	fluorescein isothiocyanate, fluorophore
FL	fluorescence
FLER	fluorine-18 labelled fleroxacin
FLI	fluorescence image
FRI(s)	fracture-related infection(s)

G

GN	Gram-negative
GP	Gram-positive
Gram	Gram staining

H

h	hours
HACEK	*Haemophilus parainfluenzae*, *Haemophilus aphrophilus* and *Haemophilus paraphrophilus* (currently referred to as *Aggregatibacter aphrophilus* and *Aggregatibacter paraphrophilus*), *Haemophilus influenzae*, *Aggregatibacter actinomycetemcomitans*, *Cardiobacterium hominis*, *Eikenella corrodens*, *Kingella kingae* and *Kingella denitrificans*
haem	*Staphylococcus haemolyticus*
HIG	human polyclonal immunoglobulin
his_6	6-Histidine-tag
hom	*Staphylococcus hominis*
HPLC	high performance liquid chromatography
humAb	human monoclonal antibody

I

ICG	indocyanine green, fluorophore
ICU	intensive care unit
IDT	integrated DNA technologies
i.e.	that is (Latin: *id est*)
IE	infective endocarditis
IgG	immunoglobulin G

^{111}In	indium-111, unstable radioactive isotope of indium
ITLC	instant thin layer chromatography
Isa A	immunodominant staphylococcal antigen A, antigen exposed on the bacterial cell surface
ΔisaA	*Staphylococcus aureus* mutant strain lacking isaA
IQR	interquartile range

K

kBq	kilobecquerel, unit for radioactivity
keV	kilo-electronvolts, unit for energy
kg	kilogram
K. pneumoniae	*Klebsiella pneumoniae*

L

L	left / litre
LB	Lysogeny Broth
LDS	lithium dodecyl sulphate (buffer)
L. lactis	*Lactococcus lactis*
LLL	left lower lobe
Log	Laplacian of Gaussian, spot detection filter
LPS	lipopolysaccharide
lug	*Staphylococcus lugdunensis*
LUL	left upper lobe

M

M	male / growth medium fraction
MALDI-TOF	matrix-assisted laser desorption/ionization time-of-flight (mass spectrometry)
MALT	fluorine-18 labelled maltose / maltodextrin-based optical tracer
MBq	megabecquerel, unit for radioactivity
µCi	microcurie, unit for radioactivity
METc	medisch ethische toetsingscommissie
µg	microgram
mg	milligram
min	minutes
µL	microlitre
mL	millilitre
µm	micrometre

mm	millimetre
µM	micromolar
mM	millimolar
µmol	micromole
MN	micrococcal nuclease, secreted by *Staphylococcus aureus*
µPET	micro positron emission tomography
MRI	magnetic resonance imaging
MRSA	methicillin-resistant *Staphylococcus aureus*
ms	millisecond
M. tuberculosis	*Mycobacterium tuberculosis*
mW	milliwatt, unit of power or radiant flux

N

n	number
NaCl	sodium chloride
Na_2CO_3	sodium carbonate
NBD	7-nitrobenz-2-oxa-1,3-diazole, fluorophore
NEG	negative (culture negative)
NIR	near-infrared
nm	nanometre
nmol	nanomole
NP	no probe
ns	nanosecond
NSIP	non-specific interstitial pneumonia
NUC	activatable nuclease-targeted optical tracer (*Staphylococcus aureus*-directed)
Δnuc / *Δnuc Δnuc2*	*Staphylococcus aureus* with mutations in the nuc and nuc2 gene(s), which are responsible for respectively the secretion of nuclease and the expression of a surface-bound nuclease
Nuc2	a surface-bound nuclease

O

O_2	oxygen
OD	optical density

P

P. aeruginosa	*Pseudomonas aeruginosa*
pas	*Staphylococcus pasteuri*

PAT	photoacoustic tomography
PBS	phosphate buffered saline
pCLE	probe-based confocal laser endomicroscopy
PCR	polymerase chain reaction
PDT	photodynamic therapy
pet	*Staphylococcus pettenkoferi*
PET	positron emission tomography
PJI(s)	prosthetic joint infection(s)
P. mirabilis	*Proteus mirabilis*
POS	positive (culture positive, infected)
PRO	prothrombin-based optical / radiolabelled tracer
PTS	phosphotransferase system
ΔptsG / *ΔptsI*	*Bacillus subtilis* containing a mutation in the phosphotransferase system (deletion strains)
PtsG	glucose transporter
PtsI	involved in the phosphorylation of internalised glucose, making its uptake by PtsG irreversible
pyo	*Streptococcus pyogenes*

R

R	right
RLL	right lower lobe
RML	right middle lobe
RNA	ribonucleic acid, carrier of messenger instructions of DNA
ROI(s)	region(s) of interest
RPM	revolutions per minute, rotational speed
RPMI	Roswell Park Memorial Institute, growth medium
RUL	right upper lobe

S

s	seconds
Sa	*Staphylococcus aureus*
SAB	Sabouraud dextrose, culture medium / *Staphylococcus aureus* bacteraemia
sap	*Staphylococcus saprophyticus*
SAP	*Staphylococcus aureus* SAP231
S. argenteus	*Staphylococcus argenteus*
S. aureus	*Staphylococcus aureus*

Sbi	protein known to bind to the Fc portion of human immunoglobulin G1
S. capitis	*Staphylococcus capitis*
S. caprae	*Staphylococcus caprae*
SD	standard deviation
S. delphini	*Staphylococcus delphini*
sec	seconds
SEM	standard error of the mean
S. epidermidis	*Staphylococcus epidermidis*
S. haemolyticus	*Staphylococcus haemolyticus*
S. hominis	*Staphylococcus hominis*
S. hyicus	*Staphylococcus hyicus*
S. intermedius	*Staphylococcus intermedius*
S. lugdunensis	*Staphylococcus lugdunensis*
S. microti	*Staphylococcus microti*
SNase	staphylococcal nuclease
SOR	fluorine-18 labelled sorbitol
Spa	protein known to bind to the Fc portion of human immunoglobulin G1 (protein A)
Δspa / *Δspa Δsbi*	*Staphylococcus aureus* Newman wild-type containing mutations in proteins known to bind to the Fc portion of human immunoglobulin G1
S. pasteuri	*Staphylococcus pasteuri*
SPECT	single-photon emission computed tomography
S. pettenkoferi	*Staphylococcus pettenkoferi*
S. pneumoniae	*Streptococcus pneumoniae*
S. pseudintermedius	*Staphylococcus pseudintermedius*
S. pyogenes	*Streptococcus pyogenes*
S. saprophyticus	*Staphylococcus saprophyticus*
S. schleiferi	*Staphylococcus schleiferi*
S. schweitzeri	*Staphylococcus schweitzeri*
SSI(s)	surgical site infection(s)
S. simiae	*Staphylococcus simiae*
S. simulans	*Staphylococcus simulans*
S. warneri	*Staphylococcus warneri*

T

t / T	time point
T/B	target-to-background (ratio)
^{99m}Tc	technetium-99m, metastable nuclear isomer of techneticum-99 which is an unstable radioactive isotope of techneticum
TCA	trichloroacetic acid
^{99m}Tc-HMPAO	techneticum-99m hexamethylpropylene amine oxime
TFLI	targeted fluorescence imaging
T/N	target-to-normal (tissue ratio)
TNase	thermonuclease
Tris-HCl	tris-hydrochloride
TSB	Tryptic Soy Broth, growth medium

U

U	units
UBI	ubiquicidin / techneticum-99m labelled ubiquicidin
UMCG	University Medical Center Groningen
US	ultrasound
USDA	United States Department of Agriculture

V

VAN	vancomycin based optical tracer
vanco-800CW	vancomycin-IRDye800CW

W

war	*Staphylococcus warneri*
WL	white light
WLI	white-light image
wt	wild-type

Z

^{89}Zr	zirconium-89, unstable radioactive isotope of zirconium

Biography

Marjolein Heuker was born on the 8th of December 1992 in Groningen, the Netherlands. She went to high school at *rsg de Borgen*, the *Lindenborg*, in Leek, where she graduated in 2011. After studying biology for a year at the University of Groningen, she started medical school at the University of Groningen in 2012. In 2013, Marjolein became involved in the research group of Prof. G.M. van Dam, Prof. J.M. van Dijl and Dr. M. van Oosten, focusing on fluorescence imaging of bacterial infections. She received her medicine bachelor's degree, including 'Junior Scientific Masterclass honours' distinction in 2015.

Marjolein received a grant from the Graduate School of Medical Sciences of the University Medical Center Groningen (UMCG) as an MD-PhD student, resulting in the combination of her medical internships with research at the department of Medical Microbiology. Marjolein followed her internships at the UMCG and at the *Treant zorggroep*, with the main location at the *Scheperziekenhuis* in Emmen. After her last medical internship at the emergency department and intensive care, she completed her medical studies in 2020. During her studies, Marjolein was active in study-related committees and followed various courses. She also worked as the chair of the 'coraad' of the *Treant zorggroep*. After graduating, Marjolein completed her research, resulting in this thesis.

Biografie

Marjolein Heuker werd geboren op 8 december 1992 te Groningen, Nederland. Haar middelbare school doorliep zij aan rsg de Borgen, de Lindenborg, in Leek, waar zij in 2011 haar atheneum diploma behaalde. Na een jaar biologie te hebben gestudeerd aan de Rijksuniversiteit Groningen, startte zij in 2012 met de opleiding geneeskunde. In 2013 raakte Marjolein betrokken bij de onderzoeksgroep van prof. dr. G.M. van Dam, prof. dr. J.M. van Dijl en dr. M. van Oosten, met als aandachtsgebied fluorescentie beeldvorming van bacteriële infecties. Zij ontving haar geneeskunde bachelor diploma, inclusief 'Junior Scientific Masterclass honours' onderscheiding in 2015.
Marjolein ontving een beurs van de *Graduate School of Medical Sciences* van het Universitair Medisch Centrum Groningen (UMCG) als MD-PhD student, zodat zij haar coschappen kon combineren met het verrichten van promitieonderzoek bij de afdeling Medische Microbiologie. Marjolein volgde haar coschappen in het UMCG en bij de Treant zorggroep, met als hoofdlocatie het Scheperziekenhuis te Emmen. Na haar semi-arts stage op de spoedeisende hulp en de intensive care rondde zij in 2020 haar studie geneeskunde af. Tijdens haar studie was Marjolein actief in studie-gerelateerde commissies en heeft zij verschillende cursussen gevolgd. Tevens was zij werkzaam als voorzitter van de 'coraad' van de zorggroep Treant. Na haar afstuderen heeft Marjolein haar onderzoek afgerond, resulterend in de totstandkoming van dit proefschrift.

List of publications *(Publicatielijst)*

Heuker M, Gomes A, van Dijl JM, van Dam GM, Friedrich AW, Sinha BNM, van Oosten M. Preclinical studies and prospective clinical applications for bacteria-targeted imaging: the future is bright.
Clinical and Translational Imaging, 2016

Heuker M, Sijbesma JWA, Aguilar-Suárez R, de Jong JR, Boersma HH, Luurtsema G, Glaudemans AWJM, van Dam GM, van Dijl JM, Slart RHJA, van Oosten M. *In vitro* imaging of bacteria using ^{18}F-Fluorodeoxy-glucose micro positron emission tomography.
Scientific Reports, 2017

Romero Pastrana F[*] , Thompson JM[*], **Heuker M**, Hoekstra H, Dillen CA, Ortines RV, Ashbaugh AG, Pickett JE, Linssen MD, Bernthal NM, Francis KP, Buist G, van Oosten M, van Dam GM, Thorek DLJ, Miller LS[#], van Dijl JM[#]. Noninvasive optical and nuclear imaging of *Staphylococcus*-specific infection with a human monoclonal antibody-based probe.
Virulence, 2017

Rosman CWK, Romero Pastrana F, Buist G, **Heuker M**, van Oosten M, McNamara JO, van Dam GM, van Dijl JM. *Ex vivo* tracer efficacy in optical imaging of *Staphylococcus aureus* nuclease activity.
Scientific Reports, 2018

Heuker M[*], Koser U[*], Ott A, Karrenbeld A, van Dijl JM, van Dam GM, de Smet AMGA, van Oosten M. Yeast Infections after Esophagectomy: A Retrospective Analysis.
Scientific Reports, 2020

Schoenmakers JWA, **Heuker M**[*], López-Álvarez M[*], Nagengast WB, van Dam GM, van Dijl JM, Jutte PC, van Oosten M. Image-guided *in situ* detection of bacterial biofilms in a human prosthetic knee infection model: a feasibility study for clinical diagnosis of prosthetic joint infections.
European Journal of Nuclear Medicine and Molecular Imaging, 2020

López-Álvarez M, **Heuker M**[*], Schoenmakers JWA[*], van Dam GM, McNamara JO, van Dijl JM, van Oosten M. The smart activatable P2&3TT probe allows accurate, fast, and highly sensitive detection of *Staphylococcus aureus* in clinical blood culture samples.
Scientific Reports, 2020

Bispo M, Anaya-Sanchez A, Suhani S, Raineri EJM, López-Álvarez M, **Heuker M**, Szymański W, Romero Pastrana F, Buist G, Horswill AR, Francis KP, van Dam GM, van Oosten M, van Dijl JM. Fighting *Staphylococcus aureus* infections with light and photoimmunoconjugates.
The Journal of Clinical Investigation (JCI) Insight, 2020

Heuker M[*], López-Álvarez M[*], Sjollema KA, van Dam GM, van Dijl JM, IJpma FFA[#], van Oosten M[#]. Bacteria-targeted fluorescence imaging for visualisation of fracture-related infections in orthopaedic trauma surgery.
Under revision for publication in the European Journal of Nuclear Medicine and Molecular Imaging

Heuker M[*], Koser U[*], van de Wauwer C, Erasmus ME, Timens W, van Dam GM, Nagengast WB, Marshall ADL, Dhaliwal K, van Dijl JM[#], Verschuuren EAM[#], van Oosten M[#]. *Ex vivo* visualisation of bacterial infection and pulmonary microbiological colonisation in resected human and porcine lungs using targeted optical endomicroscopy.
To be submitted

[*],[#] These authors contributed equally to this work.

Acknowledgements *(Dankwoord)*

De afgelopen jaren zijn voorbij gevlogen, continu wisselen tussen de kliniek en het onderzoek was intensief. Ik heb mij af en toe afgevraagd waar ik aan begonnen was, maar ik had het voor geen goud willen missen. Inmiddels is het zover, afgelopen jaar officieel een echte kleine dokter, en nu mag ik ook mijn onderzoekstraject afronden. Ik moet wel toegeven, een proefschrift maak je niet alleen. Dit proefschrift is tot stand gekomen met dank aan alle personen die hieraan hebben bijgedragen. Graag wil ik de volgende mensen in het bijzonder bedanken.

Allereerst wil ik mijn promotor **prof. dr. J.M. van Dijl** bedanken. Beste Jan Maarten, het was een genoegen om samen met jou dit onderzoekstraject te doorlopen. Als jonge geneeskunde studente ben ik met open armen ontvangen bij jullie in de groep. Ik ben gestart met oriënterende kleine onderzoeksprojecten, als onderdeel van het *Junior Scientific Masterclass Honours* programma. Ik had absoluut niet de intentie om te promoveren, maar gaandeweg werd ik enthousiast. Jij nam altijd de tijd en moeite om mij persoonlijk te begeleiden, hetgeen ik enorm gewaardeerd heb. Ik heb zelfs op ieder *pilot project* feedback ontvangen, wat zeker niet vanzelfsprekend schijnt te zijn. Dit heeft mij enorm geholpen om mijn onderzoekvaardigheden verder te ontwikkelen. Jij hebt de afgelopen jaren altijd voor mij klaar gestaan, daar kon ik blind op vertrouwen. Jij gaf mij het vertrouwen en de kans om promotieonderzoek te doen, en hier heb ik geen moment spijt van gehad. Jan Maarten, ik had mij geen betere promotor kunnen wensen. Ik heb veel bewondering voor je enthousiasme, optimisme en wetenschappelijke inzichten waarmee je veel projecten succesvol afrondt. Ik wil je tevens bedanken voor alle goede adviezen en steun tijdens mijn promotietraject. Daarnaast wil ik ook je vrouw Rita bedanken voor de 'van Dijl' spellingscontrole. Tevens heeft zij jou vaak moeten missen om de promotietrajecten van je vele promovendi af te kunnen ronden. Ik heb genoten van onze tijd samen in Nepal, en hoop ook deze mijlpaal nogmaals samen met jullie te kunnen vieren.

Mijn promotor **prof. dr. G.M. van Dam**, beste Go, dankzij jou ben ik bij de Medische Microbiologie terecht gekomen. Al snel bleek tijdens onze kennismaking dat mijn affiniteit niet bij de Chirurgie ligt. Ik had interesse in de biologie, waarna jij mij hebt laten kennismaken met de fluorescentie beeldvorming bij infectieziekten. Je begeleiding op persoonlijk vlak verdient een compliment, je hebt geluisterd naar wie ik ben en jouw ideeën waren inspirerend. Ik wil je bedanken voor alle persoonlijke gesprekken die mij hebben geholpen om verdere keuzes te durven maken.

Mijn copromotor, **dr. M. van Oosten**, beste Marleen, wat hebben wij samen een geweldige tijd meegemaakt! Het is lastig in woorden te vatten, maar dit traject heeft naast een goede begeleider ook een fantastische vriendin opgeleverd. Wij hebben de afgelopen jaren veel meegemaakt. Het boterde meteen goed. Ik was jouw eerste student, in jouw voetsporten tredend. En ja, ik stond zelfs bekend als 'mini-Marleen'. (Kennelijk zijn de meeste arts-microbiologen en overige collega's wat

stil vergeleken ons gekakel). Onze 'werkafspraken' waren heerlijk, lekker samen wijntjes drinken en eten. Iets waar wij beiden enorm van houden. Toen ik besloot een promotietraject te gaan doen, werden de verhoudingen opeens anders. Waar wij eerst vriendschappelijk onderzoek verrichtten voor het plezier, was je nu opeens mijn officiële baas. Nog steeds kon ik altijd bij jou terecht. Ik heb veel van jou geleerd, niet alleen op onderzoeksgebied, maar zeker ook op persoonlijk vlak. We hebben veel gelachen en zelfs gehuild. Ieder promotietraject kent bergen en dalen, maar jij hebt mij behoed voor de diepe kraters. Er stond altijd thee of een wijntje klaar met een portie goed advies. Ik heb genoten van de afgelopen jaren en ben trots op wat wij samen hebben bereikt. Ik wens jou, samen met Hans, Elise, James en de derde kleine spruit, heel veel geluk toe en hoop in de toekomst nog vaak met jullie te mogen proosten.

Graag wil ik de leden van beoordelingscommissie, **prof. dr. H.J. Busscher**, **prof. dr. R.A.J.O. Dierckx** en **prof. dr. J.A.G. van Strijp**, hartelijk bedanken voor het lezen en beoordelen van dit proefschrift.

Mijn paranimfen, **Jorrit**, **Lisanne** en **Mafalda**. Jorrit, jij bent de meest relaxte collega die ik ken! De vele kopjes koffie in het UMCG of in Groningen centrum bij een goed gesprek waren altijd welkom. Samenwerken in het lab verliep uitstekend met als hoogtepunt de *post-mortem* experimenten. Hier ontpopte jij je tot een ware orthopeed! Lisanne, jij bent echt een toppertje! Je bent ontzettend behulpzaam en hebt een fantastisch creatief brein. Dank voor alle hulp bij de vormgeving van dit proefschrift. Naast alle creatieve sessies heb ik ook ontzettend genoten van de kopjes thee, dansen met een biertje en ons tripje naar Edinburgh. Mafalda, és uma fantástica companheira de escritório e uma pessoa espetacular. Adorei o tempo que passamos juntas, a jantar, com muito vinho a mistura, ou a dancar durante toda a noite. Estou feliz que tu e o Tiago fiquem na Holanda, para que possamos continuar a ter mais jantares internacionais e diversão. Obrigado por estares sempre disponível para mim, não apenas nos bons momentos mas também nos mais difíceis. Thank you all for organising the social program of my special day and being wonderful friends to me. I'm thankful we've met and hope we will spend more time to celebrate life!

I would like to thank the rest of our Imaging Group, especially **Usma** and **Marina** for the intensive collaboration. Usma, thank you for learning me to practice yoga. Yoga is still part of my life these days and definitely helped me staying relaxed during my research years. You're already back in Scotland for a while, and I miss our laughs and sports together. Even the experiments during the night were always fun! Thank you for learning me to cook your family recipes. I hope we can catch up soon, I would love to visit you in Scotland. Marina, thank you for all the fun we've had and skills you've learned me. You are a real imaging expert. *Gracias* for the delicious Spanish *jámon* and knife, which we still love to use!

I would like to thank all other old and current colleagues of the Molecular Bacteriology (MolBac) lab and the Optical Molecular Imaging Group (OMIG). Thanks for all the feedback during our meetings and, even more important, the fun we've had during conferences and lab days.

Daarnaast wil ik alle coauteurs en samenwerkende partners bedanken voor hun bijdrage aan de totstandkoming van het onderzoek beschreven in dit proefschrift. Ook het secretariaat van de Medische Microbiologie, het Skills center en de analisten van het diagnostisch laboratorium wil ik bedanken voor alle logistieke hulp.

Een promotietraject kent natuurlijk altijd haar ups en downs, waarbij onvoorwaardelijke steun en liefde van vrienden en familie van groot belang is. Ik zou graag de onderstaande personen nog in het bijzonder willen bedanken.

Mijn lieve vrienden, **Peter** & **Kirsten**, **Erwin** & **Heleen** en **Mark** & **Gonneke**, bedankt voor alle gezelligheid. Jullie staan altijd voor mij klaar, ook als alles even iets minder goed lijkt te gaan. Kirsten, Heleen en Gon, wij kennen elkaar al jarenlang en delen inmiddels lief en leed. Het voelt voor mij nog altijd als in onze tienerjaren, samen als één (korfbal)team. Inmiddels is de groep uitgebreid met de kleine man, Niek, en ook de nieuwe jongens zijn op komst! Ik kijk er enorm naar uit om samen met jullie nog vele mooie herinneringen te mogen maken.
Daarnaast wil ik in het bijzonder Peter van Studio Apenzaken bedanken voor het maken van de fantastische video voor Hoofdstuk 8. En Heleen, creatief als jij bent, heb jij ons InDesign aangeleerd. Resulterend in een toch best aardige lay-out! Bedankt voor al je hulp en ondersteuning bij het ontwerpen van dit proefschrift.

Ook deze vriendschap gaat al jaren terug, lieve **Marc** & **Marlot**, **Dennis**, **Wouter**, **Jasper** en **Roy** & **Nicolien**, bedankt voor alle avonden waarin wij enorm kunnen lachen! Marlot, wij zijn al sinds de eerste klas van de middelbare school onafscheidelijk. Jij staat altijd voor mij klaar en met jou is het altijd feest! Bedankt voor het helpen uitzoeken van mijn jumpsuit, het was toch echt een klein 'say yes to the jumpsuit' moment!

De afgelopen jaren heb ik te veel bezuinigd op de tijd met mensen die mij dierbaar zijn. Hoewel ik dankbaar ben dat ik de kans heb gekregen om te promoveren, is de belangrijkste levensles geweest dat goede vrienden en familie het allerbelangrijkst zijn!

Lieve schoonfamilie, **Wilko** & **Gonny**, **Tim** & **Evelien** en **Jelmer** & **Kars**, en lieve familie, **Pap** & **Mam** en **Edwin** & **Janine**, bedankt dat het bij jullie altijd voelt als thuiskomen. Bedankt voor de interesse en ondersteuning de afgelopen jaren. Jullie vormen stuk voor stuk een luisterend oor, een troostende schouder en voorzien mij van een portie goed advies. Ik heb ontzettend veel geluk met jullie als familie en hoop de komende jaren nog veel mooie momenten samen te kunnen delen.

Lieve **Tobias**, bedankt voor al jouw steun tijdens mijn promotietraject. Jij weet als geen ander hoe het is om 'alle ballen in de lucht te houden' en was altijd positief en vrolijk als ik thuis kwam van een onderzoeksdag of uit de kliniek. Bedankt voor al je geduld, een luisterend oor en zo nu en dan een kritische noot. Ik hoop dat, nu ik mijn boekje klaar heb, wij meer tijd voor elkaar zullen maken en blijven genieten van het leven. Ik ben al jaren ontzettend blij en gelukkig met jou en hoop dit nog jaren vol te houden! Wij gaan samen een fantastische toekomst tegemoet, daar heb ik alle vertrouwen in!

Tot slot, wil ik afsluiten met een verwijzing naar de voorkant van dit proefschrift, mede mogelijk gemaakt door mijn schoonmoeder. Zoals gezegd kon dit proefschrift alleen maar ontstaan door al jullie betrokkenheid. Het gezicht van dit proefschrift zijn wij dus allemaal. Bedankt!

-Marjolein

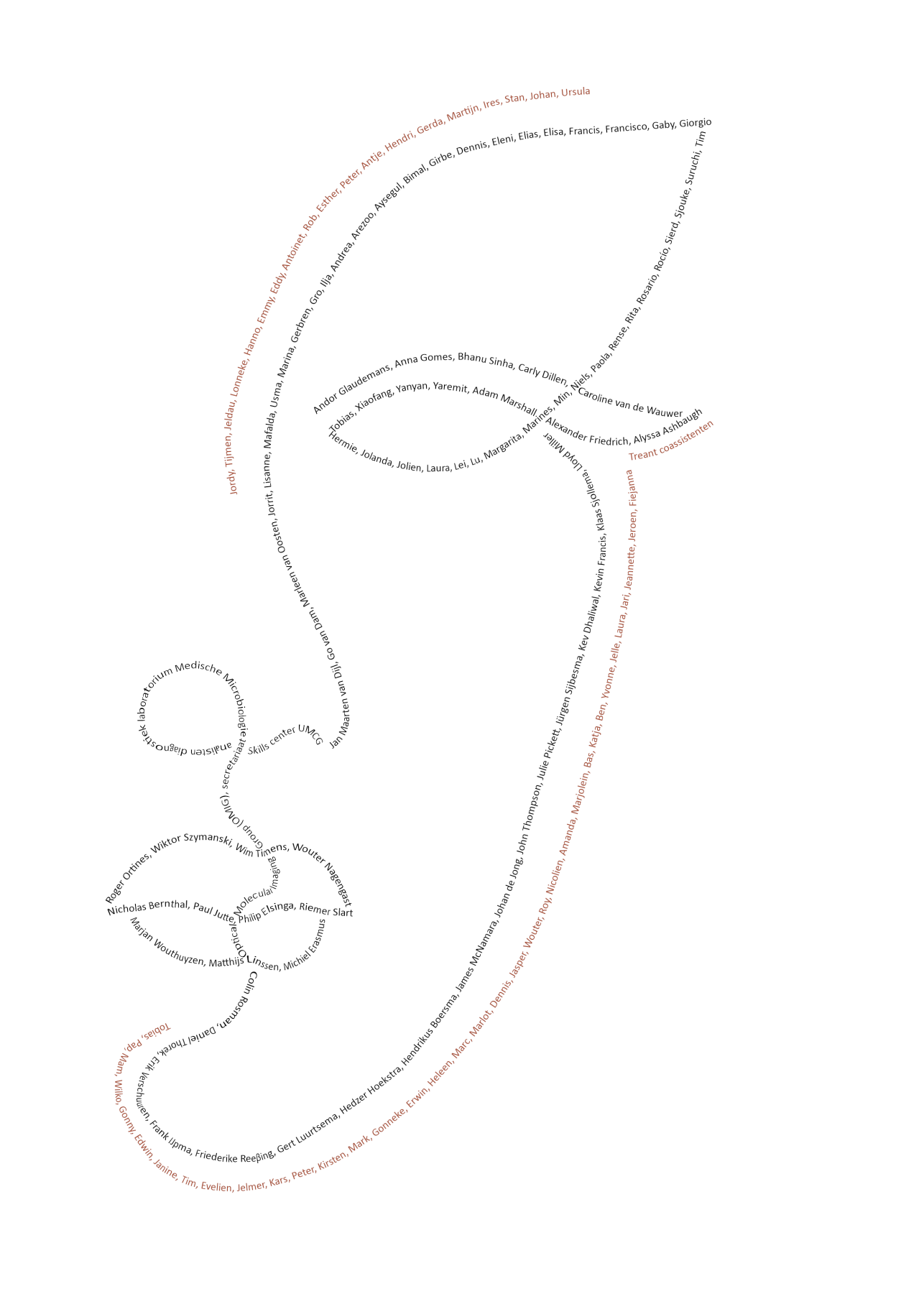
Jordy, Tijmen, Jeldau, Lonneke, Hanno, Emmy, Eddy, Antoinet, Rob, Esther, Peter, Antje, Hendri, Gerda, Martijn, Ires, Stan, Johan, Ursula
Andor Glaudemans, Anna Gomes, Bhanu Sinha, Carly Dillen, Niels, Paola, Rense, Rita, Rosario, Rocio, Sierd, Sjouke, Suruchi, Tim
Jobias, Xiaofang, Yanyan, Yaremit, Adam Marshall, Marines, Min, Caroline van de Wauwer
Hermie, Jolanda, Jolien, Laura, Lei, Lu, Margarita, Alexander Friedrich, Alyssa Ashbaugh
Treant coassistenten
Jan Maarten van Dijl, Go van Dam, Marleen van Oosten, Jorrit, Lisanne, Mafalda, Usma, Marina, Gerbren, Gro, Ilja, Andrea, Arezoo, Ayşegul, Bimal, Girbe, Dennis, Eleni, Elias, Elisa, Francis, Francisco, Gaby, Giorgio
Lloyd Miller, Klaas Sjollema, Kevin Francis, Kev Dhaliwal, Jürgen Sijbesma, Julie Pickett, John Thompson, James McNamara, Johan de Jong, Hedzer Hoekstra, Hendrikus Boersma, Gert Luurtsema, Frederike Reeßing, Frank Ijpma, Erik Wesselius, Daniel Thorek, Colin Rosman, Marjan Wouthuyzen, Matthijs Linssen, Michiel Erasmus
Roger Ortines, Wiktor Szymanski, Wim Timens, Wouter Nagengast
Nicholas Bernthal, Paul Jutte, Philip Elsinga, Riemer Slart
Skills center UMCG
Laboratorium Medische Microbiologie
Analisten diagnostiek
secretariaat
Group (OMIG)
Molecular imaging
Optical
Willo, Gonny, Edwin, Janine, Tim, Evelien, Jelmer, Kars, Peter, Kirsten, Mark, Gonneke, Erwin, Heleen, Marc, Marlot, Dennis, Jasper, Wouter, Roy, Nicolien, Amanda, Marjolein, Bas, Katja, Ben, Yvonne, Jelle, Laura, Jari, Jeannette, Jeroen, Fiejanna
Tobias, Pap, Mart,

Bacteria-targeted infection imaging
Towards a faster diagnosis of bacterial infection

Het gezicht op de voorpagina staat symbool voor de kijk naar de toekomst en refereert naar ‘the future is bright’. De lijn symboliseert het pad dat is doorlopen om dit proefschrift tot stand te laten komen. Tot slot, het gezicht is geplaatst deels over de rug van het boek, en kijkt hiermee om de hoek. Dit symboliseert dat medici en onderzoekers meer buiten de kaders moeten denken en creatief moeten blijven om nieuwe technieken te ontwikkelen.